UNIVERSITY OF BELGRADE
FACULTY OF CIVIL ENGINEERING

Moamen Awad Habib Gad

DETERMINATION OF THE REFERENCE HEIGHT SURFACES IN THE REGIONS WITH SPARSE GRAVITY DATA

Doctoral Dissertation

Belgrade, 2022

UNIVERZITET U BEOGRADU

GRAĐEVINSKI FAKULTET

Moamen Awad Habib Gad

ОДРЕЂИВАЊЕ РЕФЕРЕНТНИХ НИВОСКИХ ПОВРШИ ВИСИНА У ПОДРУЧЈИМА СА НЕПРАВИЛНИМ ПРОСТОРНИМ РАСПОРЕДОМ РЕЗУЛТАТА ОПАЖАЊА ПАРАМЕТАРА ПОТЕНЦИЈАЛА ЗЕМЉИНЕ ТЕЖЕ

Doktorska disertacija

Beograd, 2022

MENTOR:

Prof. dr Oleg Odalović, Associate professor,
University of Belgrade – Faculty of Civil Engineering

MEMBERS OF THE COMMISSION:

Prof. dr Ivana Vasiljevic, Associate professor,
University of Belgrade - Faculty of Mining and Geology

Prof. dr Dragan Blagojević, professor,
University of Belgrade - Faculty of Civil Engineering

Doc. dr Sanja M. Grekulović, Assistant professor,
University of Belgrade - Faculty of Civil Engineering

DATE OF DEFENSE OF DOCTORAL DISSERTATION:

MENTORI:

Prof. dr Oleg Odalović, vanredni profesor,
Univerzitet u Beogradu – Građevinski Fakultet

ČLANOVI KOMISIJE:

Prof. dr Ivana Vasiljevic, vanredni profesor,
Univerzitet u Beogradu – Rudarsko-Geološki Fakultet

Prof. Dragan Blagojević, redovni profesor,
Univerzitet u Beogradu – Građevinski Fakultet

Doc. dr Sanja M. Grekulović, docent,
Univerzitet u Beogradu – Građevinski Fakultet

DATUM ODBRANE:

Acknowledgments

My gratitude goes to the people and government of the republic of SERBIA for their generous hospitality during study my Ph.D.

My special thanks and warm appreciation to my fantastic mentor Prof. Oleg Odalović for his incredible steadfast support and strive to do more through his kindness, patience, motivation, and immense knowledge throughout countless days, besides giving me incredible knowledge, guidance, and push me in calculations process. Also, I would like to thank my thesis committee: Prof. dr Ivana Vasiljević for conducting the highest quality research with her guidance and insights, and Doc. dr - Sanja M. Grekulović, and Prof. dr Dragan Blagojević for their insightful comments and encouragement.

Also, my appreciation runs to Bureau Gravimetric International (BGI) organization for providing me with some data, and my deepest gratitude goes to Dir. Mohamed Sobh, Institute of Geophysics and Geoinformatics, Freiberg, Germany, for providing me GETECH gravity data for Egypt.

My profound personal gratefulness to my great family, my Wife Phepy Dawod, my children Rose, Fady, and Andrew for being here, for their support did this thesis, and to all Serbian friends who always encouraged support with their assistance throughout this journey.

Determination of the reference height surfaces in the regions with sparse gravity data

SUMMARY

The research aims to create a methodology that would lead to a mathematical model of referent surfaces and apply that created model in areas where it is not possible to provide a large number of observations, Global geopotential models, digital models of topographic masses, and available observations were used to model the Earth's potential field parameters to be distributed appropriately and be sufficient in the relevant area.
Then, the reference surfaces (geoid and quasi-geoid) are determined from observations and newly modeled parameters of the Earth's gravity potential.

The research methods that were used are the method of analysis and synthesis of existing results, mathematical modeling (interpolation, extrapolation, prediction, ...), the process of experiments, the technique of comparing the obtained results, the theory of Earth's gravitational potential, through statistical methods and collocations.

The experimental part of the research was performed in two steps using already existing and well-distributed data called Area 01 as the first step, while in the second step, Area 02 was used for sparse data region or the rest area of Egypt territory.

The results conclude that it is possible to model the Earth's gravity potential parameters in Area 02, with small numbers and irregular spatial distribution of observation results, in sufficient numbers and with sufficient accuracy.

The obtained accuracy for Area 02 geoid was ± 0,479 cm as internal accuracy in terms of Standard deviation compared with 162 GPS/H points.

Based on Area 01 results, geoid solutions for Area 01 have been fitted using 80 GPS/leveling stations. In comparison, 100 GPS/leveling stations were used as an external check; the obtained internal accuracy by the LSC technique in terms of the standard deviation was ±0.338 m of the differences, which is considered rather satisfactory. In contrast, external check accuracy was ±0.262 m, considered adequately related to the poor distribution of the available GPS/leveling data in this area.

Evidently, from the two obtained Area 01 and Area 02 geoid accuracies, Area 01 geoid has better accuracy, nearly 30%, than Area 02 geoid as an internal check.

Key words:
EGYPT geoid determinations; geoid determination for sparse data regions; least square collocation for geoid solution; geoid; a few centimetres geoid for EGYPT; sparse gravimetric data.

Academic Expertise: Geodesy

Field of Academic Expertise: Determination of the gravitational field

Table of Contents

List of Figures

List of Tables

List of Abbreviations

Preface

Geodesy is the science of accurately measuring and understanding three fundamental properties of the Earth; its geometric shape, its orientation in space, and its gravity field, as well as the changes of these properties with time. Calculating position with repeatable accuracy is the central problem for the geographical reference of terrestrial information and the principal function of geodesy.
The geographical location on the Earth's surface can be determined by a mathematically defined reference surface instead of the Earth's physical surface (very close to the rotational ellipsoid).
Reference surfaces should have two fundamental characteristics:

- they could be mathematically defined;
- they closely fit the physical surface.

Reference surfaces used are very often are:

- the ellipsoid of rotation,
- the geoid.

Reference surface (ellipsoid) has an arithmetical definition. It is used for horizontal positioning, while the geoid surface has a physical meaning and relationship with the reference ellipsoid for height/separation value. A three-dimensional position is defined by two horizontal coordinates and a vertical component, the height above the reference surface (Fig. 1).

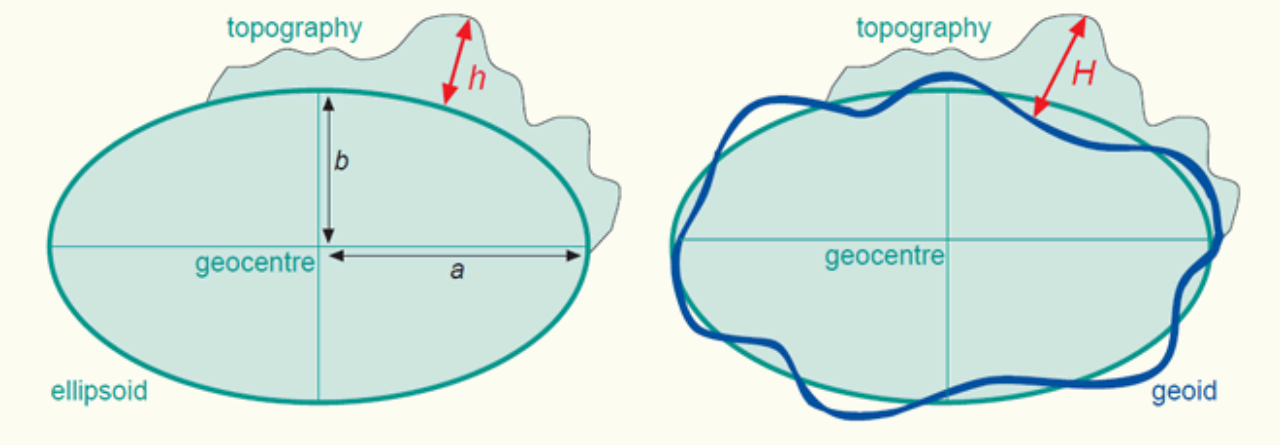

Figure 1 The general relationship between geoid, ellipsoid, and the physical shape of the Earth.
https://kartoweb.itc.nl/geometrics/Reference%20surfaces/refsurf.html

1.1 Thesis Objectives

Solving the positioning problem involves using three surfaces: the physical surface of the Earth, the rotational ellipsoid, and the geoid (Moritz 1990).

By defining and determining the mentioned surfaces within an adopted geodetic reference system, the problem of positioning is reduced by combining the geometric parameters associated with the mentioned surfaces.

Up to date, definitions of these surfaces are the result of international cooperation (IERS, 2010) through activities carried out by the International Association of Geodesy (IAG), one of the eight current associations of the International Union of Geodesy and Geophysics (IUGG) (Yearbook, 2021).

On the other hand, determining the mentioned surfaces in principle differs according to the territory under consideration, so they are most often differentiated: global, regional, and local determinations. Regardless of the region (area) under consideration, each determination implies the disposal of many observation results of almost all quantities observed in geodesy, collected on the physical surface of the Earth, inside its body, or in space outside it.

By applying modern geodetic techniques such as Long Basis Interferometry - Very Long Basis Interferometry (VLBI), Lunar Laser Ranging (LLR) (Williams et al., 2006), Satellite Laser Ranging (SLR) (Otsubo et al., 2016), Doppler observations (DORIS – Doppler Orbitography and Radio-positioning Integrated by Satellite) (Willis et al., 2016) and final observations of Global Navigation Satellite Systems (GNSS) (Beutler et al. 2009), the results of observations necessary for the creation of the International Reference Geodetic Framework (ITRF) are taken over. Within the system, continuous monitoring of the movement of tectonic plate masses (Bosy, 2014) makes it possible to determine geocentric rectangular coordinates or geodetic coordinates of relevant points using the most economical GNSS technique.

It is necessary to pre-determine the geoid to transform specific coordinates into coordinates within the Earth's gravitational field.

Nowadays, the possibility to determine the geoid with a centimeter level of accuracy that, may be achieved if the relevant area has (Sansò and Sideris 2013):

- Global Geopotential Models (GGM),
- digital models of topographic masses (masses of the Earth's crust above the geoid),
- digital models of the mass density of the Earth's crust, and
- the results of observations of the parameters of the Earth's gravitational potential (in the following part of the text, referred to as the results of observations).

Alongside geoid, it is possible to use a quasi-geoid (Molodensky, 1958) determined from the same data for transformation. Still, its determination does not imply a reduction in the results of observed parameters of the Earth's gravitational potential (Forsberg and Tscherning, 1997). Moreover, nowadays, geoid and quasi-geoid are usually determined simultaneously. However, the International Height Reference System (IHRS) is based on the geoid (Ihde et al., 2017); nevertheless, it should be noted that the quasi-geoid is not the equipotential surface of the Earth's gravitational potential.

The subject of this research is the determination of geoid and quasi-geoid in areas where only the irregular spatial distribution of observation results is available, and among other things, includes the following:

- the number of observation results is too small concerning the area under consideration,
- observation results are grouped in only one part of the relevant area and very rarely in other regions, and especially

• the results of observations cannot be taken over by classical geodetic methods due to the inaccessibility or continuous change of the Earth's physical surface of the relevant area.

1.2 Research goal

The research aims to create a methodology that would lead to a mathematical model through which, in areas where it is not possible to provide a large number of observations, the following would be possible:

• economical survey using GNSS in terms of homogeneous height,
• preliminary data for a large number of local geophysical surveys,
• providing preliminary data for all future projects in the field of gravitational field determination and geodetic reference systems, and
• monitoring changes in the Earth's physical surface in the relevant areas.

1.3 Research methods

The research methods that will be used are the method of analysis and synthesis of existing results, mathematical modeling (interpolation, extrapolation, prediction, ...), the process of experiments, the technique of comparing the obtained results, the theory of Earth's gravitational potential, through statistical methods and collocations (Moritz, 1980). The experimental part of the research will be performed using existing data from Egypt.

1.4 Historical research

Previous research in this area is numerous; it has intensified significantly since the middle of the last century, when work on establishing modern geodetic reference systems and mass gravimetric and astrogeodetic surveys began in almost all countries (Torge, 1989, 2001).

Then, the reference systems were established, and the collected observation results enabled the determination of reference surfaces to the level of accuracy from a few meters to a few decimetres, most often in relation to ellipsoids that were adopted for cartographic representations.

In the next seventy years, advances in technology, especially in satellite geodesy and the production of terrestrial relative gravimeters, have led to the determination of reference height surfaces with an accuracy of several dec centimeters. A detailed overview of all these achievements is in the publication (Sansò and Sideris 2013) by IAG. The cited research implies that it is necessary to obtain the results by observing the parameters of the Earth's potential at the level of at least one point per one, two, to five square kilometers. In areas where this is not the case, the techniques listed in (Sanso and Sideris, 2013) are only theoretically directly applicable.

There are numerous ways to determine reference surfaces in areas with small numbers of irregularly spatially distributed observation results. Only some of them are given in (Ulotu, et al. 2009), (Ågren et al. 2008), (Tierra and de Freitas, 2005), (Rabah and Kaloop, 2013), (Chen et al., 2003), (Bjelotomić et al. 2015).

The above determinations used the techniques described in (Sansò and Sideris 2013) or the KTH method (Ågren et al., 2008; Ulotu et al., 2009). The quality of these determinations can be checked by calculating the differences from conditionally correct values (discrete values of undulations or height anomalies) or by determining the range of these differences. In all works, the reference

surfaces were determined in the range of differences of approximately 1 m (Ulotu et al., 2009) up to 21 cm (Bjelotomić et al., 2015).

1.5 The framework structure of the dissertation

The structure of this thesis is presented in seven chapters, the first of which is the Preface. The contents of the remaining six chapters will be summarized below.

Chapter two reviews some aspects of the gravity field and its geodetic implementations. Firstly, the basic concepts of the Earth's gravity field are reviewed. The gravitational and centrifugal potentials have been discussed. Laplace's equation and the potential in terms of spherical harmonics were described. Then, the different types of gravity anomalies and terrain reductions were highlighted. After that, the standard approaches and methods for modeling the outer gravity field of the Earth are discussed. Finally, the various sources of errors in gravimetric geoid determination are outlined.
Chapter three illustrates an overview of Global Geopotential Models (GGMs), digital models of topographic masses, and observations of the Earth's gravitational potential parameters, whereas; the first part is GGMs which contains background about the disturbing potential as a harmonic function.

Afterward, the statistical and mathematical properties of Spherical Harmonic Computations (SHC) and the spectral meaning inherent to spherical harmonic coefficients, and a detailed review of the concepts of the spherical harmonic analysis and spherical harmonic synthesis techniques are discussed. Recent and proposed satellite missions for recovering the global gravity field signals are mentioned. The global harmonic analysis using various global gravity field data sources and the different classes of the derived global harmonic models are presented. After that, the concept of tailored geopotential harmonic models is clarified. Thenceforth, in the second part, a brief explanation of the DEM concept of calculations and modeling.

Chapter four presents a detailed review of the existing world geoid determination attempts and a detailed historical timeline of the Egyptian geoid determinations attempts.

Chapter five contains a proposed methodology to create mathematical models for determining reference surfaces.

Chapter six describes the numerical research as:

a. Creating a mathematical model,

b. Determination of reference surfaces,

c. Internal and external quality control of the obtained solutions.

Chapter seven summarizes the main topics studied in this thesis. It also outlines the main conclusions based on the obtained results. In addition, the appropriate recommendations are drawn.

2. Basic Concepts And Background Of The Earth's Gravitational Field

Overview

Most importantly, geoid modeling is a vital tool for determining the figure of the Earth, and it helps define and refine the mean Earth ellipsoid, which best fits the geoid globally. The geoid is the main issue in establishing the best fitting relative datum for a specific region on a local and regional basis.

This chapter reviews some aspects of the gravity field and its geodetic implementations. Firstly, the basic concepts of the Earth's gravity field are reviewed. The gravitational and centrifugal potentials have been discussed. Laplace's equation and the potential in terms of spherical harmonics were described. Then, the different types of gravity anomalies and terrain reductions were described, and the potential in terms of spherical harmonics. Then, the different types of gravity anomalies and terrain reductions are highlighted. After that, the standard approaches and methods for modeling the outer gravity field of the Earth are discussed. Finally, the various sources of errors in gravimetric geoid determination are outlined.

2.1 Basic Concepts of The Earth's Gravitational Field

The total force on a body at rest on the Earth's surface results from gravitational force, and the centrifugal force of the Earth's rotation (Fig. 2) is called gravity (Wellenhof and Moritz, 2005).

A fundamental quantity that describes the Earth's gravity field is the gravity potential W, which is given at a certain point p as

$$W = V + Vc, \tag{2.1}$$

where V is the gravitational potential that results from the attraction of the Earth's mass and is expressed

$$V = G \iiint_e \frac{\rho(x, y, z)}{l} \, dx \, dy \, dz, \tag{2.2}$$

where the integration is carried out over the entire Earth, l is the distance between the computation point p and the running point q (x,y,z), ρ(x,y,z) is the mass density at q, dxdydz is the infinitesimal volume element at q, G is the Newtonian gravitational constant,

$$G = 6.672 * 10^{-11} \, m^3 s^{-1} kg^{-1},$$

and Vc is the potential of the centrifugal force given by

$$Vc = ½ \ \omega 2 \ (X2 + Y2), \tag{2.3}$$

where ω is the mean angular velocity of the Earth's rotation, and X, and Y are the geocentric rectangular coordinates of point p, relative to the (right-handed) average terrestrial reference frame having the Z-axis coincident with the mean Earth rotation axis (Wellenhof and Moritz, 2005).

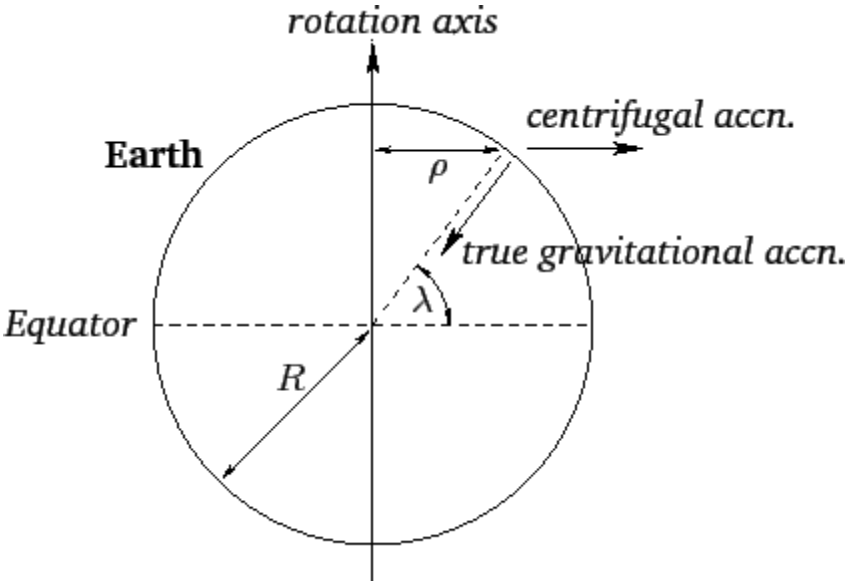

Figure 2 Attraction and Centrifugal Force.

http://shop04004.uygkjhg.ru/content?c=centrifugal%20acceleration%20of%20earthandid=2

The gravity vector ğ is the spatial gradient of W (Heiskanen and Moritz, 1967),

$$\check{g} = \text{grad } W = (\partial w/\partial x \quad \partial w/\partial y \quad \partial w/\partial z) = (w_x \quad w_y \quad w_z), \tag{2.4a}$$

The magnitude (or norm) of the gravity vector ğ is the gravity (acceleration) g,

$$g = \|g\|, \tag{2.4b}$$

which is conventionally expressed in the units of Gals, derived from Galileo,
where 1 Gal = 1 cm/s^2 = $1x10^{-2}$ m/s^2

The direction of the gravity vector is the direction of the actual vertical or plumb line. The gravity acceleration shows a systematic increase as one departs from the equator to the poles' direction due to the centrifugal force's decrease and the geocentric radius of the point of interest. Also, the Earth's gravity decreases systematically with height due to the increase of the geocentric vector.

In modeling the gravity field of an ellipsoid, one must consider an appropriate mass for that (geocentric) ellipsoid and assume that the ellipsoid rotates with the Earth. Furthermore, the ellipsoid's surface is defined as an equipotential surface of its own (theoretical) gravity field using mathematical conditions. Such an ellipsoid is the mean Earth ellipsoid or the absolute ellipsoid (Nassar et al. 1993). In general, surfaces with constant theoretical potential

are denoted as the sphero-potential (or normal level) surfaces, everywhere perpendicular to the normal gravity vector. The magnitude of that vector is the normal gravity, γ, which is longitude independent. The gravity field of the ellipsoid is called the normal gravity field, and the reference ellipsoid itself is sometimes referred to as the level ellipsoid (Fig. 3).

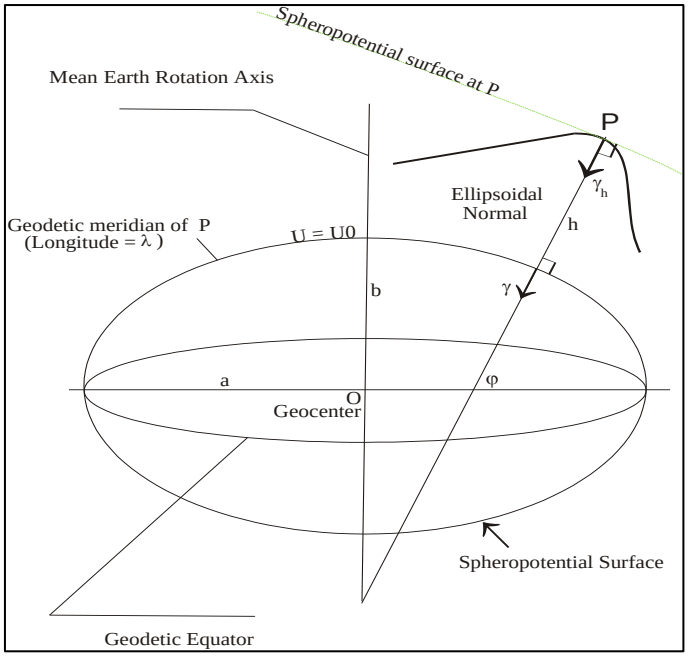

Figure 3 Level Ellipsoid and normal gravity vector (Nassar et al. 1993).

Regarding the model of the Earth, it can be shown that the normal gravity potential and its spatial derivatives are entirely specified by four defining constants, which are briefly expressed as

$U = f(a, b, GM, \omega)$

where

(a, b) are the semi-major and semi-minor axes of the ellipsoid, respectively,

ω is the mean angular velocity of the Earth,

GM is the product of Newton's gravitational constant and the mass of the mean Earth ellipsoid.

As a practical matter, the constants of the normal ellipsoid are defined by continuous research in geodesy and related fields and are adopted by international conventions. Most popular is the WGS84 reference ellipsoid, which simultaneously works as the geometric reference frame of the GPS geodetic observations

Simple mathematical formulas can express functions of the normal gravity field. For example, the normal gravity on the ellipsoid surface, defined to be the magnitude of the gradient of the normal gravity potential, is given by Somigliana's closed formula

$$\gamma = (a\,\gamma_e \cos^2\varphi + b\,\gamma_p \sin^2\varphi) / (a^2\cos^2\varphi + b^2\sin^2\varphi)^{1/2}, \quad (2.5)$$

where φ is the geodetic latitude, γ_e and γ_p are the normal gravity at the equator and pole, respectively, and are uniquely determined from the four parameters defining the normal potential Eq. (2.5). The normal gravity above the ellipsoid, (Fig. 3) is given as (Heiskanen and Moritz, 1967),

$$\gamma h = \gamma\,[1 - 2/a\,(1 + f + m - 2f\sin2\varphi)\,h + (3/a2)\,h2], \quad (2.6)$$

where f is the geometric flattening of the ellipsoid, h is the height above the ellipsoid, and $m = (\omega^2 a^2 b/GM)$ is the geodetic parameter of the reference ellipsoid, which is equal to the ratio of the centrifugal acceleration and normal gravity at its equator. Finally, γ is the relevant normal gravity on the ellipsoid.

If ρ_n denotes the hypothetical ellipsoidal mass density, which generates the normal gravitational potential, it follows that

$$V_n = G \iiint_e \frac{\rho_n(x,y,z)}{l} \, dx \, dy \, dz, \tag{2.7}$$

$$U = V_n + V_c, \tag{2.8}$$

$$T = W - U = V - V_n, \tag{2.9}$$

where U, Vn, Vc, and T denote the normal gravity potential, the normal gravitational potential, the centrifugal potential, and the disturbing (or anomalous) potential, respectively. Again, as with the actual gravity field, the normal gravity field determination does not necessitate the knowledge of the normal density distribution (Heiskanen and Moritz, 1967)**.** The disturbing potential is the slight difference between the gravity potential W of the Earth and the normal gravity potential U.

In other words, this anomalous quantity carries the spatially random nature of the Earth's actual gravity field deviation from the model field induced by the reference ellipsoid. It can be considered as being produced by a disturbing density $\delta\rho = (\rho - \rho_n)$ as follows

$$T = G \iiint_e \frac{\delta_\rho(x,y,z)}{l} \, dx \, dy \, dz, \tag{2.10}$$

If ∇^2 denotes the Laplacian operator, it can be proved that (Heiskanen and Moritz, 1967)**,**

$$\nabla^2 V = \begin{cases} 0 & \text{outside the Earth's surface,} \\ -4\pi G\rho & \text{inside the Earth's surface,} \end{cases} \tag{2.11}$$

$$\nabla^2 W = \begin{cases} 2\omega 2 & \text{outside the Earth's surface,} \\ -4\pi G\rho + 2\omega 2 & \text{inside the Earth's surface,} \end{cases} \tag{2.12}$$

$$\nabla^2 Vn = \begin{cases} 0 & \text{outside the ellipsoid's surface,} \\ -4\pi G\rho n & \text{inside the ellipsoid's surface,} \end{cases} \tag{2.13}$$

$$\nabla^2 U = \begin{cases} 2\omega 2 & \text{outside the ellipsoid's surface,} \\ -4\pi G\rho n + 2\omega 2 & \text{inside the ellipsoid's surface,} \end{cases} \tag{2.14}$$

$$\nabla^2 T = 0 \quad \text{outside the Earth's surface.} \tag{2.15}$$

Mathematically, if the Laplacian operator of a specific function vanishes, this function is harmonic. Eq. (2.15) is Laplace's equation for the anomalous potential. From the above, it is clear that the outer gravitational, normal, and anomalous potential are generally harmonic and can be expanded in spherical harmonic series. The harmonicity condition is one of the fundamental properties satisfied by the Earth's outer gravitational and anomalous fields. In (Eqs. 2.11 and 2.13), the inner and normal

gravitational fields, respectively, ∇^2 is not zero. In this case, they are said to obey Poisson's equation, not Laplace's condition. Fortunately, the geodetic applications only need to determine the outer (harmonic) gravity field elements.

All the gravity field elements are related to the disturbing potential and each other by closed functional relationships. These observable gravimetric quantities, which are also harmonic functions in outer space, are geoidal heights, deflections of the vertical, gravity anomalies, and gravity disturbances.

These elements are considered residual quantities, are supposed to be unique and smooth, and are mathematically referred to as signals. The geoid undulation (Fig. 4), defined as the geodetic height of the geoid over the reference ellipsoid, is related to the anomalous potential T, at the geoid, via the well-known Bruns' equation (Hotine, 1969).

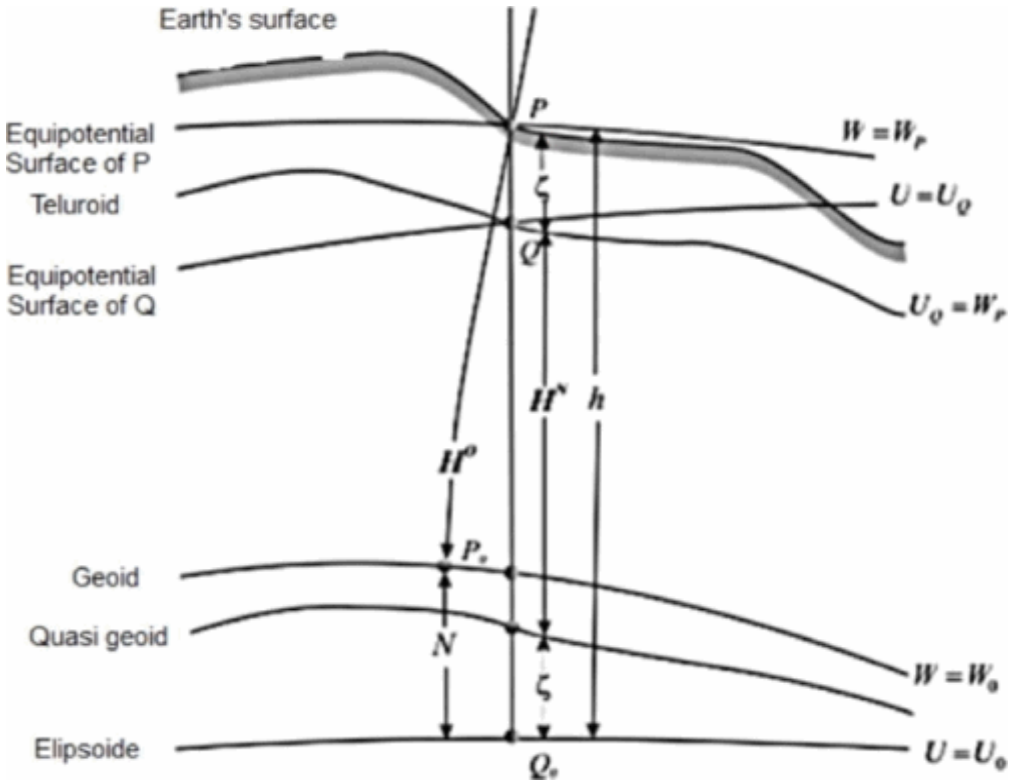

Figure 4 Geoidal height

https://www.earthdoc.org/content/papers/10.3997/2214-4609.201702624#dataandmedia

$$N = h - H = (W_P - U_P) / \gamma_Q = \frac{T}{\gamma_Q} \qquad (2.16)$$

The above expression is based on the assumption that the potential of the normal ellipsoid U_0 equals the potential of the geoid W_0.

The locus of such points is (as the terrain) a non-equipotential surface, which is usually referred to as the telluroid (or terroid) (Fig. 5). The telluroid could be considered the first approximation of the Earth's physical surface or crudely called the "normal" topography. The height anomaly ζ is the separation between that surface and the topographic surface, measured along the normal plumb line. On the other hand, the height of the telluroid above the ellipsoid, measured along the normal plumb line, is usually called the normal height H_N, thus.

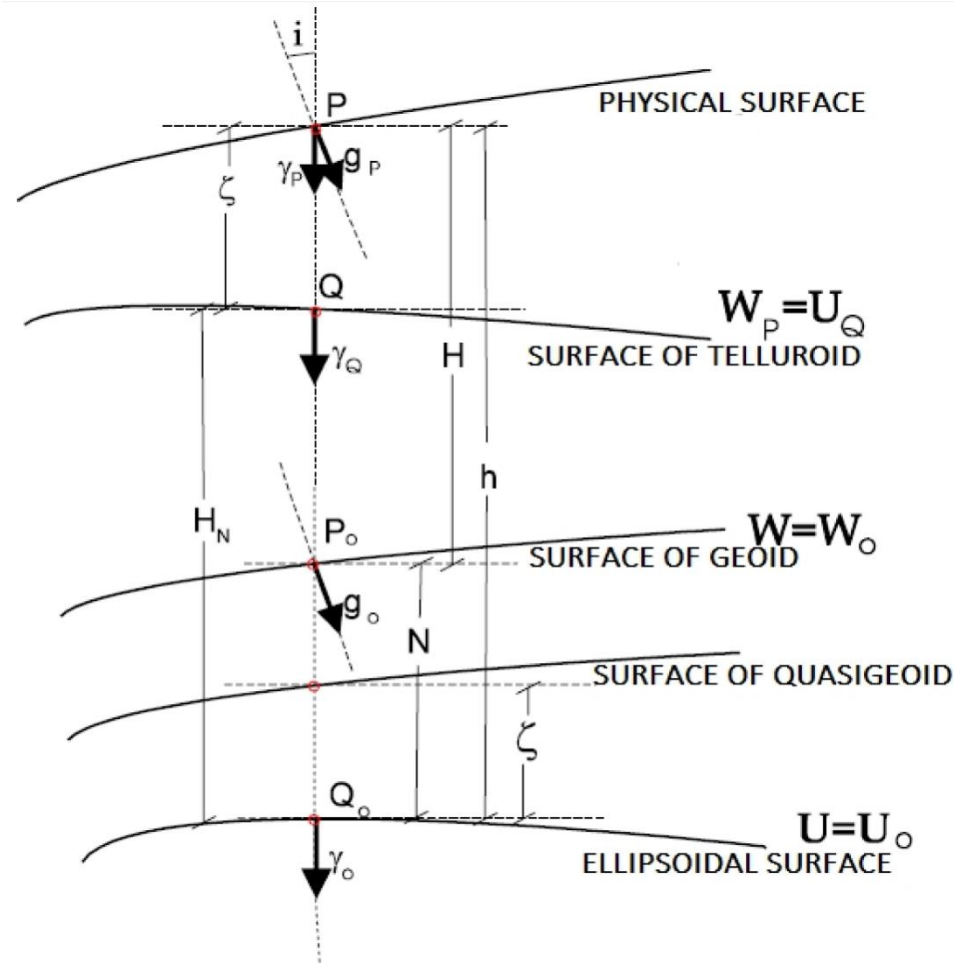

Figure 5 Telluroid and height anomaly

https://www.scielo.br/j/bcg/a/xPcsrP6g8T4HMdrQMbbqjSQ/?lang=en#ModalFigf1

If the height anomalies are plotted above the reference ellipsoid, one obtains the so-called quasi-geoid surface, a non-level surface (El-Fatairy, 1983) that closely approximates the geoid, particularly in relatively moderate topography. Considering (Fig. 5), Bruns' equation gives the height anomaly (or quasi-geoid) as follows

$$\zeta = h - H_N = \frac{(W_p - U_p)}{\gamma_Q} = \frac{T_P}{\gamma_Q}, \qquad (2.17)$$

where T_p is referred to as the disturbing potential at the surface point, P and γ_Q is the normal gravity at the telluroid point Q (having geodetic height $h = H_N$). Hence, the terrain point P is said to correspond to a height anomaly (quasi-geoidal height) ζ and has a normal height H_N above the quasi-geoid, all measured along the ellipsoidal normal.

The angular misalignment (or the relative slope) of the geoid concerning the reference ellipsoid is the deflection of the vertical Θ. The two components, ξ

and η, of the deflection angle Θ, are expressed as the spatial gradients of the geoid, at P_0, in both directions as follows:

$$\xi = -\left(\frac{1}{\mathrm{r}}\right)\frac{\partial \mathrm{N}}{\partial \theta} = -\left(\frac{1}{\mathrm{r}\gamma}\right)\frac{\partial \mathrm{T}}{\partial \theta}, \tag{2.18}$$

$$\eta = -\left(\frac{1}{\mathrm{r}\sin\theta}\right)\frac{\partial \mathrm{N}}{\partial \lambda} = -\left(\frac{1}{\mathrm{r}\gamma\sin\theta}\right)\frac{\partial \mathrm{T}}{\partial \lambda}, \tag{2.19}$$

where r, θ, and λ are the geocentric radii till the geoidal point P_0, the spherical co-latitude and geodetic longitude, respectively, and γ is the normal gravity at the point Q_0 on the ellipsoid. One distinguishes between the deflection angle Θ at the geoidal foot point P_0 and Q_0 which is the relative slope of the equipotential surface at the surface point P relative to the spheropotential surface at the relevant telluroid point Q (Fig. 5). The difference between the two angles, which is usually small, depends on the curvature of both the actual and normal plumb lines and the height of the surface point.

The negative gradient of the anomalous potential at the geoidal point P, along the direction of the normal plumb line, is referred to as the gravity disturbance δg, which is given as

$$\delta_{\mathrm{g}} = -\frac{\partial T}{\partial h} = \mathrm{g}_P - \gamma_P, \tag{2.20}$$

At the Earth's surface, the gravity disturbance becomes

$$\delta_{\mathrm{gt}} = -\frac{\partial T_t}{\partial h} = \mathrm{g}_{P_t} - \gamma_{P_t}. \tag{2.21}$$

Another important anomalous element is the gravity anomaly, which is given at the geoidal point P as

$$\Delta\mathrm{g} = \mathrm{g}_P - \gamma_Q = \frac{1}{\gamma}\frac{\partial \gamma}{\partial h}.T - \frac{\partial T}{\partial h} \tag{2.22}$$

Similarly, one obtains the gravity anomaly at the surface point Pt as follows

$$\Delta\mathrm{g}_{\mathrm{t}} = \frac{1}{\gamma_{\mathrm{t}}}\frac{\partial \gamma_{\mathrm{t}}}{\partial \mathrm{h}}.\mathrm{T}_{\mathrm{t}} - \frac{\partial \mathrm{T}_{\mathrm{t}}}{\partial \mathrm{h}} \tag{2.23}$$

2.2 The disturbing potential and derived gravity field functional

With the introduction of the reference ellipsoid and its physical parameterization, the actual gravity field is linearized and split up into a first approximation represented by the normal gravity field and a remaining and comparably small residual part. In terms of potential, these deviations are denoted as the disturbing potential or anomalous potential T.

The difference between the normal potential U and the actual gravity potential W is beneficial in physical geodesy (Heiskanen and Moritz, 1967):

$$T = W - U\,. \tag{2.24}$$

By building this difference, we can see that the centrifugal part, which is the same in W and U, cancels and thus does not have to be considered. Therefore, the disturbing potential T still satisfies the Laplace equation $\Delta T = 0$ outside the Earth's masses so that it can also be expanded into a spherical harmonic's series.

The function T is a harmonic outside the Earth, i.e., it satisfies the Laplace's equation (Heiskanen and Moritz, 1967):

$$\Delta T = \partial 2T/\partial x2 + \partial 2T/\partial y2 + \partial 2T/\partial z2 = 0\,. \qquad (2.25)$$

Furthermore, this is used to determine the Geoid by introducing some substantial functional, i.e., the gravity anomaly, the gravity disturbance, the geoid height, and the height anomaly.

Assume the point P on the geoid is projected onto the point Q of a reference ellipsoid along the ellipsoidal normal in (Fig. 6).

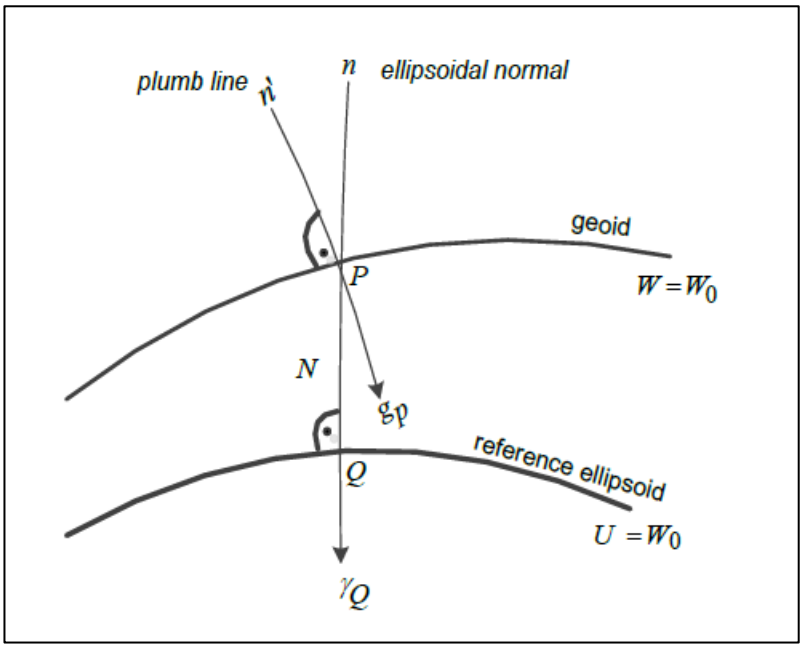

Figure 6 Geoid and reference ellipsoid (e.g., Moritz, 1980).

The previously mentioned anomalous quantities are defined as follows:
The gravity anomaly Δg: the difference between the gravity g_P value at point P on the equipotential surface $W_{(P)}$ (in particular, the geoid) and the normal gravity γ_Q at point Q on the corresponding ellipsoidal potential at its surface $U_{(Q)}$ such that $U_{(Q)} = W_{(P)}$ and Q is an orthogonal projection of P onto $U_{(Q)}$ (in particular the ellipsoid)

$$\Delta g = g_P - \gamma_Q\,; \qquad (2.26)$$

The gravity disturbance δg: the difference between the gravity value g_P at point P and the normal gravity γ_P at the same point

$$\delta g = g_P - \gamma_P\,; \qquad (2.27)$$

The geoid height N: the separation distance PQ between the geoid surface and the reference ellipsoid measured along the ellipsoidal normal. It is also called geoid undulation. The mathematical relationship between the disturbing potential T, which is a purely physical quantity, and the geoid height N, which is a purely geometrical quantity, according to *Bruns' formula* (Wellenhof and Moritz, 2005):

$$N = T_P/\gamma_Q \tag{2.28}$$

where T_P is the disturbing potentials at the geoid surface, and γ_Q is the normal gravity values at the reference ellipsoid.

The fundamental equation of physical geodesy can be derived regarding the Bruns' formula (Eq. 2.28) and the definition of the gravity anomaly (Eq.2.26). It describes the relationship between the gravity anomaly which can be measured and the disturbing potential (Heiskanen and Moritz, 1967)

$$\frac{\partial \mathrm{T}}{\partial \mathrm{h}} - \frac{1}{\gamma}\frac{\partial \gamma}{\partial \gamma} + \Delta \mathrm{g} = 0 \tag{2.29}$$

Some merits exist when the sphere is considered an approximation of the Earth's shape instead of a reference ellipsoid. The differences are minute and in terms of flattening. In many problems, it is an acceptable approximation. Then, this boundary condition takes the form (Moritz, 1989):

$$\frac{\partial \mathrm{T}}{\partial \mathrm{r}} + \frac{2}{\mathrm{R}} + \Delta \mathrm{g} = 0 \tag{2.30}$$

or

$$\frac{\partial \mathrm{T}}{\partial \mathrm{r}} + \frac{2\bar{\mathrm{g}}}{\mathrm{R}} N + \Delta \mathrm{g} = 0 \tag{2.31}$$

where R is the mean radius of the Earth, $\bar{\mathrm{g}}$ is the mean value of gravity over the Earth, $\partial/\partial h$ and $\partial/\partial r$ are partial differentials along the ellipsoidal normal and the radial, respectively. This is a fundamental property in geodesy since it implies that harmonic functions can represent the gravitational potential.

2.3 The Gravitational Potential Into Spherical Harmonics

For global problems, expanding the gravitational potential into spherical harmonics is useful (Torge, 1989), which is a unique solution of Laplace's equation (Eq. 2.11).

In the exterior space, a representation in terms of spherical coordinates (r, θ, λ) is:

$$\mathrm{V}(\theta, \lambda, \mathrm{r}) = \frac{\mathrm{GM}}{r}\left[1 + \sum_{\mathrm{n}=2}^{\infty}\left[\frac{\mathrm{a}}{\mathrm{r}}\right]^{\mathrm{n}} \sum_{\mathrm{m}=0}^{\mathrm{n}} (\mathrm{C_{nm}} \cos \mathrm{m}\lambda + \mathrm{S_{nm}} \sin \mathrm{m}\lambda)\mathrm{P_{nm}}(\cos\theta)\right] \tag{2.32}$$

where:

a	the equatorial radius of the Earth,
C_{nm} and S_{nm}	the conventional unitless Spherical Harmonic Coefficients (SHC) of the Earth's Gravitational potential of degree n and order m,
$P_{nm}(\cos\theta)$	the conventional associated Legendre function of degree n and order m,

with

$P_{nm}(\cos\theta) = (1/2^n\, n!)\,(1-\cos^2\theta)^{m/2}\ [d^{\,n+m}/d\cos\theta^{\,n+m}\ (\cos^2\theta - 1)^n\ ]$

$= (1-\cos^2\theta)^{m/2}\ [d^{\,m}/d\cos\theta^{\,m}\ (P_n(\cos\theta))\ ],$ (2.33)

$$P_{nm}\cos\theta = \frac{1}{2^n} n!\,(1-\cos^2\theta)^{\frac{m}{2}}\left[\frac{d^{n+m}}{d\cos\theta^{n+m}(\cos^2\theta-1)^n}\right] \quad (2.33a)$$

where $P_n(\cos\theta)$ is the conventional Legendre polynomial of degree n, which is given as

$P_n(\cos\theta) = P_{n0}(\cos\theta) = (1/2^n\, n!)\,[d^n/d\cos\theta^{\,n}\ (\cos^2\theta - 1)^n\ ].$ (2.33b)

$$P_n\cos\theta = P_{n0}(\cos\theta) = \frac{1}{2^n} n!\left[\frac{d^n}{d\cos\theta^n(\cos^2\theta-1)^n}\right] \quad (2.33c)$$

The C_{nm} and S_{nm} are spherical harmonics coefficients given by (Torge, 2001)**,**

$$C_{n0} = \frac{1}{M}\iiint_{earth}\left(\frac{r}{a}\right)^n Pnm(\cos\theta)\,dm \qquad m = 0 \quad (2.33d)$$

$$\begin{Bmatrix} C_{nm} \\ S_{nm} \end{Bmatrix} = \frac{2}{M} * \frac{(n-m)!}{(n+m)!}\iiint_{earth}\left(\frac{r}{a}\right)^n Pnm(\cos\theta)\begin{Bmatrix} C_{nm} \\ S_{nm} \end{Bmatrix} dm \qquad m \neq 0 \quad (2.33e)$$

Here dm is a mass element, and M is the Earth's mass.

2.4 Height System

Earth surface Heights can be defined in several ways. Two specifications are necessary to define a local height reference system (Marti and Schlatter 2002)**.**

2.4.1 Geopotential Numbers

The difference between the potential at the geoid and the potential at the points on the earth are the Geopotential numbers, they can be computed by integration of those differences along a leveling line from the reference point O located on the geoid to a corresponding point P on the earth surface (Wellenhof and Moritz, 2005)**,**

$$C_P = W_0 - W_P = \int_0^P g\,dn \sim \sum_0^P g\,\delta n. \quad (2.34)$$

Where g is the gravity, δn is the vertical levelling increment,
Δn_{oP} the height differences from sprit levelling without gravity measurments on the path of integration:

$$\Delta n_{oP} = \int_0^P g\,dn \sim \sum_0^P g\,\delta n. \quad (2.35)$$

The advantage of the geopotential numbers is that they can be determined by a combination of spirit leveling and gravity measurements without making any hypotheses.

2.4.2 Dynamic Heights

The dynamic heights is obtained by dividing the geopotential number C by the normal gravity value γ. computed on the Geodetic Reference System of 1980 (GRS 80) ellipsoid at 45 degrees latitude (Marti and Schlatter, 2002).

$$H^{dyn} = \frac{C}{\gamma_o} \tag{2-36}$$

where $\gamma_o = \gamma_{45} = 9.806199203\ ms^{-2} = 980.6199203$ gal. To convert the measured height differences Δn_{AB} between two surface points A and B directly into a difference of dynamic heights H^{dyn}_{AB} , a so-called dynamic correction DC_{AB} has to be added:

$$\Delta H^{dyn}_{AB} = \Delta n_{AB} + DC_{AB} = \int_A^B \frac{g-\gamma_\circ}{\gamma_\circ} dn. \tag{2-37}$$

2.4.3 Orthometric Heights

Orthometric heights are defined as the heights above the geoid.. They can be obtained by dividing the geopotential number by a mean gravity (Heiskanen and Moritz, 1967)**,**

$$H = \frac{C_p}{\bar{g}} \tag{2.38}$$

where, $\bar{g} = \frac{1}{H}\int_P^{P_0} g dH$ is the mean gravity along the plumb-line between points P and P_0 (Fig. 7).

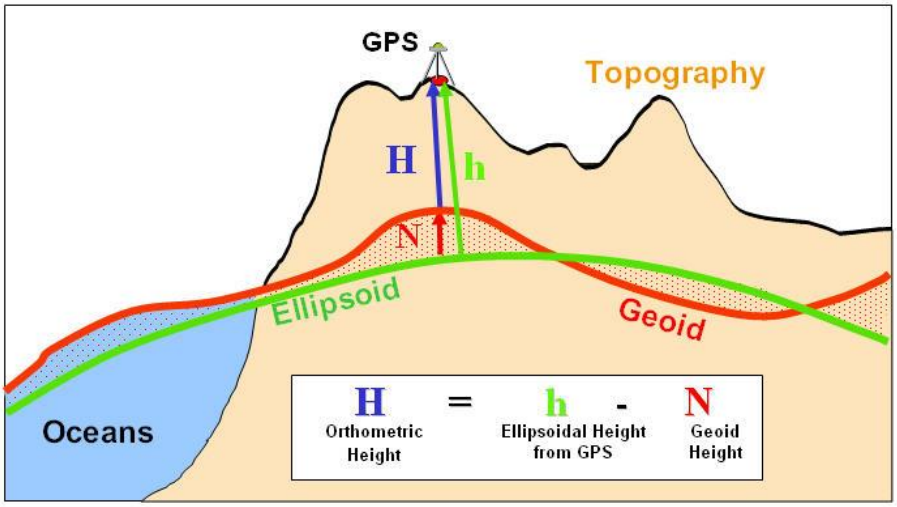

Figure 7 Orthometric height (el shouny et al., 2017)

The orthometric heights cannot determine exactly and base on a hypothesis, this disadvantage because the mean gravity cannot be measured within the earth.
There are some basic approaches for approximating the gravity within the crust as the Prey-reduction approach:

With this approach, the orthometric height H results in the Helmert height (Wellenhof and Moritz 2005, Jekeli 2000)

$$H = \frac{C}{g+0.0424\frac{mGal}{m}H} \tag{2.39}$$

where C in kilo gal*m, g in gal and H in km.

The measured height difference Δn_{AB} between two surface points A and B can be converted to a difference in orthometric height ΔH_{AB} by adding an orthometric correction OC_{AB} (Vanicek et al. 1986).

$$\Delta H_{AB} = \Delta n_{AB+} OC_{AB} = \sum_A^B \frac{g-\gamma_\circ}{\gamma_\circ}\delta_n + \frac{\bar{g}_A-\gamma_\circ}{\gamma_\circ}H_A - \frac{\bar{g}_B-\gamma_\circ}{\gamma_\circ}H_B \tag{2.40}$$

where

g_A and g_B are the mean values of gravity along the plumb lines at A and B, $\gamma_o = \gamma_{45}$ is the normal gravity at a latitude of 45°, H_A and H_B are the orthometric heights of A and B and δ_n is the leveling increment.

2.4.4 Normal Heights

Normal height is a physical height system introduced by (Heiskanen and Moritz 1967) Instead of the orthometric heights, which can be determined without any hypotheses, normal heights denoted by H_P^N can be obtained as follows (Vanicek, 1986):

$$H_P^N = \frac{C_p}{\bar{\gamma}} \tag{2.41}$$

where

$C_P = U_O - U_P = W_O - W_P$.

The abovementioned formula eq. 2.41 means that H_P^N specifies a point P`, which lies on the plumb-line through the surface point P. These kinds of points P', for which eq. 2.41 is fulfilled and lies on a surface called the telluroid. Its form is similar to the physical surface of the Earth.

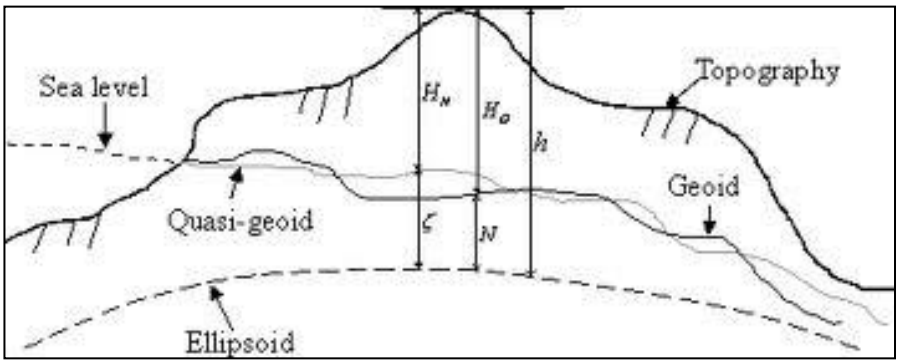

*Figure 8 Normal height (*Vanicek, 1986).

On the other hand, if we are going from any surface point along the plumb-line with the length of the normal height, we obtain a surface called the quasi-geoid, which is close to the geoid and coincides with the geoid at sea (Wellenhof and Moritz 2005).

2.4.5 Ellipsoidal Heights

Ellipsoidal Height or geodetic height of that the same point on the earth surface and its corresponding point on the typical reference ellipsoid is the World Geodetic System 1984 (WGS84), which is defined by the four parameters given in Table 1 and Fig. 9 (Featherstone and Kuhn, 2006).

Table 1 Parameters of the World Geodetic System 1984.

Parameter	value	Description
a	6378137 m	semi-major axis
GM	$3.986004418 \cdot 10^{14} m^3 s^{-2}$	the geocentric gravitational constant of the Earth
J2	$1.081874 \cdot 10^{-3}$	the dynamical form factor of the Earth (excluding the permanent tidal deformation)
ω	$7.292115 \cdot 10^{-5}$ rad s^{-1}	angular velocity of the Earth

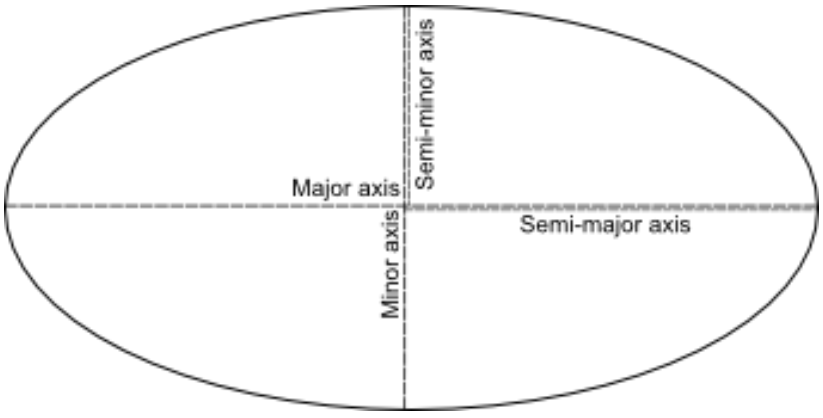

Figure 9 Parameters of the World Geodetic System 1984 (Featherstone and Kuhn, 2006).

2.5 Different Types of Gravity Anomalies and Terrain Reductions

The topographical effect is one of the most important components in solving the geodetic Boundary Value Problem (BVP). It should be adequately treated in the determination of a precise geoid. Therefore, the gravity acceleration value g, at the terrain surface, is not directly comparable with normal gravity (γ), referring to the ellipsoid's surface. A reduction of gravity (*g*) to sea level (geoid) is necessary. Since there are masses above sea level, the reduction methods differ depending

on how to deal with these topographic masses (Heiskanen and Moritz, 1967). Gravity anomalies reveal rock density variations, with the anomaly amplitude proportional to the density contrast and thickness of the anomalous body. Consequently, the problem of investigating the anomalous gravity field can be reduced to comparing actual gravity field parameters at the geoid and the corresponding normal gravity field parameters at the mean Earth ellipsoid. The basic elements of the anomalous gravity field include: gravity anomalies, height anomalies, disturbing potential, deflection of the vertical, geoid undulations, etc. (Nassar, 1976)

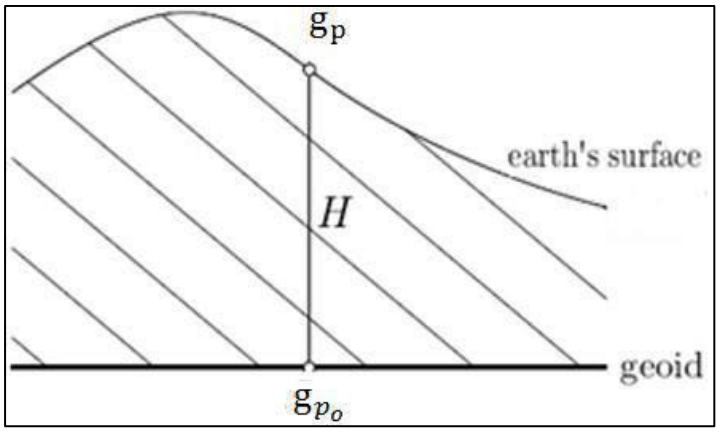

Figure 10 Gravity reductions (Nassar, 1976)

It should be noted that two conditions should be achieved to use Stokes' formula (Wellenhof and Moritz, 2005). The first condition is that the gravity Th station is lowered from the Earth's surface (g_p) to the geoid surface (g_{po}) as shows in Fig. 10. The second condition is that there must be no masses outside the geoid .

Molodensky's solution is the other fundamental solution to the geodetic BVP. This modern solution gives the quasi-geoid but not a level surface (geoid) as in Stokes's solution.
The following sections present some of the gravity reduction methodologies.
There are several types of gravity anomalies based on treating the masses between the terrain and the geoid. The most important gravity anomalies are the free-air anomaly, the Bouguer anomaly, and the isostatic anomaly. The remainder of this section will give the simple formulas of those gravity anomalies without derivations (P. Vanicek, 1975).

2.5.1 The free-air gravity anomalies

The free-air reduction is based on a simple assumption: there are no masses above the ellipsoid, so the observation station is imagined to be hanging free in the air.

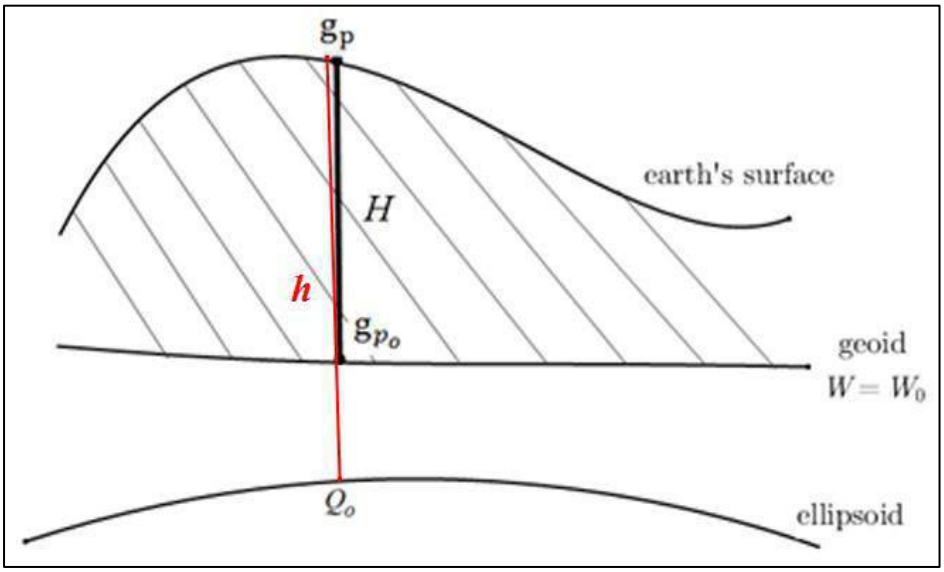

Figure 11 Free-air reduction (Wellenhof and Moritz, 2005).

We need the vertical gradient of gravity for a theoretically correct reduction of gravity to the geoid. $g_{P_\circ}$ refer to the gravity value on the geoid, according to Taylor expansion (Wellenhof and Moritz, 2005), is equal to:

$$g_{P_\circ} = g_P - \frac{\partial g}{\partial H} H \qquad (2.42)$$

where H is the orthometric height and $\frac{\partial g}{\partial H} H$ is the vertical gradient.

Suppose there are no masses above the geoid, we have:

$$g_{P_\circ} = g_P + F \qquad (2.43)$$

where $F = -\frac{\partial g}{\partial H} H$ is the free-air reduction.

For practical purposes, it is sufficient to use normal gradient of gravity $\frac{\partial \gamma}{\partial h}$ instead of $\frac{\partial g}{\partial H}$ (Heiskanen and Moritz, 1967):

$$F = -\frac{\partial g}{\partial H} H = -\frac{\partial \gamma}{\partial h} h = -0.3086h \text{ (mGal)}, \quad h \text{ in meters.} \qquad (2.44)$$

Then, from (Fig. 11), the free-air gravity anomalies (Δg_F) are given by the following formula (Heiskanen and Moritz, 1967):

$$\Delta g_F = g_{P_\circ} - \gamma_{Q_o} \qquad (2.45)$$

where point (Qo) is on the ellipsoid. Theoretical normal gravity (γ_{Q_o}), the magnitude of the gradient of the normal potential function *U*, is given at the surface of the ellipsoid by the closed formula of Somigliana given by (Torge, 2001):

$$\gamma_{Q_o} = \gamma_e \frac{1+k\sin^2\varphi}{(1-e^2\sin^2\varphi)^{1/2}} \quad \text{with} \quad k = \frac{b\gamma_p}{a\gamma_e} \tag{2.46}$$

Where

a, b semi-major and semi-minor axes of the ellipsoid, respectively,

γ_p, γ_e theoretical normal gravity at the poles and equator, respectively,

e^2 square of the first ellipsoidal eccentricity,

φ geodetic latitude.

In this study, we used the World Geodetic System 1984 (WGS-84), , as shown in Table 2.

Table 2 WGS 84 Ellipsoid Derived Geometric and Physical Constants
https://www.icao.int/NACC/Documents/Meetings/2014/ECARAIM/REF08-Doc9674.pdf

Parameters	Notation	Value	Unit
Semi-major axis	a	6378137.0	m
Semi-minor Axis	b	6356752.3142	m
First Eccentricity Squared	e^2	0.00669437999014	unitless
Normal gravity at the equator	γ_e	9.7803253359	m S^{-2}
Normal gravity at the Poles	γ_p	9.8321849378	M S^{-2}
Formula Constant K	K	0.00193185265241	unitless

2.5.2 The simple and complete Bouguer reduction

The Bouguer reduction removes all the topographic masses above the geoid contained in the Bouguer plate, which can be expressed in an analogous way as the topographic vertical attraction using the following integral equations (Wellenhof and Moritz, 2005):

$$BC = G\int_x\int_y\int_0^{H_p} \frac{\rho\,(H_p-H)(H_p-z)}{\left((x_p-x)^2+(y_p-y)^2+(H_p-z)^2\right)^{3/2}}\; d_x d_y d_z\,. \tag{2.47}$$

In Bouguer reduction (Fig. 12), the area around the gravity station is assumed as completely flat, and so-called Bouguer plate approximates the topography masses with radius $r \to \infty$, which is represented by a horizontal cylinder of thickness equal to H_P and constant density ρ (ρ = 2670 kg m^{-3}). Hence, the simple (or incomplete) Bouguer reduction BC
is computed as (Heiskanen and Moritz, 1967):

$$BC = 2\pi G\rho H \sim 0.1119 H_p\ [\text{mGal}]\,. \tag{2.48}$$

and the simple Bouguer gravity anomaly reads

$$\Delta g_B = g - \gamma - BC. \tag{2.49}$$

Furthermore, the terrain effect refines the Bouguer plate attraction concerning the deviation of actual topography from the Bouguer plate. In this case, the corresponding gravity anomaly is called the refined (or complete) Bouguer anomaly. The classical terrain correction C at the computation point $P(x_P, y_P, H_p)$ is given by an integral over the irregularities of the topographic mass relative to a Bouguer plate, i.e. Δm^+ and Δm^-,
(I. N. Tziavos and Sideris, 2013) as:

$$C = G \int_x \int_y \int_H^{H_p} \frac{\rho\,(H_p - H)(H_p - z)}{\left((x_p - x)^2 + (y_p - y)^2 + (H_p - z)^2\right)^{3/2}}\; d_x d_y d_z. \tag{2.50}$$

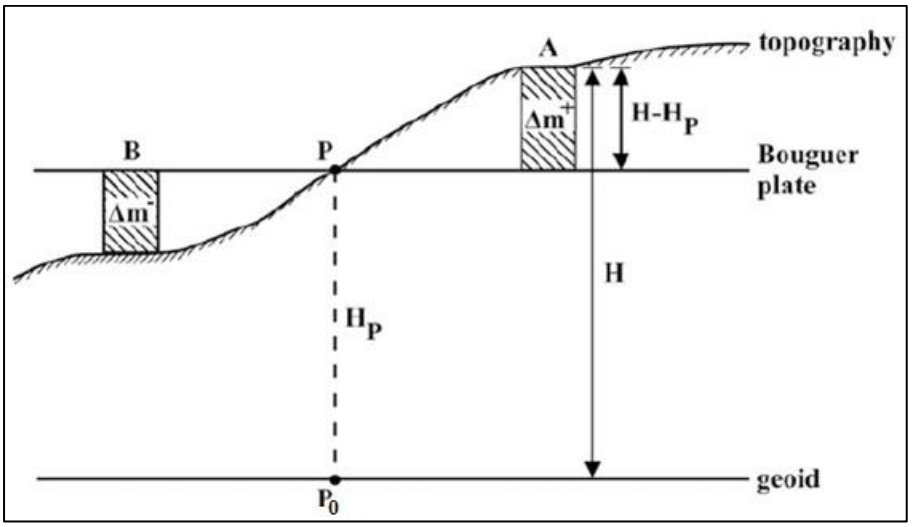

Figure 12 The geometry of the planar Bouguer reduction and the terrain correction (I. N. Tziavos and Sideris, 2013).

2.5.3 Isostatic Reduction

In the general concept of isostasy, the topographic mass excesses (*mountains*) and deficiencies (*waters*) are compensated by a corresponding mass distribution in the interior of the Earth (Torge, 2001).There are two main theories about the isostatic compensation applications, one following the Airy-Heiskanen model and another following the Pratt-Hayford model.

2.5.3.1 Airy-Heiskanen Isostatic Model

According to this model, the mountains are floating on some kind of higher density fluid, meaning that there is a mass deficit (*roots*) below the mountains and mass surpluses (*anti-roots*) below the oceans (Sansò and Sideris 2013). The Airy-Heiskanen model (Fig. 13) is based on the assumptions that the isostatic compensation is complete and local, the density of the mountains is constant and equal to $(\rho_\circ = 2.67 \mathrm{gcm}^{-3})$. The density of Earth's mantle is equal to $(\rho_M = 3.27 \mathrm{gcm}^{-3})$ and the normal crust thickness $T_\circ$ is equal to 30 km (Wellenhof and Moritz, 2005), assuming a constant density of $(\rho_W = 1.027 \mathrm{gcm}^{-3})$ for the ocean water. The condition of floating equilibrium can be written as (Sansò and Sideris 2013) for the continental cases:

$$(\rho_M - \rho_\circ)\, d = \rho_\circ H \tag{2.51}$$

and for the oceanic areas

$$(\rho_M - \rho_\circ) d' = (\rho_\circ - \rho_W) H' \tag{2.52}$$

where ,
d n thickness of the *root*,
d' thickness of the anti-root,
H height of the topography and
H' height of the ocean, i.e., the depth.

Given the density values for the crust, the mantle, and ocean water mentioned above, Eq. (2.51) and Eq. (2.52) can be written as (Wellenhof and Moritz, 2005)

$$d = 4.45H \qquad d' = 2{,}73H'. \qquad (2.53)$$

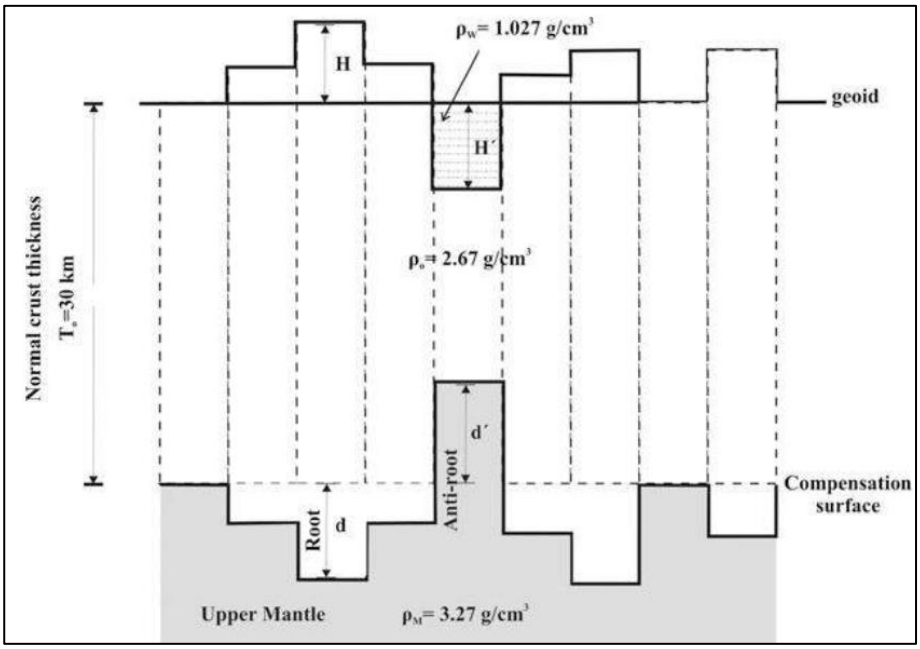

Figure 13 Airy-Heiskanen Isostatic Compensation Model (Sansò and Sideris 2013).

2.5.3.2 Pratt-Hayford Isostatic Model

This compensation system was outlined by *Pratt* and put into a mathematical form by *Hayford*. The principle is illustrated in (Fig. 14).

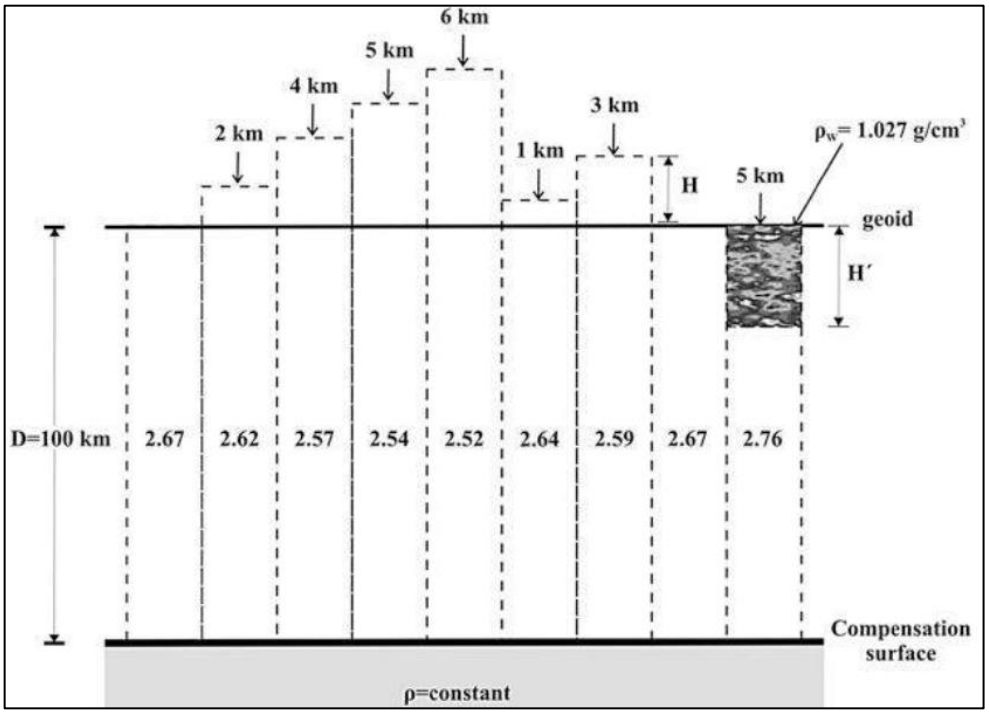

Figure 14 Pratt-Hayford Isostatic Compensation Model (Sansò and Sideris 2013).

According to (Wellenhof and Moritz, 2005) and, the Pratt-Hayford isostatic reduction considers that the level of compensation has a constant and uniform depth D assumed equal to 100 km measured from sea level (Fig. 14). The topographic masses are delineated into columns of the cross-section with height H that allowing changes in density to obtain isostatic equilibrium. Considering that a normal column (H = 0) has constant density $\rho_\circ$, the continental columns generate densities smaller than $\rho_\circ$ while the oceanic columns are denser. The equilibrium conditions for the continental column of height D+H (H representing the height of the topography) with density ρ_{cont} satisfies the equation (Sansò and Sideris 2013):

$$(\mathrm{D}+\mathrm{H})\rho_{\mathrm{cont}} = \mathrm{D}\rho_\circ \tag{2.54}$$

$$\Delta\rho_{\mathrm{cont}} = \rho_\circ - \rho_{\mathrm{cont}} = \rho_\circ \frac{\mathrm{D}}{\mathrm{D}+\mathrm{H}}\,. \tag{2.55}$$

In the ocean area with density ρ_{ocean}, the density is increased. It is given by

$$(\mathrm{D}-\mathrm{H}')\rho_{\mathrm{ocean}} + \mathrm{H}'\rho_W = \mathrm{D}\rho_\circ \tag{2.56}$$

$$\Delta\rho_{\mathrm{ocean}} = \rho_{\mathrm{ocean}} - \rho_\circ = (\rho_\circ - \rho_{\mathrm{W}})\frac{\mathrm{H}'}{\mathrm{D}-\mathrm{H}'} \tag{2.57}$$

The *topographic isostatic reduction* is the difference in the attraction between the topographic masses $\mathrm{A_T}$ and the compensated masses $\mathrm{A_C}$ (Wellenhof and Moritz, 2005):

Finally, the topographic-isostatically reduced gravity on the geoid becomes:

$$\Delta g_{\mathrm{TI}} = \Delta g_{\mathrm{F}} - \mathrm{A_T} + \mathrm{A_C}\quad . \tag{2.58}$$

Where,

A_T equals the attraction of Bouguer plate combined with terrain correction $A_T = A_B - A_{TC}$

A_C is the attraction of the compensation masses given by Airy-Heiskanen and Pratt-Hayford isostatic model.

2.6 The residual terrain modelling (RTM) reduction

In the Residual Terrain Modelling (RTM) reduction, as shown in (Fig. 15), two topography surfaces, the detailed surface and the reference surface, are used. The detailed surface represents the actual topography obtained from a high-resolution digital elevation model (DEM). The reference surface may be any smooth surface representing mean elevations of the area, usually obtained by applying a suitable low-pass filter to the detailed surface. The topography potential induced by the residual between these two surfaces is considered within the reduction process. The topography effect on gravity in the RTM reduction dg_{RTM} is approximated as (Forsberg, 1984):

$$dg_{RTM} = 2\pi G\rho(H - H_{ref}) - C \tag{2.59}$$

where C is the classical terrain correction given by Eq. (2.50), H presents the topographic height of the gravity point an H_{ref} is the height of the mean elevation surface.

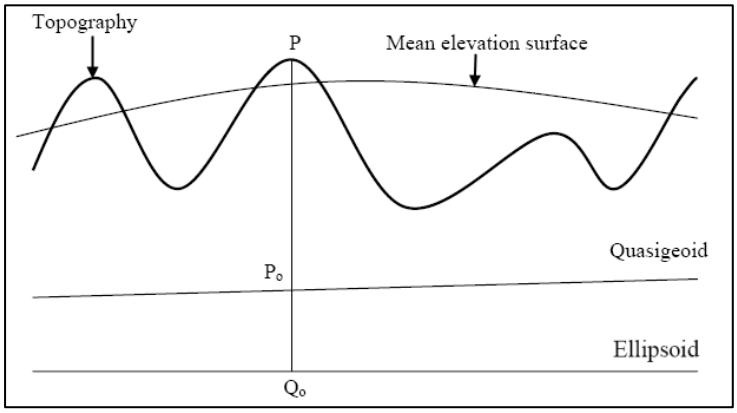

Figure 15 The residual terrain model (RTM) method (Forsberg, 1984).

The RTM anomaly $\Delta g_{RTM}$is given by (Forsberg, 1984):

$$\Delta g_{RTM} = g - dg_{RTM} - F - \gamma \tag{2.60}$$

where F is obtained from (eq. 2.60
The RTM effects on the geoid are expressed in planar approximation as:

$$\zeta_{RTM} = \frac{G\rho}{\gamma} \iint_{-\infty}^{\infty} \int_{H_{ref}}^{H} \frac{1}{r}\, d_x d_y d_H = \frac{G\rho(H - H_{ref})}{\gamma} \iint_{-\infty}^{\infty} \frac{1}{r_\circ} d_x d_y d_H$$
$$\approx \frac{G\rho(H - H_{ref})}{\gamma} . \frac{1}{r_\circ} \tag{2.61}$$

where r_0 is the planar distance.

2.7 Common Approaches for Representing the Outer Gravity Field

There is a wide range of geodetic methods which are used or have been proposed for the representation of the gravity field. These methods may be generally regarded as belonging to one of the two approaches of physical geodesy, namely, the model approach and the operational approach. In the first approach, a mathematical model is set up and determines the required quantity from a given set of data. The problem is then to obtain the data. On the other hand, the operational approach starts with the available data and asks how these data can be combined in the best way to obtain the required quantity. In a certain sense, the two approaches are complementary (C. C. Tscherning, 1981).

2.7.1 The Model Approach

The known relationships between the anomalous potential T and the different types of gravity field observables are used in the model approach. Presupposing the harmonicity of T in outer space and its regularity at infinity, an estimate of T (or any of its functions) will be the solution of different geodetic boundary value problems. The solutions manifest themselves as integral formulas; examples are Stokes, Vening Meinesz, and Hotine formulas. The data necessary for such numerical evaluations must be available in a regular grid around the computational point. The grid values are generally determined from irregularly spaced data by reliable interpolation techniques (Amin 1983, El-Sagheer 1995). In what follows, a review of the relevant methods is outlined.

2.7.1.1 Astrogeodetic Leveling

The technique of astrogeodetic geoid determination also belongs to the model approach (C. C. Tscherning, 1981). The model is very simple, and harmonicity or regularity of the disturbing potential is not required. The anomalous potential restricted to the reference ellipsoid is regarded as a function of the latitude and longitude only. The vertical deflections are then associated simply with the geoidal height through the horizontal derivatives. Then, the geoidal height is determined through numerical integration. However, this model requires that the vertical deflections are somehow reduced to the geoid. The method has the drawback that the two-dimensional numerical integration may break down if only one component of the vertical deviation is available. Only geoid profiles can be determined in this situation, or the one-component stations are left out.

2.7.1.2 Geodetic Boundary Value Problems (GBVPs)

GBVPs represent the well-established scientific basis of the analysis of terrestrial geodetic measurements for modeling the Earth's gravity field as well as the geoid or quasi-geoid (Lehmann, 1999). They can be defined mathematically as finding the disturbing potential T, so that

$$\begin{aligned} &T = T(S) \\ &B(T) = F, \end{aligned} \tag{2.62}$$

where the boundary surface S is the topographic surface, outside which the mass density is zero and on which the input data F is given, and B, which corresponds to F, is a zero or first-order derivative operator or a combination of them. After a relevant reduction of the anomalous potential, S can be the telluroid, the geoid, the reference ellipsoid or the mean terrestrial sphere, centered at the center with radius R. Hence, according to the type of input data, there exist various kinds of geodetic boundary value problems (GBVPs).

In the third GBVP, the input data are the orthometric height H or the normal height H^* and the gravity g on the topographic surface. Such data can be obtained via leveling and gravimetry. The output is the geoidal height, quasi-geoid (the ellipsoidal height h and topographic surface), and the external gravity potential. Hence, if F in (Eq. 2.62) is the gravity anomaly data Δg on the topographic surface $S_{top.}$ and B is a combination of the first and zero-order derivative operators, thus, the mathematical expression of the third GBVP is

$$T = T(S_{top.})$$
$$\frac{1}{\gamma}\frac{\partial \gamma}{\partial h} T - \frac{\partial T}{\partial h} = \Delta g \qquad \text{on the topographic surface,} \qquad (2.63)$$

where the derivatives are taken along the normal plumb line. The above expressions are called the Molodensky's problem (Heiskanen and Moritz, 1967). After transforming the disturbing potential, it reduces to the ordinary Stokes' problem, in which the boundary surface S is the geoid.

Regarding the second GBVP, the input data are the topographic surface of the Earth (the geodetic height h) and the gravity g on it, which GPS and gravity observations can obtain. The outputs are the geoid undulation or the quasi-geoid (hence the orthometric height H or the normal height H^*) and the external gravity potential. Thus, if F in (Eq. 2.62) is the gravity disturbance data δg on the topographic surface and B is the first-order derivative operator, the associated mathematical expression is given as

$$T = T(S_{top.})$$
$$T/\partial h = -\delta g \qquad \text{on the topographic surface.} \qquad (2.64)$$

The second GBVP is called the Hotine problem if the boundary surface is the geoid. The first GBVP, also regarded as the Dirichlet's problem, has the disturbing potential T0 and the topographic surface as input. The output is the value of gravity on the Earth's physical surface. Thus, F in (Eq. 2.62) is the disturbing potential data (expressed by the geoidal height or quasi-geoid) on the topographic surface, obtained by leveling and GPS observations on land or via satellite altimetry over the ocean. These (space) methods of geoid determination are called the "geometric" methods. The relevant mathematical expression reduces to

$$T = T(S_{top.})$$
$$T = T_0. \qquad \text{on the topographic surface.} \qquad (2.65)$$

From the solution of the above problem gravity anomaly and gravity disturbance can be computed by Eqs. (2.26) and (2.27), respectively. The determination of the gravity anomaly or gravity disturbance on the geoid, based on the geoidal height data, is referred to as the inverse Stokes or inverse Hotine problem.

The geodetic data situation on land and sea differs according to the kinds of data, the data accuracy, and coverage. When formulating GBVPs, the differences should be taken into account, arriving at what is called the altimetry-gravimetry problems (AGP). Problems of this kind are usually formulated as mixed GBVP. The relevant B operator will be a composite operator that depends on the data type and its location, whether on land or sea. More about the mixed GBVP can be found in (Lehmann, 1999) and (Lehmann, 2000).

2.7.1.3 Integral Formulas

There are two fundamentally different approaches to solving geodetic boundary value problems. The first (and most common) approach is the analytical solution, which aims at a

reformulation of the situation in such a way that they become analytically solvable, e.g., by integral formulas (or numerical integrations), in which the disturbing potential (or its functions) is generally expressed directly as an analytic function of the observed gravity, as will be seen below. The second approach is the numerical solution using finite differences, finite elements, boundary elements, wavelets, and other methods (Lehmann and Klees, 1999).

From the definitions of the GBVPs, it is clear that these problems are non-linear with respect to the geopotential since the relevant observable elements are non-linear functions of the generating potential. This ambiguity is solved by using the mean gravity GM/R^2, denoted as a spherical approximation in gravity space (Moritz, 1980). The corresponding approximation in the geometry space is that the geoid is assumed to form the mean terrestrial sphere, with mean radius R, and that it encloses all masses (Heiskanen and Moritz 1967, Martinec 1998)**.**

In spherical approximation, assuming that the reference ellipsoid is an absolute one, the geoidal height can be computed from the well-known Stokes' formula as follows

$$N = (R / 4\pi\gamma) \iint_\sigma S(\psi)\, \Delta g\, d\sigma, \tag{2.66}$$

where R is the earths radius and γ is the relevant normal gravity on the level ellipsoid, Δg the gravity anomaly at the running point, ψ the spherical distance between the computation point and the integration point, $d\sigma$ the element of the unit sphere σ at the running point and $S(\psi)$ is the Stokes' function (or kernel), which is given by

$$S(\psi) = \operatorname{cosec}(t) - 6\sin(t) + 1 - 5\cos(2t) - 3\cos(2t)\ln[\sin(t) + \sin^2(t)], \tag{2.67}$$

with $t = \psi/2$. The above integration is taken over the unit sphere, and the gravity anomalies refer to the geoid. Similarly, the relevant deflection of the vertical components, ξ and η, are given by the Vening-Meinesz integral formula (I. N. Tziavos and Andritsanos, 1997)**,**

$$\begin{Bmatrix} \xi \\ \eta \end{Bmatrix} = \left(\frac{1}{4\pi\gamma}\right) \iint_\sigma \Delta g\ V(\psi) \begin{Bmatrix} \cos\alpha \\ \sin\alpha \end{Bmatrix} d\sigma\,, \tag{2.68}$$

where α is the azimuth (at the computational point) of the geodesic line between the computation point and the running point and $V(\psi)$ is the Vening-Meinesz function, which is given by

$$V(\psi) = (1- s^2)^{0.5} \{-1/2s^2 + 16s - 6 + 3(s-1)/(2s(1-s^2)) + 6s \ln(s + s^2)\}, \tag{2.69}$$

with $s = \sin(\psi/2)$. Stock's and Vening-Meinesz problems are two complementary issues that solve the third GBVP on the geoid. The Hotine formula represents a solution for the second GBVP (or Neumann's GBVP). Particularly, it computes the geoidal height in terms of gravity disturbances (Zhang, 1998)

$$N = (R / 4\pi\gamma) \iint_\sigma H(\psi)\, \delta g\, d\sigma, \tag{2.70}$$

where $H(\psi)$ is the Hotine kernel, which is given as

$$H(\psi) = 1/\sin(t) - \ln(1 + 1/\sin(t)), \tag{2.71}$$

again with $t = \psi/2$.

A new integral formula, derived by (Hwang 1998), is the deflection-geoid formula, which solves the geoid undulation in terms of the deflections of the vertical, as follows

$$N == \frac{R}{4\pi}\iint_{\sigma}\frac{dC(\Psi)}{d\Psi}\,\Theta_{\alpha}\,d\sigma, \tag{2.72}$$

where Θ_α is the component of deflection of the vertical in the direction (of azimuth α) connecting the computation point and the integration point, and $C(\psi)$ is the associated kernel that is given by

$$C(\psi) = -2\log\sin(t) - 1.5\cos(2t) - 1, \tag{2.73}$$

and

$$dC(\psi)/d\psi = -\cot(t) + 1.5\sin(2t). \tag{2.74}$$

The above-stated integral formulas have the common drawback of demanding a homogeneous data type and distribution, as shown below. It should be mentioned that the Stokes, Vening Meinesz, and Hotine formulas have well-developed inverse versions, which have reversed input and output items. More about such inverse formulations can be found in (Hwang, 1998) and (Wang, 1999).

2.7.1.4 Space Domain and Spectral Domain Evaluation of Integral Formulas

Theoretically, the integral formulas for the various problems presuppose that the entire boundary surface should be continuously covered with observed gravity field quantities. This fictitious data coverage is impossible, and the integration is practically carried out over a limited spherical cap of an appropriate radius ψ_0 around each computational point. Taking Stokes' formula as an example, the integral in (Eq. 2.66) will be given as

$$N = \left(\frac{R}{4\pi\gamma}\right)\int_0^{2\pi}\int_0^{\pi} S(\psi)\Delta g\sin\psi\;d\psi\,d\alpha =$$

$$= \left(\frac{R}{4\pi\gamma}\right)\int_0^{2\pi}\int_0^{\psi 0} S(\psi)\Delta g\sin\psi\;d\psi\,d\alpha + \int_0^{2\pi}\int_{\psi 0}^{\pi} S(\psi)\Delta g\sin\psi\;d\psi\,d\alpha. \tag{2.75}$$

The first term in Eq.(2.75) is regarded as the inner (or near zone) contribution to the geoidal height. This near-zone term corresponds to the gravitational observations in the limited integration cap. The second term is the far (or remote) zone contribution, induced by the gravity field data outside the integration cap and is in principle extended to cover the rest of the Earth.

In modern geoid determination approaches, the geoidal height is spectrally decomposed into three components, according to the relevant wavelengths or spatial frequency, via the so-called remove-restore technique. Particularly, the far zone (long-to-medium wavelength) contribution is supposed to be provided by an adequate high-resolution global geopotential harmonic model. The local (or regional) gravity data provides the medium-to-short wavelength component. Finally, the short and very short detailed features are accounted for through the effect of the local topographic features (Featherstone et al. 1996; Higgins et al. 1996). Accordingly, the second term in the above integral is provided by the geoid (N_{GGM}) computed from a suitable harmonic global geopotential model, as will be discussed later. On the other hand, the detailed high-frequency features (N_h) are generally implied by a high-resolution digital elevation model for the area under study, whereas the intermediate component is modeled via the integral formula as follows

$$N = N_{GGM} + N_{Integral} + N_h$$

$$= N_{GPM} + \left(\frac{R}{4\pi\gamma}\right)\int_0^{2\pi}\int_0^{\psi 0} S(\psi)\Delta g^{r}\sin\psi\;d\psi\,d\alpha + N_h \tag{2.76}$$

were Δg^r are the residual gravity anomalies (after being reduced for the reference geopotential model and the topographic effect). In other words, the gravity anomalies resulting from the removal procedure,

$$\Delta g^r = \Delta g_{obs} - \Delta g_{GGM} - \Delta g_h. \quad (2.77)$$

The above integral is the modified (or spheroidal) Stokes' formula (Featherstone and Olliver, 1993; Vaníček and Featherstone, 1998). Due to the discontinuous coverage of the gravitational observations even within the integration cap, the integral in Eq.(2.76) is replaced by discrete summations as follows (Kirby et al. 1997)

$$N_{integral} = \frac{R}{\gamma} \sum_0^{\psi 0} \overline{\Delta g^r}\,(\psi)\;\; F(\psi)\, \delta\psi, \quad (2.78)$$

where $F(\psi) = \frac{1}{2} S(\psi) \sin \psi$. The $\Delta g^r(\psi)$ are the mean residual gravity anomalies, averaged over the annulus bounded by ψ and $(\psi+\delta\psi)$, as follows

$$\Delta g^r(\psi) = \left(\frac{1}{2\pi}\right) \sum_0^{2\pi} \Delta g^r\, \delta\alpha, \quad (2.79)$$

$\delta\alpha$ and $\delta\psi$ being appropriately chosen discrete intervals of azimuth and spherical distance, respectively. It should be emphasized that efficient computer software exists for manipulating the above ring-integration procedure**.** (Higgins et al., 1997; Kearsley et al., 1998)

It is well known that the discrete summation can be more efficiently carried out over a rectangular grid (with equal spacing $\Delta\varphi$ and $\Delta\lambda$) around the computation point, with the mean residual data predicted at the grid nodes. In this case, the discrete summations in (Eqs. 2.78 and 2.79) will be given as:

$$N_{\text{integral}} = \frac{R}{4\pi\gamma} \sum_\varphi \sum_\lambda \overline{\Delta g^r} S(\psi)\, \cos\varphi\, \Delta\varphi\Delta\lambda. \quad (2.80)$$

The above space domain numerical integral procedures and the remove-restore technique are applicable for all the integral formulas, considering the appropriate modifications according to the handled items. It should be mentioned that the singularity of the kernels at the computation points should be taken into account. In addition, the kernel functions should be weighted in such a way to account for their rapid change in the vicinity of the computation point (Featherstone and Olliver, 1994)**.** Furthermore, some trends exist according to which the integration kernels are modified to be compatible with the size of the integration cap or equivalently with the resolution of the reference geopotential field. More about the modification methods can be found in (Featherstone et al. 1998; Featherstone and Sideris 1998; Nsombo 1998)**.**

If the numerical integration, e.g., Eq. (2.55), is computationally tedious (e.g., by large data organizations), then the Fast Fourier Transform (FFT) technique would be an efficient alternative. The FFT methods are referred to as the spectral domain methods, as both the gravitational data and the relevant kernels are transformed from the space domain into the spectral (or frequency) domain (Dahl and Forsberg 1998; Tsuei et al. 1994; Tziavos and Andritsanos 1997).

The FFT technique is applicable to all numerical integration algorithms encountered in physical geodesy, including topographic reductions. FFT methods include the spherical 1D-FFT, the planar 2D-FFT, the spherical 2D-FFT, and the spherical multi-band FFT method. Regarding Stokes formula, for a given parallel of latitude φ_p, the application of the spherical 1D-FFT gives

$$N_{\varphi_p}(\lambda) = \left(\frac{R\Delta\varphi\Delta\lambda}{4\pi\gamma}\right) \frac{1}{F_1} \left\{ \sum_{\varphi p} F_1\left(\Delta g_q \cos\varphi q\right) F_1\left[S_\varphi\left(\lambda_p - \lambda_q\right)\right] \right\}. \quad (2.81)$$

.

where F_1 and F_1^{-1} stand for the discrete 1D Fourier transform and its inverse, respectively. Eq. (2.81) can be repeated for all parallels of latitudes for the area of interest. It should be mentioned that the results obtained by this 1D-FFT are precisely the same as those obtained by direct numerical integration on the sphere. On the other hand, the spherical multi-band FFT is a generalization of the spherical 2D-FFT, and both methods are approximations of the numerical integration. Details about the FFT methods can be found in (Dahl and Forsberg, 1998; Tsuei et al., 1994; I. N. Tziavos and Andritsanos, 1997). Finally, the FFT technique evaluates geodetic integrals over rectangular grids only.

2.7.1.5 Downward Continuation

In the standard Stokes formulation of the geodetic boundary value problem, the solution, T, is sought above the boundary, the geoid, while the observed gravity values are available on the surface of the Earth. The observations thus have to be reduced from the Earth's surface onto the geoid to obtain the boundary values, and this reduction is referred to as the downward continuation. The downward continuation may be applied to the observed gravity anomaly values, gravity disturbances, the disturbing potential T, or combinations of these quantities. Once one knows how to continue T downward, the downward continuation of the other quantities can be derived (p Vanicek et al., 1986)**.**

Mountainous topography affects gravity field modeling, in two possibilities, a strong gravity signal is due to the gravitational attraction of the topographic mass itself or the second possibility implies that the terrain corrections are applied to regularize the problem. (Forsberg and Tscherning, 1997)**.**

One of the impacts of local terrain reductions is to remove the correlation of free air anomalies with height (Forsberg and Tscherning, 1997)**.** There are different methods of terrain reduction for gravitational quantities. In all forms, the topographic masses between the terrain and the geoid are computationally removed at the considered point so that the Earth's mass and the geocenter are unchanged (Heiskanen and Moritz, 1967). The removal of masses is followed by the downward continuation of the observed elements as if in free air, using the relevant vertical gradient. This downward continuation is thus theoretically valid since the harmonicity of the continuation zone is formally guaranteed.

The reduction methods are different according to how the removed topographic masses are dealt with. In Helmert's second condensation method, the removed masses are computationally condensed as a single layer on the geoid, the effect of which is added to the reduced observations. During the masses' restoration, that layer's effect is subtracted (Veronneau, 1996). As an approximation of the Helmert's reduced anomalies, the Faye anomalies are usually used, in which the effect of local terrain irregularities concerning a Bouguer plate at the considered point (classical terrain correction, TC) is added to the free air anomalies (Veronneau, 1996; Wang, 1993)**.** In the complete (Bouguer) topographic reduction, the removed masses are assumed to be shifted inside the geoid. This reduction amounts to removing a Bouguer plate and then accounts for the classical TC effect relative to that plate. Ideally, such reduction should be accompanied by a relevant model of isostasy. In such a case, the masses are removed along with their isostatic compensation, and subsequently, the same features are restored.

2.7.1.6 Ellipsoidal Corrections

Stokes' formula for the gravimetric determination of the geoid requires, besides other assumptions, that the input gravity anomalies are referred to as a sphere in geometry and gravity space. According to Heiskanen and Moritz (1967), the relative error introduced by that approximation

is of the order of 3×10^{-3}. Such an error level is not acceptable at a time when the "1 cm geoid", or even a few centimeter geoid, is the target. Hence, developing the theory of geoidal height determination as precisely as possible is a step towards obtaining the geoid with a relative accuracy, which would be compatible with the achievable relative accuracy of ellipsoidal heights via the GPS technique (Martinec and Grafarend, 1997).

Some partially enhanced computational trends have appeared in the geodetic literature. The mean radius in the "spherical" Stokes' formula is replaced by the rigorous ellipsoidal geocentric radius, r, of the foot point on the reference ellipsoid. However, Martinec and Grafarend (1997) have proceeded much more precisely. They have solved the Stokes' boundary value problem for gravity anomalies distributed on an ellipsoid of revolution in the geometry and gravity space. The ellipsoidal approximation of the geoid reflects a reality, which is much better than the spherical approximation since the actual shape of the geoid deviates from an ellipsoid of revolution by about 100 m at the most.

The formulation of the ellipsoidal Stokes' formula encounters the treatment of the GBVP in ellipsoidal coordinates and the usage of the complex Legendre functions of the 2^{nd} type (Martinec and Grafarend, 1997). In this formulation, the "spherical" Stokes' function had a correction in terms of the ellipsoidal Stokes' function, which described the ellipticity of the boundary, up to the order of the square of the first eccentricity of the reference ellipsoid (i.e. (e^2)). Hence, treating the geoid concerning an ellipsoid of revolution in an appropriate normal gravity field, particularly as a boundary condition prescribed on the approximate geoid surface (the reference ellipsoid of revolution), may cause relative errors in the order of 1.5×10^{-5}. The absolute error, relevant to that "ellipsoidal approximation", in the geoidal heights computed from the ellipsoidal Stokes' integral does not exceed 2 mm and 0.2 mGal in the gravity (anomaly) space (Martinec, 1998). A preliminary numerical application of the ellipsoidal integral showed that the near-zone ellipsoidal correction term, concerning the spherical integral, is as high as 10 cm. Accordingly, the ellipsoidal Stokes' integral seems unavoidable (Ardestani and Martinec, 2000).

2.7.2 The Operational Approach

Generally speaking, the methods of the operational approach are more capable than those of the model approach. Notably, the input data types can freely be heterogeneous and should not necessarily be observed on the surface of the terrain (or sea). For example, the data could be heterogeneous, non-homogeneous, and observed at airborne or satellite altitudes. Moreover, the output of the operational techniques has the same general optional scheme of the input data, i.e., predictions of any type could be estimated everywhere. A typical characteristic of the relevant methodologies is that they require estimating intermediate (auxiliary) parameters from the input data via the solution of a system of normal equations (or an integral equation). In general, such methods follow a space domain fashion. In what follows, a review is outlined for the common techniques belonging to the operational approach.

2.7.2.1 Spherical Harmonic Synthesis

Spherical harmonic synthesis amounts to expanding the various gravimetric quantities in spherical harmonic series. The relevant "intermediate" parameters are the unitless spherical harmonics of global geopotential in spherical harmonic representations. The most straightforward spherical harmonic formulation is generally given as

$$f(\psi', \lambda) = \sum_{n=0}^{\infty} \sum_{m=0}^{n} (\bar{C}_{nm} \cos m\lambda + \bar{S}_{nm} \sin m\lambda) \bar{P}_{nm}(\sin\psi'), \quad (2.82)$$

where

ψ' the geocentric latitude,

λ the geodetic longitude,

$\bar{C}_{nm}$ the fully normalized spherical harmonic C - coefficients of degree n and order m,

$\bar{S}_{nm}$ the fully normalized spherical harmonic S-coefficients of degree n and order m,

$\bar{P}_{nm}(\sin\psi')$ the fully normalized associated Legendre function of degree n and order m.

According to the above equation, the "synthesized" function $f(\psi', \lambda)$ can be computed at any point on the unit sphere. Belonging to the operational approach (C. C. Tscherning, 1981), the spherical harmonic synthesis can predict any kind of gravitational field functions, provided the global geopotential coefficients are previously known via the functional relationships among the various gravimetric quantities. In that sense, spherical harmonic synthesis could be a tool for transforming the gravimetric elements from the Fourier frequency domain into the space domain. The harmonic coefficients themselves can be estimated from any type of (heterogeneous) data via spherical harmonic analysis.

2.7.2.2 Runge-Krarup's Theorem

Runge-Krarup's theorem is the theoretical basis for the operational approach, or equivalently, for the discrete boundary value problem. There is a very close connection between the problem of the Bjerhammar sphere and the convergence of spherical harmonics, or better, the question of approximation of the geopotential by spherical harmonic series (Bjerhammar, 1973; Moritz, 1980). Runge-Krarup's theorem states that: "Any harmonic function T, regular outside the Earth's surface, may be uniformly approximated by harmonic functions T* regular outside an arbitrarily given sphere inside the Earth, in the sense that for any given $\varepsilon > 0$, the relation

$$|T - T^*| < \varepsilon \quad (2.83)$$

holds everywhere outside and on any closed surface surrounding the Earth's surface". This sphere, enclosed inside the Earth (Fig. 2.16), is referred to as the Bjerhammar sphere. The number ε may be arbitrarily small, and the surrounding surface may be arbitrarily close to the Earth's surface.

Moreover, if the Earth's surface is sufficiently regular (e.g., continuously differentiable), this outer surface may even be taken to coincide with the Earth's surface. In this case, one gets the Keldysh-Lavrentiev theorem (Moritz, 1980): "Any function T, harmonic outside the Earth's surface and continuous outside and on it, may be uniformly approximated by harmonic functions T* regular outside an arbitrarily given sphere inside the Earth, in the sense that for any given $\varepsilon > 0$, the relation.

$$|T - T^*| < \varepsilon$$

holds everywhere outside and on the Earth's surface".

Since ε can be chosen arbitrarily, one may consider a sequence

$\varepsilon_1 > \varepsilon_2 > \varepsilon_3 \ldots\ldots\ldots \rightarrow 0.$

and find a function T^*_k for each ε_k. In this way, one obtains a sequence of harmonic functions T^*_1, T^*_2, T^*_3 … regular in the whole space outside the given Bjerhammar sphere, that converges uniformly to the given function T on and outside the Earth's surface.

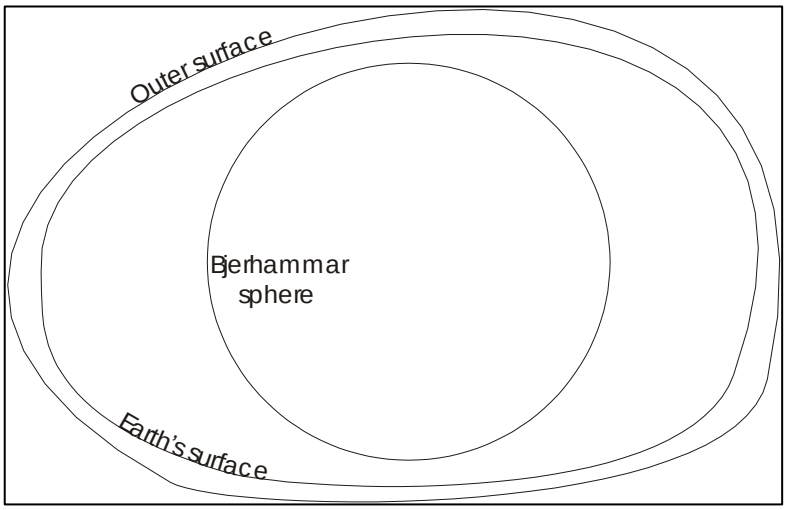

Figure 16 Bjerhammar sphere (Bjerhammar 1973).

From the above, it is obvious that the disturbing potential T, which is harmonic and regular outside the Earth's surface, can be very well approximated outside the Earth's surface by another potential T^*, which is harmonic and regular outside the Bjerhammar sphere. The sphere's radius, R_b, is theoretically supposed to be less than or equal to the semi-minor axis of the mean Earth ellipsoid. The appropriate requirement is that any point on the Earth's surface lies in the exterior of that (geocentric) sphere (Bjerhammar, 1973). According to Runge and Keldysh theorems, the anomalous potential, T, on or outside the surface of the Earth can be analytically continued downward onto the geoid or onto the Bjerhammar sphere, which is referred to as the harmonic downward continuation. Of course, if the observed gravitational elements are previously reduced to the geoid, such theorems are still valid in the sense of the classical GBVPs. This is guaranteed since, in such a case, the disturbing potential T will be harmonic and regular outside the geoid; hence, T^* will approximate T very well on and outside the geoid (Moritz, 1980).

2.7.2.3 Discrete Boundary Value Problem and Least-Squares Collocation

Bjerhammar problem can be summarized as follows: *"A finite number of gravity data is given for a non-spherical surface, and it is required to find such a solution that the boundary values for the data are satisfied in all given points"* (reference). For example, suppose gravity anomalies are known from gravity observations at discrete points of known orthometric heights at the Earth's surface. In that case, the problem is determining a gravity field that is consistent with these observations. This problem is regarded as the *discrete boundary value problem* (Bjerhammar, 1973). This formulation is more realistic than the usual formulation in terms of the classical GBVPs since the observations are taken at discrete points in reality. The solution of this problem is not unique, the additional requirement restricts that the computed gravity field should be as smooth as possible.

The non-uniqueness of the solution of Bjerhammar problem corresponds to the non-uniqueness of the interpolation problem. Thus, in the sense of the least standard error, one expects that the optimum interpolation corresponds to an optimum solution for that problem, in the sense of an optimally smooth gravity field (Moritz, 1974)**.** The solution to that problem corresponds to the least-squares prediction in physical geodesy, in which the input data and the predictions are of the same type, e.g., gravity anomalies (Heiskanen and Moritz, 1967). The principle is so flexible that it was generalized so that the input and output items could be of any heterogeneous nature. In such a case, one deals with the least-squares collocation technique, which represents the most capable and flexible prediction technique in geodesy, particularly for modeling the outer gravity field of the Earth. The least-squares collocation (LSC) method combines adjustment, filtering, and prediction in its more general scheme. A key role in this method is estimating the covariance function and the relevant modeling parameters.

2.7.2.4 Least-Squares Collocation and Integrated Geodesy

Any geodetic measurement, without exception, may (after linearization) be split into three components. The first constitutes a systematic part AX, which comprises effects of the ellipsoidal reference system, station coordinates and other geometric parameters, and systematic measuring errors. The second component is a random signal part, t, which expresses the effect of the anomalous gravity field on the observed quantity. The last part is the random observational errors, n, inherent in any measurement. Hence, each geodetic observation can be represented by the general mathematical model of the (LSC) technique, given as

$$l = AX + t + n, \tag{2.83}$$

which is regarded as the general observation equation for physical geodesy (Moritz, 1980).

Thus, the (LSC) principle is so flexible that it could incorporate all terrestrial geodetic observations, observed elements of the gravity field, and GPS observations into a unified adjustment, filtering, and prediction scheme. Particularly, besides all observable gravimetric elements and GPS measurements, observed horizontal and zenith angles, spatial distances, astronomic azimuths and coordinates, orthometric heights, geopotential differences, etc., all these data can be efficiently handled in an (LSC) algorithm (Moritz, 1974). This general computational trend is regarded as the integrated geodesy adjustment.

The principle of integrated geodesy allows for simultaneous processing of all possible geodetic data, which have a two-fold output. One output is the adjusted station geodetic coordinates relative to the reference ellipsoid and the relevant orthometric heights. The second output is the desired elements of the disturbing potential, such as geoidal heights, vertical deflections, and gravity anomalies or disturbances. In summary, the integrated geodesy implicitly accounts for all reductions of terrestrial observations to the reference ellipsoid, performs 2D or 3D adjustment of control stations (Shaker, 1982), models the anomalous gravity field, and performs GPS height and any eventual datum parameters estimation (Hein et al. 1989). More about the geometrical applications of collocation can be found in (Moritz, 1980).

2.7.3 The Combined Methods

Regarding both the operational (LSC) and model approaches, the use of an appropriate high-resolution model of global geopotential as a reference field provides the long-wavelength contribution and results in a smooth residual field, which is a theoretical property treating the anomalous elements as signals (with possibly zero mean and standard deviation). On the other hand, subtracting the terrain effects should smooth the input data more while accounting for the short-

wavelength component of the field (C. C. Tscherning and Forsberg, 1986a). Thus, in both approaches, local terrestrial gravity and Digital Terrain Model (DTM) data are combined with a harmonic model of global geopotential, originally constructed from satellite dynamics analysis.

It is well known that the (LSC) technique may be computationally tedious when the number of data points and predicted signals is very large. Hence, another alternative is to use the collocation method as a technique for gridding the data, and then the FFT techniques may be used. Furthermore, the Fast collocation method, discussed in the following chapter, can also be used.

The astro-gravimetric method (or astro-gravimetric leveling) uses the main advantages and avoids the fundamental defects of both the astro-geodetic method and the gravimetric one to compute a better geoid. Particularly, the astro-geodetic (as well as the GPS-leveling method) can determine the fine structure of the geoid. However, using this method, the position of the (local) datum origin with respect to the geocenter will be unknown. In addition, the observed astro-deflections could be poorly distributed. On the contrary, the gravimetric method deals with a geocentric datum, but some factors could affect its long wavelength components, particularly the zero degree term (Heiskanen and Moritz, 1967). As the densification of deflections by astronomical observations is laborious and uneconomic, it is more efficient to predict the deflections gravimetrically at the wanted new positions. Amin (1983) gives a comparison among some methods for Astro-gravimetric leveling.

2.8 General Sources of Errors in Gravimetric Geoid Determination

Keeping in mind that the Remove-Compute-Restore (RCR)technique has been the standard tool for gravity field modeling, the gravimetric geoid encounters many sources of errors, which could be of a random or systematic nature. While the random errors are unavoidable, the systematic errors can be a consequence of the practical approximations in theory, not properly accounting for reductions, or the lack of global and local data coverage. In this sense, according to the available information and computational techniques, the systematic errors could be completely or partially accounted for.

The basic sources of random errors are the random observational errors inherent in the input gravity data and the uncertainty in the used geopotential spherical harmonic models. The noise inherent in the geopotential coefficients, up to a specific degree and order, is usually called the commission error. Such error is best described in terms of the error degree variances of the harmonic model, which will be discussed in the proceeding chapters.

On the other hand, there are many sources of non-random errors. Obviously, the input gravity observations should be efficiently corrected for tidal effects, drift, etc., via appropriate mathematical models or special observational techniques (G. Dawod, 1998). A significant error could be due to the used Earth's constants. If the best updated Earth's constants are considered, then no error will be committed regarding the Earth's defining parameters. Otherwise, an error of the order of about one meter could be the consequence (Featherstone and Olliver, 1993). Moreover, as was previously mentioned, the spherical approximation yields a considerable error in geoid computation. Fortunately, the remove-restore technique is acknowledged to significantly decrease the effect of spherical approximation (Martinec, 1998).

Regarding the classical GBVPs, discretization error is another problem (Rapp, 1973). This error typically results from gravity data's non-continuous coverage of the far and near zone (integration cap) areas. The discretization error is thus the amount of information lost when replacing the integrals with discrete numerical summations regarding the near zone computations. On the other hand, the far zone component of that error is the amount of the lost features due to the construction of geopotential coefficients from global discrete data. The improvement of global data coverage can only reduce such errors. Theoretically, if a continuous global data coverage were achieved, this would

correspond to a (fully determined) global geopotential model with a maximal degree of infinity, and a statistical treatment of the Earth's gravity field would have no sense.

It is well known that the objective of the remove-restore technique is to account for the truncation error (or the omission error), which is the error resulting from neglecting the information outside the limited integration cap. This amounts to the long-to-medium wavelength contribution. However, the used geopotential model could have no data contribution from the investigated area. Consequently, it would not recover the long and intermediate wavelength features for that region in a reliable manner. In particular, residual long wavelength features would result (Stewart and Hipkin, 1989) and a long wavelength error in the computed local geoid will be the consequence. This shortcoming can be considered as a partial removal of the truncation error by the geopotential harmonic model. Finally, another source of gravimetric geoid errors is the neglection or improper modeling of the topographic gravitational signal in a remove-restore fashion.

3. Global geopotential models, digital models of topographic masses

Overview

This chapter introduced the statistical and mathematical properties of the spherical harmonic functions and discussed the spectral meaning of the spherical harmonic coefficients. Then, the principles of spherical harmonic analysis and spherical harmonic synthesis are clarified. The global harmonic analysis using various global gravity field data sources and the different classes of the derived global harmonic models are presented. After that, the concept of tailored geopotential harmonic models is clarified. A theoretical review of the various applications of global harmonic models is then presented. After then, the concept of DEM is introduced.

3.1 Global geopotential models

The global Geopotential Model is a mathematical function that describes the Earth's gravity field in 3-dimensional space. The determination of the Earth's global gravity field is one of the main tasks of geodesy: it serves as a reference for geodesy itself, and it provides essential information about the Earth, its interior, and its fluid envelope for all geosciences. from such gravity potential all related gravity field functionals can be obtained (Barthelmes, 2014).

As mentioned in chapter two, section 2.2. that the gravitational potential of the Earth, V, when calculating the effects of Earth's gravity on a satellite we need to solve for the geopotential at a specific location outside of the Earth by integrating the geopotential over a series of
Mass elements dM that comprise the Earth (Fig. 17)

$$V = G \iiint_{Earth} \frac{dM}{l} \quad . \tag{3.1}$$

where no attracting masses exist (outer space), the gravitational potential is a harmonic function and satisfies Laplace's equation, which is given as:

$$\nabla^2 V = . \tag{3.2}$$

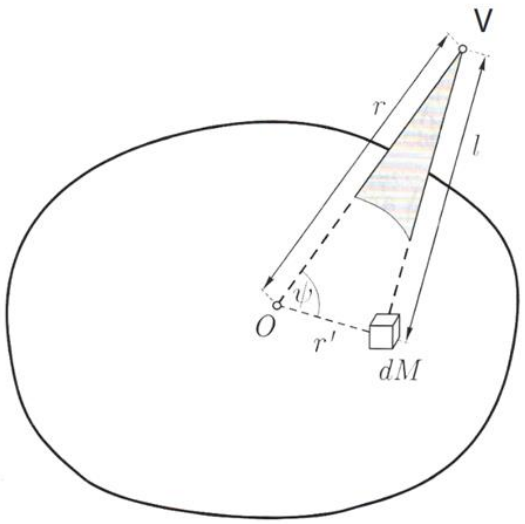

Figure 17 The potential V at a point at distance l from an attracting mass is the summation of the potential due to all mass elements dM (adapted from Wellenhof and Moritz 2005)

It can be easily shown that the reciprocal distance (1/l) is primarily a harmonic function, which can be looked upon as the gravitational potential of a point mass of m = 1/G. This is the only reason why the outer gravitational potentials of homogeneous spherical masses, point masses, surface mass layers, and even non-homogeneous solid bodies (such as the Earth) are harmonic outside the attracting masses. Furthermore, the non-harmonicity inside the attracting body is easily interpreted by the singularity of the reciprocal distance in such domains.

Analogously, the normal gravitational potential,

$$V_n = G \iiint_{Earth} \frac{dM_n}{l} \tag{3.3}$$

is harmonic in the outer space of the relevant level ellipsoid and obeys Laplace's condition, that is

$$\nabla^2 V_n = 0 \ . \tag{3.4}$$

It follows immediately that applying the Laplacian operator on disturbing potential, $T = V - V_n$, which is harmonic outside the attracting masses, gives

$$\nabla^2 T = . \tag{3.5}$$

It can be shown that the Laplacian condition (Eq.3.2), for the gravitational potential of the Earth, can be expressed in spherical coordinates as follows (Heiskanen and Moritz, 1967)

$$r^2\ \partial^2V/\partial r^2 + 2r\ \partial V/\partial r\ +\ \partial^2V/\partial\theta^2\ + \cot\theta\ \partial V/\partial\theta\ + (1/\sin^2\theta)\ \partial^2V/\partial\lambda^2\ = 0, \tag{3.6}$$

$$r^2 \frac{\partial^2 V}{\partial r^2} + 2r \frac{\partial V}{\partial r} + \frac{\partial^2 V}{\partial \theta^2} + \cot(\theta) \frac{\partial V}{\partial \theta} + \left(\frac{1}{\sin^2 \theta} . \frac{\partial^2 V}{\partial \lambda^2} \right) = 0$$

where r is the geocentric radius,

θ is the co-latitude (or the compliment of the geocentric latitude ψ') and, λ is the geodetic longitude.

The general solution of the above differential equation yields the well-known infinite spherical harmonic expansion of the Earth's gravitational potential into a series of spherical harmonic functions of degree *n* and order *m*, which is expressed by

$$V(\theta, \lambda, r) = \left(\frac{GM}{r}\right) \left[1 + \left(\frac{a}{r}\right)^n \sum_{m=0}^{n} (C_{nm} \cos m\lambda + S_{nm} \sin m\lambda) P_{nm} (\cos \theta)\right], \tag{3.7}$$

where:

a	the equatorial radius of the Earth,
C_{nm} and S_{nm}	the conventional unitless spherical harmonic coefficients of the Earth's gravitational potential of degree n and order m,
$P_{nm}(\cos\theta)$	the conventional associated Legendre function of degree n and order m.

However, it is common practice in physical geodesy to replace both the conventional spherical harmonic coefficients and the relevant associated Legendre functions by their fully normalized versions, as follows

$$\bar{C}_{n0} = \frac{C_{n0}}{(2n+1)^{1/2}}, \tag{3.8}$$

$$\begin{pmatrix} \bar{C}_{nm} \\ \bar{S}_{nm} \end{pmatrix} = \left[\frac{(n+m)!}{(2(2n+1)(n-m)!)}\right]^{1/2} \begin{pmatrix} C_{nm} \\ S_{nm} \end{pmatrix}, \qquad m \neq 0 \tag{3.9}$$

and

$$\bar{P}_{n0}(\cos\theta) = (2n+1)^{1/2}.\ P_{n0}(\cos\theta),$$

$$\bar{P}_{nm}(\cos\theta) = \left[\frac{2(2n+1)(n-m)!}{(n+m)!}\right]^{1/2}.\ P_{nm}(\cos\theta), \qquad m \neq 0 \tag{3.10}$$

Where:

$\bar{C}_{nm}$ and $\bar{S}_{nm}$ are the fully normalized unitless spherical harmonic coefficients of the Earth's potential of degree n and order m,

$\bar{\bar{P}}_{nm}(\cos\theta)$ is the fully normalized associated Legendre function of degree n and order m.

Hence, Eq. (3.7) is usually expressed as

$$V(\theta,\lambda,r) = \left(\frac{GM}{r}\right)\left[1 + \sum_{n=1}^{\infty}\left(\frac{a}{r}\right)^{n}\sum_{m=0}^{n}(\bar{C}_{nm}\cos m\lambda + \bar{S}_{nm}\sin m\lambda)\bar{P}_{nm}(\cos\theta)\right], \tag{3.11}$$

where both $\bar{S}_{n0}$ and S_{n0} are by definition equal to zero, since sin0λ=0.

Similar to the actual gravitational field of the Earth, Laplace's differential equation (3.4), as applied to the normal gravitational field, can be expressed in ellipsoidal coordinates (β, λ, u) and solved for V_n(β, λ, u) (Hobson, 1931). In this case, the solution would be the expansion of the normal gravitational field in ellipsoidal harmonics, which utilizes, besides the ellipsoidal coordinates, the complex second type of associated Legendre functions Q_{nm}, in addition to the above-mentioned associated Legendre functions, P_{nm}. Nevertheless, exploiting the relationships among the ellipsoidal and spherical coordinates, the normal gravitational field is usually expressed in the following zonal spherical harmonic expansions (Hirvonen, 1960)

$$V_n(\theta,r) = \left(\frac{GM_e}{r}\right)\left[1 - \sum_{n=1}^{\infty}\left(\frac{a_e}{r}\right)^{n}\bar{C}_{2n}\bar{P}_{2n}(\cos\theta)\right], \tag{3.12}$$

where:

$\bar{P}_{2n}(\cos\theta)$ is the fully normalized Legendre polynomial of degree 2n,

$\bar{C}_{2n}$ is the fully normalized zonal spherical harmonic coefficient, of degree 2n and order 0, of the normal gravitational potential,

M_e is the mass of the reference ellipsoid and

a_e is the respective equatorial radius.

The even zonal coefficients of the normal field are given by

$$\bar{C}_{2n} = \frac{C_{2n}}{(2n+1)^{1/2}} \ . \tag{3.13}$$

Based on the above, it is clear that the disturbing potential can be expanded in spherical harmonic series, via the subtraction of the expansion (3.12) from (3.11), as follows (Kirby and Featherstone, 1997; Smith, 1998)

$$T(\theta,\lambda,r) = \frac{GM-GM_e}{r} + \frac{GM}{r}\left[\sum_{n=1}^{\infty}\left(\frac{a}{r}\right)^n \sum_{m=0}^{n}(\bar{C}^*_{nm}\cos m\lambda + \bar{S}_{nm}\sin m\lambda)\,\bar{P}_{nm}(\cos\theta)\right] \tag{3.14}$$

$$\bar{C}^*_{n0} = \bar{C}_{n0} - \left[\frac{GM_e}{GM}\cdot\left(\frac{a_e}{a}\right)^n\right]\bar{C}^e_{n0}, \qquad m=0 \text{ and } n \text{ even}, \tag{3.14a}$$

$$\bar{C}^*_{nm} = \bar{C}_{nm} \qquad \text{otherwise}, \tag{3.14b}$$

where $\bar{C}^e_{n0}$ are the relevant even zonal coefficients of the normal gravitational potential, as given in Eqs. (3.12) and (3.13). The first term of Eq. (3.14) is the zero-degree term of the anomalous potential. If the mass of the normal ellipsoid equals that of the Earth, then that term would equal zero. Moreover, if the center of the reference ellipsoid coincides with the geocenter, then the first-degree terms would vanish. In such a case, and assuming an equal equatorial radius of both the Earth and the normal ellipsoid, one simply obtains

$$T(\theta,\lambda,r) = \frac{GM}{r}\left[\sum_{n=2}^{\infty}\left(\frac{a}{r}\right)^n \sum_{m=0}^{n}(\bar{C}^*_{nm}\cos m\lambda + \bar{S}_{nm}\sin m\lambda)\,\bar{P}_{nm}(\cos\theta)\right], \tag{3.15}$$

with

$$\bar{C}^*_{n0} = \bar{C}_{n0} - \bar{C}^e_{n0} \qquad m = 0 \text{ and } n \text{ even}. \tag{3.15a}$$

In spherical approximation, the equatorial radius, a, will be replaced by the mean radius of the Earth, R, in the harmonic expansions of the anomalous features. Moreover, the geocentric latitude will be replaced by geodetic latitude.

The harmonic expansion is practically truncated at a maximum degree N, the maximum resolution of a given global geopotential harmonic model. Utilizing the functional relationships between the anomalous potential and the various gravimetric quantities, these quantities can be similarly expanded in spherical harmonic series, as given by Eq. (3.16) through (3.17)

$$N(\theta,\lambda.r) = \left(\frac{GM}{r\gamma}\right)\sum_{n=2}^{N}\left(\frac{a}{r}\right)^n \sum_{m=0}^{n}(\bar{C}^*_{nm}\cos m\lambda + \bar{S}_{nm}\sin m\lambda)\,\bar{P}_{nm}(\cos\theta), \tag{3.16}$$

$$\Delta g(\theta,\lambda.r) = \left(\frac{GM}{r^2}\right)\sum_{n=2}^{N}(n-1)\left(\frac{a}{r}\right)^n \sum_{m=0}^{n}(\bar{C}^*_{nm}\cos m\lambda + \bar{S}_{nm}\sin m\lambda)\,\bar{P}_{nm}(\cos\theta), \tag{3.17}$$

with the zero- and first-degree terms taken equal to zero,

where:

N, Δg,	are the relevant computed, geoidal height, gravity anomaly,
θ	the geocentric latitude,
λ	the geodetic longitude,
r	the geocentric radius to the geoid,
γ(θ, r)	the normal gravity implied by the reference ellipsoid,
GM	the product of the Earth-mass by the gravitational constant,
a	the equatorial radius,

$\bar{C}^{*}_{nm}$ the fully normalized spherical harmonic C-coefficients of degree n and order m, reduced for the even zonal harmonics of the reference ellipsoid,

$\bar{S}_{nm}$ the fully normalized spherical harmonic S-coefficients of degree n and order m,

$\bar{P}_{nm}\cos\theta$ the fully normalized associated Legendre function of degree n and order m.

It should be emphasized that "a" in the above expressions is sometimes referred to as the equatorial radius scale factor of the given geopotential harmonic model. Also, GM is the geocentric gravitational constant pertaining to the model (Smith and Small, 1999). These constants can be taken from the determined Earth constants, during the construction of the respective harmonic model (Rapp, 1982). Particularly, the value of "a" is looked upon as the sphere's radius, down to which the relevant harmonic expansion is assumed to be convergent (Smith, 1998). Of course, the convergence can also be guaranteed below that radius, provided the evaluation point does not lie in the topographic masses. Nevertheless, the regularization via the topographic reductions and the concept of Bjerhammar sphere supplements the evaluation of the harmonic series down to the geoidal surface (Moritz, 1980).

3.1.1 Statistical and Mathematical Properties of Spherical Harmonics

Recall that the outer anomalous field and its observable functions can be expanded in spherical harmonic series. Such expansions are based on common orthogonal base functions (or eigenfunctions), which are usually referred to as the (fully normalized) spherical harmonic functions (or spherical harmonics). According to where the harmonic expansion is evaluated, one deals with either solid or surface harmonics.

Particularly, when the evaluation point lies on the surface of a sphere of radius a, representing the boundary surface, one speaks of the surface harmonics. Thus, any function f(θ, λ), which is defined on the surface of a sphere of radius a, can be expanded in surface harmonic series as follows

$$f(\theta,\lambda) = \sum_{n=0}^{\infty}\sum_{m=-n}^{n}\bar{K}_{nm}\ \bar{Y}_{nm}(\theta,\lambda), \tag{3.18}$$

where

$$\bar{Y}_{nm}(\theta,\lambda) = \bar{P}_{nm}(\cos\theta)\begin{pmatrix}\cos m\lambda \\ \sin|m|\lambda\end{pmatrix}, \quad \begin{matrix} m\geq 0 \\ m<0\end{matrix} \tag{3.19}$$

are the fully normalized surface harmonics of degree n and order m, and

$$\bar{K}_{nm} = \begin{pmatrix}\bar{C}_{nm} \\ \bar{S}_{nm}\end{pmatrix}, \quad \begin{matrix} m\geq 0 \\ m<0\end{matrix} \tag{3.19a}$$

are the unitless fully normalized spherical coefficients, relevant to the expanded function *f*. On the other hand, if the function is harmonic in outer space of the sphere, whose radius equals *a*, which is the case relevant to the geopotential, then it can be expanded in terms of solid spherical harmonic series as given in Eq.(3.15), or formulated as follows

$$f(\theta,\lambda,r)_o = \sum_{n=0}^{\infty}\sum_{m=-n}^{n}\left(\frac{a}{r}\right)^{n+1}\bar{K}_{nm}\ \bar{Y}_{nm}(\theta,\lambda), \tag{3.20}$$

and if such function is harmonic inside the same sphere (such as in mass layers), one obtains

$$f(\theta,\lambda,r)_i = \sum_{n=0}^{\infty}\sum_{m=-n}^{n}\left(\frac{r}{a}\right)^{n}\bar{K}_{nm}\ \bar{Y}_{nm}(\theta,\lambda), \tag{3.20a}$$

where both $\left\{\left(\frac{a}{r}\right)^{n+1}\cdot\bar{Y}_{nm}(\theta,\lambda)\right.$ and $\left.\left(\frac{r}{a}\right)^{n}\bar{Y}_{nm}(\theta,\lambda)\right\}$ are referred to as the fully normalized solid spherical harmonics.

In the sense of the above, the spherical harmonic coefficients are considered constants, which should be determined for the harmonic function under consideration. Essential for their determination is the orthogonality relations among the surface harmonics. These remarkable relations mean that the integral over the unit sphere of the product of any two different surface harmonic functions is zero. Particularly, one obtains

$$\iint_e Y_{nm}(\theta,\lambda)Y_{k1}(\theta,\lambda)d\sigma = \frac{1}{4\pi}\int_{\lambda=0}\int_{\theta=0} Y_{nm}(\theta,\lambda)Y_{k1}(\theta,\lambda)\sin\theta d\theta d\lambda = \tag{3.21}$$

$$= \begin{pmatrix} 0 & n \neq k \ or \ m \neq 1, \\ 1 & n = k \ and \ m = 1. \end{pmatrix}$$

Thus, globally, the average of the squares of the same surface harmonic equals unity, whereas the products of different harmonics average up to zero. Hence, in a statistical sense, the surface harmonics could be considered as spatially uncorrelated. Mathematically, they are said to be orthogonal. This property is essential for the applicability of spherical harmonics in physical geodesy, as will be shown in the subsequent sections.

The harmonics with m=0 (or Legendre polynomials) are polynomials of degree n in cosθ, so that they have n real zeros in the interval ($0 \leq \theta \leq \pi$), which means that they change their sign n times in this interval, and hence, divide the sphere into zones along the parallels of latitude (Fig. 18a).

On the other hand, associated Legendre functions change their sign (n-m) times in the interval ($0 \leq \theta \leq \pi$), while the functions cos mλ and sin mλ have 2m zeros in the interval ($0 \leq \lambda \leq 2\pi$). So, the longitude dependent non-zonal harmonics ($m \neq 0$) divide the sphere into compartments that are positive and negative in a staggered fashion. So, they are called tesseral harmonics (Fig.18 c). In particular, for n = m, the non-zonal harmonics have no zeros in the meridian directions. Therefore, they degenerate into functions, dividing the sphere into positive and negative sectors (Fig. 18b), and are referred to as sectorial harmonics.

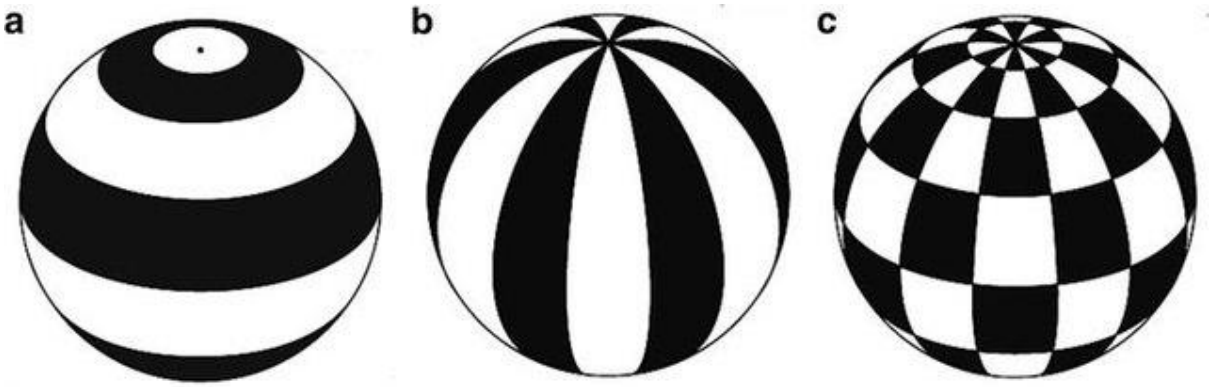

Figure 18 (a) Geometric representation of zonal harmonics (m = 0) (b) sectorial harmonics (m = n), (c) tesseral harmonics (m ≠ 0). (Skiba, 2017)

Thus, the surface harmonics provide the spatial periodicity (or frequency) of the disturbing potential, according to the respective degrees and orders.

3.1.2 Spectral Meaning inherent to Spherical Harmonic Coefficients

The zero-degree term in any harmonic expansion represents the average value of the relevant harmonic function over the evaluation sphere. The succeeding terms for higher degrees describe the harmonic deviations from that mean value. Each harmonic term has two parts. The first is the trigonometric part, represented by the surface harmonic, and it controls the frequency of the spatial oscillations of the function. The second part is a constant multiplier, represented by the respective spherical harmonic coefficient, and it controls the amplitude of these oscillations. Regarding the geopotential as a harmonic function, the power of the harmonic coefficients generally has a damping trend as the degree increases, therefore, the amplitudes of the lower degree terms are relatively larger than those of, the higher frequency ones.

The zero-degree term of the geopotential is simply the average performance of the whole Earth as a point mass, which is relevant to the planetary behaviour of the Earth in the Solar system. On the other hand, the zero-degree term of the disturbing potential expresses the discrepancy between the Earth's mass (represented by an appropriate global geopotential model) and that of the reference ellipsoid.

The first-degree terms correspond to the non-geocentricity of the normal ellipsoid and vanish when a geocentric ellipsoid is considered.

The zonal second-degree term of the disturbing potential, which is the dominant term in the expansion of the anomalous field, is a function of the discrepancy between the difference between the polar and mean equatorial mass moments of inertia of the Earth and the polar and equatorial moments relevant to the normal datum. In this sense, that second-degree zonal term is a measure of the difference between the flattening of the Earth and that of the ellipsoid.

Moreover, the second-degree tesseral terms and the sectorial S-term of the Earth’s potential express the first product moments of inertia of the Earth with respect to the axes of the average terrestrial system, and thus they represent the anti-symmetry of the Earth with respect to such axes. On the other hand, the second-degree sectorial C-term is a function of the difference between the two equatorial mass moments of inertia; hence, it is a measure of the ellipticity of the equatorial plane of the Earth (Heiskanen and Moritz, 1967).

All harmonic contributions of degrees higher than zero are super-positioned with the zero-degree term to describe the disturbing masses’ dependent structure of the anomalous field (Eq. 3.14). For example, Fig. 19 illustrates a schematic representation of the global geoid, computed from a global spherical harmonic model of the Earth’s geopotential.

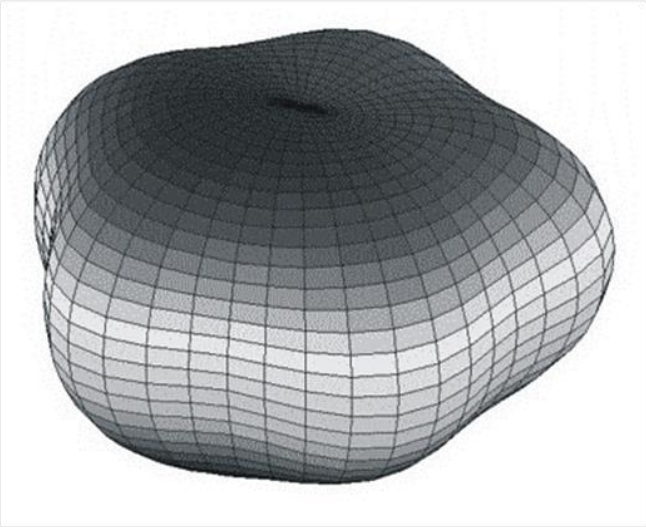

Figure 19 Spherical harmonic representation of the global geoid (Heiskanen and Moritz, 1967).

The coefficients can be viewed, in a general sense, as weighted mean values of the anomalous potential in the frequency domain, the weights being the spherical harmonics. Loosely speaking, a mean gravity anomaly field will represent an amount of information contained in a set of potential coefficients of degrees less than or equal to a specific degree, N. The magnitude of N depends on the size of the grid cells, over which the mean anomaly is computed.

The finer the grid resolution is, the higher is the maximum degree of the coefficients, which can be extracted, and vice versa. If the Earth were continuously covered with point gravity data, a geopotential model of maximum degree infinity could have been theoretically assessed. The second limiting case is obviously when one deals with the Earth as a whole (a point mass or a sphere of homogeneous mass), which corresponds to a zero-degree coefficient, where the potential would vary with the radial vector-only (C. C. Tscherning, 1974).

A mean data grid having resolution θ in both latitude and longitude directions on the Earth's surface generally produces a set of harmonic coefficients of maximal degree $N=180^o/\theta^o$ (Rapp, 1977).

This rule connects the space domain resolution, θ, with the resolution, N, relevant to the spectral domain. Resolution θ is then referred to as the half-wavelength, which is inversely interrelated with the spectral frequency N (Groten, 1981).

Thus, a GGM with a maximum of degree/ order N can recover the anomalous field with a spatial resolution, corresponding to a grid of spacing $180^o/N$ (Rapp, 1972a, 1972b).

Recall that, via the remove-restore technique in modern local geoid modeling, the geoid is usually spectrally decomposed into long - medium, medium - short and short - very short wavelength components. These components correspond to the geoid's global, regional, and residual local trends, respectively, as shown in Fig. 20. The first trend is derived from an appropriate potential harmonic model, the second part is supposed to be provided from the local gravitational data, and the third trend is represented by the very short gravity signal derived from an appropriately high-resolution digital terrain model.

Accordingly, the resolution of the low-frequency information will be compatible with that of the geopotential model. In contrast, the resolutions of the local gravity data and the digital terrain model will govern the resolution of the final detailed local geoid solution.

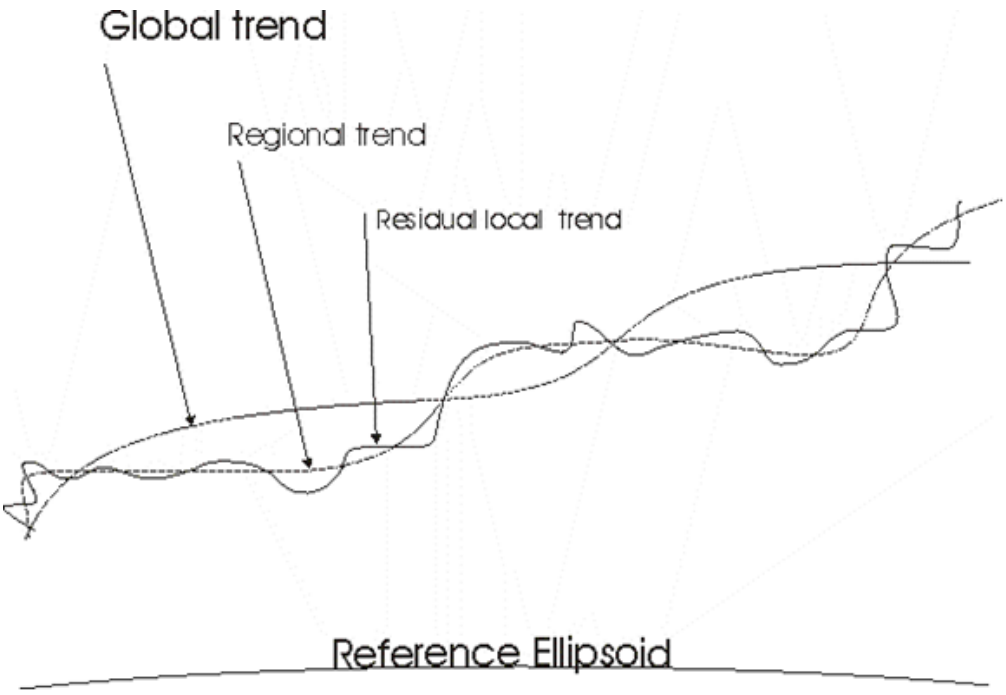

Figure 20 Reference ellipsoid

3.1.3 Spherical Harmonic Analysis and Synthesis

Spherical harmonics are among the standard mathematical tools for analysis and synthesis on the Earth and in the neighboring space. For example, geopotential models in the spherical harmonic series synthesize most of the available observational information from gravity surveys, satellite orbit tracking, and topographical height data.

The gravity anomaly (Δg) expression becomes in spherical harmonics as equations 3.16 and 3.17.

All band-limited functions on the surface of a sphere, which are square-integrable, can be expanded into a series of spherical harmonics,

$$f(\theta,\lambda) = \sum_{n=0}^{N}\sum_{m=0}^{n}(\bar{C}_{nm}\cos m\lambda + \bar{S}_{nm}\sin m\lambda)\,\bar{P}_{nm}(\cos\theta)\ . \qquad (3.22)$$

A band-limited function does not contain any power in the frequencies above a certain degree, N. Equation (3.18) is known as global spherical harmonic synthesis (GSHS), as the function $f(\theta,\lambda)$ is composed (or synthesized) of the harmonic coefficients. Such coefficients are referred to as the true ones because they represent the function. The upper bound, N, tends to infinity for a non-band-limited function, such as the potential of the Earth. The above equation can evaluate the function from a given set of coefficients in the space domain. Conversely, it is possible to compute these coefficients, if the function values are given on the sphere as follows

$$\bar{C}_{nm} = \frac{1}{4\pi}\int_{\lambda=0}^{2\pi}\int_{\theta=0}^{\pi} f(\theta,\lambda)\cos m\lambda\ \bar{P}_{nm}(\cos\theta)\sin\theta\,d\theta\,d\lambda, \qquad (3.23)$$

$$\bar{S}_{nm} = \frac{1}{4\pi}\int_{\lambda=0}^{2\pi}\int_{\theta=0}^{\pi} f(\theta,\lambda)\sin m\lambda\ \bar{P}_{nm}(\cos\theta)\sin\theta\,d\theta\,d\lambda,\ \ . \qquad (3.23a)$$

The computation of the coefficients of a function defined on the sphere is known as Global Spherical Harmonic Analysis (GSHA). Hence, the spherical harmonic analysis is the inverse algorithm of the spherical harmonic synthesis. Both algorithms belong to the Global Spherical Harmonic Computations (GSHC).

The GSHC are usually performed more efficiently by splitting them into longitude and a latitude-dependent part. This is achieved by the interchange of the summations in Eq. (3.18) over n and m, as follows

$$\sum_{n=0}^{N}\sum_{m=0}^{n} \Rightarrow \sum_{m=0}^{N}\sum_{n=m}^{N} \quad ,$$

which is the same summation. This summation swap yields the so-called two-step GSHS, which is given as (Sneeuw, 1996),

$$a_m(\theta) = \sum_{n=m}^{N} \bar{P}_{nm}(\cos\theta)\, \bar{C}_{nm} \,, \tag{3.24}$$

$$b_m(\theta) = \sum_{n=m}^{N} \bar{P}_{nm}(\cos\theta)\, \bar{S}_{nm} \tag{3.24a}$$

$$f(\theta,\lambda) = \sum_{m=0}^{N}(a_m(\theta)\cos m\lambda + b_m(\theta)\sin m\lambda) \,. \tag{3.25}$$

Furthermore, the corresponding two-step GSHA is defined as

$$a_m(\theta) = \frac{1}{(1+\delta_{m0})\pi} \int_{\lambda=0}^{2\pi} f(\theta,\lambda)\cos m\lambda \, d\lambda \,, \tag{3.26}$$

$$b_m(\theta) = \frac{1}{(1+\delta_{m0})\pi} \int_{\lambda=0}^{2\pi} f(\theta,\lambda)\sin m\lambda \, d\lambda \,, \tag{3.26a}$$

$$\bar{C}_{nm} = \frac{(1+\delta_{m0})}{4} \int_{\theta=0}^{\pi} a_m(\theta)\bar{P}_{nm}(\cos\theta)\sin\theta \, d\theta, \tag{3.27}$$

$$\bar{S}_{nm} = \frac{(1+\delta_{m0})}{4} \int_{\theta=0}^{\pi} b_m(\theta)\bar{P}_{nm}(\cos\theta)\sin\theta \, d\theta, \tag{3.27a}$$

where

$\delta_{mk} = 1$ $\quad$ $m = k,$

$\delta_{mk} = 0$ $\quad$ $m \neq k.$

Splitting the information and unknowns makes the two-step trend powerful. The order-degree swap leads to more efficient computations due to two reasons. Firstly, as can be shown by the above equations, they can be (optionally) treated by fast Fourier transformation over single parallels, in which the $a_m(\theta)$ and $b_m(\theta)$ coefficients represent the 1D-Fourier coefficients (Fig. 21). Secondly, the above relations can be evaluated for separate orders m, which is very easy to handle in computer programming (C. C. Tscherning et al., 1983).

However, the input for harmonic analysis usually consists of function values at discrete points (samples) of a continuous function. Hence, the SHA must be performed based on a set of discrete (e.g. gridded) data accompanied by relevant discrete versions of Legendre functions. In a subsequent SHS, the coefficients should represent the continuous function, not merely the function values at the data points previously input for the harmonic analysis. In this respect, the main difficulty is caused by the non-orthogonality of the discretized surface harmonics. Due to the absence of orthogonality relations, the GSHA cannot yield a unique expression for the spherical harmonic coefficients. This

leads to different methods for discrete spherical harmonic analysis, instead of one unique "exact" solution, as in the case of continuous data coverage. Three practical problems occur, resulting in sampling, data noise, smoothing, and approximation errors (C. C. Tscherning et al., 1983).

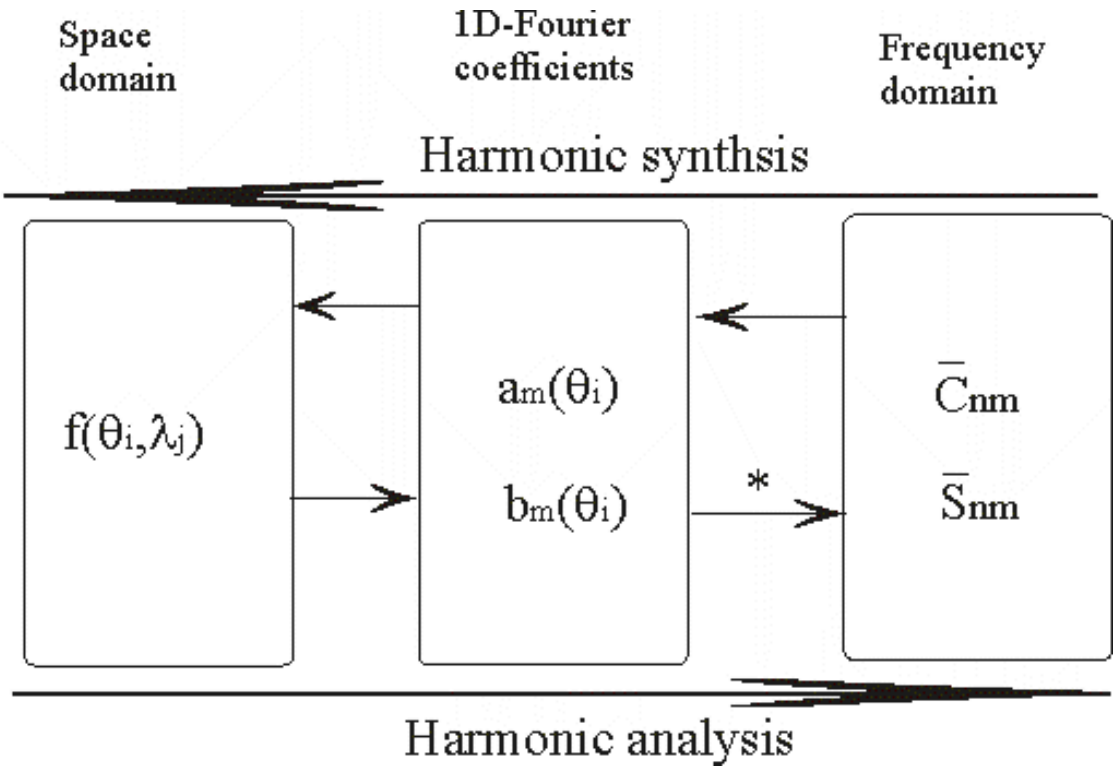

Figure 21 Principle of the two-step GSHC (Tscherning, Rapp, and Goad 1983)

Assuming a band-limited continuous signal $f(\theta,\lambda)$ with maximum frequency N is sampled on a grid by taking measurements, such measurements are usually contaminated with noise. These data can be called gridded point data or block averaged mean data. The considered gridding in both latitude and longitude directions is assumed to be equiangular. Let N_λ and N_θ be the numbers of meridians and parallels containing data. The sampling interval in longitude directions is thus $\Delta\lambda = 2\pi/ N_\lambda$. In case the poles are included, equiangular gridding in latitude direction yields a sampling interval $\Delta\theta = \pi/ (N_\theta-1)$, whereas the interval for block means is equal to $\Delta\theta = \pi/ N_\theta$. If the data were errorless, then the function would be perfectly sampled on a grid.

Moreover, if the sampling is dense enough to expand up to degree N, then this discrete function is transformed from the space domain to the frequency domain using the discrete GSHA, which different methods can accomplish. One should remember that in such methods, the samples are represented in different ways, resulting in different sets of coefficients with respect to different base functions. This implies that it is possible to transform a discrete function forth and back between these representations without any loss of information. But what is more interesting is that the coefficients of the discrete function are the same as the (true) coefficients of the continuous function. So, the continuous signal can be retrieved from its samples if the errorless data sampling is dense enough, i.e. the data resolution is finer than or equal to the Nyquist half-wavelength (Groten, 1981).

In practice, however, there exist some problems, such as aliasing, data noise, scattered data coverage and the different GSHA methods. These problems make the computed coefficients differ from the desired true coefficients, which are the best estimates of the continuous signal. An aliasing error (or sampling error) is caused by under-sampling or under-developing. In both cases, aliasing errors result in the continuous signal because the degree of expansion of the discrete function, N_{max}, is smaller than the maximum frequency, N. The problem of aliasing generally exists if the signal is

not band-limited (such as the gravitational potential), because, for practical reasons, its development has to obey a truncated fashion. Furthermore, if a band-limited continuous signal is dealt with, aliasing can also occur if the density of observations is too small to estimate all coefficients up to the band limitation. The principle of aliasing is that the high frequencies present in the signal, but not in the developed expansion (i.e. N_{max}+1 …. N) will be erroneously mapped into the estimated coefficients. The higher estimated coefficients will be affected more than the lower degree ones. Therefore, regarding the aliasing effect, the coefficients are less trusted with increasing degree n. This effect depends on the used prediction technique.

The predicted coefficients are also affected by the input gravity data noise. These errors in the data are of high frequency by nature, which is reflected in the form of an increasing coefficient error spectrum with the degree. On the other hand, it is well-known that the sampled signal is relatively smooth and has a decreasing power spectrum, according to Kaula's rule for signal decay. Usually, the power and error spectra will have an intersection point at some degree, referred to as the degree of resolution. Logically, beyond this degree, the coefficients' estimates should no longer be trusted because the estimates contain as much noise information as the signal. The GSHS model becomes inconsistent in the apace domain due to such errors. In the GSHA model, the data noise will be mapped into the relevant functional model, which again depends on the used GSHA technique.

On the other hand, averaging observations over blocks implies a smoothing of the data, which affects the estimates. The real data will mostly be irregularly distributed (scattered), where data gaps are likely to exist. Such data are transformed into a grid by some interpolation or averaging technique. Finally, the errors associated with the mathematical algorithm and numerical features of each GSHA method could be referred to as approximation errors.

The determination of the geopotential from space has been successful via precise orbit determination (POD) for the so-called low-Earth orbit (LEO) satellites. Such LEO satellites orbit the Earth at altitudes of a few hundred kilometers.

A satellite orbit is a manifestation of the Earth's gravitational pull exerted on the satellite; hence, it contains information about the gravity field.

On the other hand, satellite altimetry provides a powerful tool for the determination of marine geoidal heights and deflection components of relatively higher resolutions, which could be easily used to predict any other function of the anomalous field over marine areas.

Precise orbit determination of an LEO satellite relies on optical or radio tracking of the satellite from ground-based and/or space-borne platforms, whose positions themselves are well determined.

One newer technique that involves no ground tracking and has been proposed as especially suited for gravity signal recovery applications is the satellite-to-satellite tracking (SST) technique. SST is accomplished through the range and/or range rate observations between a pair of satellites. The two satellites may be orbiting in tandem and separated by several hundreds of kilometers in the same orbit, referred to as low-low SST. Another possibility is that one satellite is an LEO and the other is a GPS high-orbiting satellite, which constitutes the so-called high-low SST (Hwang 2001). As the gravitational signal attenuates with altitude, the lower orbit of an LEO is more efficient regarding gravity field recovery. Such measurements, representing satellite dynamics (perturbations) data, could be effectively supplemented by satellite gravity gradiometry (SGG).

Some recent satellite altimetry missions, usually of medium satellite altitudes, are GEOSAT, ERS1-GM, ERS-ERM, ERS2, Topex/Poseidon (T/P), and JASON-1. In particular, the (T/P) altimetry mission was launched in 1992 with a lifetime of six years. The (T/P) follow-on mission, JASON-1, was launched by the end of 2000. The missions LAGEOS-1 and LAGEOS-2 (1992-1998) represent passive target satellites (equipped with laser retro-reflectors) and are tracked via the satellite laser ranging (SLR) technique. Similar (SLR) missions are STARLETTE, AJISAI, STELLA,

ETALON-1, ETALON-2 and GFZ-1. The GFZ-1 mission was launched in 1995 with an altitude of 390 kms, an orbital inclination of 52º, and a lifetime of 5 years. On the other hand, some missions, which lean on the SST technique, were recently proposed, namely the CHAMP, GRACE, COSMIC, and GOCE gravity field missions (Fig. 22).

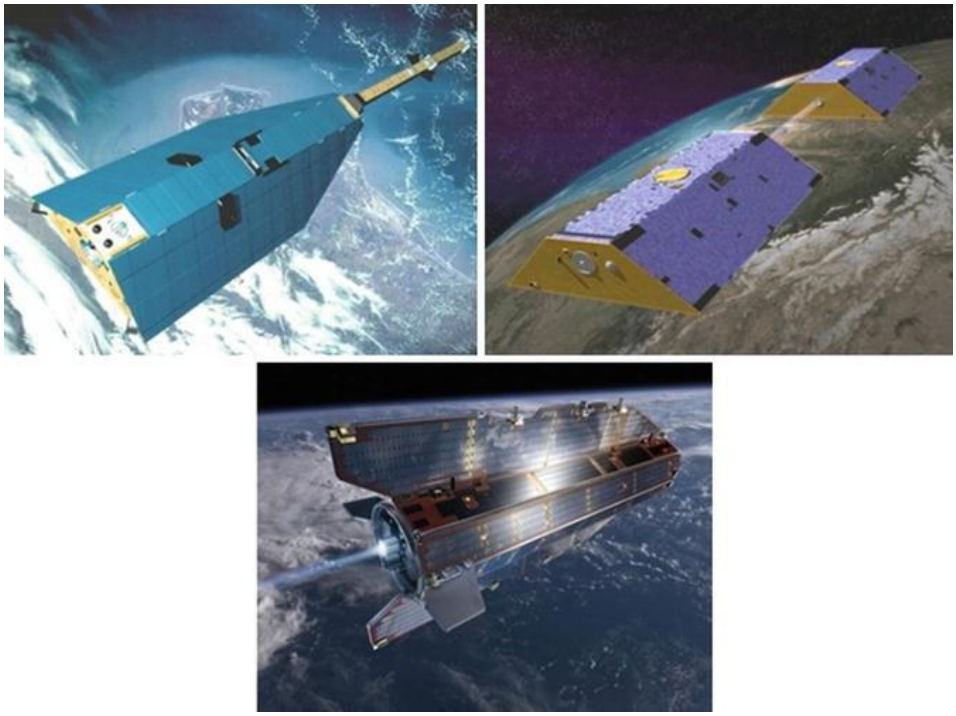

Figure 22 CHAMP-, GRACE-, GOCE-Satellite Projects

https://link.springer.com/referenceworkentry/10.1007/978-3-319-02370-0_29-1?noAccess=true#Fig1

CHAMP is a German-led mission to determine, among other things, the static and time-varying global gravity field. The LEO (454 km altitude) CHAMP satellite is tracked using the high-Earth orbiting (~ 20,000 km altitude) GPS satellites relative to a network of ground stations. The benefit of using high-low SST is that the LEO satellite will "see" many GPS satellites with good geometry relative to the entire low orbit.
The orthogonal accelerometers on board the CHAMP satellite estimate the non-gravitational perturbations. CHAMP was launched in 2000, and the mission was scheduled to run for five years.
The LEO satellite was placed in a near-circular orbit at an inclination angle of 87º to the equatorial plane. This allows for a near-global coverage of observations, with data gaps only at the poles. The CHAMP mission allowed the determination of the global gravity field at a spatial resolution of about 500 km full-wavelength at the Earth's surface. The accuracy of a derived satellite-only geopotential model had been improved by one order of magnitude.

The Gravity Recovery and Climate Experiment, or GRACE, mission flew twin spacecraft in tandem around Earth to study key changes in the planet's waters, ice sheets, and the solid Earth.
GRACE is a USA-German-led mission which followed the CHAMP mission. The mission consists of two CHAMP-identical LEO satellites following one another in nearly the same orbit (~448 km initial altitude), separated by a distance of about 170-270 km.
The low-low SST is measured using two microwave instruments, which provide very accurate observations of the inter-satellite range and the relevant rate of change. This is combined with the high-low GPS-based SST of both satellites. The low-low SST expresses the differences between the orbital perturbations of the two LEO satellites. This enables to recovery the higher resolution features

of the Earth's gravity field. Moreover, the orbital inclination angle is about 88.5º, with respect to the equator.
This five-year mission was launched in 2002, GRACE mission improved upon the CHAMP determination of the global gravity field at low frequencies and also increased the spatial resolution, up to degree and order 120.

COSMIC is a joint Taiwan-US satellite mission primarily oriented toward atmospheric studies. Besides, such mission will also recover the Earth's gravitational signal. This mission was launched in 2004 which comprised a constellation of eight micro-satellites. The satellites altitude ranging from 300 to 700 km, with an inclination angle of about 80º (Hwang, 2001).

GRACE Follow-On (GRACE-FO) continues GRACE's legacy of tracking Earth's water movement across the planet. Monitoring changes in ice sheets and glaciers, underground water storage, the amount of water in large lakes and rivers, and changes in sea level provides a unique view of Earth's climate. https://gracefo.jpl.nasa.gov/

The Gravity Field and Steady-State Ocean Circulation Explorer (GOCE) measures Earth's gravity field and model the geoid with extremely high accuracy. It was launched on 17 March 2009. GOCE is often cited as one of ESA's most elegant space probes due to its sleek shape. The mission ended on 11 November 2013 . GOCE is a European-led mission to determine, among others, the global gravity field of the Earth. GOCE used an LEO satellite (~260 km altitude) in a nearly circular orbit, a three-axis gradiometer (SGG), and a high-low GPS-based SST. This allowed the determination of the static and time-varying components of the global gravity field up to a resolution of degree and order 200, with a global accuracy of 1-cm and 1-mGal, for the computed geoid and gravity anomaly, respectively (Tscherning et al., 2000).

3.1.3.1 Global Harmonic Analysis using Satellite Dynamics, Gravimetry and Altimetry Data

Depending on the type and resolution of the gravitational data, which are input to a spherical harmonic analysis algorithm, three categories of global geopotential harmonic models exist in principle. These are satellite-only low-degree, combined low-degree and high, and ultra-high resolution harmonic models. In what follows, a general discussion regarding those models is presented.

3.1.3.2 Satellite-Only Global Geopotential Models

The processing of LEO satellite data in terms of global gravitational harmonic coefficients yields the so-called satellite-only global geopotential models. A satellite-only harmonic model for global geopotential is usually the outcome of processing a number of different LEO satellite data, regardless of their observational technique. Harmonic analysis from satellite data is based on the satellite orbit perturbations.

The orbital perturbations are primarily gravitational, which are induced by the Earth's mass anomalies and are important for gravity field recovery from LEO satellites. Whereas such gravitational perturbations could be at the sub-decimetre level for T/P mission, they could reach several tens of meters for LEO satellites (Visser and IJssel, 2000).

3.1.3.3 Combined Low, High, and Ultra-High Degree Global Harmonic Models

Due to the attenuation of the gravitational signal with altitude, not all solved-for coefficients are fully sensed by the satellites. Therefore, to enhance the resolution of the low-degree satellite-only harmonic models, they are usually combined with global low-resolution surface gravity and altimetry

data. Such an algorithm greatly reduces the satellite-only models' commission errors (Gruber et al., 1997). These combined solutions are accomplished via the use of a satellite-only model as a reference field for the low-resolution surface data in a GSHA algorithm. The resulting models are referred to as combined low-frequency harmonic models.

To obtain global geopotential harmonic models of higher resolutions, the satellite-only or the combined low-frequency models are usually augmented by global high-resolution altimetry and terrestrial gravity data, in a GSHA process.

3.1.3.4 Tailored Geopotential Harmonic Models

Using a GGM in local geoid solutions via the remove-restore technique, the respective low-frequency features would only be reliable if the model contains local gravity data from the region under consideration (Marsh et al., 1989). Global geopotential models can be refined by a process, which is referred to as tailoring. In such a process, the existing spherical harmonic coefficients, under refinement, are adapted and often extended to higher degrees, using gravity field data that may not necessarily have been used in the global solution for the geopotential model. Tailored geopotential models can be developed either globally or over a particular region. For global geopotential model tailoring, the same concept is valid, recognizing that in such case, one uses a global data set as input.

3.2 Digital elevation model

As a gravimetric quantity, the geoid undulation can be expanded in terms of global spherical harmonic coefficients as follows

$$N(\theta,\lambda.\,r) = \left(\frac{GM}{r\gamma}\right)\sum_{n=0}^{n\,max}\left(\frac{a}{r}\right)^{n}\sum_{m=0}^{n}(\bar{C}^{*}_{nm}\cos m\lambda + \bar{S}_{nm}\sin m\lambda)\,\bar{P}_{nm}\,(\cos\theta). \quad (3.28)$$

In spherical approximation, the geoid and the reference ellipsoid are geometrically represented by the mean terrestrial sphere of radius R = 6371 km. So, the equatorial radius a is replaced by the mean radius of the Earth R, the point of normal gravity γ by the mean Earth gravity GM/R^2, the rigorous geocentric radius r (at the geoid) is replaced by R, and the geocentric latitude θ by the geodetic latitude φ (Heiskanen and Moritz, 1967). Hence, substituting these values in Eq. (3.28), the geoidal height can be expanded in the following surface harmonics

$$N(\varphi,\lambda.) = \left(\frac{GM}{r\gamma}\right)\sum_{n=0}^{n\,max}\left(\frac{a}{r}\right)^{n}\sum_{m=0}^{n}(\bar{C}^{*}_{nm}\cos m\lambda + \bar{S}_{nm}\sin m\lambda)\,\bar{P}_{nm}\,(\sin\varphi). \quad (3.29)$$

The height of the Earth topography can also be expanded in surface harmonic series in analogy to the geoid in Eq. (3.29) (Burša, 1971; C. C. Tscherning and Forsberg, 1986a). This is based on the assumption that the Earth's physical surface is smooth enough to be treated as if it were a gravimetric quantity. Namely, the height H of the topography above mean sea level can be expressed as

$$H(\varphi,\lambda.) = R\sum_{n=0}^{n\,max}\sum_{m=0}^{n}(\bar{A}_{nm}\cos m\lambda + \bar{B}_{nm}\sin m\lambda)\,\bar{P}_{nm}\,(\sin\varphi), \quad (3.30)$$

where $\bar{A}_{nm}$ and $\bar{B}_{nm}$ are the fully normalized (unitless) harmonic coefficients (of degree n and order m) of the Earth's topographic height above mean sea level, $\bar{P}_{nm}\sin\varphi$ is the usual fully normalized associated Legendre function, and nmax is the maximum degree of the global topographic harmonic model. Eq. (3.30) can be rearranged as follows

$$H(\varphi,\lambda.) = R\sum_{n=0}^{n\,max}\sum_{m=0}^{n}(\bar{D}_{nm}\cos m\lambda + \bar{E}_{nm}\sin m\lambda)\,\bar{P}_{nm}\,(\sin\varphi), \quad (3.31)$$

with

$$\overline{D}_{nm} = R.\overline{A}_{nm} ,$$

$$\overline{E}_{nm} = R.\overline{B}_{nm}.$$

So, both $\overline{D}_{nm}$ and $\overline{E}_{nm}$ are still fully normalized harmonic coefficients but now have meter dimension. This reformulation is intuitively useful since the topographic height harmonic coefficients are computed in practice directly in meter units as will be clarified below.

Theoretically, if the Earth terrain height (or bathymetry in marine areas) H(φ,λ) is continuously available over the whole globe, then the corresponding fully normalized harmonic coefficients can be determined by (Burša, 1971),

$$\overline{D}_{nm} = \frac{1}{4\pi R^2} \iint_e H(\varphi,\lambda)\ \cos m\lambda\ \overline{P}_{nm}\sin\varphi.\, R^2 \cos\varphi\, d\varphi\, d\lambda \tag{3.32}$$

$$\overline{E}_{nm} = \frac{1}{4\pi R^2} \iint_e H(\varphi,\lambda)\ \sin m\lambda\ \overline{P}_{nm}\sin\varphi.\, R^2 \cos\varphi\, d\varphi\, d\lambda\ . \tag{3.32a}$$

Practically, however, the formal global terrain height data is often global mean terrain heights of a specific resolution, say I x 2I global equiangular grid cells. Then, the integrals in Eq. (3.32 and 3.32a) will be replaced with discrete summations as follows (Fan, 1998),

$$\overline{D}_{nm} = \frac{1}{4\pi R^2} \sum_{i=1}^{I} \sum_{j=1}^{2I} H(\varphi_i,\lambda_i)\ \cos m\lambda_j\, \overline{P}_{nm}(\sin\varphi_i).\, R^2 \cos\varphi_i\, \Delta\varphi\, \Delta\lambda \tag{3.33}$$

$$\overline{E}_{nm} = \frac{1}{4\pi R^2} \sum_{i=1}^{I} \sum_{j=1}^{2I} H(\varphi_i,\lambda_i)\ \sin m\lambda_j\, \overline{P}_{nm}(\sin\varphi_i).\, R^2 \cos\varphi_i\, \Delta\varphi\, \Delta\lambda \tag{3.33a}$$

where (φ_i,λ_i) are the geodetic coordinates of the running block center and Δφ, Δλ are the (equal) latitude and longitude grid intervals.

On the other hand, the immediate output of the spherical harmonic analysis of global mean sea surface height data is a set of harmonic sea surface coefficients. Such input data can be obtained from oceanic altimetry data and an oceanic geoid model, which a global geopotential model can represent. It should be mentioned that such global SSH coefficients could be predicted simultaneously during GSHA procedures for high-degree geopotential models, which utilize, among other data, global altimetry data. For instance, during the solution for the EGM96 geopotential model, a global SSH model, up to degree and order 20, was solved simultaneously, based on T/P and GEOSAT altimetry data (Lemoine et al., 1996). Being more related to oceanographic applications, the SSH harmonic models are considered outside the scope of the current investigation.

4. Detailed review of existing research

Overview

This chapter illustrated a historical narrative of Gravimetric, hybrid, or Geoid-quasi-geoid determination attempts for most countries the worldwide, with an explanation of whether the calculated geoid solution is based on only gravity observations or gravity and geometrical observations as GPS/dh, in addition to all the available geoid solutions for Egypt with more details and continuous-time frame from the pioneer geoid solutions in 1960 up to this time. It also lists in more detail the attempts to calculate the geoid with an indication of the resolution and spatial distribution of the gravity observations in the MENA region.

4.1 African geoid solutions attempt

The African Geoid Project was initially established as a Committee for Developing Countries of the IAG. After the General Assembly of the IAG in Sapporo in July 2003, the project was taken over as a project of Commission II (Gravity Field Commission) of the IAG. The project is driven by a small working group of African geodesists who collaborate to obtain data and investigate appropriate models. Ideally, there would be near-continuous data coverage at a station spacing of the order of 5-10 km. These data could then be used to interpolate gravity anomalies on a regular 5' (about 8 km) grid, from which a geoid model can be calculated. The first attempt to compute a preliminary geoid model for Africa was achieved in 2003 (Merry, 2003) . In this model, the gaps in the 5' terrestrial data set (Fig. 23) were filled using the EGM96 geopotential model (Lemoine et al., 1998), and the geoid was computed in several steps:

The African Geoid Project was initially established as a Committee for Developing Countries of the IAG. The pioneer attempt for the Africa geoid model computation was achieved in 2003 (Merry, 2003). EGM96 was used to fill the severe gaps in the available terresterial data at that time, and the geoid was computed in several steps:

- EGM96 was used to comput the long wavelength of the height anomalies quasi- geoid,
- The short-wavelength component was computed using reduced gravity anomalies in a two-dimensional convolution representation of the Stokes' integration,
- DEM was used to compute the terrain effect (Molodensky term) (Hastings and Dunbar, 1998).

The height anomalies were converted to geoidal heights using (Rapp, 1997) spherical harmonic representation of the separation between the two surfaces.

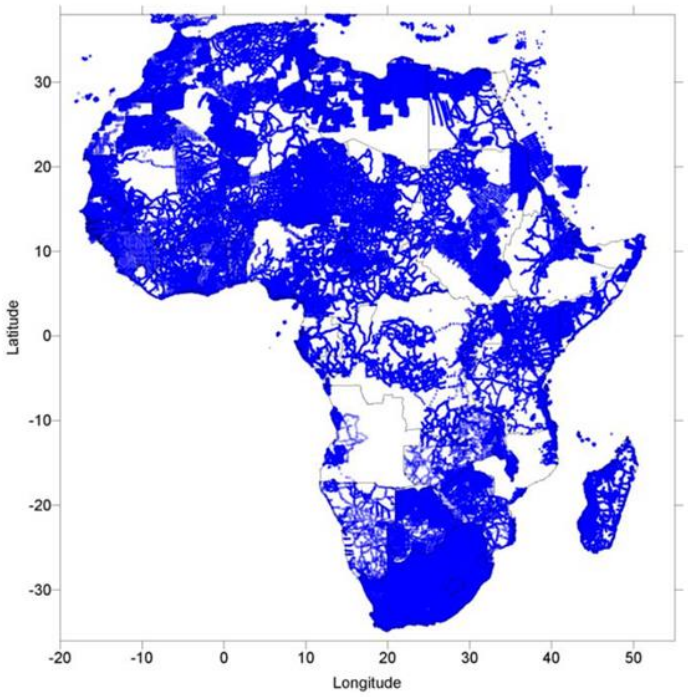

Figure 23 The terrestrial Gravity data set of Africa (Merry, 2003)

Terrestrial data sets were produced by the Universities of Leeds and Cape Town (Fairhead, 1988; Gysen and Merry, 1987). As shown in Fig. 24, there are many regions suffering from spars and poor distribution of data coverage (e.g., in the interior of Angola, Egypt) .

GPS/leveling data were used to validate the obtained geoid model (AGP2003), Data were obtained from Algeria, Egypt, and South Africa (Fig. 24). the obtained results showed significant biases existed among the three countries, Table 3 summarized those comparisons.

There is a multiplicity of potential sources for these biases:

- errors in the long-wavelength components of the EGM96 geopotential model,
- differences in the GPS reference frame used,
- biases in the vertical datums used in the different countries,
- cumulative systematic errors in the levelling networks.

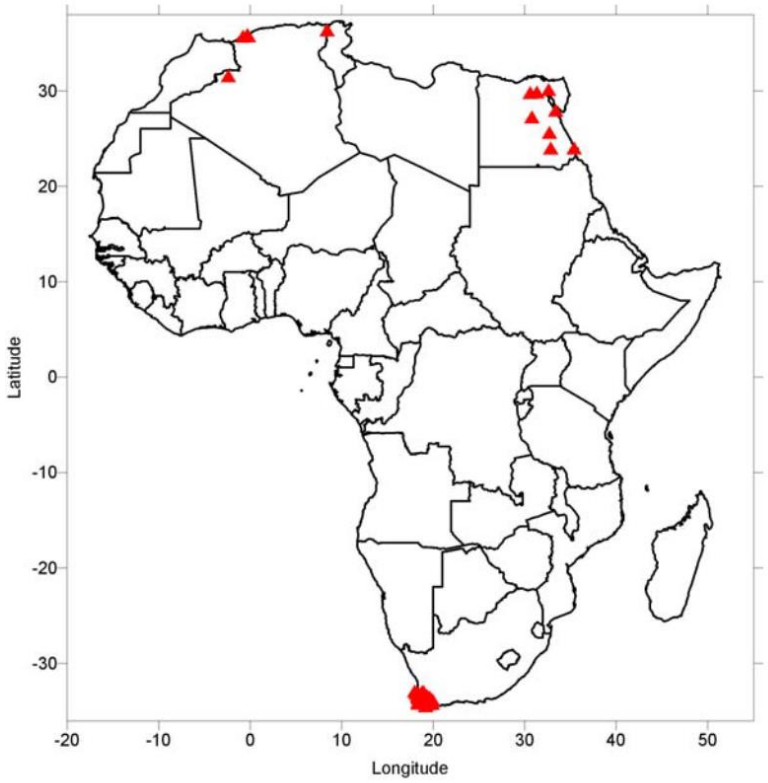

Figure 24 GPS/levelling data points (Merry 2003).

Table 3 Comparison of GPS/levelling - AGP2003 (Merry 2003)

Region	No. Pts.	Bias (cm)	Std. Dev. (cm)
Algeria	13	-17	48
Egypt	8	+124	80
South Africa	42	-63	9

A $5' * 5'$ mean gravity anomaly grid developed at Leeds University was used to compute that geoid model. We regret that this data set has never become available since then again. For the geoid computed by Merry et al. (2005), the remove-restore method was employed based on the EGM96 geopotential model (Lemoine et al. 1998).

Another geoid model for Africa (Fig. 25) has been computed by (H. A. Abd-Elmotaal et al., 2020) . This geoid model employed the window remove restore technique with the EGM2008 geopotential model (Pavlis et al., 2012), up to degree and order 2160, and a tailored reference model (computed through an iterative process), up to degree and order 2160, to fill in the data gaps, the values of the AFRgeo2019 African geoid range between -55:34 and 57.34 m with an average of 11.73 m.

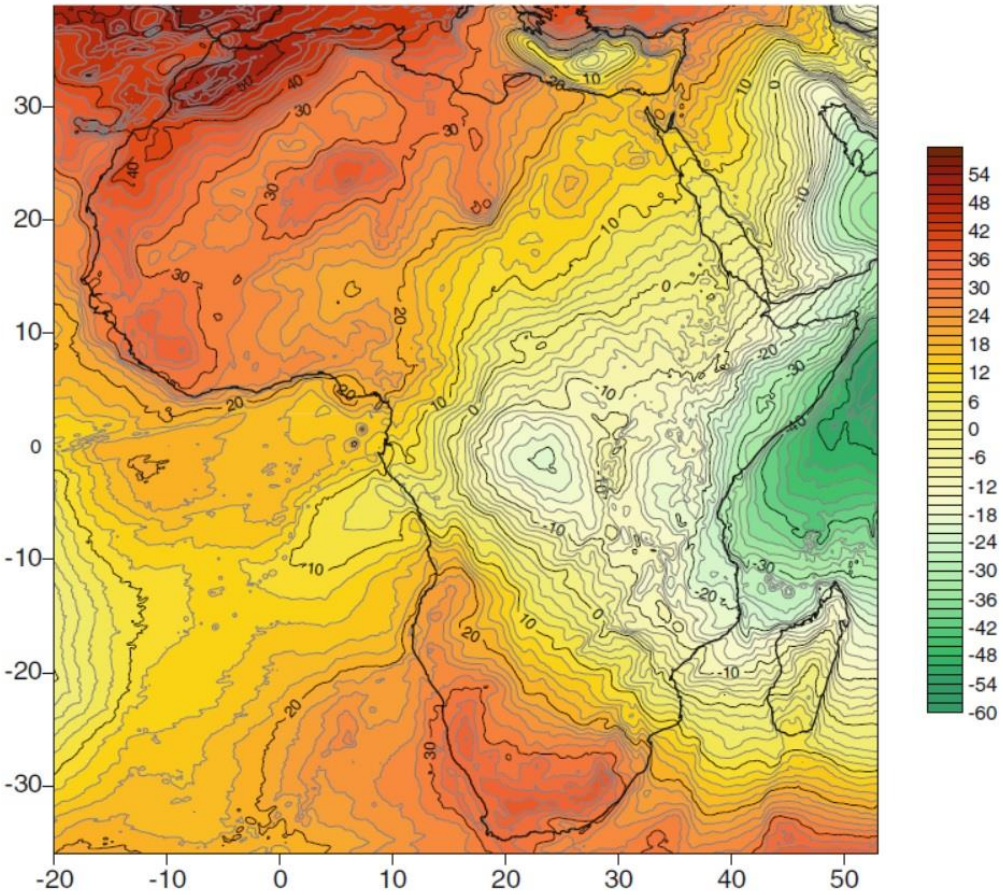

Figure 25 The AFRgeo2019 African de-trended geoid. (Abd-Elmotaal et al. 2020)

4.1.1. Egypt Geoid determination attempts

All the previous attempts to determine the geoid in Egypt from 1980 to the present have severe shortage, which reached to scarcity, in the distribution, density, and accuracy of the geoid data, as well as GPS/H data points.

Egyptian Geodetic Datum (EGD) was defined in 1907 with Helmert 1906 ellipsoid as a reference ellipsoid. Mean Sea Level (MSL) was adopted as Egypt's geoid (Cole, 1944).

The first pioneering attempt to determine the geoid of Egypt was Al- Naggar's attempt, through which he was able to determine the first geoid of Egypt using the LSC technique and heterogeneous data with an accuracy of 3.3 m in terms of RMS (Dawod, 2009).

Three attempts were carried out in 1993, El-Tokhey and Nassar et al. (1993), had developed a geoid of Egypt, while , Saad (1993) has investigated the accuracy improvements and redefinition of the Egyptian vertical control networks.

In 1995 El-Shazly (1995) continued to investigate the redefinition of Egypt's vertical datum while, El-Sagheer (1995) established a DTM called DTM-95 which was used to predict the geoid with an accuracy of 3.71 m in terms of RMS, In the same year The Egyptian Survey Authority established two national GPS geodetic control networks called HARN and NACN (Dawod, 2009).

In 1997, an accurate gravity framework for Egypt was established through the Egyptian National Gravity Standardization Network 1997 (ENGSN97). The ENGSN97 150 gravity points (plus another 100 stations) have been utilized by (Dawod, 1998).

The accuracy of the geoid began to improve relatively with the beginning of the year 2000, when the University of Ain Shams University developed a geoid called (ASU2000) with an accuracy of 0.6 m and 1m as internal and external accuracy respectively, Tscherning et al. (2001)continued for developing by computing geoid for the area of Lake Nasser with an accuracy of 0.26 m in RMS Saad and Dawod (2002).

Numerous attempts were carried out in the period between 2007 to 2015, and we mention that, for example, but not limited to, (H. Abd-Elmotaal, 2006), who developed a geoid by combining gravity anomalies with EGM96, as well as Dawod (2008) attempt for computing a precise geoid for Egypt.(Dawod, 2009), and also (Al-Krargy et al., 2014) attempt was developed with an accuracy of ±18.4 cm.

(El-Ashquer et al., 2017) had improved Egypt's hybrid local geoid model, with hybrid residual height anomalies ranging from –1.5 m to +0.9 m.

On December 20 (Gad et al., 2020) were checked the possibility of determining the geoid of Egypt using the LSC technique, but due to data lack and irregular distribution, a data window was selected for computing the geoid, and the obtained accuracy for this area was 11 cm in terms of standard deviation.

Although during the past two decades, more data were collected for the gravity field of Egypt, as the Fig. 26 shows, there is a heterogeneity data distribution over the entire area of Egypt, as well as a few numbers, and sparsely data in some regions, as it is obvious from Fig. 26 there are no data in the western and eastern desert.

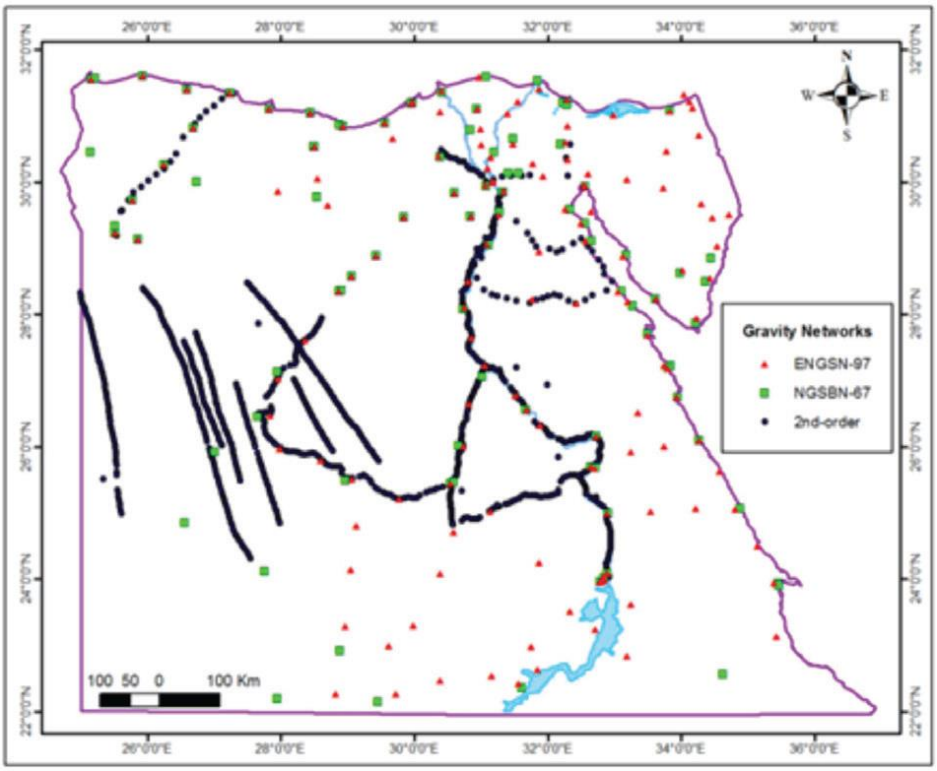

Figure 26 Spatial distribution of the available gravimetric data utilized up to the year 2017 (Dawod and Hosny, 2017)

4.1.2. Libya Geoid determination attempts

The first attempt, a geoid map based on 19 levelled Doppler, was computed by IGN - French Mapping Agency (Institut Géographique National). In that attempt, IGN database have been used, as the only source of data, the vertical deflections obtained from the comparison of the astronomical coordinates and their respective WGS72 to the levelled Doppler points above the same ellipsoid. From these computations, IGN drew the map (Fig. 28) of Libyan geoidal undulations (Swassi, 2000).

Aero - Service Corporation (ASC) computed a second geoidal map. Two geoidal maps related to two different datums were added, one concerning the local datum, European Libyan datum 1979 (ELD79), and the other one with relation to the WGS72 datum (Swassi, 2000).

In 1997 the third attempt to determine gravimetric geoid for the area of Libya was achieved using data as: (a) 5'x 5' gridded value of Bouguer anomalies (onshore) and free-air anomalies (offshore) based on the African Gravity Project, and released for geoid computation by Geophysical Exploration Technology University of Leeds (GETECH), (b) global (5'x5') Terrain Base digital terrain model and (c) the OSU91A and EGM96 geopotential models. Two geoid/quasigeoid models have been computed. The first model is OSU91A and the second one is the EGM96 global model (Łyszkowicz and Wahiba, 1998).

Due to the lack of appropriate data, a rough estimation of the computed geoid/ quasigeoid model (Fig. 27) have been inevitable, and the accuracy of geoidal height difference depends on the accuracy of the three components: $\Delta N_{GGM,}$ $\Delta N_{\Delta g,}$ $\Delta N_{TOPO,}$

That average error in ppm for contribution from the geopotential model is below two ppm. The other two contributions are relatively small, which were below one ppm. Thus the total relative accuracy of these geoid/quasigeoid models is estimated on a few ppm (about two ppm) (Łyszkowicz and Wahiba, 1998).

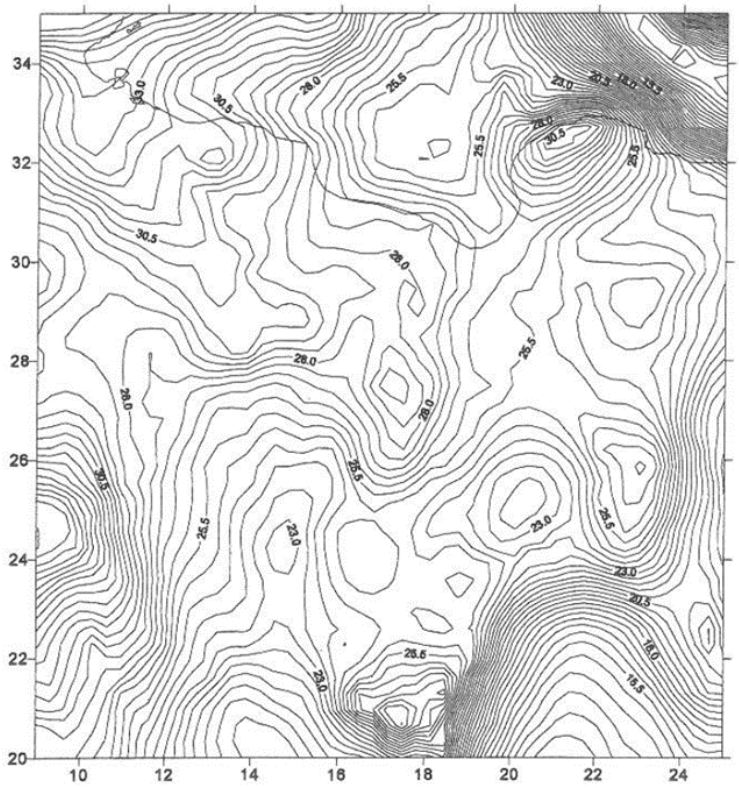

Figure 27 Geoid (quasi geoid) for the area of Libya (Łyszkowicz and Wahiba 1998)

The fourth geoid determination for Libya, by A. M. Swassi, was conducted in 2000. He used a method based on the remove-restore technique to 360 x 360 spherical harmonic reference model OSU91A with the terrain effect consideration (Fig. 28) (Swassi, 2000).

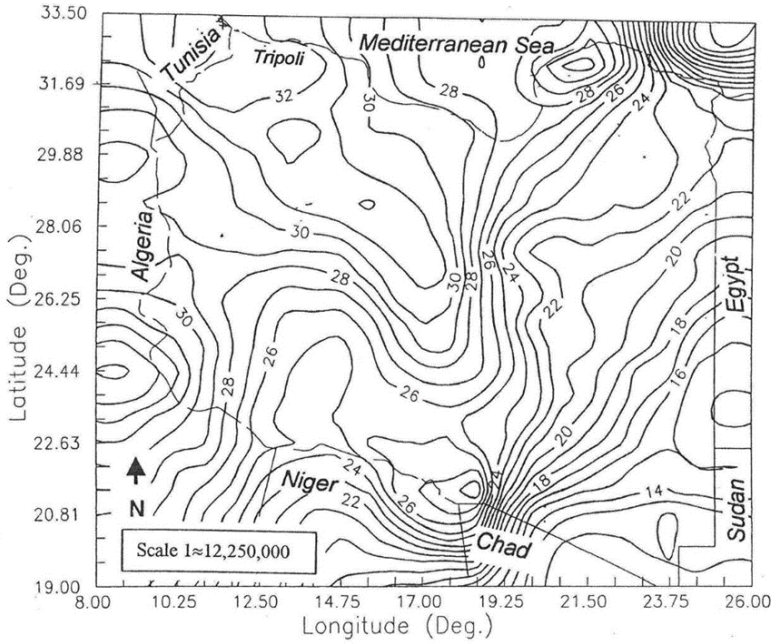

Figure 28 The geoidal undulation map with 1 m *interval (Swassi 2000)*

4.1.3. Sudan Geoid determination attempts

The first geoid model for the area of Sudan was developed by Adam (1967) at Cornell University, USA. This geoid model was based on deflections of the vertical determined on 46 astrogeodetic stations. Due to a lack of data, the accuracy of this model has not been estimated. The next gravimetric geoid model based on terrestrial gravity data, topography data, and the Goddard Earth Model (i.e., GEM-T1) was developed by Fashir (1991) using a modified Stokes' kernel. The accuracy of the following geoid model developed by Fashir et al. (1997) using the same method, the same terrestrial and topography data, and the EGM96 (Earth Gravitational Model 1996) was estimated to be 1.43 m using Doppler/levelling data. The latest geoid model for the area of Sudan was developed by Abdalla (2009). His model is based on terrestrial gravity data and the GRACE-based GGM (i.e., EIGEN-GRACE02S) up to d/o 120 using the least-squares modification of Stokes integration formula, developed at the Royal Institute of Technology (KTH), Stockholm, Sweden. The fit of this model to the available GNSS/levelling data is 30 cm in terms of the standard deviation of differences.

In 2014, The Sudanese SUD-GM2014 gravimetric geoid model was computed from the available terrestrial mean free-air gravity anomalies and TIM-R4 GOCE-only global geopotential model, and the high-resolution SRTM30_PLUS global digital elevation model; the computation has been performed by using the remove-compute-restore procedure and the least-squares collocation method.

The SUD-GM2014 model (Fig. 29) has been evaluated using geoid heights at 19 GNSS/levelling points distributed over the country, showing an overall accuracy of 30 cm (Godah and Krynski, 2014).

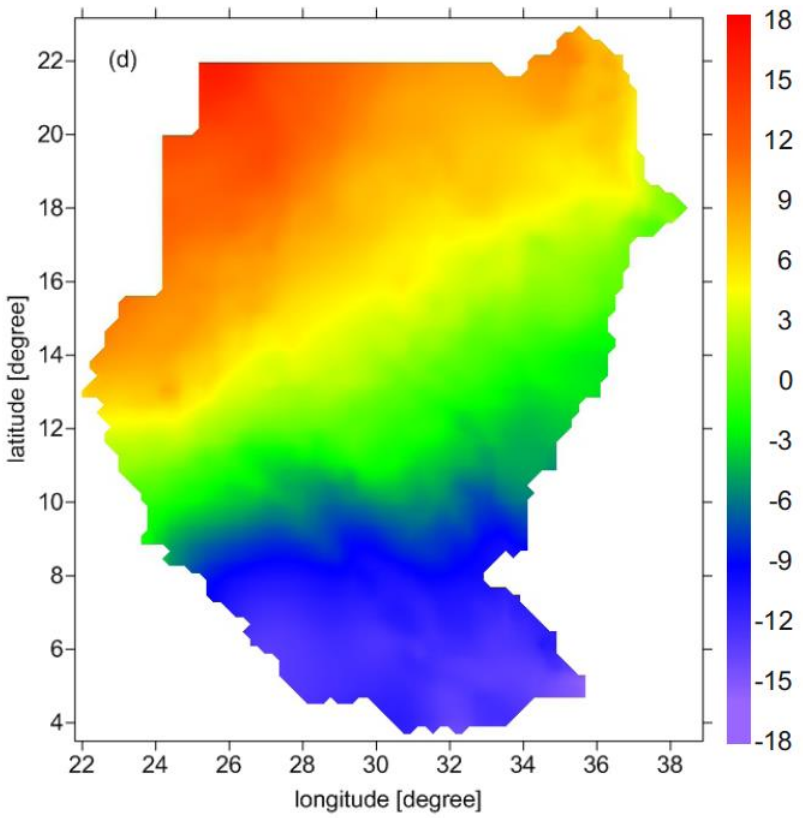

Figure 29 The gravimetric geoid model SUD-GM2014 [m] *(Godah and Krynski 2014)*

4.1.4. Algeria Geoid determination attempts

The first determination of a preliminary geoid in a small zone in the north of Algeria was done in 1997 (Benahmed Daho and Kahlouche, 1998), using the Least Squares Collocation (LSC) method and the Gravsoft software.

In the second gravimetric solution over the whole of Algeria territory, the BGI gravity data and topographic information were included (Benahmed Daho, 2000).

In 2004 Algerian quasi-geoid was computed via Fast Fourier Transformation using the Remove-Restore procedure by integrating the new gravity data supplied by GETECH through the agreement between the National Centre of Space Techniques/Geodetic Laboratory and the University of Leeds/GETECH.

The comparisons of the new quasi-geoid with GPS/Levelling data provide, after fitting, RMS differences of about ± 11 cm for the north part of Algeria (Fig. 30) (Mammar 2019)et al. 2019).

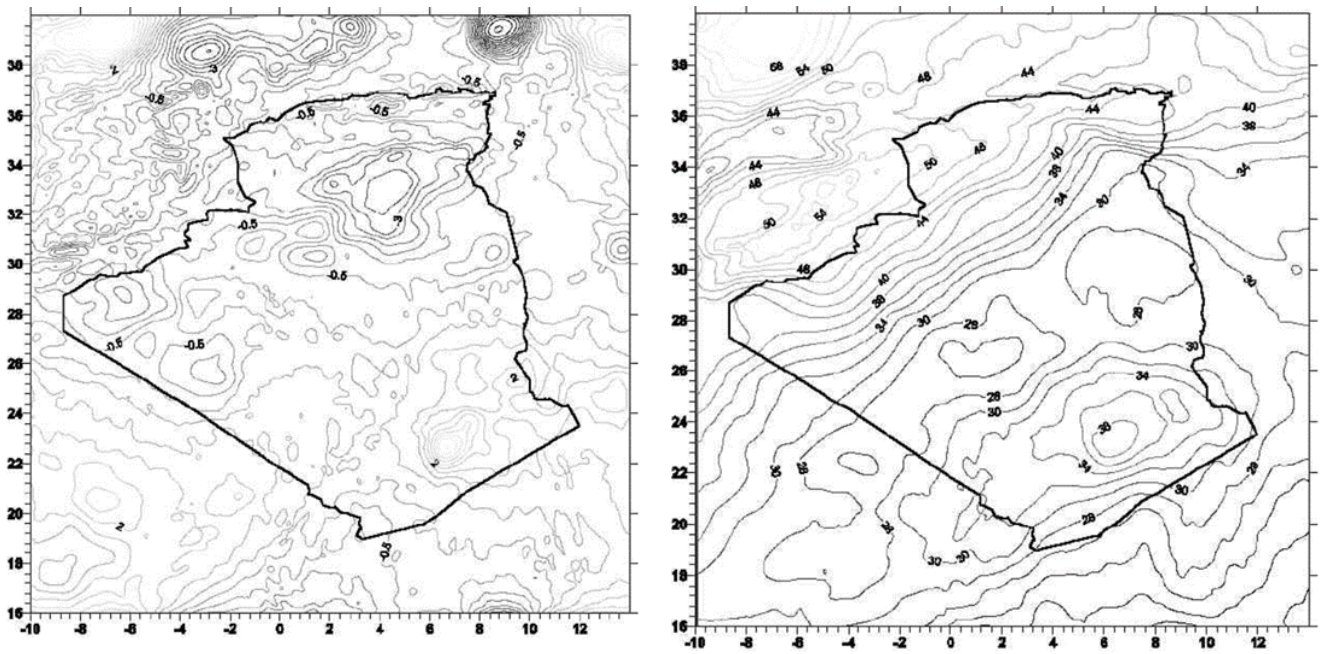

Figure 30 Maps of the Residual quasi-geoid (left picture) and the quasi-geoid solution (right picture) in Algeria. The statistics of the total quasi-geoid values are ranging from 17.69 *to* 60.65*, with mean value* 35.15 *and standard deviation* 8.83 m*. (Mammar et al. 2019)*

4.1.5. Morocco Geoid determination attempts

Several studies have taken geoid computations in Morocco and the surrounding area as an objective (Benaim 1995; Benaim et al. 1998; Groten and Roehrich 1989; Sevilla 1995, 1997). Unfortunately, only MGG97 (Benaim et al., 1998) covers Morocco completely; the other geoids partially cover the northern part. MGG97 is the official geoid model used in Morocco to calculate the geoid undulations. These calculated geoid and previous geoids existing for this study area (MGG97 and EIGEN-CG01C) are compared to the geoid undulations corresponding to Morocco's 6 GPS/levelling points. The Moroccan geoid (MORGEO) improves precision and reliability, fitting the geoidal heights of these 6 GPS/levelling points with more accuracy than the previous geoids.

The Moroccan geoid (MORGEO) shows a minor discrepancy (Fig. 31) with the observed geoid undulations obtained for the 6 GPS/levelling points available in Morocco compared to previous geoids. This improvement is most remarkable when we compare this new geoid with the official geoid model for Morocco (MGG97) because that geoid has a standard deviation of 29.5 cm instead of the 41.3 cm corresponding to MGG97 (Corchete et al., 2007).

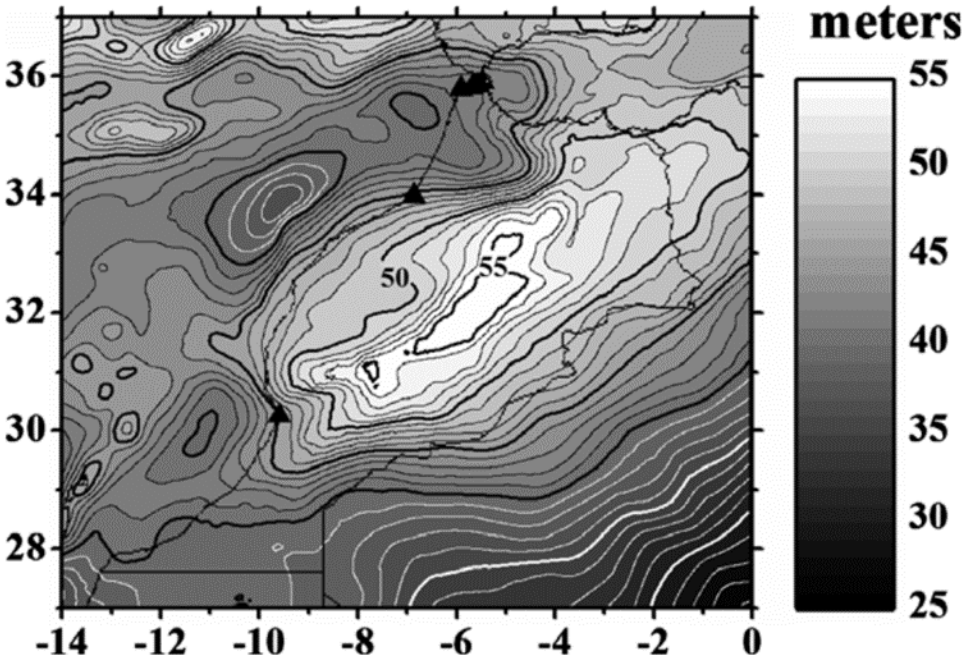

Figure 31 Spatial distribution of the GPS/levelling points used as control data set projected on Moroccan geoid (MORGEO). Contour interval: 1.0 m*(Corchete et al. 2007)*

An attempt for Morocco Geoid determination was recently calculated in 2020 by "Moroccan Geoid Determination from Spatial Gravity Using Recent GGM," (El Hassan, 2020). Depending on the considered area, we notice that the amplitude of the differences changes and remains between 10 and 15 cm for the best cases. We also note a variable value of bias that reaches 50 cm in certain areas. This shows the need to apply a model for fitting geoid grid to GPS levelling measurements and many more points to use this model properly.

The reset of African attempts for geoid determinations is listed in Table 4 hereafter below.

Table 4 The list of historical attempts for geoid determination of African continent

No.	Country	Model Name	Model Type	Data Used	Year	References
1	South Africa	SAGEOID10	Hybrid Geoid	better than 10cm	2010	(Chandler and Merry, 2010)
2	Ethiopia	ETH-GM21/ETH-QM21	Gravimetric Geoid and Quasi-Geoid		2021	(Belay et al., 2021)
3	Tanzania	N/A	Gravimetric Geoid		2007	(Olliver, 2007)
		TZG08			2008	(Ulotu, 2009)
4	Nigeria-Lagos State	N/A	Gravimetric Geoid	2.37 cm of RMS	2016	(Odumosu et al., 2016)

No.	Country	Model Name	Model Type	Data Used	Year	References
5	Zambia	d ZG201	Gravimetric Geoid	7 cm of RMS	2016	(Saka, 2019)
6	Madagascar		Hybrid Geoid	0.7 m of RMS	1998	(Bonneville et al. 1988)
7	Botswana	-	Geometric Geoid		2016	(Manisa et al., 2016)
8	Kenya	-	Geometric Geoid	about 1 cm of RMS and STD. dev.	2014	(Odera et al. 2014)
9	Cameroon	CGM05	Gravimetric Geoid	About 11cm STD. dev.	2005	(Kamguia et al., 2007)
10	Zimbabwe	-	Gravimetric Geoid	N/A	1997	(Nyamangunda, 1997)
11	Papua New Guinea	PNG94	Gravimetric Geoid	N/A	1994	(Kearsley and Ahmad, 1996)
		PNG08	Gravimetric Quasi-Geoid	0.2 m STD.dev.	2011	(Stanaway, 2012)
12	Ghana	GGG2017	Gravimetric Geoid	45.7 cm STD.dev.	2017	(Yakubu et al. 2017)
13	Uganda	UGG2014	Gravimetric Geoid	7.0 cm STD.dev	2014	(Ssengendo et al. 2015)
14	Tunisia	TNG	Gravimetric Geoid	1.64 cm STD.dev	2018	(Ismail, 2016)
15	Benin	-	Gravimetric Geoid	0.412m RMS		(Olujimi et al. 2019)

4.2. Attempts for geoid determination of the Australian continent

Many regional models of the geoid /quasi-geoid have been available for the Australian continental since 1967. These models were historically used to reduce geodetic surveying measurements to the non-geocentric Australian National Spheroid (ANS)(Mccubbine et al., 2021).

While the first geoid-ANS separation model, published by Fischer and Slutsky (1967), was computed from ~600 astrogeodetic deflection observations, the latest model (AUSGeoid2020) was calculated by Featherstone et al. (2018) with an accuracy (of one sigma) of 50–60 mm across most of the Australian landmass, increasing to ~100 mm in regions of steep horizontal gravity gradients or the mountains.

The most recently released official model for GPS/GNSS surveyors, AUSGeoid2020, was explicitly calculated to determine Australian Height Datum heights from Geocentric Datum of Australia 2020 ellipsoidal heights in a more direct manner without the need for post-surveying adjustments.

Most of the historical attempts for Australian continental are listed in Table 5 to describe the models with their development and accuracy from 1993 to 2020.

Table 5 The list of historical attempts for geoid determination of the Australian continent

No.	Country	Model Name	Model Type	Data Used	Year	References
1	Australia	(AUSGEOID93)	Gravimetric Geoid	N/A	1993	(Steed and Holtznagel, 1994)
2		(AUSGEOID98)		0.364 m RMS	1998	(Featherstone et al., 2001)
3		(AUSGEOID09)		N/A	2009	(Featherstone et al., 2010)
4		(AUSGEOID2020)	Hybrid Quasi-Geoid	27 mm STD.dev	2018	(Featherstone et al., 2018)
5	New Zealand	(NZGEOID05)	Gravimetric Quasi-Geoid	8 cm STD.dev	2005	(Amos, 2007)
6		(NZGeoid09)		6 cm STD.dev	2009	(Claessens et al., 2011)
7		(NZGM2010)		7 cm STD.dev	2010	(Abdalla and Tenzer, 2011)
8		(NZGeoid2016)		3 cm STD.dev	2016	(Amos, 2016)

No.	Country	Model Name	Model Type	Data Used	Year	References
9		(NZGeoid2017)		±48 mm STD.dev	2017	(McCubbine et al., 2018)
10	Papua New Guinea	(PNG94)	Gravimetric Geoid	N/A	1994	(Kearsley and Ahmad, 1996)
		(PNG08)	Gravimetric Quasi-Geoid	0.2 m STD.dev	2011	(Stanaway, 2012)

4.3. Attempts for geoid determination of Asian continent

Many Asian and Asia-Pacific (AP) region countries have invested various sources in improving the accuracy of the geoid models. They have increased the use of new satellite gravity data and remote sensing satellite data to update the accuracy of digital elevation models, which are essential for geoid calculation. Other countries increase GPS/levelling observations used to evaluate and control the computed gravimetric geoid; all these efforts lead to the enhancement geoid for Asian countries. In the following, several of these attempts have been listed and placed in Table 6 to give a historical overview of all these attempts with the type and accuracy of the calculated geoid.

Table 6 The list of historical attempts for geoid determination of the Asian continent

No.	Country	Model Name	Model Type	Data Used	Year	References
1	Russia	(RGG-2003)	Gravimetric Quasi-Geoid	N/A	2003	(Medvedev and Nepoklonov, 2003)
2	Kazakhstan	(KazGM2015)	Gravimetric Geoid	0.177 m STD.dev	2015	(Shoganbekova et al. 2015)
3	Iran	(IRG2016)	Gravimetric and Hybrid Geoid	23 cm RMS	2016	(S. A. Saadat, 2016) (Saadat et al. 2018)
4		(IRG2018)		24 cm STD.dev	2018	(Ramouz et al., 2019)
5		(IRLG2020_Tehran)	Gravimetric Geoid	8.9 cm. STD.dev	2020	(Ramouz and Safari, 2020)

No.	Country	Model Name	Model Type	Data Used	Year	References
						(Ramouz et al., 2020)
6	China	Xinjiang and Tibet	Gravimetric Geoid	18 cm STD.dev	2013	(Shen and Han, 2013)
7	Japan	(JGEOID93)	Gravimetric Geoid	8.6 cm STD.dev	1993	(Kuroishi, 1995)
		(GSIGEO96)	Hybrid Geoid	7 cm RMS	1996	(Fukuda et al., 1997)
		(JGEOID98)	Gravimetric Geoid	Improved by 29 % than JGEOID93	1998	(Kuroishi, 2001)
		(GSIGEO2000)	Hybrid Geoid	4 cm throughout nearly the whole region	2000	(Kuroishi et al. 2002) (Nakagawa et al., 2003)
		(JGEOID2000)	Gravimetric Geoid	14.3 cm. STD.dev	2000	(Kuroishi, 2001)
		(JGEOID2004)	Gravimetric Geoid	9.2 cm STD.dev	2004	(Kuroishi and Keller, 2005)
		(JGEOID2008)	Gravimetric Geoid	10 cm. STD.dev	2008	(Kuroishi, 2009)
		(GSIGEO2011)	Hybrid Geoid	1.8 cm. STD.dev	2011	(Miyahara et al. 2014)
8	South-East of Asia	South-East	Gravimetric Geoid	N/A	1999	(Kadir et al. 1999)
9	Brunei	-	Gravimetric Geoid	± 0.3 m. STD.dev	2014	(Lyszkowicz et al. 2014)

Table 6 summarizes Asian countries' attempts for geoid determination with their accuracies and the types of obtained geoid solutions during the period from 2003 up to 2020. We can note that many countries in the region have invested considerable resources in improved geoid models where these investments have achieved some of their goals for determining the geoid and introduced alternative height references for these countries with incredible accuracies as a few centimeters in Japan and sub-decimeter in Iran while unfortunately, the rest countries of Asian region are still suffering from insufficient of terrestrial gravity field data coverages.

4.4. Attempts for geoid determination of the European continent

The Institute of Geodesy (IfE) stated European geoid and quasi-geoid calculations in the early 1980s using mean gravity values. After the 1980s, a combination of point gravity values with digital topography models and global satellite gravity field solutions was introduced. Based on local to regional research, corresponding continental calculations for Europe were carried out from the beginning of the 1990s. This work has been carried out since 1990 with the support of the International Association for Geodesy (IAG).

With the support of the IAG, gravity and topographic data were regularly updated and computed in combination with current satellite gravity field models into high-resolution geoid- and quasi-geoid models, as shown in Fig. 32 (https://www.ife.uni-hannover.de/en/).

The following gravimetric solutions became more important, while the detailed historical attempts for geoid determination for the European continent have been listed hereafter in table 7

- **EGG1997** (European Gravimetric (Quasi) Geoid 1997), (Denker and Torge, 1998),
- **EGG2008**, (Denker, 2013),
- **EGG2015**, (Denker et al., 2018).

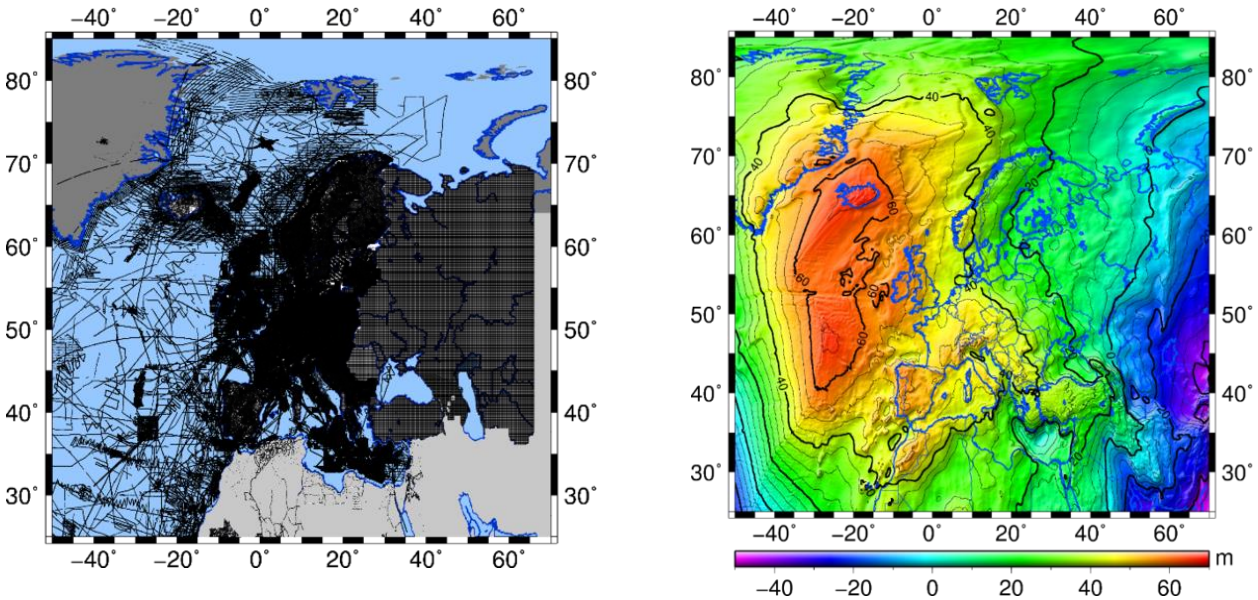

Figure 32 EGG2015 - Gravity field data (left picture, black: terrestrial; blue: altimetric; grey: global fill values), and EGG2015 – European Gravimetric (Quasi)Geoid 2015 (right picture), (https://www.ife.uni-hannover.de/en/)

Table 7 The list of historical attempts for geoid determination of the Asian continent

No.	Country	Model Name	Model Type	Data Used	Year	References
1	Ukraine	(UFM/UFMC)	Gravimetric Geoid	N/A	1995	(Marchenko et al. 1995)
		(UGG2013)		N/A	2013	(Corchete, 2013b)
2	Ukraine and Moldova	(UQG2006)	Gravimetric Quasi-Geoid	8 cm STD .dev	2006	(Marchenko et al. 2007)
		(UQG2007)		4 cm RMS	2007	(Marchenko and Kucher, 2008)
		(UQG2011)		smaller than 4 cm STD .dev	2011	(Marchenko et al. 2015)
3	France	(QGF96)	Gravimetric Quasi-Geoid	12.8 cm STD .dev	1996	(H. Duquenne, 1997b)
		(RAF96)	Hybrid Quasi-Geoid	standard deviation of 2.5 cm and a bias at the 1 cm level	1996	(H. Duquenne, 1997a)
		(GGF97)	Gravimetric Geoid	STD. dev from 10 to 15 cm in plain areas and from 30 to 50 cm on the reliefs	1997	(I.G.N., 1998, p. 97) (Kadaj and Świętoń, 2016)
		(QGF98)	Gravimetric Quasi-Geoid	10.9 cm STD. dev	1998	(Duquenne, 1998)
		(RAF98)	Hybrid Quasi-Geoid	the overall precision of 2 to 3 cm, degrading to 4 cm in mountain areas.	1998	(Duquenne 1998)

No.	Country	Model Name	Model Type	Data Used	Year	References
		(RAF09)	Hybrid Quasi-Geoid	between one and two centimeters.	2009	(F. Duquenne, 2010) (I.G.N., 2010)
		(QGF16)	Gravimetric Quasi-Geoid	6.7 cm	2016	(L'Ecu, 2017)
		(RAF18/RAF18B)	Hybrid Quasi-Geoid	1 cm. STD. dev	2018	(I.G.N., 2018)
4	Spain	Iberian Peninsula (IBERGEO95)	Gravimetric Geoid	1.0 ppm. STD. dev	1995	(Sevilla, 1995)
		Iberian Peninsula (IGG2005)		N/A	2005	(Corchete et al. 2005)
		Iberian Peninsula (IBERGEO2006)		0.62 ppm. STD. dev	2006	(Sevilla, 2006)
		Iberia and Macaronesia (ICAGM07)		overall precision of 8-10 cm	2007	(Catalao et al. 2007) (Catalao and Sevilla, 2009)
		Iberian Peninsula (IBERGEO2008)	Hybrid Geoid	N/A	2008	(Sevilla, 2006)
		Northern Andalusia	Gravimetric Geoid	5 cm. STD. dev	2001	(Lacy et al., 2001)
		North Iberia (NIBGEO)		N/A	2008	(Corchete, 2008)
		South Spain and the Gibraltar Strait Area (SOSGIS)		N/A	2008	(Corchete et al., 2008)
5	SWEDEN	Baltic Region	Gravimetric Geoid	N/A	1995	(Vermeer, 1995)
		Baltic Region and Nordic Area (NKG96)		The model shows a fit at the level of 10 cm	1996	(Forsberg et al. 1997)

No.	Country	Model Name	Model Type	Data Used	Year	References
		Baltic Region and Nordic Area (NKG2004)	Gravimetric Quasi-Geoid	9.0 cm. STD. dev	2004	(Forsberg et al. 2004)
		Sweden (SWEN08_RH70)	Hybrid Geoid	The standard uncertainty has been 10-15 mm	2008	(Ågren et al., 2008)
6	Norway	NMA2013v22	Gravimetric Geoid	an accuracy of 5.6 cm	2013	(Borge, 2013)
7	Germany	(GCG2011-NORTH)	Hybrid Geoid	about 1-2 cm	2010	(Rülke et al., 2012)
		(GCG2016)		The overall accuracy about 1 cm	2016	(Schwabe et al. 2016)
8	Finland	FIN2005N00	Gravimetric Geoid	2cm STD. dev	2010	(Bilker-Koivula, 2010)
9	Poland	(quasi09c)	Gravimetric Quasi-Geoid	Between 3.2 cm and 1.8 cm STD. dev	2010	(Lyszkowicz, 2010)
		(PL-geoid-2011)	Hybrid Quasi-Geoid	N/A	2011	(Kadaj and Świętoń, 2016)
		(KTH-PL-GEOID2015)	Gravimetric Geoid	2 cm. STD. dev	2015	(Kuczynska-Siehien et al. 2016)
		(PL-quasi-geoid2021)	Hybrid Quasi-Geoid	1.9 cm STD. dev	2021	(Geodesy and Cartography, 2021)
10	Italy	(ITALGEO83)	Quasi-Geoid	0.5 m RMS	1983	(Benciolini et al., 1984)
		(ITALGEO90)		The precision is of the order of meter in absolute and	1990	. (Barzaghi et al. 2002)

No.	Country	Model Name	Model Type	Data Used	Year	References
				about 5 ppm in relative.		
		(ITALGEO99)		sub-decimetric precision	1999	(Barzaghi et al., 2002)
		(ITALGEO05)		Overall precision of around 3 cm over the entire Italian area.	2005	(Barzaghi et al., 2007)
		(ITG2009)	Gravimetric Geoid	N/A	2009	(Corchete, 2010)
11	Northwest Italy and Switzerland	(GISGEO2012)		N/A	2012	(Gilardoni et al. 2013)
12	Great Britain	(OSGM02)	Hybrid Geoid	2 cm RMS in the UK and \3-4 cm RMS in other areas	2002	(Iliffe et al., 2003)
		(OSGM15)		The estimated accuracy is of 1 cm RMS for Mainland GB, Outer Hebrides and Scilly Isles, 2 cm for Orkney and Shetland, and 3 cm for Isle of Man, while it is 2.3 cm std for Republic of Ireland and 1.4 cm std for Northern Ireland.	2015	(Greaves et al. 2016)
13	Romania	-	Gravimetric Quasi-Geoid	8.5 cm STD. dev	2018	(Avramiuc et al., 2019)
14	Greece	(GreekGeoid2010)		The mean accuracy of the geoid model is	2010	(Tziavos et al. 2010)

No.	Country	Model Name	Model Type	Data Used	Year	References
			Gravimetric Geoid	3-5 cm		
15	Attica Basin - Greece	(GEOID2015)		N/A	2015	(Georgopoulos and Telioni, 2015)
16	Bulgaria	(QBG01) (HGG2013)	Gravimetric Quasi-Geoid	N/A	2010	(Peneva, 2001)
17	Iceland	(ICEGEOID2011)	Hybrid Geoid	1.7 cm. STD. dev	2011	(Sigurdsson and Valsson, 2014)
18	Hungary	(HGG2013)	Gravimetric Geoid	3.6 cm. STD. dev	2013	(Corchete, 2013a)
19	Portugal	(GEODPT08)	Hybrid Geoid	the estimated accuracy is 4 cm.	2008	(Catalao, 2008)
20	Austria	-	Geoid and Quasi-Geoid		1996	(Erker et al., 1996)
		(GV_GEOID)	Hybrid Geoid	An estimated accuracy of the order of 2-3 cm over the whole Austrian territory.	2008	(Pail et al., 2009)
21	Czech Republic	(CR2000)	Quasi-Geoid	3.4 cm. STD. dev	2000	(Kostelecky et al., 2004)
		(CR2005)		N/A	2005	(Kostelecky et al., 2004)
22	Serbia		Gravimetric Geoid	7.7 cm. STD. dev	2003	(Odalović, 2006)
23	Ireland	-	Quasi-Geoid	less than 1 m. STD. dev	1980	(Olliver, 1980)
24	Lithuania		Gravimetric Geoid	4.2 cm STD. dev	2004	(Ellmann, 2004)

No.	Country	Model Name	Model Type	Data Used	Year	References
25	Latvia	(LV98)	Gravimetric Geoid	the estimated accuracy of about 6-8 cm.	1998	(Kaminskis and Forsberg, 1996)
		-	Gravimetric Geoid	5.6 STD. dev	2004	(Ellmann, 2004)
26	Croatia	(HRG2009)	Gravimetric Geoid	3.5 cm STD. dev	2009	(Basic and Bjelotomic, 2014)
27	Slovakia	(DVRM05)	Hybrid Geoid	34 mm RMSE	2005	(Droscak, 2014)
28	Estonia	(EST-GEOID2017)	Hybrid Quasi-Geoid	4.2 mm STD. dev	2017	(Ellmann et al. 2019)
29	Denmark	(DKGEOID12)	Hybrid Geoid	5 cm RMS	2012	(Forsberg, 2016a)
		(DKGEOID12A)		6 mm STD. dev	2012	(Forsberg, 2016b)
30	Switzerland	(CHGEO98)	Hybrid Geoid and Quasi-Geoid	±8 cm. STD. dev	1998	(Marti, 2002)
31	Switzerland and Liechtenstein	(CHGEO2004/CHGEO2004Q)	Geoid and Quasi-Geoid	N/A	2004	(Marti, 2007)
32	Northwest Italy and Switzerland	(GISGEO2012)	Gravimetric Geoid	N/A	2012	(Gilardoni et al., 2013)
33	Netherlands	(NLGEO2004)	Hybrid Quasi-Geoid	N/A	2004	(Crombaghs and Bruijne, 2004)
		(NLGEO2018)		N/A	2018	(Slobbe et al., 2019)
34	Moldova	(MOLDGEO2004A)	Hybrid Quasi-Geoid	Accuracy is better than 10 cm.	2004	(Marchenko and Monin, 2004)
		(GM2005)		5 cm. STD. dev	2005	(Kucher et al. 2005)

No.	Country	Model Name	Model Type	Data Used	Year	References
35	Belgium	(BG03)	Gravimetric Quasi-Geoid	an accuracy of about 3 cm.	2003	(Barzaghi et al., 2003)
		(hBG03)		The estimated accuracy of this model is about 2 cm.	2003	(Duquenne et al. 2005)
		(hBG18)		N/A	2018	(Slobbe et al., 2018)
36	Turkey	(Turkey-ITUGRG2021)	Gravimetric Geoid	The estimated accuracy is 10.1 cm (before-fit) and 8.6 cm (after 7-parameter fit).	2021	(Hirt et al., 2019)
37	Slovenia	(SLOAMG2000)	Hybrid Geoid	The inner accuracy of the heights is on average of 3 cm.	2000	(Pribicevic, 2000)
38	Kosovo		Quasi-Geoid	1–3 cm in most of the territory and the mountains the standard deviation occurs from 4 to 7 cm.	2015	(Ameti and Jäger, 2016)
39	Switzerland and Liechtenstein	(CHGEO2004/CHGEO2004Q)	Geoid and Quasi-Geoid	N/A	2004	(Lobianco et al., 2004)
40	Cyprus	-	Gravimetric Geoid	±0.054 RMS		(I. Tziavos et al., 2017)

A great effort has been made in European countries to determine the geoid, with used the whole available observations as inaccurate observations of the Earth's gravitational field in those countries, in addition to using gravity satellite observations as the Gravity Field and Steady-State Ocean

Circulation Explorer (GOCE) satellite, which enabled scientists to determine the long wavelength of the Earth's gravitational field with high accuracy.

These efforts have paid off for achieving geoid with incredible accuracy, as evident from Table 7, which describes the most geoid attempts for European countries as in Denmark, Italy, Slovakia, Estonia, and Spain they succeeded in determining the geoid with a precision of a few millimeters, while in France and Great Britain it has reached to 1 cm accuracy, in the other countries the rang of accuracies are between 2 cm and sub-decimeters.

4.5. Attempts for geoid determination of the South American continent

Despite a strong effort that is being carried out in several countries to improve the distribution of gravity information, to organize the gravity measurements in the continent, and validate the available gravity measurements, the obtained geoid of the content has a low accuracy, which reached up to 50 cm in terms of standard deviation.

According to The Sub Commission 2.4b of IAG commission 2 entitled Gravity and Geoid in South America held on Oct 02, 2021, for a new project established for improving the distribution of gravity information, to organize the gravity measurements in the continent to enhance the accuracy of the geoid, the main objectives of the project are:

- to re-measure existent absolute gravity stations and encourage the establishment of new stations;
- to validate fundamental gravity networks from different countries to establish a single and common gravity network for South America;
- to adjust national gravity networks and link them together;
- to obtain and maintain files with data necessary for the geoid computation like gravity anomalies, digital terrain models, geopotential models, and satellite observations (GPS) on the levelling network of different countries;
- to provide a link between the different countries and the IGFS to ensure access to proper software and geopotential models for local geoid computation;
- to compute a global geoid model for South and Central America using the available data;
- to encourage countries to cooperate by releasing data for this purpose;
- to encourage and eventually support local organizations in different countries to increase the gravity data coverage, improve the existing digital terrain models, carry out GPS observations on the levelling network, and compute a high-resolution geoid;
- to organize and encourage the organization of workshops, symposia, or seminars on gravity and geoid determination in South America (https://com2.iag-aig.org/sub-commission-24).

Summarized historical attempts for geoid determination are listed in Table 6 below for south American countries and it is indisputable that the accuracy of geoid for all countries except

Uruguay ranges from 12 to 50 cm. This accuracy needs more effort to consider geoid as a reference for the height system in South America.

Table 8 The list of historical attempts for geoid determination of the South American continent

No.	Country	Model Name	Model Type	Data Used	Year	References
1	Brazil	(MAPGEO2004)	Gravimetric Geoid	±0.5 m RMS	2004	(Lobianco et al. 2004)
		(MAPGEO2010)		±0.28 m RMS	2010	(Matos et al., 2012)
		(MAPGEO2015)		17 cm RMS	2015	(Blitzkow et al., 2016)
2	Colombia	(QGEOCOL2004)	Gravimetric Geoid and Quasi-Geoid	50 cm. STD. dev	2004	(Sánchez, 2003)
3	Argentina	(GAR)	Gravimetric Geoid	N/A	2007	(Corchete and Pacino, 2007)
		(GEOIDEAR16)		An accuracy of less than 10 cm	2016	(Piñón et al., 2016)
		Santa Fe Province		0.221 m. RMS	2018	(Cornero et al., 2018)
4	Venezuela	GEOID2010	Gravimetric Geoid	0.64 m. RMS	2010	(Matos et al., 2012)
5	Chile			1.21 m. RMS		
6	Ecuador			2.17 m. RMS		
7	Bolivia	(BOLGEO)	Gravimetric Geoid	N/A	2006	(Corchete et al. 2006)
8	Uruguay	(URUGEOIDE2000)	Gravimetric Geoid	accuracy of 13 cm	2000	(Piña et al. 2001)
		(URUGEOIDE2007)		accuracy of 2 cm	2007	(Militar, 2007)

4.6. Attempts for geoid determination of North and Central America continent

The primary objective of *the Sub Commission 2.4b of IAG commissions 2, entitled Gravity and Geoid in North America*, held on Oct 02, 2021, the regional geoid model covers the region of north America and central America by 2022 to achieve a common vertical datum. This model will serve as the official implementation of vertical datum for countries that want to adopt it.
The intention is to ensure that a suitable North American Geoid is developed to serve as a common datum for everyone in the region (https://com2.iag-aig.org/sub-commission-24).

In 2014, the United States National Geodetic Survey (NGS) started producing annual experimental gravimetric geoid models, the xGEOID models, for the upcoming vertical datum modernization in 2022, the North American-Pacific Geopotential Datum of 2022 (NAPGD2022).

For the upcoming North American-Pacific Geopotential Datum of 2022, the National Geodetic Survey (NGS), the Canadian Geodetic Survey (CGS), and the National Institute of Statistics and Geography of Mexico (INEGI) computed the first joint experimental gravimetric geoid model (xGEOID) on 1'x1' grids that cover a region bordered by latitude 0 to 85-degree, longitude 180 to 350 degree east.

xGEOID20 models are computed and then evaluated against the independent GPS/levelling data sets. The geoid comparisons with the most accurate Geoid Slope Validation Surveys (GSVS) from 2011, 2014, and 2017 indicate that the relative geoid accuracy could be around 1-2 cm baseline lengths up to 300 km for these GSVS lines in the United States (Wang et al., 2021).

Table 9 The list of historical attempts for geoid determination of the North American continent

No.	Country	Model Name	Model Type	Data Used	Year	References
1	United States	(GEOID93)	Gravimetric Geoid	10 cm STD. dev	1993	(Milbert, 1993)
		(G96SSS/GEOID96)	Gravimetric and Hybrid Geoid	5.5 cm RMS	1996	(Smith and Milbert, 1999)
		(USGG2003/GEOID03)		2.4 cm RMS	2003	(Roman et al., 2004)
		(USGG2009/GEOID09)		1.4 cm RMS	2009	(Wang et al., 2012)
		(xGEOID19B/GEOID18)		1.39 cm RMS	2019	(Li et al., 2019)
2	Colorado - USA	(ColSCA-CASM2019)		the accuracy of the quasi-geoid and geoid models	2019	(Jiang et al. 2020)

No.	Country	Model Name	Model Type	Data Used	Year	References
			Gravimetric Geoid and Quasi-Geoid	is equal to 3.1 cm and 3.5 cm, respectively		
3		(ColUNBSH2019)		the accuracy of the quasi-geoid and geoid models is both equal to 2.9 cm	2019	(Matsuo and Forsberg, 2019)
4		(ColFFTWG2020)		The mean accuracy is 2.5 cm	2020	(Grigoriadis and Vergos, 2020)
5		(ColLSMHA2021)		the accuracy of the quasi-geoid and geoid models are 2.7 cm and 2.6 cm, respectively	2021	(Işık et al., 2021)
6	Canada	(GSD91)	Gravimetric Geoid	69.5 cm STD. dev	1991	(Veronneau and Mainville, 1992)
		(GSD95)			1995	(Veronneau, 1996)
		(CGG2000)		8.7 cm STD. dev	2000	(Veronneau, 2001)
		(CGG2005)		8.4 cm STD. dev	2005	(Veronneau and Huang, 2007)
		(CGG2010)		7.4 cm STD. dev	2010	(Huang and Veronneau, 2013)
		(CGG2013/CGG2013a)		7.3 cm STD. dev	2013	(Huang and Véronneau, 2016)
7	Mexico	(MEXICO97)	Gravimetric Geoid	N/A	1997	(Smith and Milbert, 1999)
		(GGM04)		58 cm RMS	2004	(Naranjo, 2004)

No.	Country	Model Name	Model Type	Data Used	Year	References
		(GGM05)		36 cm, RMS	2005	(Naranjo et al. 2006)
		(GGM06)		35 cm, RMS	2006	(Naranjo et al. 2007)
		(GGM10)		Its estimated absolute accuracy in geoidal height values is 20 cm.	2010	(Avalos Naranjo et al. 2010)
8	Caribbean	(CARIB97)	Gravimetric Geoid	62 cm. RMS	1997	(Smith and Small, 1999)
9	Alaska	(ALASKA94)	Gravimetric Geoid	an accuracy of about 20 cm over length scales of 100 km.	1994	(Milbert, 1993)
		(GEOID96)		N/A	1996	(Smith and Milbert, 1999)
		(GEOID99)		N/A	1999	(Smith and Roman, 2001)
		(USGG2003/GEOID03)		N/A	2003	(Roman et al., 2004)
		(USGG2009/GEOID09)	Gravimetric and Hybrid Geoid	0.6 cm STD. dev	2009	(Roman et al., 2009)
		(USGG2012/GEOID12B)			2012	(Wang et al., 2012)
10	Greenland	-	Gravimetric Geoid	N/A	1996	(Forsberg et al. 2002)
		(GGEOID16)		3.7 cm, RMS	2016	(Forsberg, 2016a)

Table (9) illustrates the previous attempts for geoid determination for North American countries, and we can note that the geoid accuracy ranges from 1.4 cm up to 70 cm, except for Alaska, that has a sub-millimeter solution.

Mexico and the Caribbean need more attempts with new data coverage to obtain a better accuracy where the accuracy is 20 and 62 cm, respectively.

4.7. Antarctic Geoid attempts

In 2008 an attempt for quasi-geoid determination for Antarctica was performed by Marchenko, he had to find solutions for the insuffeciant of the local gravity data coverage to overcome this problem and used GGMs, for filling the gap with EGM96 synthesized data (Marchenko et al. 2012).

A gravimetric quasi-geoid for the Antarctic region limited by 50° S in latitude (Fig. 33) is based on marine and land gravity anomalies from BGI and ADGRAV databases and on gravity anomalies computed by KMS from the inversion of satellite altimetry.

A remove-restore procedure is then applied by using the EIGEN-CG01C global gravity model up to degree 360 and the GEBCO DTM topography model. The quasi-geoid solution is based on the Sequential Multipole Analysis (SMA) technique approximating the gridded reduced mean gravity anomalies by 20152 radial multipoles with an accuracy of 5 mGal. The obtained quasi-geoid and the corresponding SST model have been assessed by comparison with independent data from 5 tide-gauges stations (Mawson, Davis, Casey, Macquarie Island, Heard Island) of the Australian levelling network, leading to an estimated accuracy of 10 cm (Marchenko et al., 2012).

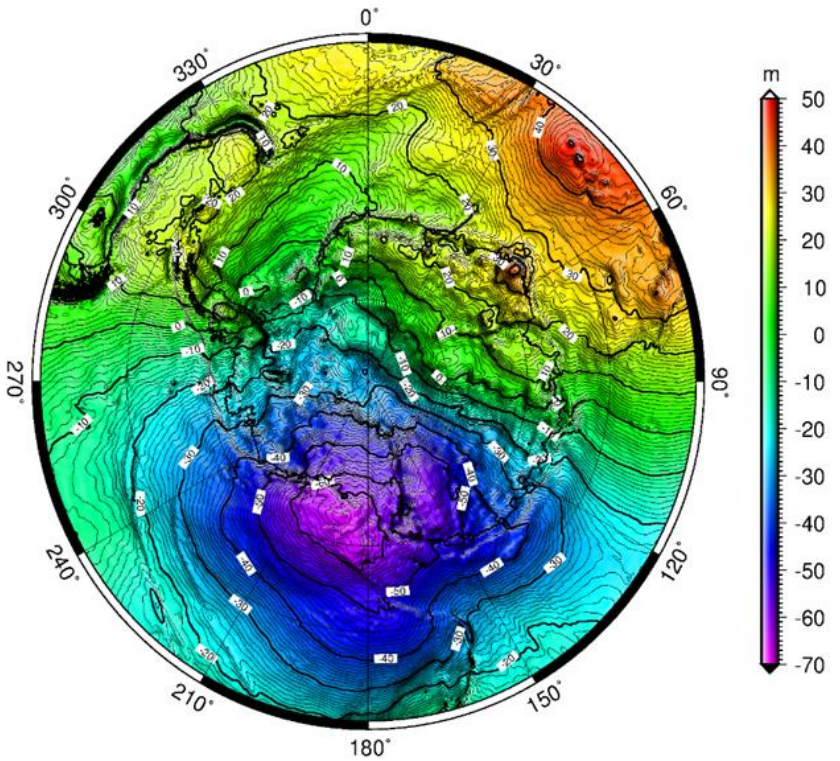

Figure 33 Gravimetric quasi-geoid [m] *solution based on the KMS, BGI, and ADGRAV free air anomalies* Δg *(Marchenko et al. 2012)*

5. Proposed methodology to create mathematical models for determining reference surfaces

Overview

This chapter discussed the statistical background and the mathematical model for the least-squares collocation (LSC) algorithm. Then, the definitions of the covariance functions and the spatial covariance function and its role are outlined. An overview of the numerical estimation of the empirical covariance function and the explanations of the degree variances and error degree variances is then presented. After that, the concept of the analytical covariance function and its role and the principle of the local covariance function, which is consistent with the remove-compute-restore technique, are discussed. Finally, the Ellipsoidal Collocation was discussed.

5.1 Background and Mathematical Expressions

The least-squares collocation (LSC) technique was firstly advocated in its general form by (Krarup, 1969). Then, it was widely investigated and applied by (Moritz, 1980) and further treated by Tscherning (C. C. Tscherning, 1994a). This method is a vital tool for gravity field modeling. Besides, being flexible in dealing with heterogeneous input and output features yields optimal results based on a particular data set. Hence, the LSC will be the standard technique used for gravity field modeling in Egypt throughout the current work. So, this chapter outlines the various aspects of local gravity field modeling by least-squares collocation.

The gravity potential, as well as the respective observable quantities, represents a spatial stochastic phenomenon. The irregularity of the gravity field is caused by the visible and invisible mass anomalies, i.e., the non-even distributions of the Earth's mass. The mass anomalies could have regular (or systematic) patterns, such as mountainous chains extending regularly. After removing such (known) systematic trends, the residuals will be somewhat irregular.

Rather, randomly distributed mass anomalies cause the residual gravitational features. In this sense, the residual gravity field elements may also be said to be spatially random (Fig. 34). The randomness exists not for time (as observational errors) but for space (the measurements are considered simultaneously but at different points).

The random behavior is theoretically independent of the position on the sphere and the direction, that is, homogeneous and isotropic (Moritz, 1978).

Usually, the least-squares collocation technique is considered a general methodology that combines least-squares adjustment and least-squares prediction (or kriging) in a unified mathematical algorithm (Heiskanen and Moritz, 1967; Moritz, 1972). In particular, the LSC technique has found many applications in physical geodesy. The most general form of the collocation model (in matrix notation),

$$l = AX + t + n, \tag{5.1}$$

illustrated in Fig. 35. The term AX represents a simple, regular, and slowly varying curve. It is a linear (or linearized) function of several parameters, X. Another function, s, called the signal and is irregularly oscillating about zero, is superimposed, giving the function AX + s. The problem is to determine the function (AX + s) using discrete observations, l, which are furthermore affected by observational errors (or noise), n. Denoting the signal part at the observational (or data) points by t, one arrives at Eq. (5.1). Thus, the curve AX+s, to be interpolated, consists of a "systematic part" AX, representing the general trend of the physical feature, and a "random part" s, representing continuous irregular fluctuations of the feature. In contrast to the signal s, the other random quantity n (the observational error) occurs only at the data points and is thus discrete. If the determination of the parameters X is viewed as adjustment, the (partial) removal of the noise as filtering, and the estimation of s at points other than the measuring points as prediction, one may say that the LSC

technique combines adjustment, filtering, and prediction (Moritz, 1972). An insight into Eq. (5.1) shows that the main difference between LSC and least-squares adjustment is the existence of the random signal part, t.

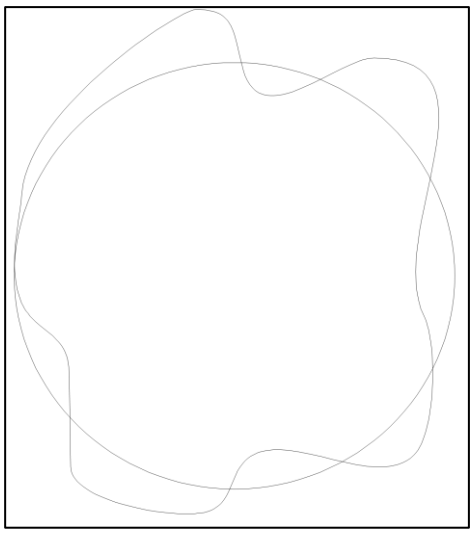

Figure 34 Spatial random rotation of a function defined on a sphere around its center

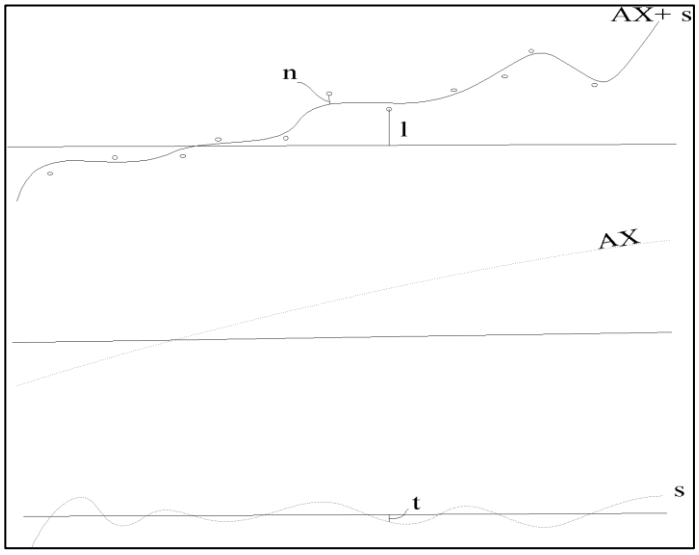

Figure 35 The collocation model

In general, the LSC solution amounts to predicting the desired signals s and the unknown parameters X, along with their uncertainties. In all geodetic applications of the collocation theory, the signal s (or t at the data point) always reflects the effect of the irregularity of the actual gravity field of the Earth, which is supposed to possess a random behavior on the geodetic measurements. Regarding gravity field modeling by collocation, the vector of observations l could comprise of any combination of heterogeneous anomalous elements at scattered data points, for example, gravity anomalies, geoidal heights, vertical deflections, airborne gravity anomalies, and 2nd order derivatives, etc. Moreover, (dynamic) satellite-tracking measurements could also be used as input (Moritz, 1972). Similarly, the signals to be estimated could be a combination of any heterogeneous features, such as discrete geoidal heights, gravity disturbances, and geopotential coefficients. In this sense, the collocation technique belongs to the space domain trend for geoid determination. On the other hand,

the vector of unknown parameters X could represent modeled systematic observational errors, a mathematical trend surface, a set of geodetic datum transformation parameters, or even a local vertical datum offset (C. Tscherning et al., 2001). The LSC solution yields the best linear unbiased estimates, based on the model (5.1), subject to the following minimum condition (Moritz, 1980),

$$s^T C_{ss}^{-1} s + n^T C_{nn}^{-1} n = \text{minimum}, \quad (5.2)$$

where C_{ss} and C_{nn} are the auto-covariance matrix of the signals to be predicted and the error variance-covariance matrix of the input observations, respectively. Of course, if there is no correlation among the random observational errors, then C_{nn} should be a diagonal matrix. In the above condition, the signals are supposed to have pure random behavior about zero; in other words, these quantities are assumed to be centered. The well-known remove-compute-restore technique of the long and short wavelength features, using appropriate high-resolution geopotential and topographic models, primarily aims at residual "centered" data of a random smooth nature. The smoothness is practically reflected by the (possibly) minimal mean and standard deviation of the input data. While removing a global harmonic model eliminates a slowly varying part of a long-wavelength nature, the topographic reduction would suppress the frequent oscillating features that could have large amplitudes (Vaníček et al., 1996).

The above minimization implies the optimal prediction accuracy and the smoothest gravitational field, which is compatible with the given data. This allows a smooth harmonic downward continuation till the Bjerhammar sphere (Tscherning 1993). Particularly, while C_{nn}^{-1} represents the classical error weight matrix, the matrix C_{ss}^{-1} carries the meaning of signal roughness (weighting) based on the variations of the treated field. In the general theory of collocation, while the observational noise has a zero expected average in the probability space, the gravity field signals are regarded as having an expected spatial mean equal to zero globally. Moreover, the random measuring errors are assumed to be uncorrelated with the random field signals. If there were no signal term in Eq. (5.2), the above minimum would reduce to the usual least-squares adjustment principle. On the other hand, if there were no observational noise, one would deal with errorless collocation.

Based on the above, it can be proved that the LSC solution is given by

$$X = [A^T D^{-1} A]^{-1} . [A^T D^{-1} l], \quad (5.3)$$

$$S = C_{st} D^{-1} (l - AX), \quad (5.4)$$

with

$$D = (C_{tt}+C_{nn}), \quad (5.5)$$

where C_{tt} is the auto-covariance matrix relevant to the input observations, S is the vector of predicted signals, D is denoted as the "total" covariance matrix, and C_{st} is the cross-covariance matrix between the predicted signals and the input observations. On the other hand, the associated error estimates are expressed by

$$E_{xx} = [A^T D^{-1} A]^{-1}, \quad (5.6)$$

$$E_{ss} = C_{ss} - C_{st} D^{-1} C_{ts} + H A E_{xx} A^T H^T, \quad (5.7)$$

with

$$H = C_{st} D^{-1}, \quad (5.8)$$

E_{xx} and E_{ss} are the estimated error variance-covariance matrices of the estimated parameters and the predicted signals, respectively, and C_{ts} (or C_{st}^T) is the cross-covariance matrix between the input observations and the predicted signals. The covariance matrices C_{ss}, C_{tt}, and C_{st}, have the relevant analytical covariances between any possible pairs of input and output gravimetric elements in the solution under consideration. These covariances are computed according to a basic covariance

function model for the anomalous potential, based on the input data and utilizing the law of covariance propagation.

On the other hand, if no parameters are needed, which is the most common case, then the LSC solution for the signals and their uncertainties reduce to

$$S = C_{st}\, D^{-1}\, l, \tag{5.9}$$

$$E_{ss} = C_{ss} - C_{st}\, D^{-1}\, C_{ts}\ , \tag{5.10}$$

where the impact of the parameters X (and their uncertainties) has disappeared altogether. In Eqs. (5.9) and (5.10), it can be shown that the signals (and their error estimates) can be independently predicted one by another, which means that no restrictions are imposed on the size of the vector S or the matrix E_{ss}. The only restriction may be the size of the D matrix to be inverted, which is equal to the number of the input observations. An insight into Eq. (5.10) shows that the first term reflects the "a-priori" roughness of the field, expressed by C_{ss}, whereas the second term represents the gain inaccuracy due to the user input data. Furthermore, in the above expressions, the input data variance (or roughness) and the noise variance are balanced in the total covariance matrix, D (C. C. Tscherning, 1994b).

Suppose the data are assumed to be errorless. In that case, they are exactly reproduced at the data points after prediction with zero error estimates, which is the original mathematical idea of collocation. Moreover, in this case, different choices of the basic model covariance function would correspond to different possible gravitational fields, which would be compatible with the given data. However, if the data are affected by random measuring errors, then the computed field matches the data not exactly but in such a way that the effect of these errors is kept as small as possible (Moritz, 1980). In this latter case, the solution amounts to filtering the data; thus, one obtains

$$t = C_{tt}\, D^{-1}\, l, \tag{5.11}$$

$$E_{tt} = C_{tt} - C_{tt}\, D^{-1}\, C_{tt}\ . \tag{5.12}$$

This gives the optimal estimate for the signal part t of the observations l themselves along with its accuracy. . In this way, the noise n is filtered out in the best possible way. One has no prediction if no computations are performed at points other than the data points. From the above, it can be said that the signal predictions at new points would be more sensitive to the field roughness, whereas the filtration of the data is more sensitive to the quality of the input data.

A unique basic model for the covariance functions, which best describes the anomalous input features, must be used throughout the collocation solution. This would guarantee a predicted field consistent with the input (heterogeneous) data. Accuracy computations Eq. (5.10) presuppose good estimates of the input covariances derived from the basic covariance model.This is much more critical than predicting the signals or the parameters themselves. A similar fact is known from least-squares adjustment, where the adjusted quantities are relatively insensitive concerning the choice of the prior weights, whereas the a-posteriori accuracies strongly depend on them. Thus, in the collocation solution, the covariances work as weights. Furthermore, Eq. (5.10) shows no dependency of the estimated signal accuracy on the measurements themselves. Combining these two facts, the LSC method can be used as a simulation tool to optimize gravimetric data types and configurations based on an approximate covariance model (Lachapelle and Tscherning, 1978).

5.2 Covariance Functions

In probability theory and statistics, covariance measures how much two variables change together. The covariance function describes the spatial covariance of a random variable process which may be used as an analytical function to fit as covariance values. In studies of the Earth's anomalous gravity field, covariance functions are of great interest. The behavior of the gravity field

is reflected in these functions. The magnitude of the variations and the roughness of the field are described. This information is essential and must be considered when gravity field-related quantities are estimated from a set of observations. The method of least squares collocation (Moritz, 1980) is widely used for this purpose; this method needs a covariance function to express the relations between the observations and the estimated quantities. The best least-squares agreements with the true potential are obtained when the empirical covariance function is used.

When conducting local studies of the gravity field, global covariance functions were estimated from gravity observations by (C. C. Tscherning and Rapp, 1974b). They derived some covariance function models, and an expression for the global covariance function was found. High-degree spherical harmonic approximations are very important when conducting studies of the gravity field in local areas. Estimations of gravity field-related quantities are carried out relative to the spherical harmonic approximations using the residual observations and the local empirical covariance function. This procedure corresponds to the stepwise collocation (Moritz, 1980).

Covariance functions are needed in estimation methods like least square collocation, and they have to be consistent with the observations used. Unfortunately, the estimations of such functions are hampered by the lack of data in the areas where the gravity field modeling is to take place. Consequently, a covariance function model has to be chosen. It is, therefore, essential to understand the variability of the local empirical covariance functions. This variability decreases remarkably when the terrain effect is taken into account, where the residual gravity field becomes more homogeneous, and choosing a covariance function model becomes easier. The basic covariance function in least-squares collocation, usually used to derive all other covariance, is the covariance function of the disturbing potential T.

If T(p) and T(q) are the disturbing potentials at two points p and q in space, then K(p,q) is defined as

$$K(p,q) = M\{ T(p), T(q) \}, \tag{5.13}$$

where M is the spatial expectation operator, defined as the mean over the whole sphere and all azimuths. It is assumed that both points lie on the surface of a sphere of radius R, representing the mean terrestrial sphere that corresponds to the reference ellipsoid, or the geoid, in the spherical approximation (Heiskanen and Moritz, 1967). Since the operator M is homogeneous (average over the whole sphere) and isotropic (average over all azimuths), the covariance K(p,q) will be a function of the spherical distance, ψ, between p and q. Hence, such function is denoted as the spherical covariance function, which is given by

$$K(p,q) = K(\psi) = M\{T(p)T(q)\} = \frac{1}{8\pi^2}\int_{\lambda=0}^{2\pi}\int_{\theta=0}^{\frac{\pi}{2}}\int_{\alpha=0}^{2\pi} T(\theta_p,\lambda_p)T(\theta_q,\lambda_q)\sin\theta \, d\theta \, d\alpha \tag{5.14}$$

where θ, λ are the spherical co-latitude and the geodetic longitude, respectively, and α is the azimuth of the arc PQ on the sphere. The spherical distance ψ can be expressed as (Heisken and Moritz 1967):

$$\psi = \cos^{-1}\left(\cos p \cos\theta_q \cos(p-\lambda_q) + \sin\theta_p \sin\theta_q\right) \quad . \tag{5.15}$$

The covariance function is harmonic outside the Earth's surface. It represents the average product of the (harmonic) anomalous potential at all possible pairs of points with the same mutual spherical distance (C. C. Tscherning, 1982). Consequently, the spherical harmonic expansion of Equation (5.14) can be written as follows

$$K(\psi) = \sum_{n=2}^{\infty} \sigma_n P_n(\cos\psi) \tag{5.16}$$

where:

P_n Legendre polynomials,

σ_n degree variance of the potential.

In practice, treating the potential field, and hence the relevant covariance functions, as being homogenous and isotropic requires the handled data to be as smooth as possible so that they behave randomly. However, this could not be accurate due to eventual regular field trends (particularly on a regional scale) or some unusual local topographic and/or geophysical variations. In particular, such (non-random) features may force the field to be an-isotropic and inhomogeneous, azimuth, and location-dependent (Tscherning 1982). Nevertheless, the modern remove-restore technique (of the known low and high-frequency signal parts) would homogenize the residual (smoothed) input information in such a manner that it could be safely considered homogenously random (D. Arabelos, 1989). A separate mathematical treatment of the an-isotropic covariance functions is required in extreme abnormal cases. There should be a further dependence on the azimuths of the lines connecting the pairs of points (C. C. Tscherning, 1999)**.** Hence, , throughout the current investigation, the treated covariance functions are assumed to be isotropic.

The extension of the covariance function (5.16) into the space outside the sphere r = R depends mainly on the definition (5.14) of K (outside r an average product of T(P) and T(Q), since T is assumed to be harmonic outside r = R. I well-known that the n^{th} degree spherical harmonic outside a sphere depends on the radius vector through $r_P r_Q^{-(n+1)}$.

Thus, K(P, Q) can be expressed in space into a series of solid spherical harmonics, and the spatial covariance function of the anomalous potential will have the following form

$$K(P,Q) = K\left(\psi, r_{P,} r_Q\right) \sum_{n=0}^{\infty} \sigma_n \left[\frac{R_b^2}{r_P\ r_Q}\right]^{n+1} P_n(\cos\psi) \qquad (5.17)$$

where:

R_b radius of Bjerhammer (1973) sphere,

$r_P r_Q$ geocentric radii to points of K(P, Q)

ψ spherical distance between (P, Q).

This is the general form of the homogeneous and isotropic spatial covariance function of the disturbing potential, which is symmetric with respect to (P, Q) and harmonic outside the sphere r = R_b (Heiskanen and Moritz, 1967).

This approach uses heterogeneous sets of essential functions associated with point masses, where the point masses are buried at varying depths covering the whole Earth (Vermeer, 1992)**.**

The empirical covariance function cov (p, q) of the point gravity anomaly Δg has fundamental characteristics because the gravity anomalies data form the main empirical material for the practical determination of the other signal covariance (Heiskanen and Moritz 1967).

There consistency between the gravity anomaly covariance function $cov_{\Delta g \Delta g}(p, q)$ has the form:

$$cov_{\Delta g \Delta g}(p.q) = \sum_{n=2}^{\infty} \sigma_n(\Delta g) \left[\frac{R_b^2}{r_p\ r_q}\right]^{n+2} P_n\left(\cos\psi_{pq}\right) \qquad (5.18)$$

with positive full power degree variances $C_n(\Delta g)$

$$C_n(\Delta g) = \frac{(n-1)^2}{R^2}\sum_{m=0}^{n}\left(\bar{a}_{nm}^2 + \bar{b}_{nm}^2\right) \quad (5.19)$$

where

C_n rrefers to the conventional harmonics,

$\bar{a}_{nm}^2$ and $\bar{b}_{nm}^2$ are the coefficients of the fully normalized harmonics.

5.3 Empirical and Analytic Covariance Functions

In particular, gravity anomalies are most popular as the input data type to estimate covariance function. Thus, the global covariance function of gravity anomalies is given by

$$C(p,q) = \frac{1}{8\pi^2}\int_{\lambda=0}^{2\pi}\int_{\varphi=0}^{\frac{\pi}{2}}\int_{\alpha=0}^{2\pi}\Delta g(\theta_p,\lambda_p)\Delta g(\theta_q,q)\sin\theta\, d\theta\, d\lambda\, d\alpha \quad (5.20)$$

where:

φ,λ are the spherical co-latitude and longitude, respectively,

α is the azimuth between p and q on the sphere, which are separated by the spherical distance (ψ).

The above integration gives the gravity anomaly covariance function, if the Earth were continuously covered with observed point gravity anomaly data, We need a statistical treatment of the global geopotential to make up for the shortfall in gravity field data. However, the terrestrial sphere is not entirely covered with gravity field data. Hence, according to the handled data format, a covariance function needs to express the relations between the observations and the estimated quantities.

The covariance of discrete point gravity anomalies on the sphere is empirically estimated, via a discrete numerical integration, as follows,

$$cov(\psi_i) = \frac{1}{M}\sum_{n=1}^{M}\Delta g(p)\,\Delta g(q) \quad (5.21)$$

where M is the number of products taken at a given spherical distance ψ .

Covariance what is called the empirical covariance function; when the gravity anomaly (Δg) is the residual gravity anomaly (Δg_r), and the points $\{P_i\}$ are taken from a local area A only, we have a local empirical covariance function.

The empirical covariance function values are evaluated using a suitable ψ interval (Tscherning and Rapp 1974).

$$\psi_i - \frac{\Delta\psi}{2} \le \psi < \psi_i + \frac{\Delta\psi}{2}$$

This interval should not be very small otherwise, a few points could be situated within that interval, and consequently, the result would be statistically useless (Kraiger, 1988). The empirical covariance function eq. (5.20) is estimated, based on the residual gravity anomaly data, after removing the long and short wavelength information. In this manner, this residual anomaly covariance function would reflect the local characteristics of the anomalous field. The input signal variance is the covariance value at zero spherical distance (M. Amin et al., 2003), thus, eq. (5.21) reduces to

$$cov_0 = \frac{1}{M}\sum_{i=1}^{M}\Delta g(P_i) \quad (5.22)$$

where M here equals the number of data points, the variance is simply the mean square of the (residual) anomaly data. On the other hand, the correlation length is defined as the spherical distance, which corresponds to a positive covariance value of ½ cov_0.

Of course, cov_0, ξ, and the first zero ψ_0 of the function (Fig. 36) can be easily determined from the data, whereas the curvature of the covariance function at ψ_0 is problematic since it depends on the horizontal gradient of gravity data, which is difficult to estimate (Kraiger, 1988; Moritz, 1980).

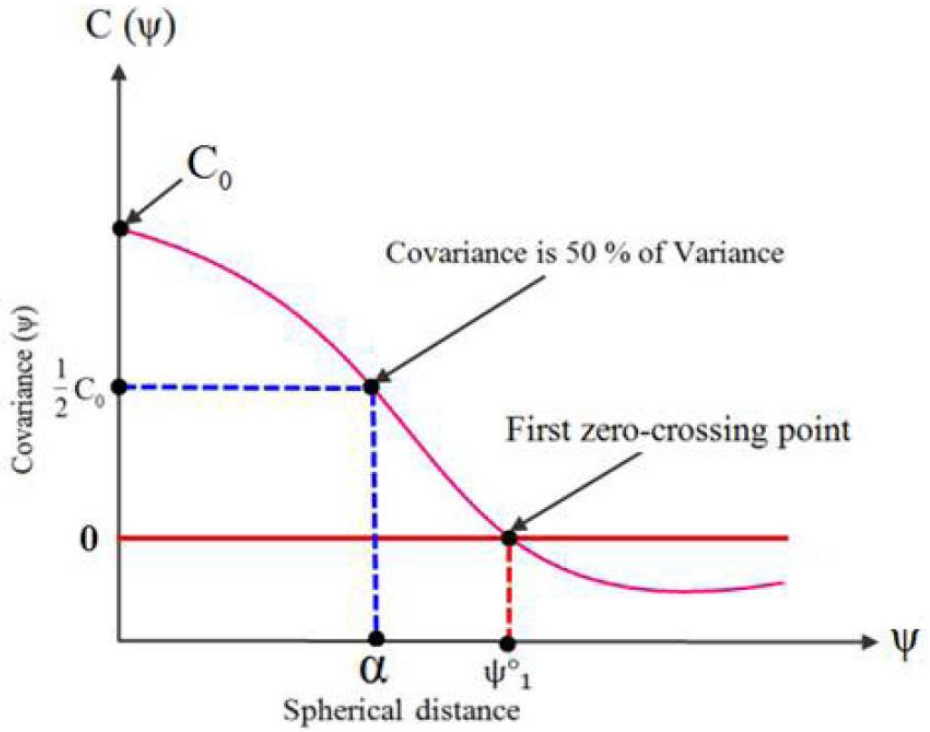

Figure 36 Schematic representation

There are three essential parameters for the local gravity anomaly covariance functions (M. Amin et al., 2002; H. H. Fashir and Kadir, 1998). These are the covariance (C_0), the correlation length (α), and the first crossing zero-point (ψ_1^0).

a) **The covariance** (C_0): This is the value of covariance function C (ψ) when the spherical distance (ψ) between the point P and Q is equal to zero

$$C = C(\psi) = C(0) \text{ at } \psi = 0 . \quad (5.23)$$

The covariance defines the statistical correlation of gravity anomalies and the average product of the anomalies at constant distances of 0', 2', 4', etc. For practical purposes, it's the variance of the residual gravity anomalies in square mGal at $\psi = 0$.

b) **The correlation length (α):** This is the value of the argument for which C (ψ) has decreased to half of its value at $\psi = 0$

$$C(\alpha) = \frac{1}{2}C_0 \quad . \quad (5.24)$$

The correlation length (α) is used to determine the most appropriate shape of the covariance function of the residual field.

c) **The first zero-crossing point** (ψ_1^0): In theory, the first zero crossing point (ψ_1^0) of the empirical covariance function of the reduced gravity anomalies up to degree N of geopotential harmonic model should be located at a distance by the rule of thumb as (D. N. Arabelos and Tscherning, 2010):

$$\psi_1^\circ = \frac{180^\circ}{(2\times N)} \ . \tag{5.25}$$

The variance and the correlation length of the empirical covariance function express the amount of smoothness of the input residual data, hence, a more stable LSC solution.

The empirical covariance function has a damping oscillatory behavior of about zero. The variance cov_0 is an important quantity as it is a scale factor for the point gravity anomaly covariance function, whereas the correlation length is regarded as the distance behind which the signals could be considered weakly correlated. Finally, it is worth mentioning that the empirical covariance function may be normalized via dividing all values by the variance cov_0. The resulting (unitless) curve is called the correlation function, which has the same shape as the covariance function and a value of unity at zero spherical distance.

5.4 Degree Variances and Error Degree Variances

The degree variance expresses how much signal power (content) is implied by all the coefficients belonging to a specific degree in a global sense. The scaled signal and error degree variances for the various quantities related to the gravity field can be computed as follows (Vergos et al., 2006):

$$\sigma_n^2(\Delta g) = \left(\frac{GM(n-1)}{a}\right)^2 \left(\frac{a^2}{R^2}\right)^{n+1} \sum_{m=0}^{n} (\bar{C}_{nm}^2 + \bar{S}_{nm}^2) \tag{5.26}$$

$$\varepsilon_{\sigma_{n(\Delta g)}}^2 = \left(\frac{GM(n-1)}{a}\right)^2 \left(\frac{a^2}{R^2}\right)^{n+1} \sum_{m=0}^{n} \left(\sigma_{\bar{C}_{nm}}^2 + \sigma_{\bar{S}_{nm}}^2\right) \tag{5.27}$$

and for geoid undulation

$$\varepsilon_{\sigma_{n(N)}}^2 = \left(\frac{GM}{\gamma a}\right)^2 \left(\frac{a^2}{R^2}\right)^{n+1} \sum_{m=0}^{n} \left(\sigma_{\bar{C}_{nm}}^2 + \sigma_{\bar{S}_{nm}}^2\right) \tag{5.28}$$

where

GM the geocentric gravitational constant,

R mean Earth radius,

a stands for the scaling factor associated with the coefficients,

n, and m are the degree and order of the harmonic expansion.

5.5 Analytical Degree Variance Models

From the previous section, it is clear that both the power and error spectra of any function of the disturbing potential can be easily computed empirically from GGMs, in terms of the relevant (reduced) harmonic coefficients and their error estimates, respectively. This is, however, only possible up to the maximum nominal resolution (or degree) of a given global harmonic model. On the other hand, it is obvious from Eqs. (5.16) and (5.17) that, theoretically, to completely describe

the potential, or equivalently, the gravity anomaly covariance function, the relevant degree variances are needed up to infinity. Practically, the maximal target degree is a function of the (global or local) data coverage and resolution. Hence, some analytical degree variance models were proposed in the geodetic literature, based on the available low degree geopotential models and/or the global gravity anomaly data. The target was to derive appropriate mathematical expressions so that one could easily assess the degree variance, in terms of
the degree n.

The anomaly degree variance model as follows (Rapp, 1972a),

$$(\sigma^2{}_n)_{\Delta g} = \frac{192}{n\left(1+\frac{3}{2}n\right)} \qquad [\text{mGal}^2]\,. \tag{5.29}$$

On the other hand, Meissl (1971) proposed a degree variance model as follows

$$(\sigma^2{}_n)_{\Delta g} = \frac{5\times10^5}{(n+250)^2} \qquad [\text{mGal}^2]\,. \tag{5.30}$$

Moreover, five analytic models for anomaly degree variance have been described by (Rapp 1972a; Tscherning and Rapp 1974), three of which are given by

$$(\sigma^2{}_n)_{1\,\Delta g} = \frac{A_1(n-1)}{n} \qquad [\text{mGal}^2] \qquad n > 1,$$

$$(\sigma^2{}_n)_{2\,\Delta g} = \frac{A_2(n-1)}{(n-2)} \qquad [\text{mGal}^2] \qquad n > 2,$$

$$(\sigma^2{}_n)_{3\Delta g} = \frac{A_3(n-1)}{(n-2)(n+B)} \qquad [\text{mGal}^2] \qquad n > 2, \tag{5.31}$$

where A_i are positive constants of dimension $mGal^2$ and B is a dimensionless constant, all of which might be determined according to some condition. Among those models, the third model was recommended for deriving closed expressions for the covariance function of the disturbing potential and the other related gravimetric quantities. Best fitting that model with the variance of the available global mean anomaly data and the empirically obtained anomaly degree variances from potential coefficients, in a least-squares procedure, it was found that the positive integer number 24 was the optimal estimate for B. In addition, a value for A_3 was estimated based on the available information. The fitting to the global data variance (in the sense of Eq. 5.26) was performed up to an extremely high degree (Tscherning and Rapp 1974). Hence, the analytical degree variance model will be given as

$$(\sigma^2{}_n)_{\Delta g} = A\,(n-1) / \{(n-2)\,(n+B)\} \quad [\text{mGal}^2], \qquad n > 2 \quad \text{and } B = 24. \tag{5.32}$$

Since its development, that degree variance model has been recommended and widely applied to global and local gravity field modeling by collocation (C. C. Tscherning, 1994a)**.** Hence, it will be used throughout the current work for modeling the covariance function of the disturbing potential and the related quantities. The use of that model in deriving an analytical closed expression for covariance functions will be discussed in the next section.

5.6 Analytical Covariance Function Modeling

Recall from section 5.2 that, to obtain a consistent LSC solution, based on the available heterogeneous data, a unique basic model for the covariance function, which best describes the anomalous input features, must be used throughout the collocation solution. This is achieved in practice by modeling the covariance function of the disturbing potential, or equivalently, gravity anomalies and then deriving the needed covariances for the input and output features using the low of covariance propagation.

The covariance between gravity anomalies at two points p and q (having a spherical distance ψ and geocentric radii r and r´, respectively), can be obtained as follows:

$$C(\psi, r, r') = \sum_{n=2}^{\infty} (\sigma_n^2)_{\Delta g} \left(\frac{R_b^2}{rr'}\right)^{n+2} P_n(\cos\psi). \quad (5.33)$$

Using the model in expression 5.33 for the anomaly degree variance, one obtains

$$C(\psi, r, r') = \sum_{n=3}^{\infty} \frac{A(n-1)}{\{(n-2)(n+B)\}} \left(\frac{R_b^2}{rr'}\right)^{n+2} P_n(\cos\psi). \quad (5.34)$$

Using the relationship between the disturbing potential and the gravity anomaly degree variances, which is given as

$$K_n = (\sigma_n^2)_T = \left\{\frac{R}{(n-1)}\right\}^2 (\sigma_n^2)_{\Delta g} \quad (5.35)$$

the corresponding expression for the disturbing potential covariance is expressed as

$$C(\psi, r, r') = \sum_{n=3}^{\infty} \frac{A R^2}{\{(n-1)(n-2)(n+B)\}} \left(\frac{R_b^2}{rr'}\right)^{n+1} P_n(\cos\psi). \quad (5.36)$$

As a practical matter, a closed expression was derived for the infinite expansion for the global anomaly covariance function (Eq. 5.34) by (C. C. Tscherning and Rapp, 1974b)**.** This expression is given as

$$\mathrm{cov}(\Delta g_p, \Delta g_q) = \left\{\frac{A S}{B+2}\right\}\left\{(B+1)\left(\frac{F_B - S}{B} - \frac{S^2 \cos\psi}{B+1} - \frac{S^3 \ P_2 \ \cos\psi}{B+2}\right) + F_{-2}\right\} \quad (5.37)$$

and the relevant closed form for the covariance between the disturbing potentials at two points is given as

$$\mathrm{cov}\left(T_p, T_q\right) = \frac{A R_b^2}{(B+2)(B+1)}\Big((B+1).F_{-2} - (B+2)(F_{-1} - s^3 P_2(\cos\psi) + \frac{F_B - S}{B} - \frac{S^2 \cos\psi}{B+1} - \frac{S^3 \ P_2 \ \cos\psi}{B+2}\Big). \quad (5.38)$$

Moreover, the closed expression for the covariance between the anomalous potential at p and the gravity anomaly at q is given as

$$\mathrm{cov}\left(T_p, \Delta g_q\right) = \frac{A R_b^2}{r(B+2)}\left\{F_{-2} - \left(\frac{F_B - S}{B} - \frac{S^2 \cos\psi}{B+1} - \frac{S^3 \ P_2 \ \cos\psi}{B+2}\right)\right\} \quad (5.39)$$

where

$s = (R_b^2 / r\, r')$ and F_{-1}, F_{-2} and F_B are functions of n, s and cosψ, which are computed by recursion algorithms.

Considering the disturbing potential analytical auto-covariance function (Eq. 5.38) as the basic covariance model, the auto and cross-covariances between any functions of the disturbing potential could be analytically derived and evaluated. For example, covariances can be assessed between any configuration pattern of heterogeneous input and output features, such as geoidal heights, deflection components, gravity anomalies and gravity disturbances. In particular, the disturbing potential covariance function is looked upon as the reproducing kernel of the anomalous field, from which any type of covariances can be easily derived, as the mutual relationships are well mentioned in chapter two. In spherical approximation, these relations are given as

$$N = \frac{1}{\gamma}\, T$$

$$\xi = -\left(\frac{1}{r\gamma}\right)\frac{\partial T}{\partial \varphi}$$

$$\eta = -\frac{1}{\gamma r \cos\varphi}\,\frac{\partial T}{\partial \lambda}$$

$$\delta g = -\frac{\partial T}{\partial r}$$

$$\Delta g = -\frac{\partial T}{\partial r} - \frac{2}{r} T\,. \qquad (5.40)$$

Using the law of covariance propagation, the covariance between any two gravitational signals S_{ip} and S_{jq} at two points p and q, respectively, is given by

$$\mathrm{cov}\left(S_{ip}, S_{jq}\right) = L_i\left(\mathrm{cov}\left(T_p, S_{jq}\right)\right) = L_i\left(L_j \mathrm{cov}\left(T_p, T_q\right)\right) \qquad (5.41)$$

where L_i and L_j are the two linear functional operators, which, when applied to the disturbing potential at p and q, yield the two signal types S_{ip} and S_{jq}, respectively. For instance, denoting covariance between the disturbing potentials at p(φ,λ,r) and q (φ',λ',r') by K (Eq. 5.38), the corresponding closed covariances between the gravimetric elements are computed from (C. C. Tscherning and Rapp, 1974b)

$$\mathrm{cov}\left(N_p, T_q\right) = \frac{1}{\gamma}\, K$$

$$\mathrm{cov}\left(N_p, N_q\right) = \frac{1}{\gamma\gamma'}\, K$$

$$\mathrm{cov}\left(T_p, \Delta g_q\right) = -\frac{\partial}{\partial r'}\, K - \frac{2}{r'}\, K$$

$$\mathrm{cov}\left(N_p, \Delta g_q\right) = \frac{1}{\gamma}\left(-\frac{\partial}{\partial r'}\, K - \frac{2}{r'}\, K\right)$$

$$= \frac{1}{\gamma}\, \mathrm{cov}\left(T_p, \Delta g_q\right)$$

$$\mathrm{cov}\left(\xi_p, T_q\right) = \frac{1}{r\gamma}\left(\frac{\partial}{\partial \varphi}\, K\right)$$

$$\mathrm{cov}\left(\xi_p, N_q\right) = \frac{1}{r\gamma\gamma'}\,\frac{\partial}{\partial \varphi}(K)$$

$$\mathrm{cov}\left(\xi_p, \Delta g_q\right) = \frac{1}{r\gamma}\,\frac{\partial}{\partial \varphi}\left(-\frac{\partial}{\partial r'}\, K - \frac{2}{r'}\, K\right)$$

$$= \frac{1}{r\gamma}\,\frac{\partial}{\partial \varphi}\left(\mathrm{cov}\left(T_p, \Delta g_q\right)\right), \text{etc}\,. \qquad (5.42)$$

This means that the functional operators, pertaining to the gravimetric elements, are applied sequentially to the basic covariance function ($K=\mathrm{cov}(T_p,T_q)$) and evaluated at the relevant positions. Recognizing that A, R_b and B are constants, it is clear that the finally encountered derivatives generally concern the spherical coordinates of both stations. Of course, any derivatives concerning φ and λ are performed first concerning cosψ, which is a function of them (Eq. 5.15). Details about the derivatives of the F_i terms in the closed form (5.38), which have s and cosψ as variables, are given in (C. C. Tscherning and Rapp, 1974b)**.** Applying the law of covariance propagation, as given above, would yield closed forms (similar to those given by Eqs. (5.37), (5.38) and (5.39)) for the covariances between any quantities.

The above expressions for the closed covariance functions can also be used in cases, where a set of empirical degree variances up to a certain degree, N, are used in connection with the model degree variances. For example, one can write the expression for the global covariance function of the anomalous potential as follows

$$K(\psi, r, r') = \sum_{n=2}^{N} (\sigma_n^2)_T \left(\frac{R_b^2}{rr'}\right)^{n+1} P_n(\cos\psi) + \sum_{n=N+1}^{\infty} \frac{AR^2}{\{(n-1)(n-2)(n+B)\}} \left(\frac{R_b^2}{rr'}\right)^{n+1} P_n(\cos\psi) \quad (5.43)$$

where $(\sigma_n^2)_T$ are the empirically determined potential degree variances, which can be computed from harmonic coefficients up to degree N (in spherical approximation) as follows

$$(\sigma_n^2)_T = \left(\frac{GM}{R}\right)^2 \sum_{m=0}^{n} (\bar{C}_{nm}^{*2} + \bar{S}_{nm}^2) \ . \quad (5.44)$$

This specific formulation of the covariance function (Eq. 5.43) enabled the inclusion of the empirical 2nd degree variance, thus avoiding the respective singularity inherent in the analytical degree variance model. Eq. (5.43) can be rewritten as

$$K(\psi, r, r') = (\sigma_2^2)_T \left(\frac{R_b^2}{rr'}\right)^{2+1} P_2(\cos\psi) + \sum_{n=2+1}^{N} (\sigma_n^2)_T - \frac{AR^2}{\{(n-1)(n-2)(n+B)\}} \left(\frac{R_b^2}{rr'}\right)^{n+1} P_n(\cos\psi) + \sum_{n=2+1}^{N} \frac{AR^2}{\{(n-1)(n-2)(n+B)\}} \left(\frac{R_b^2}{rr'}\right)^{n+1} P_n(\cos\psi) \ . \quad (5.45)$$

While the second term in Eq. (5.45) is a finite summation up to degree N, which can be evaluated easily, it is clear that the third term can be simply replaced by the closed-form (5.38). Again, the relevant functional operators are applied and evaluated for the three terms cumulatively to derive any desired covariances based on the above basic covariance function. While the third term is treated as the closed-form (5.38), the first and second terms are handled separately. Particularly, the respective functional operators of the anomalous field will be applied (and evaluated) to the empirical and analytical potential degree variances, from degree 2 up to degree N. It should be noted that applying the functional relationships to the potential degree variance amounts to the determination of a degree variance, which is consistent with the target covariance function, and may have mixed units. Namely, if the target covariance is between geoidal height and gravity anomaly, this would imply a geoid-anomaly degree variance.

So far, the modeling of an analytical global covariance function of the Earth's gravity field has been discussed. Anyway, whether one deals with only model degree variances or with a combination of empirical and model degree variances, closed forms exist for the covariance functions relevant to the various gravimetric elements. These analytical covariance models are usually modified to suit the local applications, which is the subject of the following section.

5.7 Determination of a Local Covariance Function Consistent with the Remove-Restore Technique

As the remove-restore technique has been widely adopted for local gravity field modeling, the empirical local covariance function must have as input the residual local data, reduced to an appropriate global geopotential model and to the topographic effect. Hence, a modeled local covariance function, best fitted to the input residual anomaly empirical covariance, should be derived and used. Generally, a local covariance function corresponds to a global covariance function, from which the global signal power has been removed. Ideally, if a global harmonic model of maximum degree and order N has been subtracted from the local data, it should remove N spectral degrees from it. This would correspond to be an N^{th} degree model covariance function, which has zero-degree

variances up to an inclusive degree N (Meissl, 1971; C. C. Tscherning and Rapp, 1974b)**.** Such local (potential) covariance function is derived from the global one (Eq.5.43), as follows

$$K(\psi, r, r') = \sum_{n=N+1}^{\infty} \frac{AR^2}{\{(n-1)(n-2)(n+B)\}} \left(\frac{R_b^2}{rr'}\right)^{n+1} P_n(\cos\psi)$$

$$= -\sum_{n=3}^{N} \frac{AR^2}{\{(n-1)(n-2)(n+B)\}} \left(\frac{R_b^2}{rr'}\right)^{n+1} P_n(\cos\psi) +$$

$$\sum_{n=3}^{N} \frac{AR^2}{\{(n-1)(n-2)(n+B)\}} \left(\frac{R_b^2}{rr'}\right)^{n+1} P_n(\cos\psi) \; . \qquad (5.46)$$

However, according to the discussion in Section 5.4, regarding the dependence of the local empirical covariance function on the regional accuracy of a harmonic model, there exist at least random errors inherent in the geopotential model, which are represented by the global error estimates of the respective harmonic coefficients. Thus, a procedure could be followed in which the removed empirical potential degree variances in Eq. (5.46) (up to degree N) are replaced by the corresponding empirical potential error degree variances, which can be generally scaled by a (unitless) positive scale factor, c (Meissl, 1971; Rapp, 1979; C. C. Tscherning, 1993; C. C. Tscherning and Forsberg, 1986b), as follows

$$K(\psi, r, r') = \sum_{n=2}^{N} c.\,(\sigma_{e\,n}^2)_T \left(\frac{R_b^2}{rr'}\right)^{n+1} P_n(\cos\psi) +$$

$$\sum_{n=N+1}^{\infty} \frac{AR^2}{\{(n-1)(n-2)(n+B)\}} \left(\frac{R_b^2}{rr'}\right)^{n+1} P_n(\cos\psi) \qquad (5.47)$$

where $(\sigma_e{}^2{}_n)_T$ are the empirically determined potential error degree variances, which can be computed from the error estimates of the respective harmonic coefficients up to degree N (in spherical approximation) as follows

$$(\sigma_{e\,n}^2)_T = \left(\frac{GM}{R}\right)^2 \sum_{m=0}^{n} \left(\sigma_{c^*_{nm}}^2 + \sigma_{s_{nm}}^2\right) \; . \qquad (5.48)$$

Recall from the previous section that, to exploit the available closed forms for the infinite covariance expressions, the local covariance function in Eq. (5.47) can be rearranged as follows

$$K(\psi, r, r') = c(\sigma_{e\,2}^2)_T \left(\frac{R_b^2}{rr'}\right)^{2+1} P_n(\cos\psi) + \sum_{n=3}^{N} \left[c(\sigma_{e\,n}^2)_T - \frac{AR^2}{\{(n-1)(n-2)(n+B)\}}\right] \left(\frac{R_b^2}{rr'}\right)^{n+1} P_n(\cos\psi) \; + \; \sum_{n=3}^{\infty} \frac{AR^2}{\{(n-1)(n-2)(n+B)\}} \left(\frac{R_b^2}{rr'}\right)^{n+1} P_n(\cos\psi) \qquad (5.49)$$

which is analogous to Eq. (5.45). Again, assessing the first and second terms is easy, and the closed-form replaces the third term in Eq. (5.33). Of course, the same comments regarding applying the law of variance propagation to Eq. (5.45) are still valid for the above expression, whose first and second terms have a combination of empirical error degree variances and analytical degree variances.

It is worth mentioning that the scale factor, c, is a measure of how well a specific harmonic model fits the local data low-frequency information. Thus, that scale factor describes the local variations of the global accuracy of a geopotential model (D. Arabelos, 1989)**.**

Practically, the corresponding local covariance function of gravity anomalies is fitted to the residual anomaly empirical covariance function via a nonlinear 3-parameter iterative least-squares adjustment. The local isotropic anomaly covariance function model is given as

$$C(P,Q) = C(\psi, r, r') = \sum_{n=2}^{N} c(\sigma^2_{e\,n})_{\Delta g} \left(\frac{R_b^2}{rr'}\right)^{n+2} P_n(\cos\psi) + \sum_{n=N+1}^{\infty} \left[\frac{A(n-1)}{\{(n-2)(n+B)\}}\right] \left(\frac{R_b^2}{rr'}\right)^{n+2} P_n(\cos\psi)$$

$$= c(\sigma^2_{e\,2})_{\Delta g} \left(\frac{R_b^2}{rr'}\right)^{2+2} P_n(\cos\psi) + \sum_{n=3}^{N} c(\sigma^2_{e\,n})_{\Delta g} - \left[\frac{A(n-1)}{\{(n-2)(n+B)\}}\right] \left(\frac{R_b^2}{rr'}\right)^{n+2} P_n(\cos\psi) + \sum_{n=3}^{\infty} \left[\frac{A(n-1)}{\{(n-2)(n+B)\}}\right] \left(\frac{R_b^2}{rr'}\right)^{n+2} P_n(\cos\psi) \quad (5.50)$$

where:

ψ	the spherical distance between p and q (Eq. 3.15)
r	the geocentric radial distance of point P ≈ R+H_p,
r'	the geocentric radial distance of point Q ≈ R+H_q,
R	taken ≈ 6371 km,
H	orthometric height of the respective point,
$(\sigma_e{}^2{}_n)_{\Delta g}$	the n^{th} empirical anomaly error degree variance based on the standard errors of the harmonic coefficients, as given by Eq. (5.31).

The three parameters c, A (as implied by the residual data variance at H=0), and (R_b-R) are given approximate values firstly. On the other hand, the residual anomaly empirical covariance values are input and treated as observations, whereas a relevant set of "computed" observations are assessed from the three input approximate parameters (using Eq. 5.50 and exploiting the closed forms). The adjustment is then performed iteratively until the convergence is arrived, resulting in the final three parameters c, A in $mGal^2$, (R_b-R) in meters and the point gravity anomaly variance at MSL as a by-product. Based on the local residual gravity anomaly data, these parameters are determined via its empirical covariance function. The final values are then used, along with the previously discussed closed forms, to compute all the elements of the auto-covariance matrix between the observations, the auto-covariance matrix of the signals to be predicted, and the cross-covariance matrix between the input observations and the unknown signals. This is done regarding the functional types and the relevant positions. As stated in section 5.1, these covariance matrices are the backbone of the collocation solution.

5.8 Stepwise Least-Squares Collocation for Large Data Sets

It is possible to split up the prediction by collocation into two steps. This may be done to reduce the size of the matrices to be inverted. This procedure is referred to as stepwise least-squares collocation. Particularly, in the case of collocation without parameters, the mathematical model is divided into two parts as follows

$$l_1 = t_1 + n_1$$

$$l_1 = t_2 + n_2 \quad (5.51a)$$

with

$$I = \begin{pmatrix} I_1 \\ I_2 \end{pmatrix} \tag{5.51b}$$

and

$$A = \begin{pmatrix} A_1 \\ A_2 \end{pmatrix} \tag{5.51c}$$

where l_1 and l_2 are the vectors of the two groups of observations and A_1 and A_2 are the corresponding matrices of parameter coefficients. Accordingly, the matrices D and C_{st} are partitioned as follows

$$D = \begin{pmatrix} D_{11} & D_{12} \\ D_{21} & D_{22} \end{pmatrix} \tag{5.51d}$$

$$C_{st=(C_{st} \;\; C_{st})} \tag{5.51e}$$

where D_{11} and D_{22} are the total auto-covariance matrices of the two data groups, D_{12} and D_{21} are the total covariance matrices between the two groups of observations and C_{st1} and C_{st2} are the cross-covariance matrices between the unknown signals and the two data sets, respectively. According to Eqs. (5.9) and (5.10), the LSC solution for the signals and the relevant error estimates is given by

$$S = (C_{st1} \;\; C_{st2}) \begin{pmatrix} D_{11} & D_{12} \\ D_{21} & D_{22} \end{pmatrix}^{-1} \begin{pmatrix} I_1 \\ I_2 \end{pmatrix} \tag{5.52a}$$

$$E_{ss} = C_{ss} - (C_{st1} \;\; C_{st2}) \begin{pmatrix} D_{11} & D_{12} \\ D_{21} & D_{22} \end{pmatrix}^{-1} (C_{st1} \;\; C_{st2})^T \; . \tag{5.52b}$$

It can be shown that the above expressions reduce to (Moritz, 1980; C. C. Tscherning, 1974)

$$S = [C_{st1}\, D^{-1}{}_{11}\, l_1] + [(C_{st2} - C_{st1}\, D^{-1}{}_{11}\, D_{12})\, (D_{22} - D_{21}\, D^{-1}{}_{11}\, D_{12})^{-1}\, (l_2 - D_{21}\, D_{11}{}^{-1}\, l_1)]$$

$$= S_1 + S_2, \tag{5.53a}$$

$$E_{ss} = C_{ss} - [C_{st1}\, D^{-1}{}_{11}\, C_{st1}{}^T] - [C_{st2}\, D^{-1}{}_{22}\, C_{st2}{}^T]$$

$$= C_{ss} - E_{ss1} - E_{ss2}, \tag{5.53b}$$

where S_1 and S_2 are the contributions of the two data groups, l_1 and l_2, to the predicted signals and E_{ss1} and E_{ss2} are the respective gains in accuracy. Hence, it is clear that the inversion would be necessary only for the diagonal blocks D_{11} and D_{22}. If the second group contains one observation at a time, then one deals with sequential collocation, where D_{22} would diminish to a single element.

Thus, the main advantage of using stepwise collocation is that the normal matrices inverted are smaller than the original D matrix. Hence, the total storage requirements are not reduced. So, when using PCs with a high storage capability, which are available nowadays, the stepwise solution of the normal equations will be of no real advantage (C. C. Tscherning, 1974)**.** However, such a technique could be used to incorporate an additional set of new observations to improve a previous LSC solution.

5.9 Fast Collocation

When using the (LSC) technique, the CPU time will vary depending on the number of observations, the used covariance functions, the number of signals to be predicted, and their error estimates. It is well known that the total covariance matrix D, to be inverted in the LSC, is symmetric for any data distribution pattern.

Particularly, for a data set of u observations, one obtains the total covariance matrix of the observations as follows

$$D_{u,u} = \begin{pmatrix} d_{11} & d_{12} & \cdots & \cdots & \cdots & d_{1u} \\ & d_{22} & d_{23} & \cdots & \cdots & d_{2u} \\ & & d_{33} & \cdots & \cdots & d_{3u} \\ & & & \ddots & \cdots & \vdots \\ & & & & \ddots & \vdots \\ & & & & & d_{uu} \end{pmatrix} . \quad (5.54)$$

Every off-diagonal element is the sum of the covariance function and the relevant error covariance (if the data noise is correlated), whereas every diagonal element equals the sum of the variance and the respective error variance.

Considering the arrangement of data in a planar grid and assuming homogeneous data types, equal error variances, and uncorrelated data noise, it can be shown that the total covariance matrix D will be a symmetric block Toeplitz matrix, and each block is itself a symmetric Toeplitz matrix. Thus, one obtains a Toeplitz/Toeplitz structure (Barzaghi et al., 2003), which can be exploited to obtain a fast collocation solution. Particularly, if a planar data grid has u = r . m observations, where r and m are the number of rows (latitudes) and columns (longitudes), respectively, then the total covariance matrix, D, will show the following symmetric block Toeplitz structure

$$D_{u,u} = \begin{pmatrix} k_{11} & k_{12} & \cdots & \cdots & k_{1,r-1} & k_{1r} \\ & k_{22} & k_{23} & \cdots & \cdots & k_{2r} \\ & & k_{33} & \cdots & \cdots & k_{3r} \\ & & & \ddots & \cdots & \vdots \\ & & & & \ddots & k_{r-1,r} \\ & & & & & k_{rr} \end{pmatrix} \quad (5.55)$$

where each K_{ij} block is an (m x m) matrix that carries the mutual covariances (plus the noise terms) between the points along the i^{th} and j^{th} latitudes. It should be noted that the block Toeplitz structure implies that $K_{11}=K_{22}=\ldots.=K_{rr}$, $K_{12}=K_{23}=K_{34},\ldots..=K_{r-1,\,r}$, $K_{13}=K_{24}=K_{35}=\ldots.=K_{r-2,\,r}$ and $K_{1,\,r-1}=K_{2r}$. Moreover, each block has its own symmetric Toeplitz structure as follows

$$K_{ij(m,m)} = \begin{pmatrix} k_1 & k_2 & k_3 & \cdots & k_{m-1} & k_m \\ & k_1 & k_2 & k_3 & \cdots & k_{m-1} \\ & & k_1 & k_2 & k_3 & \vdots \\ & & & \ddots & \cdots & k_3 \\ & & & & \ddots & k_2 \\ & & & & & k_1 \end{pmatrix} . \quad (5.56)$$

Combining Eqs. (5.54) and (5.55), one obtains the total covariance matrix in the following form

$$D_{(u,u)} = \begin{pmatrix} d_1 & d_2 & d_3 & \cdots & d_{u-1} & d_u \\ & d_1 & d_2 & d_3 & \cdots & d_{u-1} \\ & & d_1 & d_2 & d_3 & \vdots \\ & & & \ddots & \cdots & d_3 \\ & & & & \ddots & d_2 \\ & & & & & d_1 \end{pmatrix} . \quad (5.57)$$

It is clear that, due to that special structure, the storage of the covariance matrix is much reduced since the knowledge of the first row is sufficient to construct the whole matrix. In the fast collocation methodology, this very simple form of the total covariance matrix is combined with an efficient inversion algorithm to reduce the CPU time required by collocation greatly. It should be mentioned that the block Toeplitz structure (and not the Toeplitz structure within each block) is

destroyed if the data grid is expressed in geodetic coordinates, as a consequence of the convergence of meridians. Nevertheless, this drawback can be overcome by an iterative procedure (ibid.). The fast collocation procedure could be optimally used to merge some existing national geoid solutions into a unified regional solution (C. C. Tscherning et al., 1987). The main disadvantages of the fast collocation algorithm are the approximations in the input data noise, the use of only homogeneous data types, and the restriction on the data distribution, which greatly constrain the flexibility of the collocation technique.

5.10 Ellipsoidal Collocation

The spherical approximation is used in gravity modelling because the surface to which a boundary value problem is related is a sphere and is considered twofold. On the one hand, the position of a point in terms of geocentric latitude, geodetic longitude, and radial distance is equal to the geodetic latitude, geodetic longitude (unchanged) and the radial distance is set equal to R+h. Frequently one further approximation is made, where the orthometric or normal height replaces the ellipsoidal height h. This is referred to as a spherical approximation in geometry space. On the other hand, the reference ellipsoid is approximated by a sphere of radius R. Furthermore, the relevant normal gravity is replaced by the mean gravity (GM/R^2) and the derivatives in the vertical direction (in the functional relationships between the various gravitational quantities) are taken in the direction of the radius vector. This is looked upon as a spherical approximation in the gravity space.

Using an ellipsoidal boundary surface (instead of the geoidal surface) will improve the ellipsoidal approximation. In least-squares collocation, however, the use of an ellipsoidal boundary leads to very complicated numerical procedures, making such a method an extremely heavy task. In spherical approximation, the LSC solution is expressed as a linear combination of base functions, which are harmonic outside the Bjerhammar sphere that is enclosed inside the Earth. The basic covariance function is rotationally invariant on spheres which are harmonic outside the Bjerhammar sphere, such as on the Earth's mean surface. Furthermore, spherical approximation enables representing a large class of covariance functions in simple closed expressions.

On the other hand, if no spherical approximation is used, the rotational invariance will be lost. It is easy to notice that in the case of non-spherical approximation, the degree variances and covariance functions would be dependent on the equatorial radius, a, and on r and γ of the evaluation point, as it would generally be latitude dependent, thus violating the isotropy assumption (Colombo, 1980). This means that the LSC solution would depend on the latitude. One possible method to solve this problem is to use an-isotropic covariance functions or covariance functions based on the complex ellipsoidal harmonics. Such non-isotropic kernels would imply a harmonicity domain down to "a Bjerhammar ellipsoid" with a semi-minor axis smaller than or equal to the semi-minor axis of the Earth. However, closed expressions for such ellipsoidal covariance functions have not been developed yet. Such closed forms should be the aim of theoretical gravity field research. Therefore, throughout the current work, all the encountered collocation solutions will be performed in spherical approximation. This seems admissible since the remove-restore technique is used (Martinec, 1998).

6. Numerical research

The methodology, numerical research, creating a mathematical model, and determination of reference surfaces are presented in this chapter.

The distribution of the available data over the entire territory of Egypt is inconsistent, as the data are intense in some northern regions but sparse in the southern and western regions.

Data deficiency still exists at this time, therefore, it's not adopted to use a prediction technique as Least Square Collocation (LSC) for the determination of the geoid, whereas the essential conditions are not suitable for the whole area of Egypt. Therefore, a selected "data window" called AREA01 was chosen for applying the LSC technique in this research.

The outcome solution from the LSC technique will be used as a reference to assist the geoid solution from the proposed mathematical model through areas where it is impossible to provide many observations. The following would be possible:

• economical survey using GNSS in terms of homogeneous height,

• preliminary data for a large number of local geophysical surveys,

• providing preliminary data for all future projects in the field of gravitational field determination and geodetic reference systems, and

• monitoring changes in the Earth's physical surface in the relevant areas.

The modified Stokes' formula that combines local terrestrial data with a global geopotential model (GGM) is often used nowadays. The optimum modification of Stokes' formula, introduced by (Sjöberg, 2003), is employed to minimize the expected mean square error of the combined geoid height. According to this stochastic method, the approximate geoid height is first computed from the modified Stokes' formula using surface gravity data and a GGM. The precise geoid height is then obtained by downward continuation and by adding topographic and ellipsoidal corrections to the approximate geoid height.

The commonly adopted and applied approach to regional gravimetric geoid determination is the so-called Remove-Compute-Restore (RCR) technique (Schwarz et al., 1990). The complete expansion of GGM is used in conjunction with regional terrestrial gravity data via the spherical Stokes' integral. In principle, in the RCR technique, any a priori known signal features are first removed from the observed data before the prediction process and then appropriately added back (restored) to the predicted features. Moreover, a suitable (DTM) is usually used to account for local topographic effects (Fig. 37).

The LSC algorithm is a flexible tool for combining all possible heterogeneous data in one unified solution to solve any desired type of anomalous signals. The LSC estimated signals, which have minimum error variance among all other solutions, could also be evaluated at any point (Moritz, 1978, 1980). This study's main objective is whether it is possible to determine the geoid at the centimeter level in the territory of Egypt by using LSC.

A schematic diagram of the general computation procedure, which is considered one of the possible solutions, is depicted in Fig. 38.

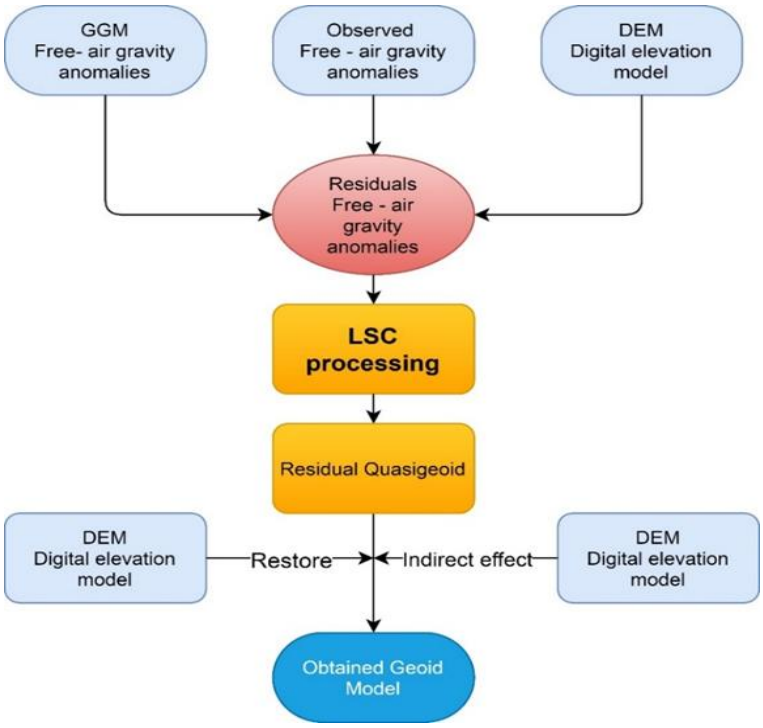

Figure 37 Overview of data processing steps for the remove-compute-restore procedure

The processing procedures consist of:

1. data collection,
2. data preparation,
3. formation of final data sets,
4. quality analysis and data selection, and then determination geoid for Data Window Selection Area
5. long-wave characteristics of anomalous potential functionals (free-air anomaly and anomalous heights),
6. short-wave characteristics of the anomalous potential functional (free-air anomaly and anomalous heights),
7. residual functionalities of anomalous potential (anomaly of free air and anomalous heights),
8. residual anomalous heights,
9. short-wave characteristics of anomalous heights,
10. long-wave characteristics of anomalous heights,
11. quasi-geoids,
12. differences between quasi-geoids and geoids,
13. geoid in the spherical approximation of ellipsoids by terrestrial sphere,
14. ellipsoidal corrections,
15. geoid,
16. translation parameters,
17. combined solution,

18. assess the residual,

19. and finally, the surface of the transformation.

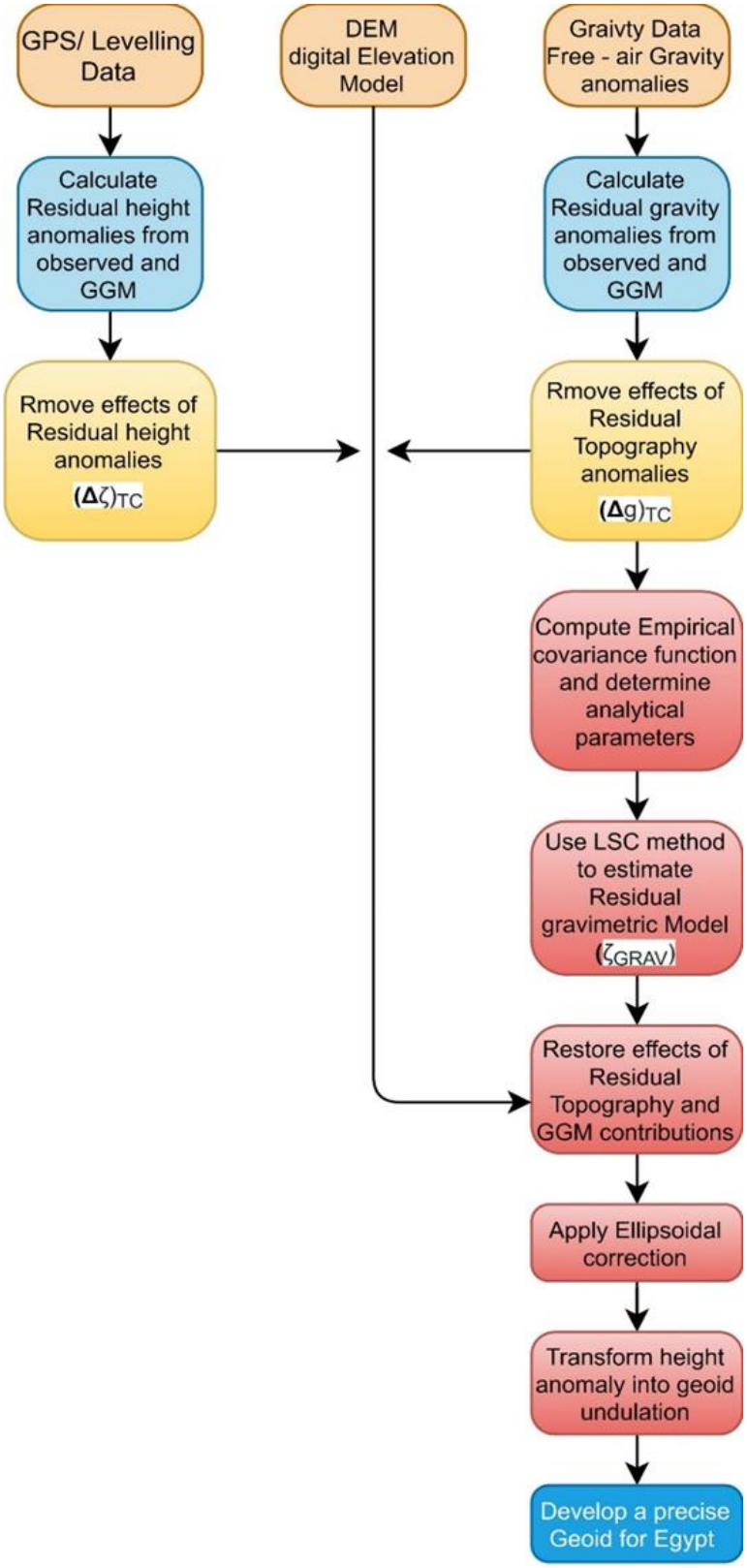

Figure 38 Flowchart of the procedure of developing a precise geoid model for Egypt

6.1. Available Data

6.1.1. Gravimetric Observation

The local gravity anomaly data used in this research was gathered from two sets. The first set mostly consists of previously available free-air gravity anomalies gathered at 1000 points with -4.57 mGal as mean (average) and 32.37 mGal as standard deviation. The sources of these data are documented in previous works (M. Amin et al., 2002, 2003; El-Tokhy, 1993). Besides, two sets of free-air gravity anomaly values at 267 and 333 points were obtained from the Bureau Gravimetric International (BGI), where the mean value is -6.09 mGal, and the standard deviation is 19.57 mGal. The total number of points in the first set is 1600 data points.

The second set consists of 55,250 observational data points provided by Getech company and obtained under the African Gravity Project (Fairhead, 1988) see (Fig. 39). Some of these data were observed in the pre-GNSS/GPS era, therefore, the major sources of errors that contaminate the data are the inaccurate estimates of the positions and heights of the stations, but the data provider recommended an accuracy of 1.0 mgal. Getech did not provide enough information about the methods of processing the data, but recommended the 1.0 mGal accuracy.

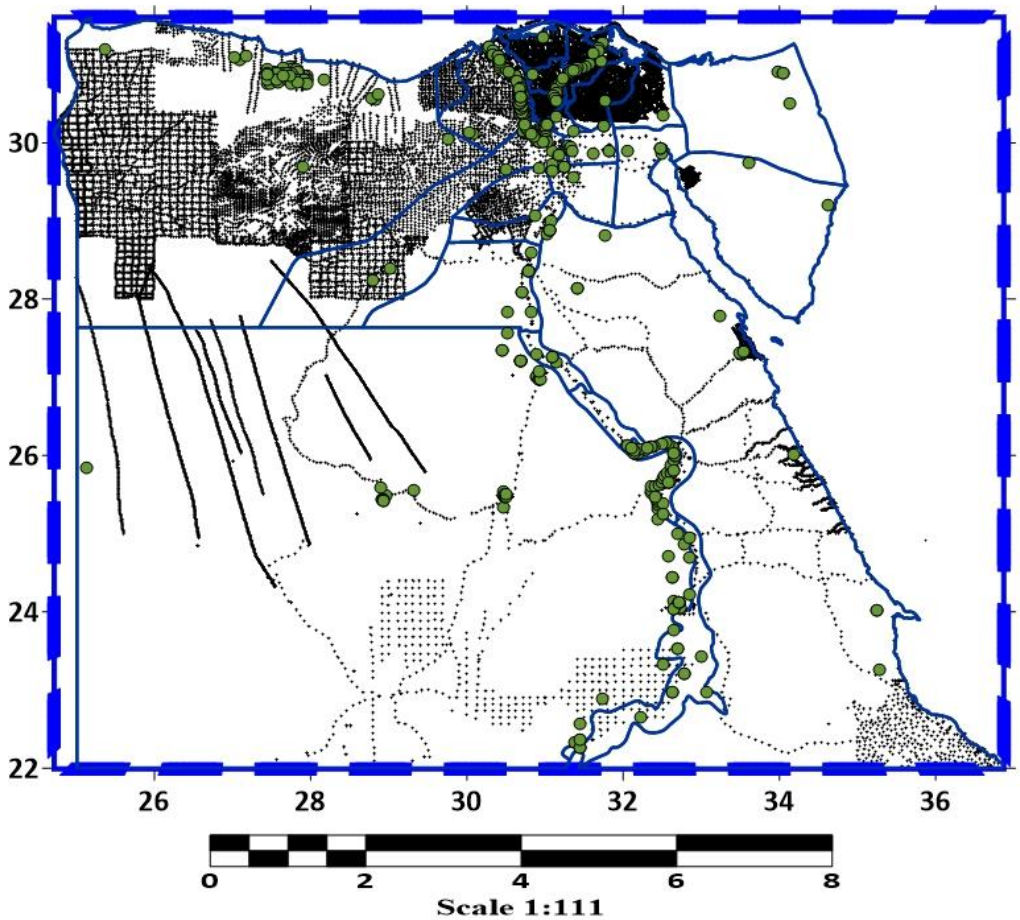

Figure 39 The available local gravimetric data (black dots represent free-air gravity anomalies)and discrete GPS/dh data points represent green dots.

6.1.2. Discrete Values of Anomalous Heights

This group contains 453 discrete values of anomalous heights from GPS/H data stations, and their distribution as 7 discrete anomalous heights determined in relation to the system of orthometric

height for National Egyptian vertical Datum and ellipsoidal heights values in fundamental benchmarks of High Accuracy Reference Network (HARN) that covers the entire Egyptian territory and consists of 30 stations with approximate separation of 200 km, the relative precision level of HARN is 1:10,000,000.

In addition to 49 data points from the National Agricultural Cadastral Network (NACN), which covers the Nile valley and the Delta, with relative a precision 1:1,000,000 (Dawod and Ismail, 2005).

In addition to 83 data points of the reference Egyptian Surveying Authority ESA network, 138 from old collections and 28 data points were obtained from the article published in the Arabian Journal of Geosciences (Rabah and Kaloop, 2013) in addition to 148 stations from various national projection (Fig. 40). Most of those data sources have been published in many researches (Amin et al., 2002, 2003; El-Tokhy, 1993).

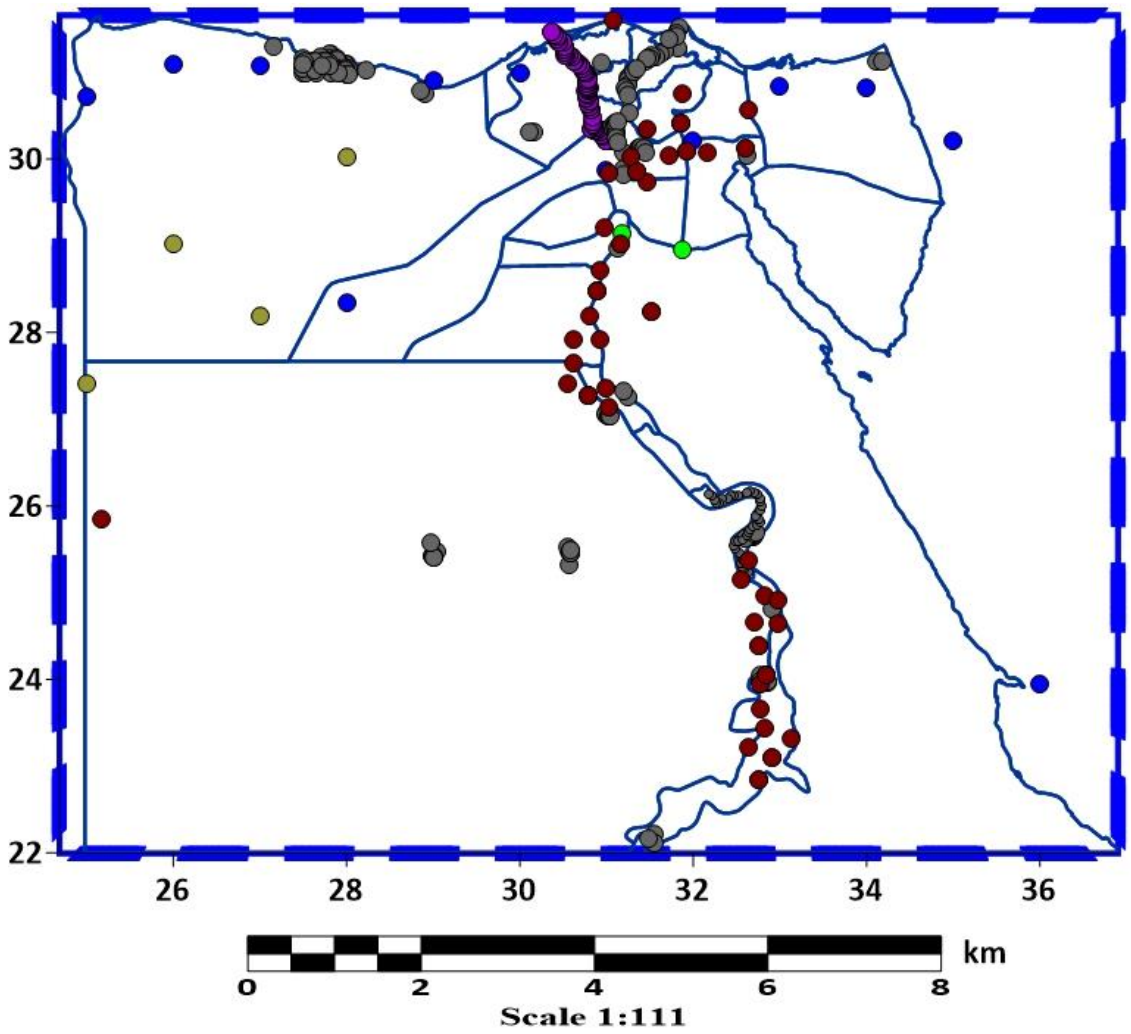

Figure 40 The available local GPS/dh data (green dots represent (Rabah and Kaloop (2013) data, blue dots represent old collections data, dark red dots represent NACN data, light green dots represent HARN data, gray dots represent data points collected from several projects, purple dots represent ESA GPS/H discrete data points)

6.1.3. Digital Elevation Model

Shuttle Radar Topography Mission (SRTM), with a resolution of three arc second in both directions (Fig. 41), was used for determining the short-wave characteristics of the anomalous

potential functional beyond those provided by the maximum degree/order GGM by computing the so-called Residual Terrain Model (RTM) (Forsberg, 1984), Such data of SRTM are distributed for free via the public web service (https://lta.cr.usgs.gov/SRTM) (Farr and Kobrick, 2000).

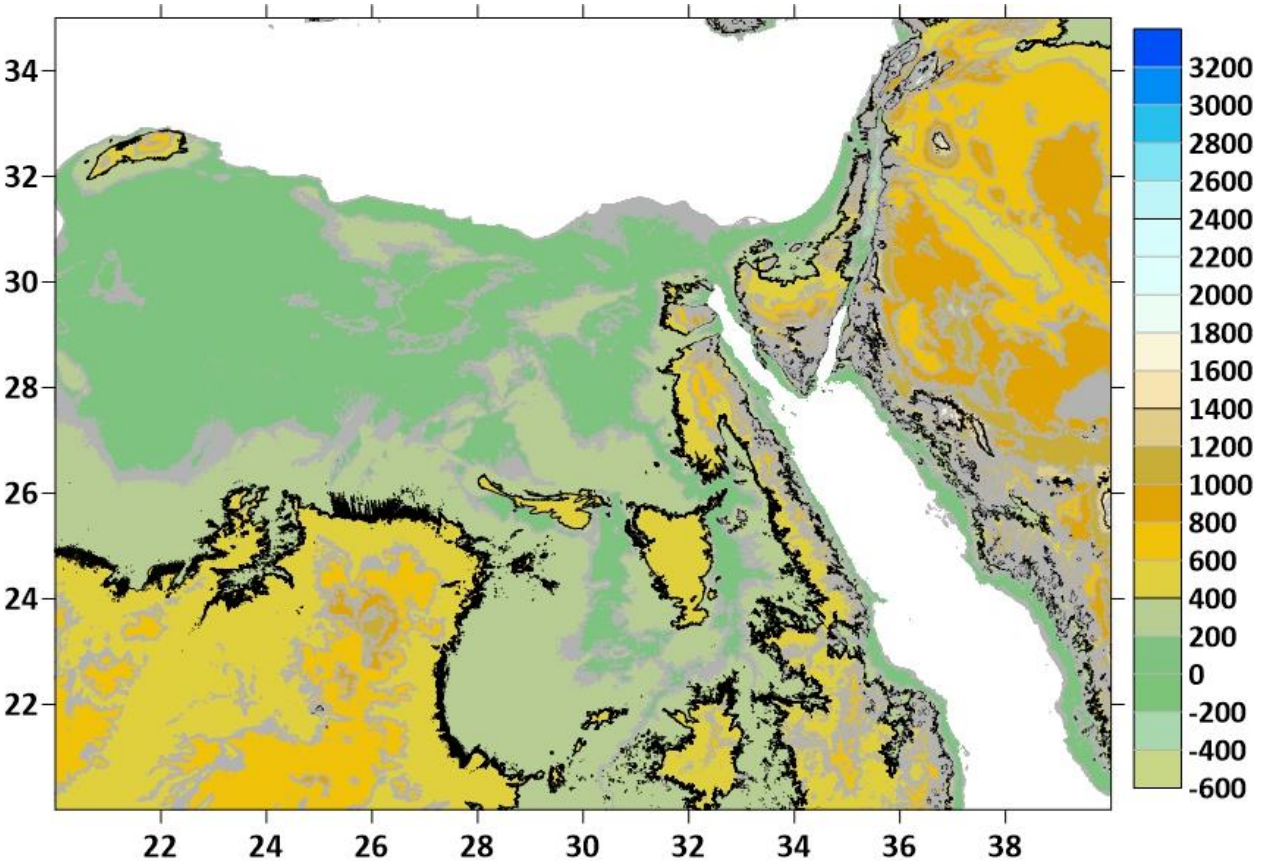

Figure 41 SRTM Digital Elevation model for whole Egypt territory which was used to calculate short wave length effects, unit in m

6.1.4. Global Geopotential Model

Table 10 illustrates the three GGMs used for determining the long-wave characteristics of the anomalous potential functional , the first one GOCO05c is a combined GGM up to degree and order 720 based on GOCO05S and altimetric/terrestrial gravity anomaly data set also GOCO05c is an independent of EGM2008. (Fecher et al., 2016)

The second GGM is A High-Resolution Earth's Gravity Field Model SGG-UGM-2 was developed by combining the observations of the Gravity Field and Steady-State Ocean Circulation Explorer (GOCE), the normal equation of the Gravity Recovery and Climate Experiment (GRACE), marine gravity data derived from satellite altimetry data, and EGM2008-derived continental gravity data. (Liang et al., 2020)

The third GGM XGM2019e is a combined global gravity field model, which included data from GGM GOCO06s combined with a ground gravity grid which also covers the shorter wavelengths. (Zingerle et al., 2020)

Table 10 Global Geopotential Models *(*A is for altimetry, S is for satellite (e.g., GRACE, GOCE, LAGEOS), G for ground data (e.g., terrestrial, shipborne, and airborne measurements), and T is for topography*)*

Global Geopotential Model	Degree/order	Data	References
GOCO05c	720	A, G, S	(Fecher et al., 2016)
SGG-UGM-2	2190	A, (EGM2008, Grace), S(Goce)	(Liang et al., 2020)
XGM2019e	2190	A, G, S(GOCO06s), T	(Zingerle et al., 2020)

6.1.4.1. Evaluation of the Performance of the Chosen GGMs Over Egypt Territory

All models were downloaded from the website http://icgem.gfz-potsdam.de/home. However, GGM models are compared to 56850 terrestrial gravity data points and 453 GPS/H data points to choose the best performance GGM over Egypt, where GGM is necessary in determining the geoid of Egypt.

The statistical computations show GGM XGM2019e has a superior precision of the residuals deferences of free-air gravity anomalies and corresponding values computed from XGM2019e in terms of Standard deviation than Goce05c on the other hand, it has not same precision with respect to residuals from GPS/H and height anomalies. Tables 11 and 12 summarize the numerical results of the comparison operation.

Table 11 Statistical computation residuals of the free- air gravity anomaly data points and corresponding from GGMs (unit: mgal)

	Model	Degree/order	Min	Max	Mean	Std. Dev.
$\delta\,\Delta g$ [mGal]	GOCO05c	720	-56.821	53.435	-0.232	9.713
	SGG-UGM-2	2190	-97.865	41.159	-0.089	8.681
	XGM2019e	2910	-52.471	41.144	0.422	7.779

Table 12 Statistical computation residuals of discrete GPS/H data points and corresponding from GGMs (unit: m)

	Model	Degree/order	Min	Max	Mean	Std. Dev.
$\delta\,N[m]$	GOCO05c	720	-1.904	0.893	-0.330	0.435
	SGG-UGM-2	2190	-0.939	1.809	0.570	0.449
	XGM2019e	2910	-2.036	0.837	-0.371	0.487

We can notice from Tables 11, 12, and Figs. 42, 43, 44, 45, 46, and 47, the residual free air anomaly difference between GOCO05c and XGM2019e models is 1.9 mGal in terms of standard deviation, while there is a 5 cm difference at discrete GPS/H data points in terms of standard deviation. That means the two mentioned GGMs have almost the same accuracy regarding the free air gravity anomaly residuals, but GOCO05c is better by 5 cm less of the residuals from discrete GPS/H points over Egypt. Therefore, GOCO05c has been used as a reference model in this research .

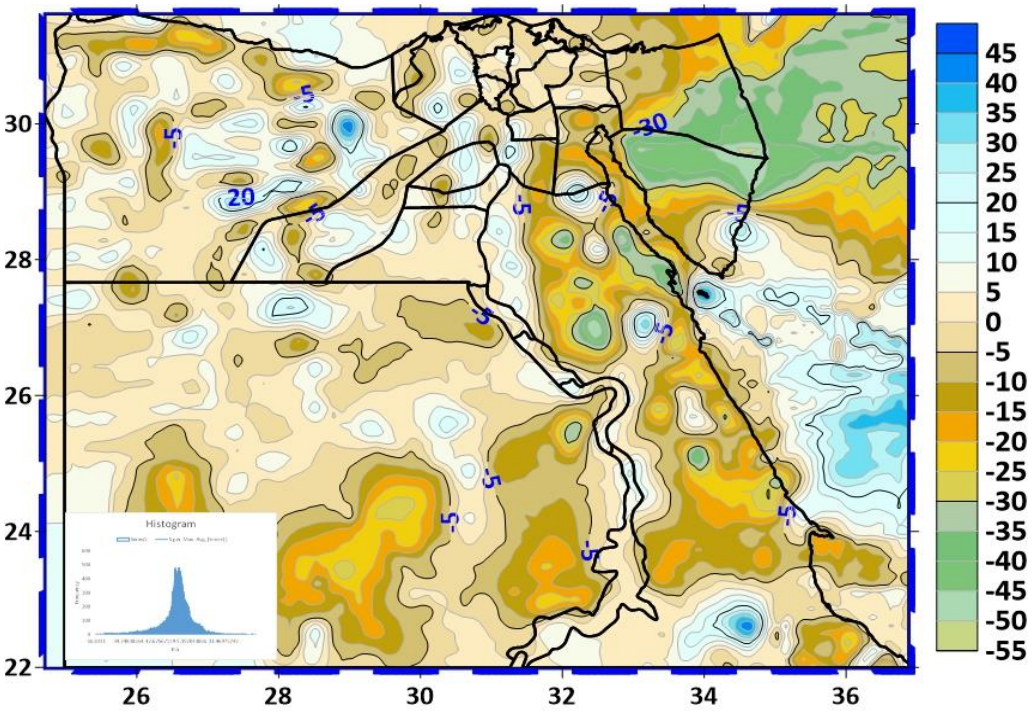

Figure 42 Free air gravity anomaly residuals obtained from GGM GOCO05c and discrete Free air gravity anomaly values over whole territory of Egypt. The histogram of residuals is shown on the below left corner of the map.

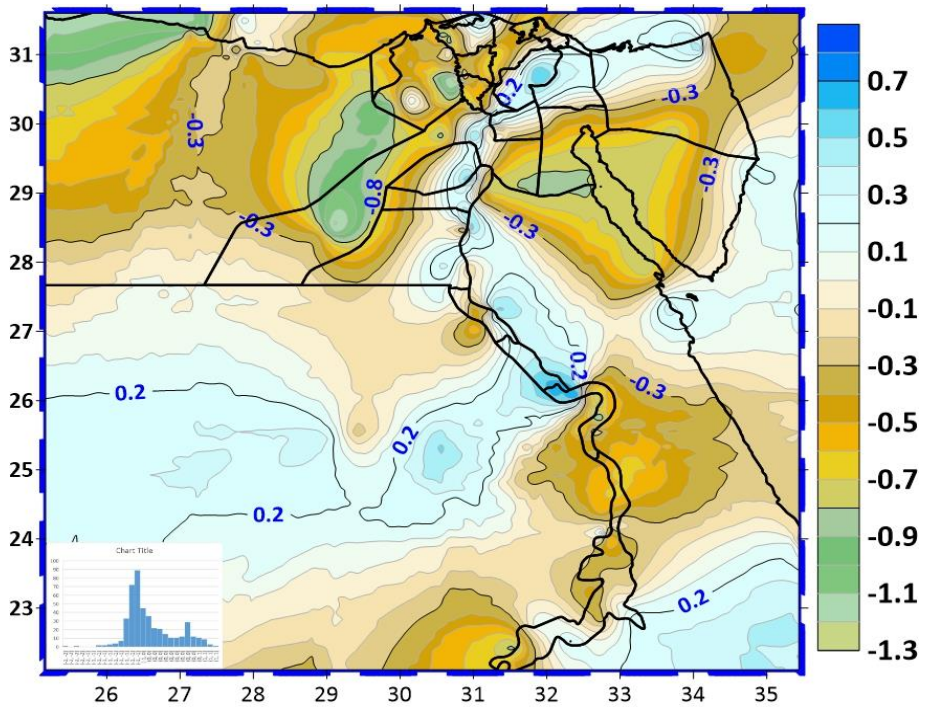

Figure 43 Height anomaly residuals obtained from GGM GOCO05c and discrete GPS/H over whole territory of Egypt. The histogram of residuals shown on the below left corner of the map.

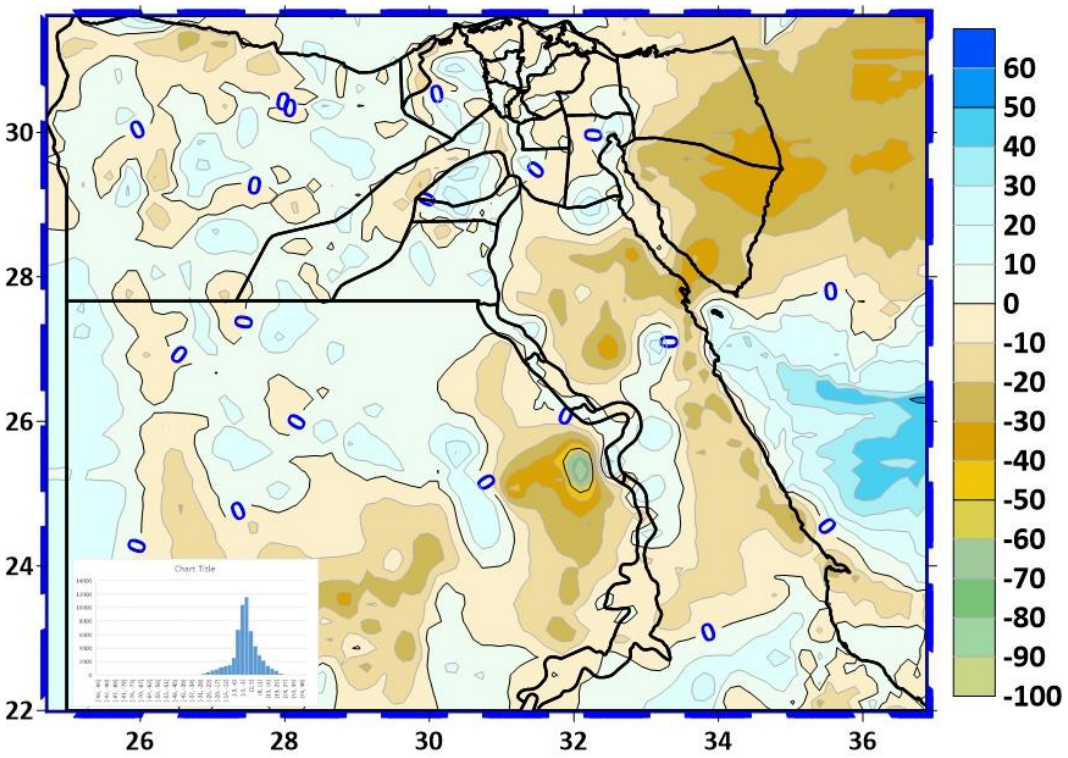

Figure 44 Free air gravity anomaly residuals obtained from GGM SGG-UGM-2 and discrete Free air gravity anomaly values over whole territory of Egypt. The histogram of residuals shown on the below left corner of the map.

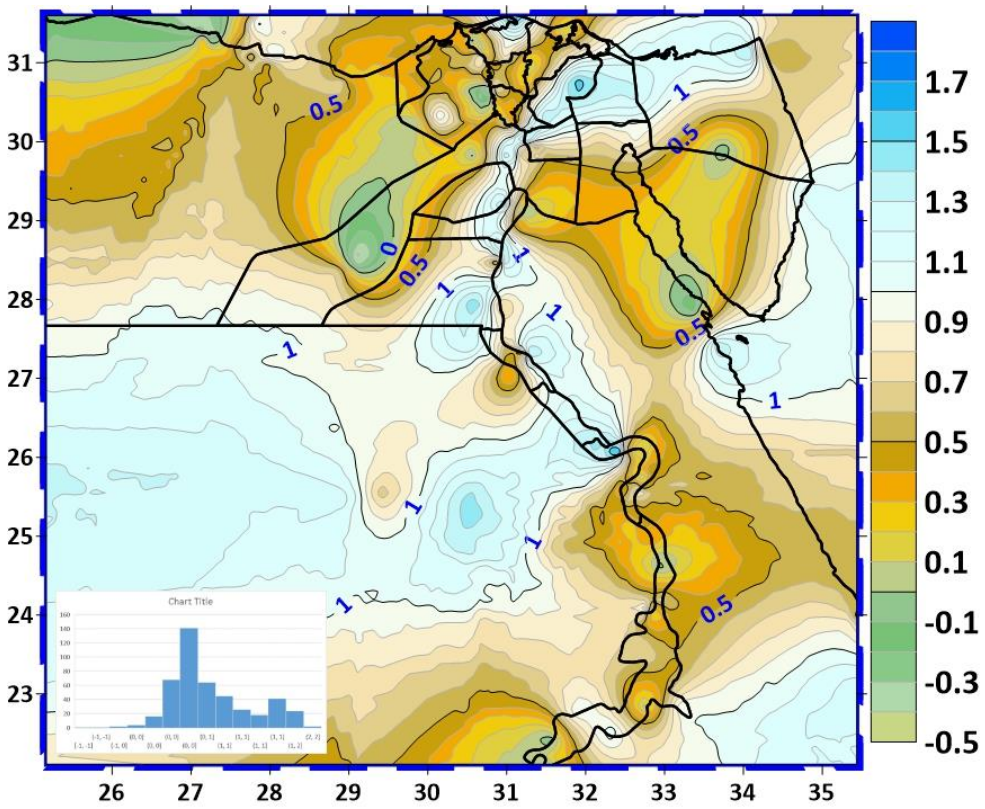

Figure 45 Height anomaly residuals obtained from GGM SGG-UGM-2 and discrete GPS/H over whole territory of Egypt. The histogram of residuals shown on the below left corner of the map.

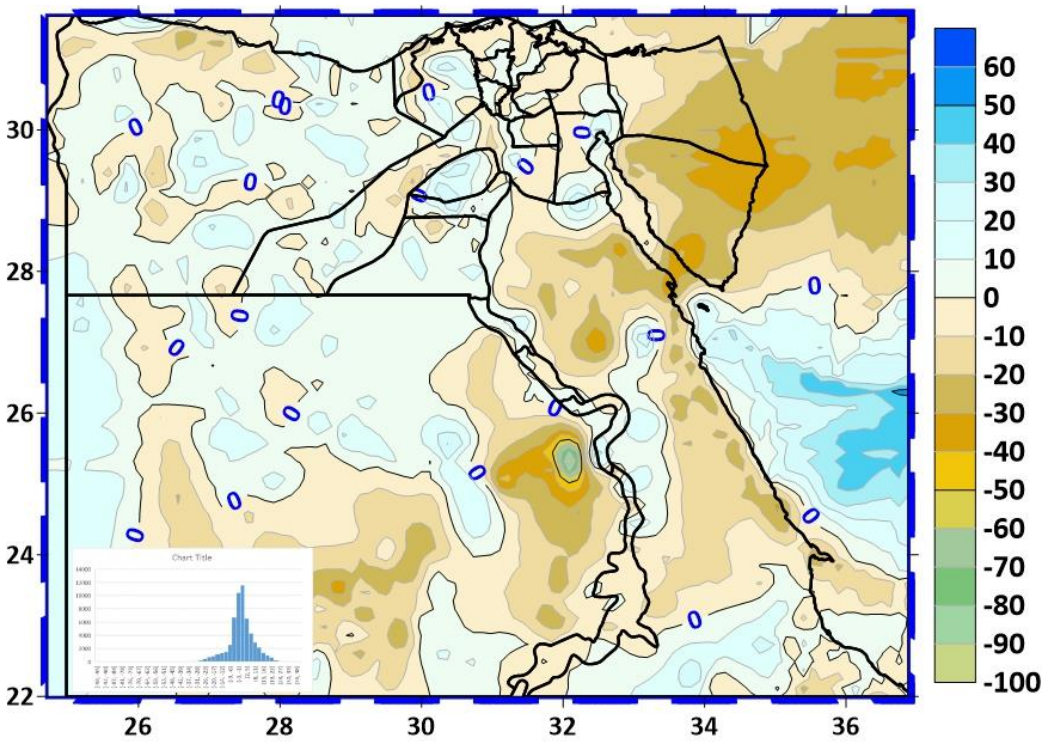

Figure 46 Free air gravity anomaly residuals obtained from GGM XGM2019e and discrete Free air gravity anomaly values over whole territory of Egypt. The histogram of residuals shown on the below left corner of the map.

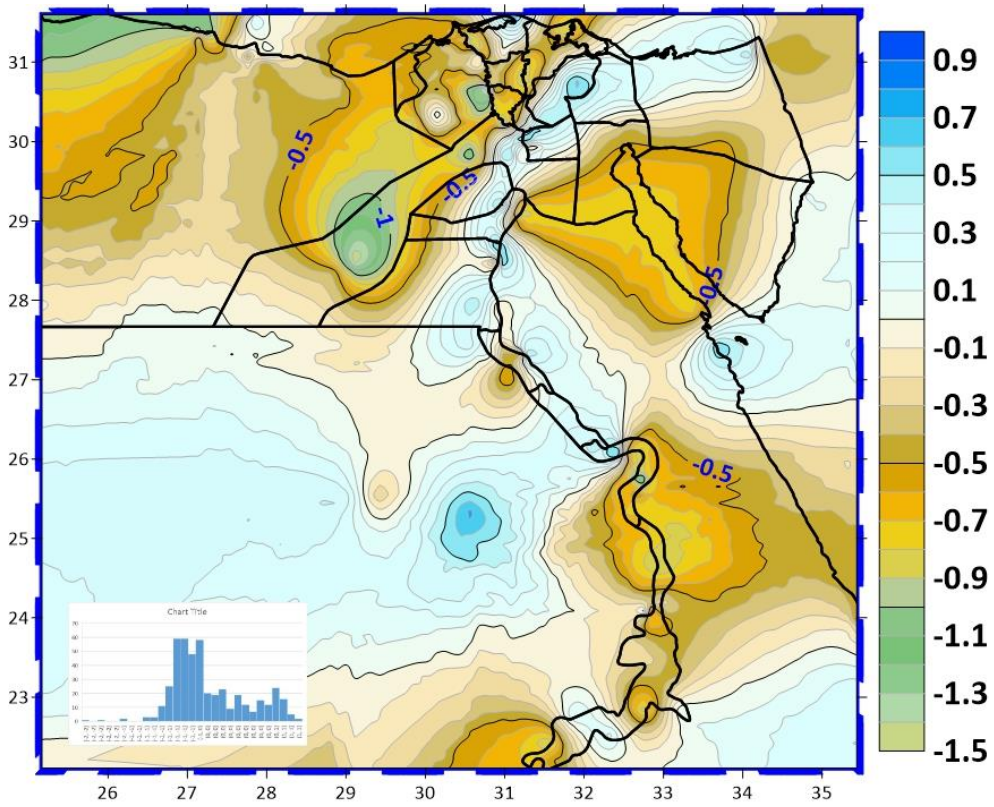

Figure 47 Height anomaly residuals obtained from GGM XGM2019e and discrete GPS/H over the whole territory of Egypt. The histogram of residuals is shown on the below-left corner of the map.

6.2 Geoid Determination for Data Window Selection Area 01

Good coverage and distribution of local gravimetric data are needed to determine a centimeter's accurate geoid by applying the LSC. Unfortunately, this condition cannot be achieved all over Egypt territory.

Therefore, an area with dense data was chosen as a window for calculations, as shown in Fig. 48. Hence, 38150 data points of free-air gravity anomalies and 180 GPS/dh discrete values were used to determine geoid solutions for this Area01.

The data set window referred to the WGS84 and IGSN71 and extended 4 degrees in the south-north direction and 7 degrees in the west-east direction, the statistical calculations for those values are shown in Tables 13 and 14.

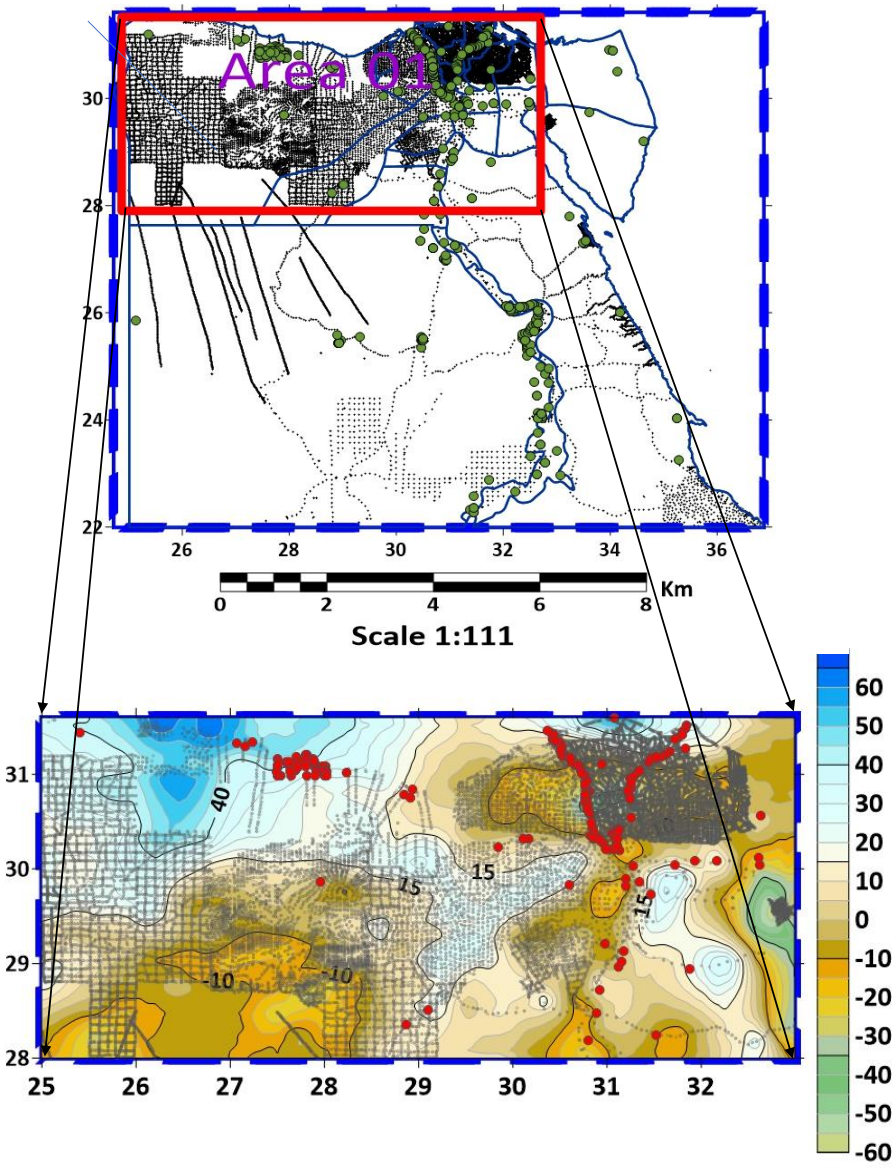

Figure 48 The location and contour map of available free air gravity anomaly data set with an interval of 5 mGal, *and discrete GPS/H points of the selected dense data Area01 (red dots represent GPS/H data points while light grey dots represent Free Air gravity anomaly data points)*

6.2.1 Formation of Final Data Sets

The formation of final data sets refers to the determination of the anomalous potential functional in accordance with theoretically defined relations:

$\zeta_P = h_P - \zeta_P$ (6.1)

$\Delta g_P = g_P - \gamma_P$ (6.2)

where

ζ_P anomalous height,

Δg_p Free air anomaly.

All the presented relations refer to the approximation of the ellipsoid by the terrestrial sphere, where it is assumed that no reductions of the measurement results were applied. All quantities refer to the point P, which is located on the Earth's physical surface, i.e., to the point Q, which is by definition the point of the telluride.

6.2.2 Long-Wave Characteristics of The Anomaly Potential Functional

The long-wavelength characteristic of the functional was determined using the global geopotential model GOCO05c.

The basic expression for the value of long-wavelength characteristics of anomalous potential functionals is the expression for anomalous potential as a function of (orthonormal) spherical harmonics (Rapp, 1997):

$$T = \frac{kM}{r}\sum_{n=2}^{\infty}\left(\frac{a}{r}\right)^n \sum_{m=0}^{n}\left[\left(\bar{J}_{nm} - \bar{J}^U_{nm}\right)\cos m\lambda + \bar{K}_{nm}\sin m\lambda\right]\bar{P}_{nm}(\cos\theta) \quad (6.3)$$

where

a the semi major-axis of the ellipsoid in the plane of the equator,

K Universal gravitational constant,

M the mass of the body of the Earth,

$\bar{J}_{nm}$, $\bar{K}_{nm}$ orthonormal coefficients of spherical harmonic development of the Earth's acceleration potential,

$\bar{J}^U_{nm}$ orthonormal coefficients of spherical harmonic expansion of the Earth's acceleration potential,

$\bar{P}_{nm}$ orthonormal Legendre functions.

By replacing the sign ∞ in the previous equation with , N_{max}, maximum degree of GGM as well as unknown theoretical values of the coefficients, $\bar{J}_{nm}$, $\bar{K}_{nm}$ coefficients of the global model, $\bar{J}`_{nm}$, $\bar{K}`_{nm}$, we get an expression for determining the long-wave anomaly potential at any point:

$$T_{GGM} = \frac{kM}{r^2}\Sigma_{n=2}^{Nmax}\left(\frac{a}{r}\right)^n \Sigma_{m=0}^{n}\left[\left(\bar{J}`_{nm} - \bar{J}^U_{nm}\right)\cos m\lambda + \bar{K}`_{nm}\sin m\lambda\right]\bar{P}_{nm}(\cos\theta)\ . \quad (6.4)$$

Based on the previously presented expression and theoretically defined relations of the anomalous potential and its linear functionals, the following expressions for long-wavelength characteristics of the functional are given

- acceleration anomaly

$$\Delta g_{GGM} = \frac{kM}{r^2}\sum_{n=2}^{N_{max}}(n-1)\left(\frac{a}{r}\right)^n \sum_{m=0}^{n}\left[\left(\bar{J}_{nm} - \bar{J}^{U}_{nm}\right)\cos m\lambda + \bar{K}_{nm}\sin m\lambda\right]\bar{P}_{nm}(\cos\theta) \qquad (6.5)$$

- anomalous height

$$\zeta_{GGM} = \frac{kM}{r\gamma}\sum_{n=2}^{N_{max}}\left(\frac{a}{r}\right)^n \sum_{m=0}^{n}\left[\left(\bar{J}_{nm} - \bar{J}^{U}_{nm}\right)\cos m\lambda + \bar{K}_{nm}\sin m\lambda\right]\bar{P}_{nm}(\cos\theta)\,. \qquad (6.6)$$

The above expressions were applied to 38150 free air anomaly values and 180 discrete values of anomalous heights, table 15 contains statistically computation of the terrestrial free air gravity anomaly and the residuals from the comparison of those terrestrial data and the corresponding values obtained from Goco05c, while table 14 illustrated statistical computations for observed anomaly height GPS/H and the corresponding anomaly heights obtained from GOCO05c model. The residuals of these comparisons were represented by contour maps, as shown in Figs. 49 and 50.

Table 13 Residuals from the discrete gravity anomaly data points and corresponding points from GGM for the selected Area 01 (unit: mgal)

Free air gravity anomaly	Min	Max	Mean	Std. Dev.
Δg Terrestrial	-58.844	64.639	-1.562	19.408
δ Δg GOCO05c	-56.963	46.833	0.976	8.437

Table 13 Residuals from the discrete GPS/H data points and corresponding points from GGM for the selected Area 01 (unit: m)

GPS/H and Height anomaly	Min	Max	Mean	Std. Dev.
Observed GPS/H	-123.936	658.419	62.458	83.805
δ N GOCO05c	-0.939	1.809	0.570	0.449

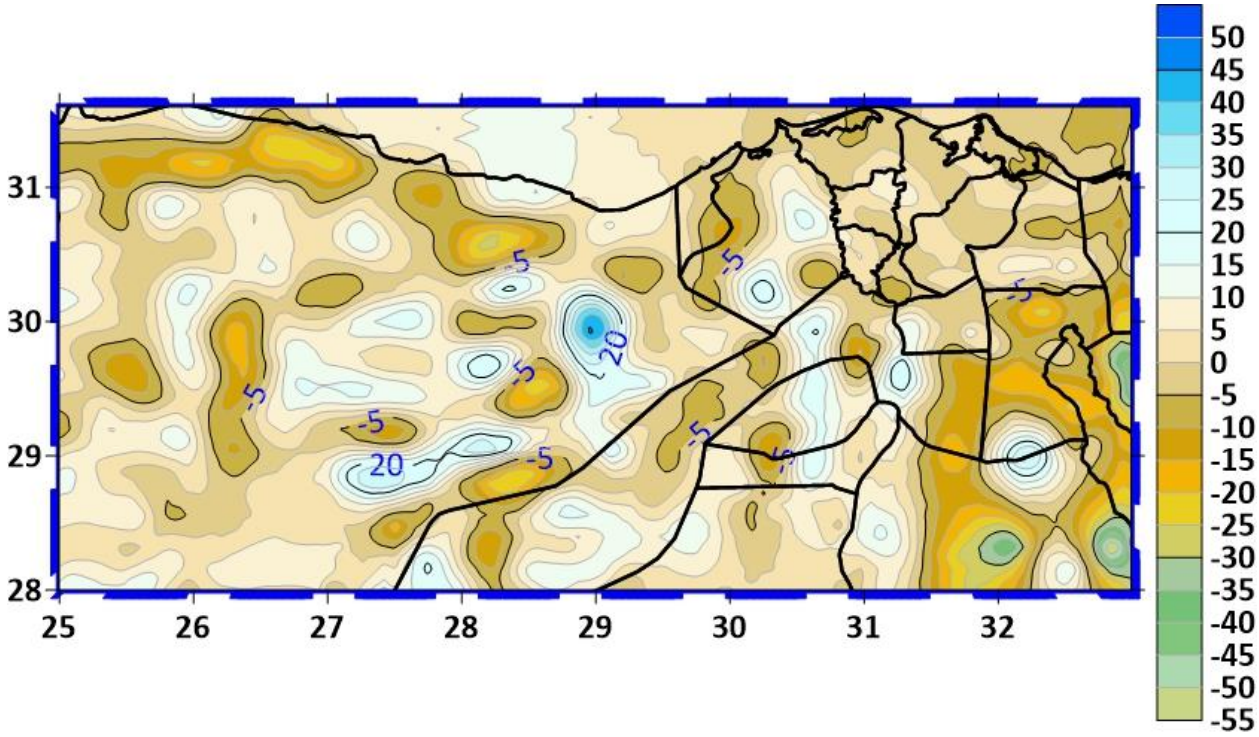

Figure 49 Free air gravity anomaly residuals obtained from GGM GOCO05c and discrete Free air gravity anomaly values over Area 01

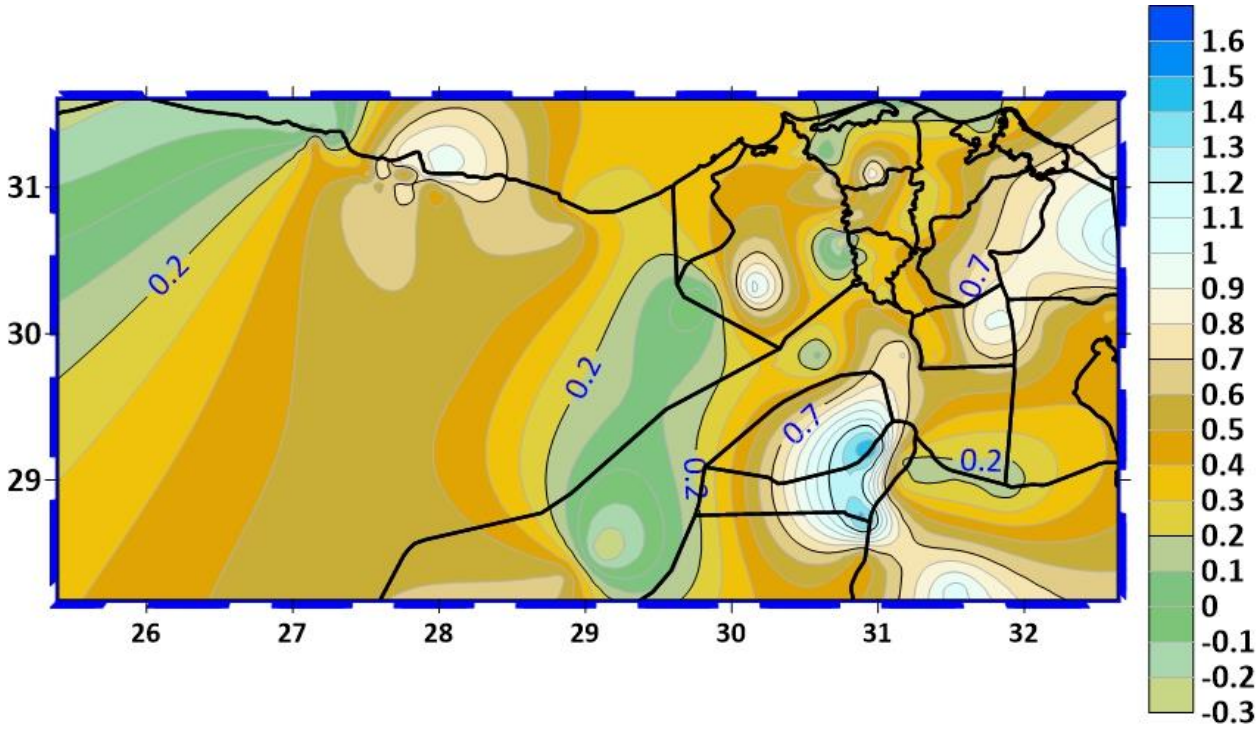

Figure 50 Height anomaly residuals obtained from GGM GOCO05c and discrete GPS/H over Area 01

6.2.3 Determination of Short-Wave Characteristics of Anomalous Potential Functionals for the Purpose of Determining the Geoid of Area 01

Short wave characteristics of the functional of anomaly potential were determined using STRM 3 arc-sec in both directions (Fig. 51), which also plays an important role in the smoothing strategy for the formation of final data sets. The DEM with this resolution has been chosen because the selected area is generally flat, and this resolution is less demanding in terms of computation time needed.

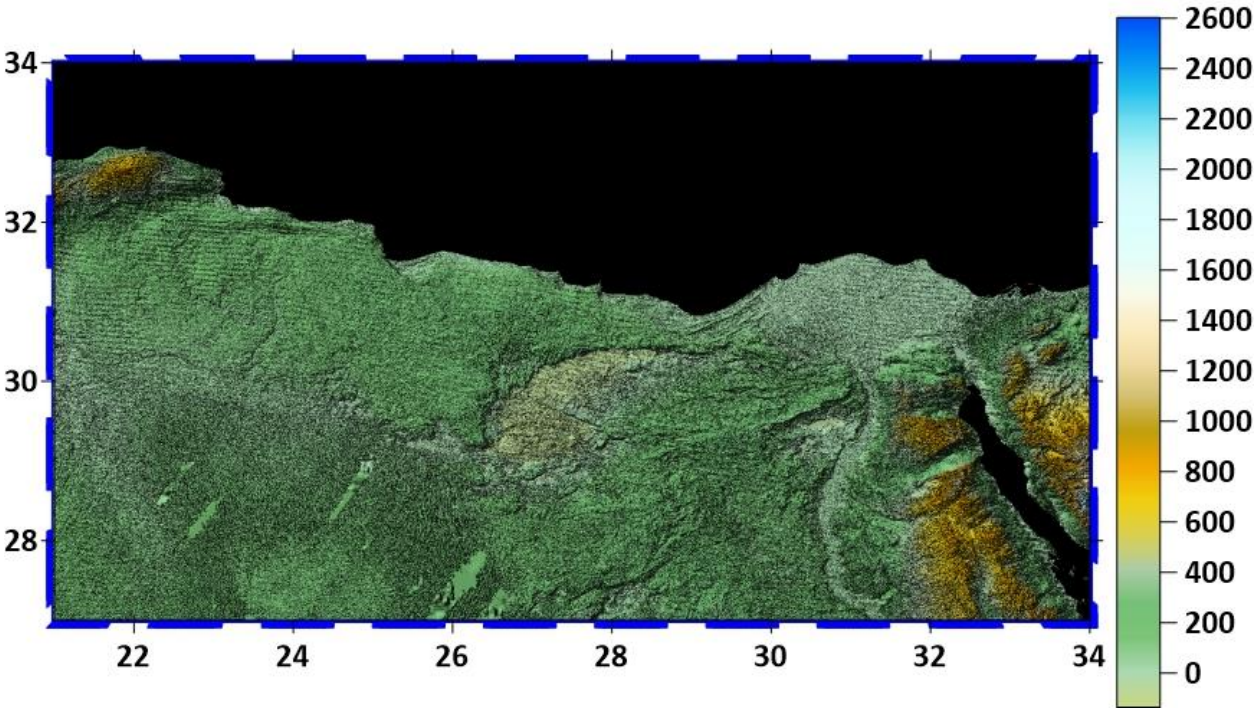

*Figure 51 SRTM 3*3 arcsec DEM for the selected Area 01*

6.2.3.1 Residual Terrain Model

The concept of RTM was introduced by (Forsberg and Tscherning, 1981), and the basic settings of the model are as follows:

• one part of the influence of all topographic masses (topographic masses of the Earth's body), is already contained in the long-wave characteristics determined by the application of the global geopotential model;

• the part contained in the long-wave characteristics is "limited" to the surface called the reference or mean elevation surface. Reference surface resolution corresponds to the resolution of the global geopotential model, from which it follows that the reference surface "roughly" defines the topographic masses (Fig. 52);

• topographic masses, around the point P where the short-wave characteristic is determined, are divided into bodies of regular geometric shape τ_i, $i = 1, \ldots, n$ (bodies whose gravitational influences are defined by closed-form equations);

• the part of the short-wavelength characteristic $t_L^{\tau_i}$ of the observed functional that arises as a consequence of each individual element τ_i is determined,

• and then the overall shortwave characteristic of the observed functional through numerical integration is determined as:

$$t_L = \sum_{i=1}^{n} t_L^{\tau_i} \quad . \tag{6.7}$$

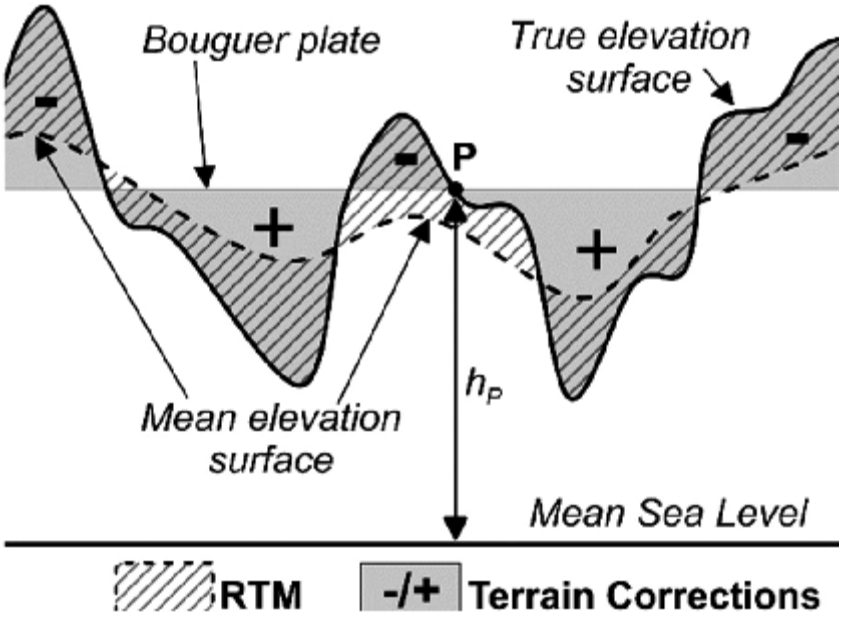

Figure 52 Residual Terrain Model (RTM) and terrain corrections (Forsberg 1984)

The RTM terrain effect may be computed in a spherical cap around the computation point, provided the cap is sufficiently large, so the remote residual topography has a negligible impact. In this study, the mean elevation surface was determined from the DEM data by applying the moving average method. The RTM gravity terrain effect in the planner approximation is given by a volume integral (Bucha et al., 2019).

After the advent of electronic computers, the division of topographic masses was exclusively dictated by the application of digital terrain models (DTM). The bodies τ_i reached by this division of masses are prisms with the most common rectangular (quasi-rectangular) base, where the foreign bases are defined by the steps of the digital model, ΔB and ΔL (Fig. 53).

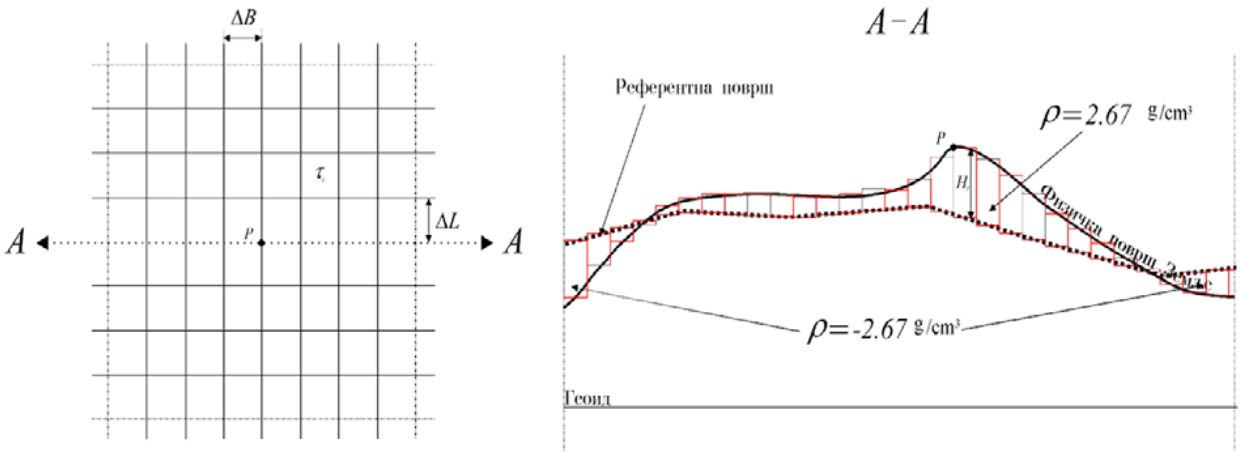

Figure 53 Division of topographic masses by applying a digital terrain model to prisms with a rectangular base

The heights of the prisms can be determined by the expression

$$\mathrm{H_P} = \sum_{\mathrm{i=1}}^{4} \mathrm{H_i^0} - \mathrm{H_i^{Ref}} \Big/ 4\,, \tag{6.8}$$

where $\mathrm{H_i^0}$ are the orthometric heights of the vertices of the upper base of the prism, $\mathrm{H_i^{Ref}}$ are orthometric heights of the vertices of the lower base of the prism (orthometric heights of the points of the reference surface).

where the reference surface is constant along the entire base of the prism therefore, Eq. 6.8 can be written as follows:

$$\mathrm{H_P} = \frac{\sum_{\mathrm{i=1}}^{4} \mathrm{H_i^0}}{4} - \mathrm{H^{Ref}}. \tag{6.9}$$

A digital terrain model defines all the data needed to determine the gravitational influence of the prism, and thus the complete topographic influence. Namely, the heights of the reference surface points are determined by using the heights of the digital terrain model by eliminating a certain number of its species and columns or by linear (square) interpolation, collocation, and other methods.

6.2.3.2 Expressions for Determining Short-Wavelength Characteristics of Anomalous Potential Functionals

After determining all parameters (parameters ΔB, ΔL and $\mathrm{H_P}$) that define a constant density prism in the geometric sense, it is possible to determine the expression for the acceleration potential of the prism's gravitational force based on it the prism's gravitational influence on anomalous potential functionals. If a rectangular coordinate system, with a coordinate origin in point P, is defined as in Fig. 54, then the acceleration potential of the gravitational force of the prism, in rectangular coordinates x, y, and z, is defined by the expression (Petrović, 1996):

$$\Delta g_{TOPO} = G\rho \int_{x_1}^{x_2} \int_{y_1}^{y_2} \int_{z=z_m(x,y)}^{z=z(x,y)} \frac{z - z_1}{[(x_2 - x_1)^2 + (y_2 - y_1)^2 + (z_2 - z_1)^2]^{3/2}}\, dx_2\, dy_2\, dz_2 \tag{6.10}$$

where

z are the topographic heights.

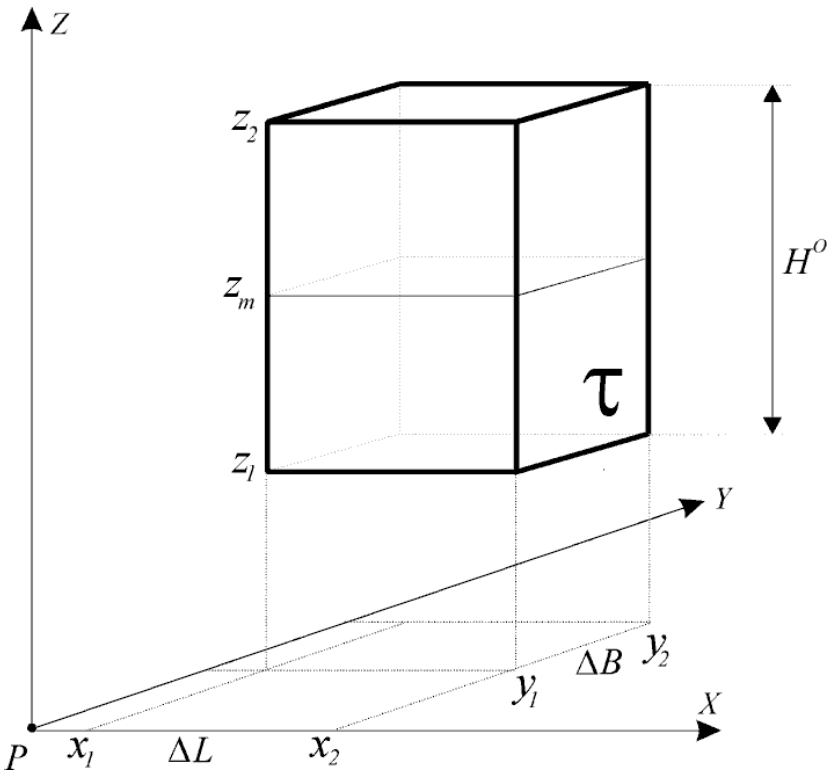

Figure 54 Prism of constant density with a rectangular base

6.2.4 Residual Anomalies and Residual Anomaly Heights

To determine the geoid of Area 01, short-wave characteristics were determined using a residual terrain model for 38150 free air anomalies (Fig. 55 and Table 15) and 180 anomaly heights using the following expressions:

$$\Delta g_R = \Delta g - \Delta g_{GGM} - \Delta g_{TOPO} \quad (6.11)$$

$$\zeta_R = \zeta - \zeta_{GGM} - \zeta_{TOPO} \quad (6.12)$$

and finally, before the prediction of residual anomaly heights, the value of atmospheric correction (δ_{ATM}) was added to the residual anomalies, which was determined based on the expression 6. 13 and the statistical computations results and summarized in Table16 and represented with a contour map Fig. 56:

$$\delta_{ATM\,[\mu ms^{-2}]} = 8.74 - 9.9 * 10^{-4} H_{[m]} + 3.56 * 10^{-8} H^2_{[m]} \ . \quad (6.13)$$

Table 14 Basic statistical data for short-wave characteristics of free air anomalies (unit: mGal).

Parameter	Number of points	Min	Max	Mean	Std. Dev.
Δg_{TOPO}	38150	-58.844	64.639	-1.562	19.408

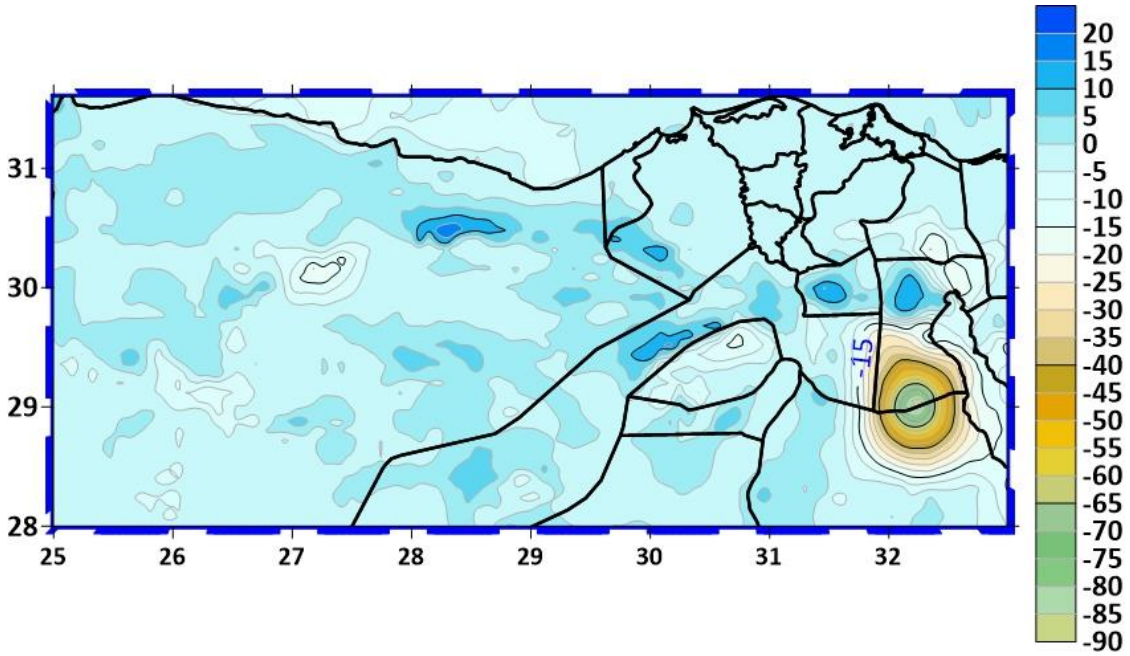

Figure 55 The map of shortwave characteristics of free air anomalies (contour interval 5 mGal*)*

Table 15 Basic statistical data for atmospheric correction of free air anomalies (unit: mGal).

Parameter	Number of points	Min	Max	Mean	Std. Dev.
δ_{ATM}	38150	0.810	0.886	-0.868	0.008

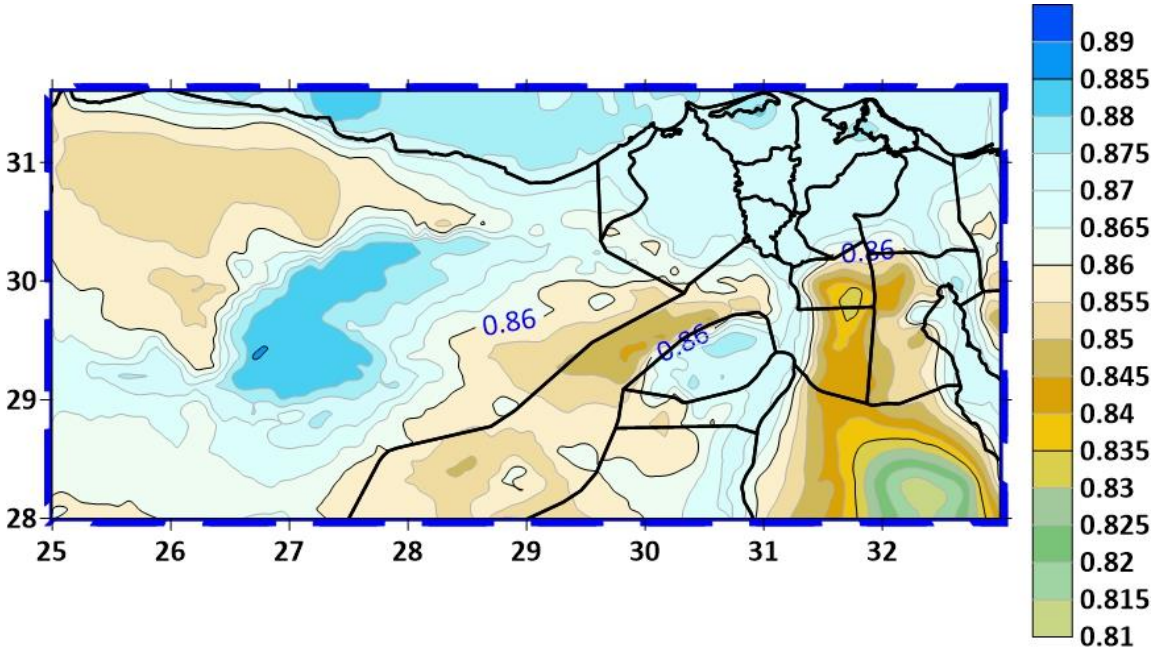

Figure 56 The map of atmospheric correction of free air anomalies (contour interval 0.005 mGal*)*

Residual functionals were formed based on a series of determinations mentioned in the previous section using Eq. 6. 11, Table 17 illustrated the statistical calculation of the residuals anomalies, while represented by Fig. 57 as a counters map.

Table 16 Basic statistics of residual anomalies (unit: mGal).

Parameter	Number of points	Min	Max	Mean	Std. Dev.
Δg_R	38150	48.482	120.911	3.180	9.099

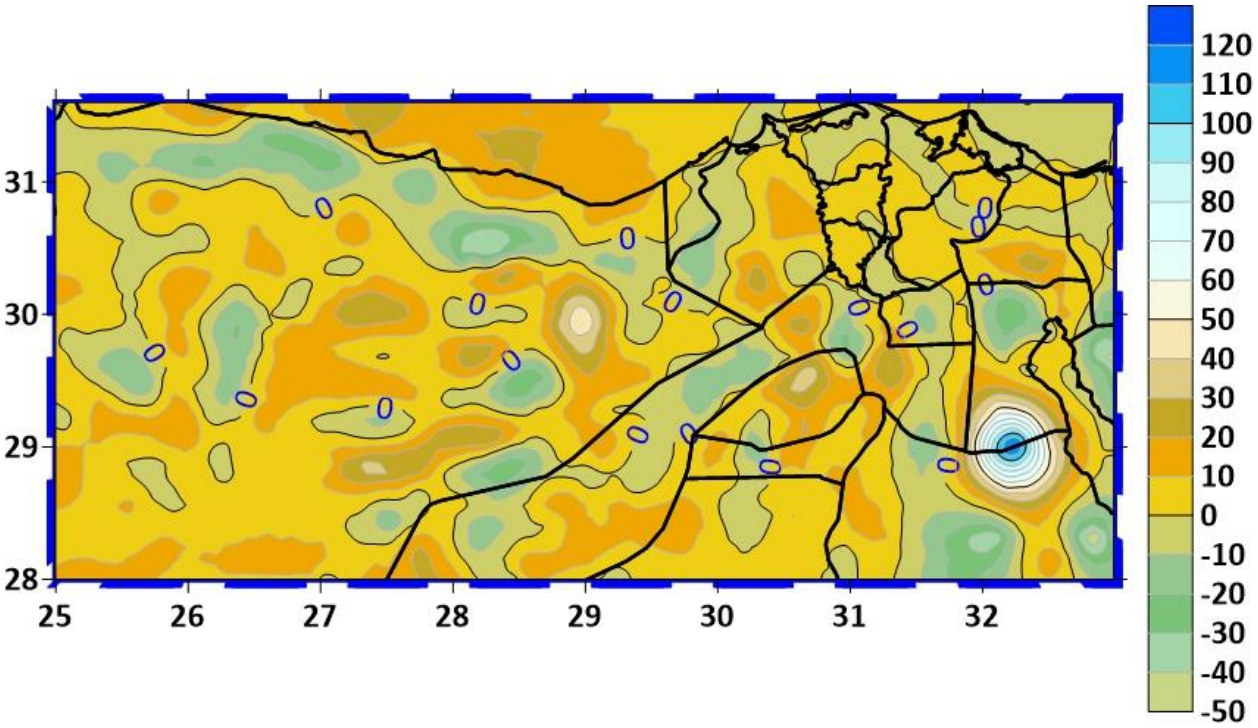

Figure 57 General surface shape of residual anomalies (in mGal*)*

6.2.5 Prediction of Residual Anomaly Heights

The prediction of residual anomalous heights was determined by applying collocation with an adequate estimate of empirical covariances as well as the selection and determination of analytical functions of covariances. The theoretical value of the covariance of any two anomalous potential functionals s and t is defined by the covariance function on the surface of the sphere (Moritz, 1980):

$$C(\psi) = \frac{1}{4\pi} \int_{\theta=0}^{\pi} \int_{\lambda=0}^{2\pi} \int_{\alpha=0}^{2\pi} s(\theta,\lambda)\ t(\theta',\lambda')\sin\theta d\theta d\alpha d\lambda \qquad (6.14)$$

where

s, t anomalous potential functionals,

Ψ spherical distance.

Expression (6.14) implies that the functional ones are known in all points of the physical surface of the Earth, i.e., the unit or terrestrial sphere.

In practical works, only a discrete set of results of observations s_i' and t_j', $i = 1, \ldots, n$ and $j = 1, \ldots, m$ functional of anomalous potential s and t, so it is necessary to apply numerical integration when determining covariance.
Covariances determined by applying numerical integration from observation results are called empirical covariances. In the process of determining empirical covariances, the physical surface of the Earth is divided into blocks $A_k, k = 1, \ldots, k$ bounded by meridians and parallels, where the "widths" and "heights" of blocks ΔB_k and ΔL_k are determined according to the distribution and number of results of observations.

If the result of the observation s_i' is joined by the part of the physical surface of the Earth A_i within which the observation is located, and in the same way the observation t_j' is joined by the part of the physical surface of the Earth A_j, then empirical covariance can be calculated from the expression:

$$C(\psi) = \frac{\sum s_i' t_j' A_i A_j}{\sum A_i A_j}, \tag{6.15}$$

where ψ is the spherical distance between the points to which the observations are s_i' and t_j'.

In practical applications, the value of the spherical distance is defined from the conditions

$$\psi - \frac{\Delta\psi}{2} < \psi_{ij} < \psi + \frac{\Delta\psi}{2}, \tag{6.16}$$

where the interval $\Delta\psi$, as in the case of the intervals ΔB and ΔL, is adopted depending on the distribution and number of observation results.

Several forms of covariance analytical functions have been proposed over time for geoid determination. The 4th model of (C. C. Tscherning and Rapp, 1974a) is almost exclusively used, which defines the analytical function of covariances of anomalous potential

$$K(P,Q) = \alpha \sum_{n=2}^{N} \varepsilon_n \left(\frac{R_E^2}{r_P r_Q}\right)^{n+1} P_i(\cos\psi) + \sum_{n=N+1}^{\infty} \sigma_i \left(\frac{R_B^2}{r_P r_Q}\right)^{n+1} P_n(\cos\psi), \tag{6.17}$$

α scale factor,

N degree of global geopotential model used,

ε degree variance errors,

R_E radius of the terrestrial sphere,

R_B radius of the Bjerhammer sphere,

P_n Legendre polynomials of degree and,

where the degrees of variance σ_n are defined as functions of unknown parameters A and B:

$$\sigma_n = \frac{A}{(n-1)(n-2)(n+B)}. \tag{6.18}$$

Once determined, the covariance function must satisfy a number of requirements: it must be defined and continuous for the area for which it is determined, a real function whose variables are also from the set of real numbers, harmonic at all points of definition, homogeneous-isotropic, positive definite and also on the surface of the sphere represents the best approximation of empirical covariances.

There are basically two types of covariance analytical functions: global and local covariance functions.

Global covariance functions are determined by using the results of observations of anomalous potential functionals that are properly distributed over the entire surface of the Earth, and local covariance functions are determined by using observation results that cover the local area.

It can be said that almost all expressions for local covariance functions, which are used today in determining the mid-wave characteristics of functionals, are only special forms of expressions derived in determining global covariance functions.

The global covariance functions must meet the above conditions that are tough to achieve in practical determinations. This is especially true for the homogeneity property, which depends on the arrangement and number of results of the anomalous potential functional observations. In theoretical considerations, only isotropic covariance functions are always discussed, and verifying the homogeneity property is a special problem in determining global (or local) covariance functions.

The starting point for determining the global covariance functions is the spatial covariance function of the Earth's acceleration anomalies:

$$C_{\Delta g_P \Delta g_Q} = \sum_{n=2}^{\infty} \sigma_n \left(\frac{R^2}{r_P r_Q}\right)^{n+2} P_n(\cos\psi)\,, \tag{6.19}$$

and the first step is to define a series of models for degrees of variance of acceleration anomalies, c_n , i.e a series of nonlinear functions through which degrees of variance are represented as functions of degree n and unknown parameters $A_{i,}\ i = 1, \ldots\ldots, k$

$$\sigma_n = \sigma_n\left(n, A_{i,}\ i = 1, \ldots\ldots, k\right).$$

After defining the model of power variances, the obtained covariance functions are analyzed on a global level, which means the comparison of the values of modeled degrees of variance with the values of empirical degrees of variance, i.e., variances that can be determined using the coefficients of the global geopotential model through expression (Rapp, 1997):

$$\hat{\sigma}_n = \left(\frac{kM}{a^2}\right)^2 (n-1)^2 \sum_{m=0}^{n} (\bar{J}'^2_{nm} + \bar{K}'^2_{nm})\,, \tag{6.20}$$

as well as comparing functions in terms of simplicity of closed forms.

Functions whose degrees of variance "follow the behavior" of empirically determined variants and functions with a simpler closed form fit into empirically determined variants. Using the least-squares method based on the function selected for the degrees of variance, unknown parameters are determined for each model, where the empirical degrees of variance are considered "measured quantities".

After determining the global covariance function of acceleration anomalies, the global covariance function of anomalous potential and all other covariance functions necessary for collocation application are determined, which follow from the application of "covariance transfer law" to anomaly potential covariance function.

The fourth model, which was defined by (C. C. Tscherning and Rapp, 1974b), has been utilized in this research:

$$C_n = \frac{A(n-1)}{(n-2)(n+B)}, \tag{6.21}$$

and almost exclusively used in the application of collocation to determine the undulation of geoids / anomalous heights.

For the local covariance function of anomalous potential, the function is adopted which is obtained when all members of the order from $n = 2$ to $n = n_l$ are subtracted from the global covariance function, where the power n is called the order of the local covariance function (Chen and Schwarz, 1985; Schwarz and Lachapelle, 1980; C. C. Tscherning and Rapp, 1974b). The adoption of this covariance function for the local follows from the fact that the first members of the order of the global function are constant in the local area, and that subtracting the first members of the global function leads to a function that describes the stochastic properties of residual observation results (Moritz, 1980).

The local function is considered determined when the order of local covariance function and unknown parameters of the adopted analytical form, i.e., unknown parameters of the adopted model of power variances, are determined from the results of observations from the local area (local empirical covariances).

Determining the order of a local function and unknown parameters of the degree variance model is the basic problem of collocation application in determining the anomalous potential functional, and there are a number of proposals that indicate ways to determine the order of function and the fit covariances (Odalović, 2000)

All the expressions presented in this chapter were used to estimate the empirical covariances and fit the fourth Tscherning and Rap model, and the obtained results are shown in Fig. 58 and Table 18.

Table 17 Parameters of the analytical function of covariances of residual anomalies

α [−]	$R_B - R_E$ [km]	$C_{H=3.18}$ [mGal^2]	C_0 [mGal^2]	ζ [arc minute]
0.154434	-1.1680	82.80	60.88	5.00

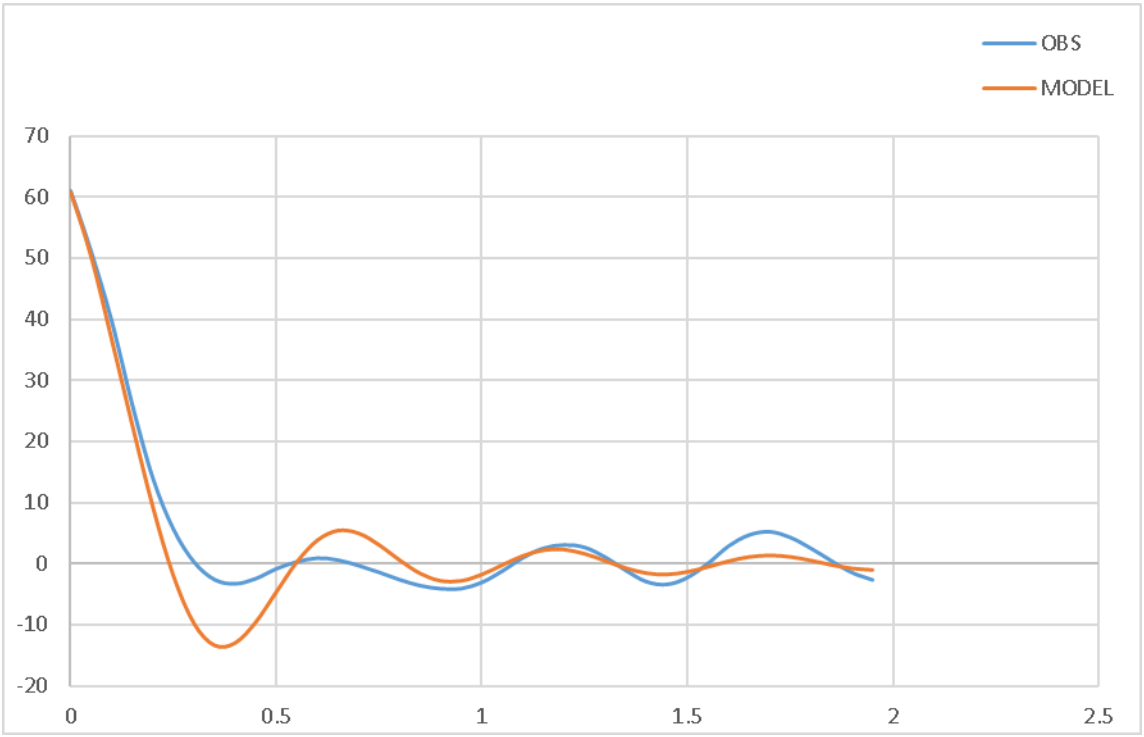

Figure 58 Empirical covariances and analytical function of covariances

Prediction of residual anomalous heights was made using a predetermined analytical function of covariance and expression

$$\zeta_{\text{Coll}}(\text{P}) = \frac{\widetilde{\text{T}}\,(\text{P})}{\gamma_{\text{P}}} \tag{6.22}$$

,

where

$$\widetilde{\text{T}}\,(\text{P}) = \text{C}_{\text{P}}^{\text{T}}(\text{C} + \text{D})^{-1}\text{X}\,, \tag{6.23}$$

and where they are

C_{P} matrix of cross covariances of anomalous potential and linear functionals,

C functional covariance matrix,

D matrix of variances of noise vector elements,

X vector of residual functionals of anomalous potential.

The values of residual anomalous heights (Table 19 and Fig. 59), were determined in 180 points where discrete values of undulations are known, as well as in 93961 points correctly distributed on the chosen AREA01 at a distance of 2 km (TG - geoid points), with heights determined based on digital terrain model SRTM 3 arc-sec.

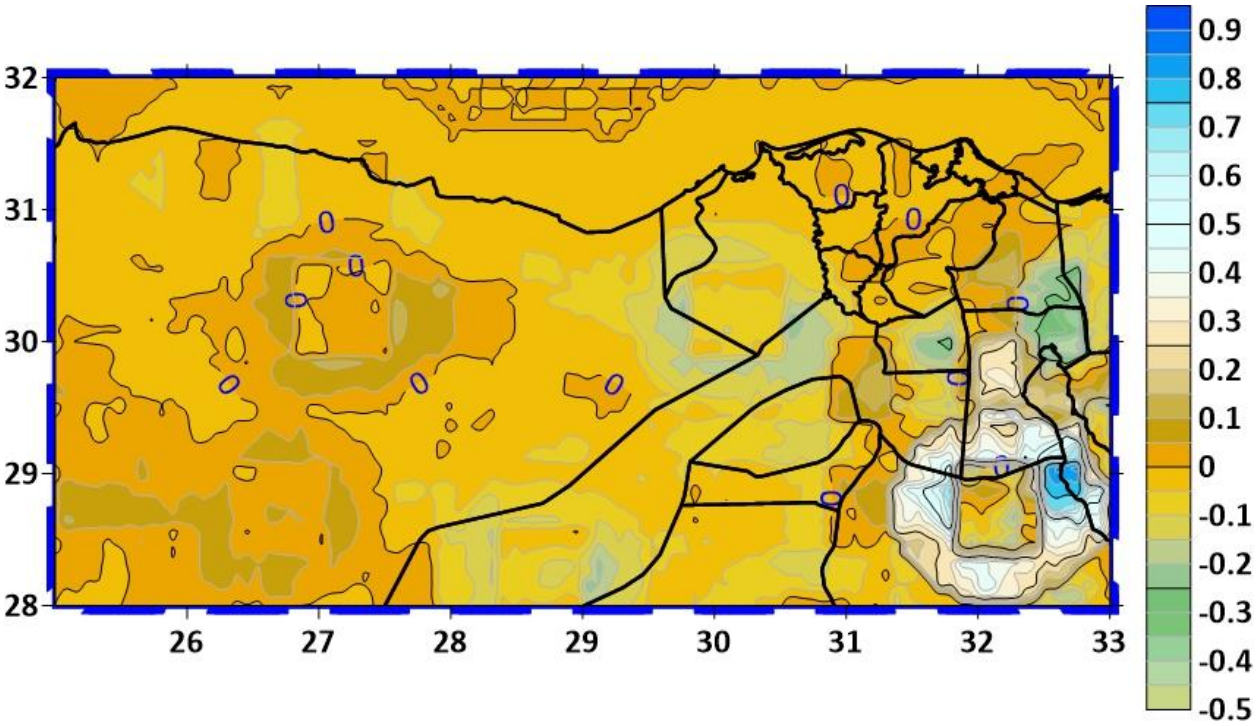

Figure 59 Residual anomalous heights (in m*)*

Table 18 Basic statistics of residual anomalous heights (unit: m).

Parameter	Number of points	Min	Max	Mean	Std. Dev.
ζ_{Res}	93961	-0.480	0.901	-0.001	0.110

6.2.6 Short Wave Characteristics of Anomaly Heights

The short-wave characteristic must be calculated using the terms shown in the aforementioned verse 6.2.3 based on the same digital terrain models and parameters applied in the remove phase in forming residual functionalities of anomalous potential in all TG (Table 20 and Fig. 60).

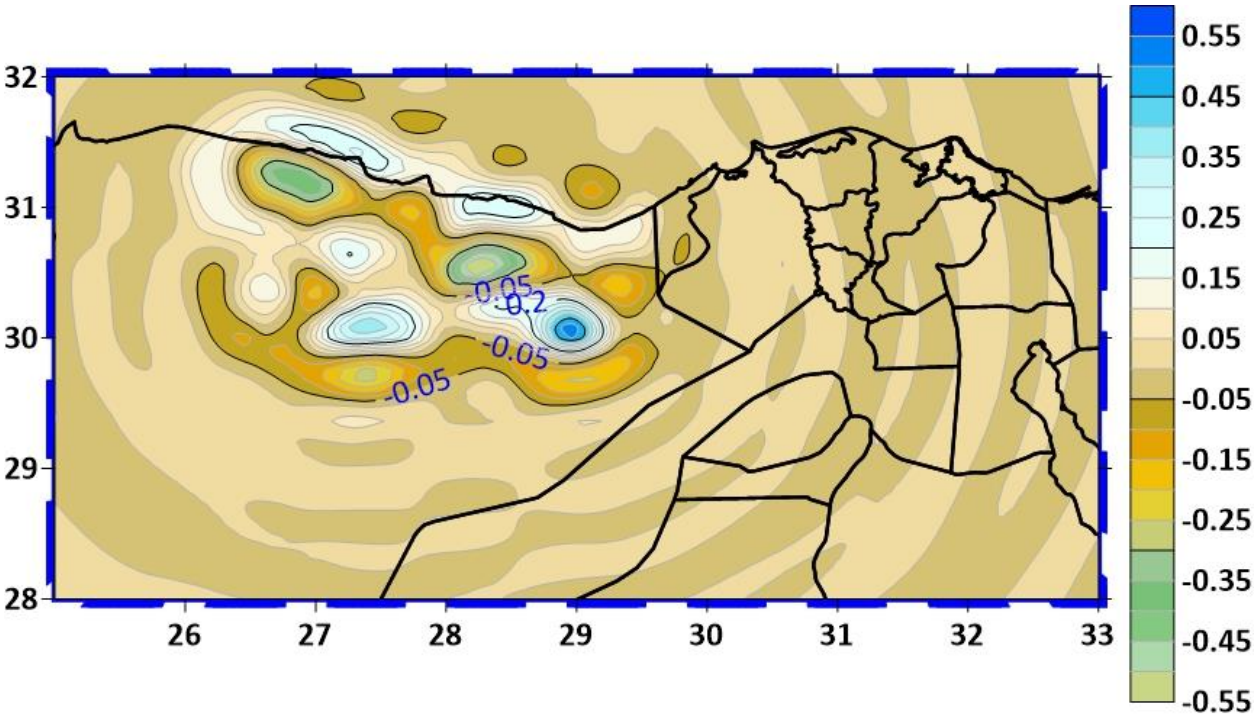

Figure 60 Shortwave characteristics of anomalous heights (unit: m).

Table 19 Basic statistics of short wave characteristics of anomalous heights (unit: m).

Parameter	Number of points	Min	Max	Mean	Std. Dev.
ζ_{TOPO}	93961	-0.552	0.545	-0.000	0.071

6.2.7 Long Wave Characteristics of Anomaly Heights

Long-wave characteristics are determined using Eq. 6.6 and global coefficients of the GOCO05c geopotential model used in the remove phase in all TGs.

The statistical computations of the Area 01 grid TGs anomaly heights have been illustrated in Table 21, while the spatial representations show by the contour map Fig. 61.

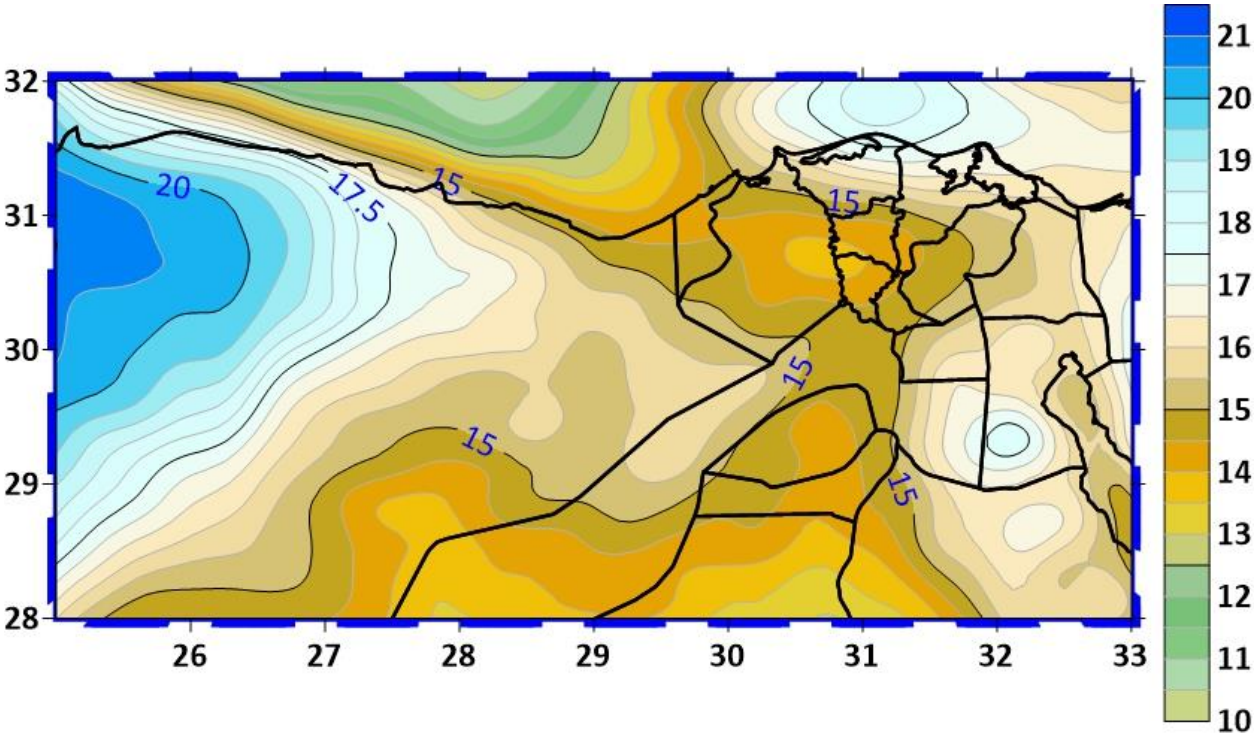

Figure 61 General shape of the surface of long-wave characteristics of anomalous heights (in m*)*

Table 20 Basic statistics of the long-wave characteristics of anomalous heights (unit: m).

Parameter	Number of points	Min	Max	Mean	Std. Dev.
ζ_{GGM}	93961	10.274	20.842	15.879	1.995

6.2.8 Total Anomaly Heights

Total anomalous heights are determined by summing the determination of the restore phase, where it is necessary to form two groups of total anomalous heights:

• total anomalous heights in TG (93961 points)

$$\zeta^{TG} = \zeta^{TG}_{R} + \zeta^{TG}_{GGM} + \zeta^{TG}_{TOPO} \quad , \tag{6.24}$$

• and total anomalous heights at points where discrete values of undulations / anomalous heights are known (180 points)

$$\zeta^{GPS/dh} = \zeta_R^{GPS/dh} + \zeta_{GGM}^{GPS/dh} + \zeta_{TOPO}^{GPS/dh} \quad . \tag{6.25}$$

At the end of this phase, the total anomalous heights at a grid TGs of 2 km spacing in each direction were obtained, i.e., after this phase, a high-resolution quasi-geoid has been determined on the chosen AREA 01, where it has a range from 10.264 to 20.820 with a mean value 15.78 m and 2 m as a standard deviation all these quantities listed in Table 22, while Fig.62 describe the spatial representation of the obtained Quasi-geoid over Area 01.

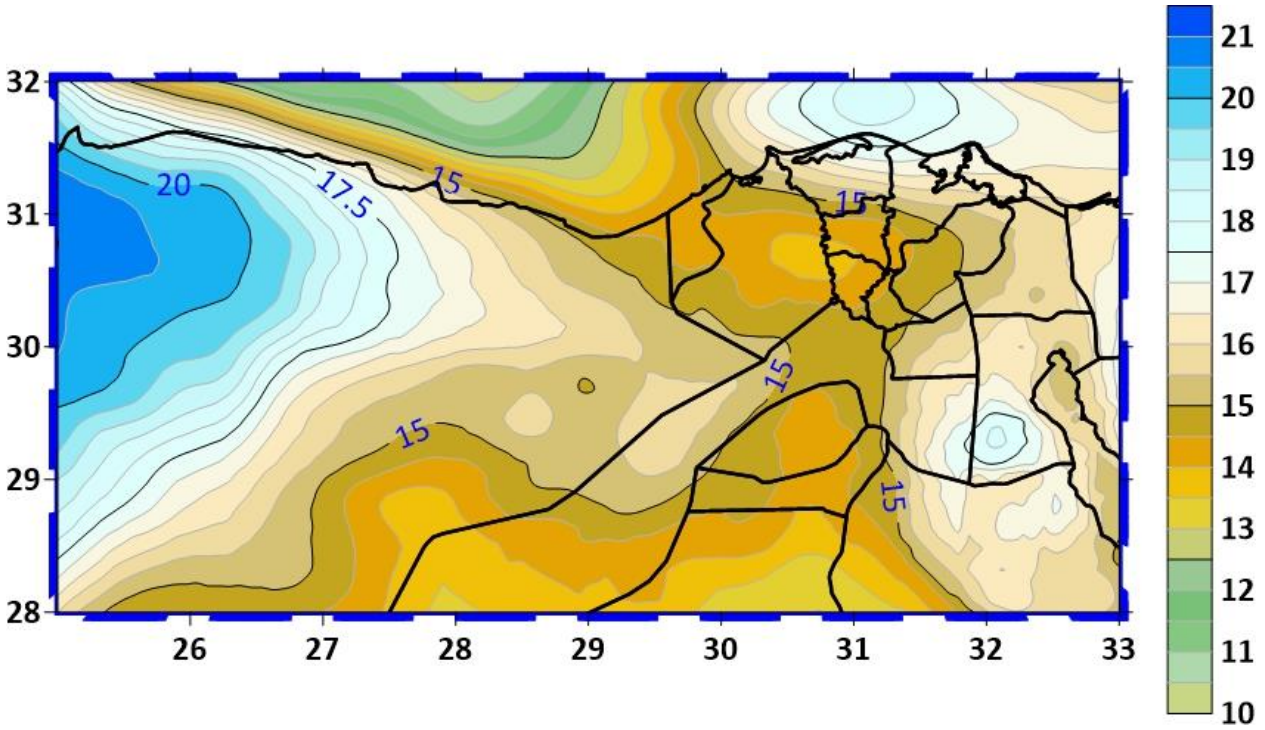

Figure 62 Quasi-geoid of the chosen AREA01 (in m*)*

Table 21 Basic statistical data for quasi-geoid of the chosen AREA01 (unit: m).

Parameter	Number of points	Min	Max	Mean	Std. Dev.
ζ	93961	10.264	20.820	15.878	2.007

6.2.9 Difference Between Geoid and Quasi-Geoid

To determine geoid undulations based on previously determined values of anomalous heights, it is necessary to determine the difference between geoid and quasi-geoid using the expression:

$$\Delta N_\zeta = N - \zeta = \frac{\Delta g_B}{\bar{\gamma}} H^0 , \tag{6.26}$$

Δg_B Bouguer Anomaly

$\bar{\gamma}$ the mean value of the normal acceleration along the normal height of the point at which the difference between the geoid and the quasi-geoid is determined.

Bouguer anomalies (Δg_B) can be determined at all points where the acceleration of the Earth's gravity is known, as well as their orthometric height and if the value of the density (ρ) of the Earth's crust masses is adopted using the expression:

$$\Delta g_B = g' - 2\pi k\rho H^0 + FH^0 - \gamma \quad (6.27)$$

where

g' - measured value of acceleration on the physical surface of the Earth,
F - vertical gradient of normal acceleration,
γ - the value of the normal acceleration on the geoid.

The value for the density of the Earth's crust of 2.67 g/cm^3 is most often used in determining Bouguer anomalies, and the value of $0.3086.10^{-5}\ 1/s^2$ is used for the value of the normal gradient.

As Bouguer anomalies are very suitable for interpolation, it is possible to estimate the value of Bouguer anomaly at all points for which the total anomaly heights are determined, and thus, by using expression (6.27). The differences between geoid and quasi-geodes were too small to represent in a table or figure, but they have been considered in the calculations process. The standard deviation is about 2 millimeters, therefore, it is obvious that Geoid/quasi-geoid separation is close to zero in the chosen Area01 because this area is almost flat.

6.2.10 Geoid in Spherical Approximation

Using previously calculated differences between geoids and quasi-geoids at all points where the differences between geoids and quasi-geoids are determined, it is necessary to calculate the values of undulations of geoids in the spherical approximation using the expression:

$$N = \zeta + \delta N\zeta .$$

6.2.11 Ellipsoid correction

To eliminate the introduced spherical approximation at all points where the differences between geoids and quasi-geoids are determined, it is necessary to calculate ellipsoidal corrections using the expression:

$$EC = e^2 \left(\frac{1}{4} - \frac{3}{4}\sin^2 B\right) N , \quad (6.28)$$

where

e^2 is the first numerical eccentricity,

B is the latitude of the point.

6.2.12 Geoid

The final values of geoid undulations should be determined by adding the values of certain ellipsoidal corrections to the values of undulations at the spherical approximation:

$$N_E = N + EC. \quad (6.29)$$

Such undulations define the geoid, often called the scientific geoid and can be considered as the high-resolution geoid of the chosen AREA 01 (Table 23 and Fig. 63).

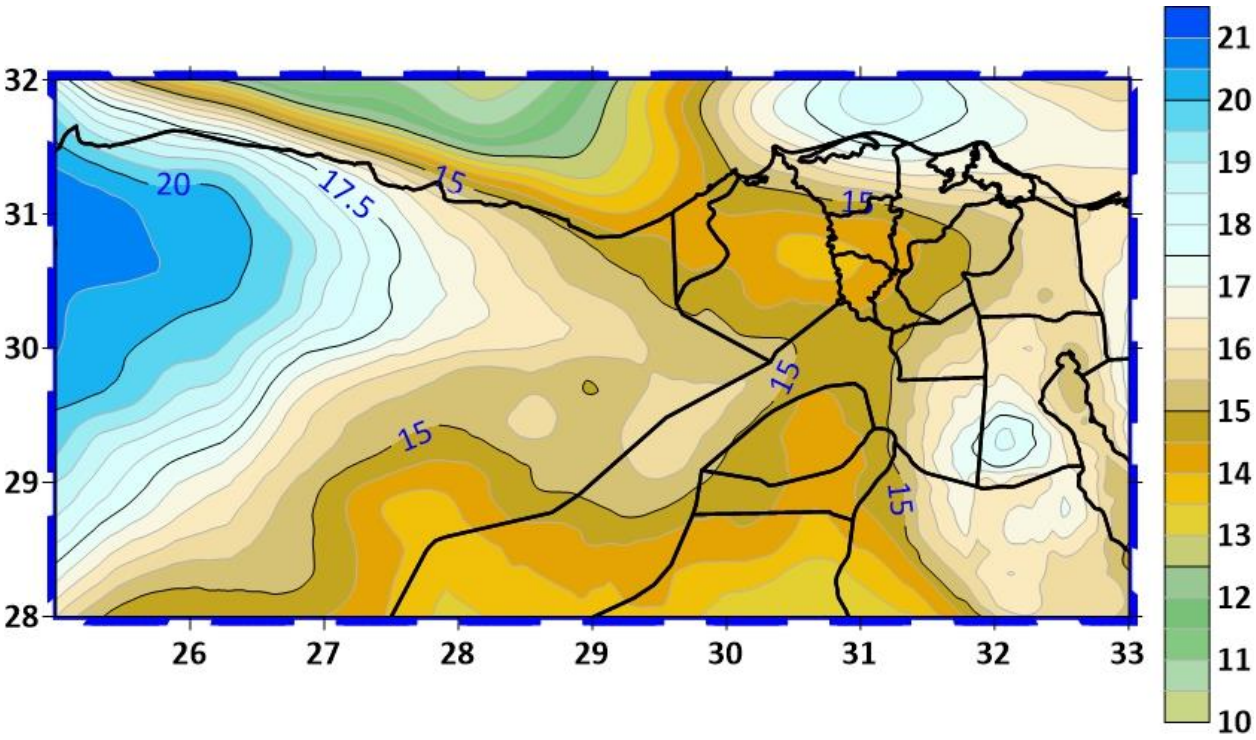

Figure 63 General Surface of the high-resolution geoid of Area 01 (in m*)*

Table 22 Basic statistical data for the geoid of Area01 (unit: m).

Parameter	Number of points	Min	Max	Mean	Std. Dev.
N_E	93961	10.268	20.824	15.883	2.007

6.2.13 Evaluation of Translation Parameters

After the finally determined undulations, it is necessary to fit the geoid into the national Egyptian height system.

The first step is to eliminate the influence of hypotheses that are present in the process of determining N_E undulations.

When creating global geopotential models and defining the analytical functions of covariances, hypotheses are introduced that the reference system's center of mass coincide with the Earth's real center of mass. As it is stated that the coincidence in practical works is very difficult to achieve in the estimates of undulations N_E remain part of the above discrepancies.

Differences of undulation determined by expression:

$$t = N_E - N_{GPS/dh}, \qquad (6.30)$$

at points where discrete undulation values are known can be interpreted as a consequence of the mismatch of the mentioned centers and presented in the form of a function of the position of the points and unknown translation parameters $\Delta X, \Delta Y, \Delta Z$

$$t = \cos B \cos L \, \Delta X + \cos B \sin L \, \Delta Y + \sin L \Delta Z \, . \qquad (6.31)$$

The previous expression refers to points whose coordinates are known. As the values of t can be determined from (6.30), it follows that unknown translation parameters can be determined using the least-squares method, for which is necessary to adopt:

• expression (6.31) for the connection function, i.e., the functional part of the mathematical model of the least square's method,

• and the same accuracy of determining differences by applying (6.31) as the starting point of the stochastic part of the mathematical model of the least square's method.

The above parameter evaluation procedure and the obtained parameter values are given in Table 24.

Table 23 Estimates of translation parameters (unit: m).

Parameter	Value
$\Delta\hat{X}$	0.032
$\Delta\hat{Y}$	4.597
$\Delta\hat{Z}$	-4.731

Table 25 and Fig. 64 show the differences t for GPS/H in order to fit the obtained geoid N_E into the national Egyptian height system.

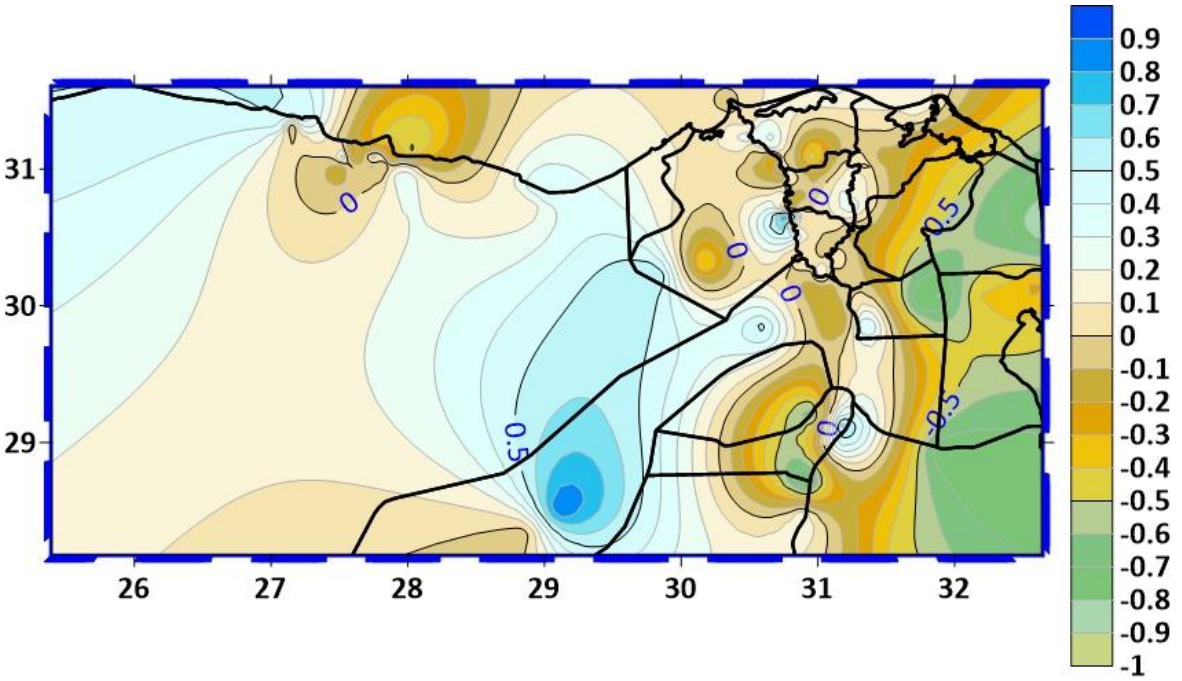

Figure 64 General surface of differences t for GPS/H (in m)

Table 24 Basic statistical data of differences t (unit: m).

Parameter	Number of points	Min	Max	Mean	Std. Dev.
t	180	-0.936	1.457	0.000	0.319

6.2.14 Combined Solution

After the estimated translation parameters, it is possible to determine the effect of the introduced hypotheses at each point of the Grid of 2 km spacing (TG) and evaluate the differences (Table 26 and Fig. 65)

$$\hat{t} = \cos B \cos L\, \Delta\hat{X} + \cos B \sin L\, \Delta\hat{Y} + \sin L \Delta\hat{Z}\,, \qquad (6.32)$$

and then a combined solution (Table 27 and Fig. 66) is obtained as

$$N_c = N_E - \hat{t}\ . \qquad (6.33)$$

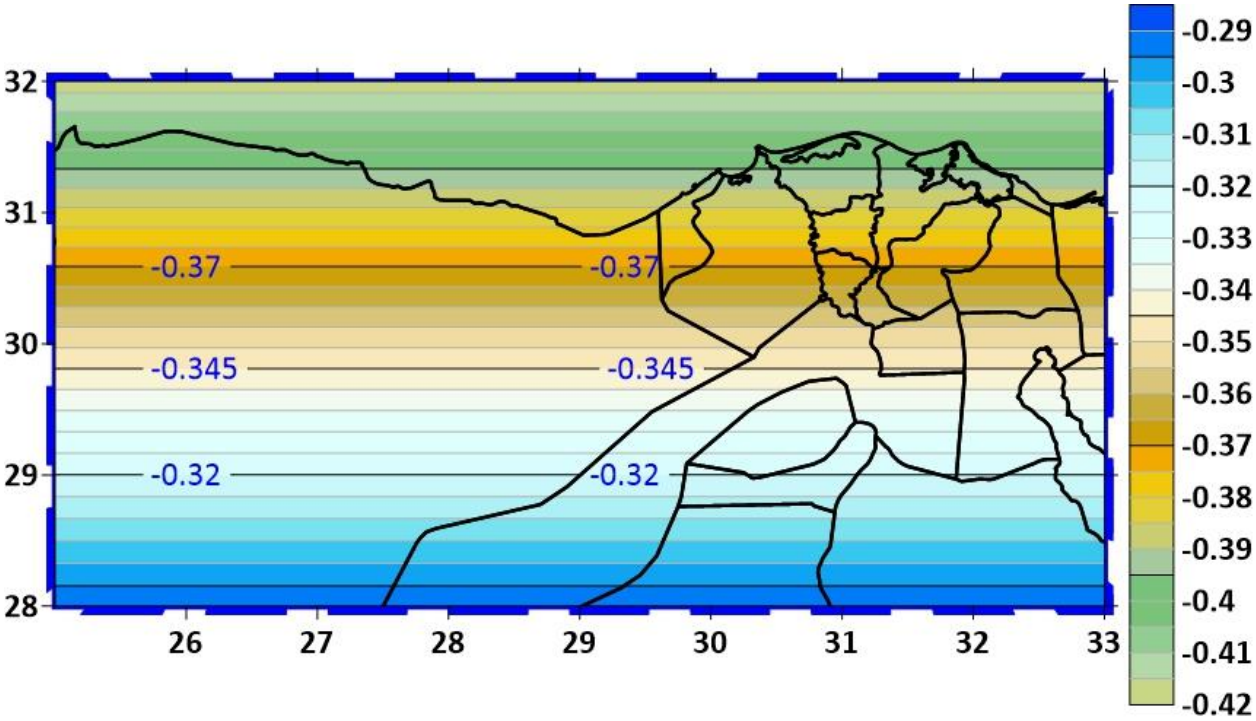

Figure 65 General Surface of differences $\hat{t}$ (in m*)*

Table 25 Basic statistical data of differences $\hat{t}$ (unit: m).

Parameter	Number of points	Min	Max	Mean	Std. Dev.
$\hat{t}$	93961	-0.418	-0.291	-0.352	0.037

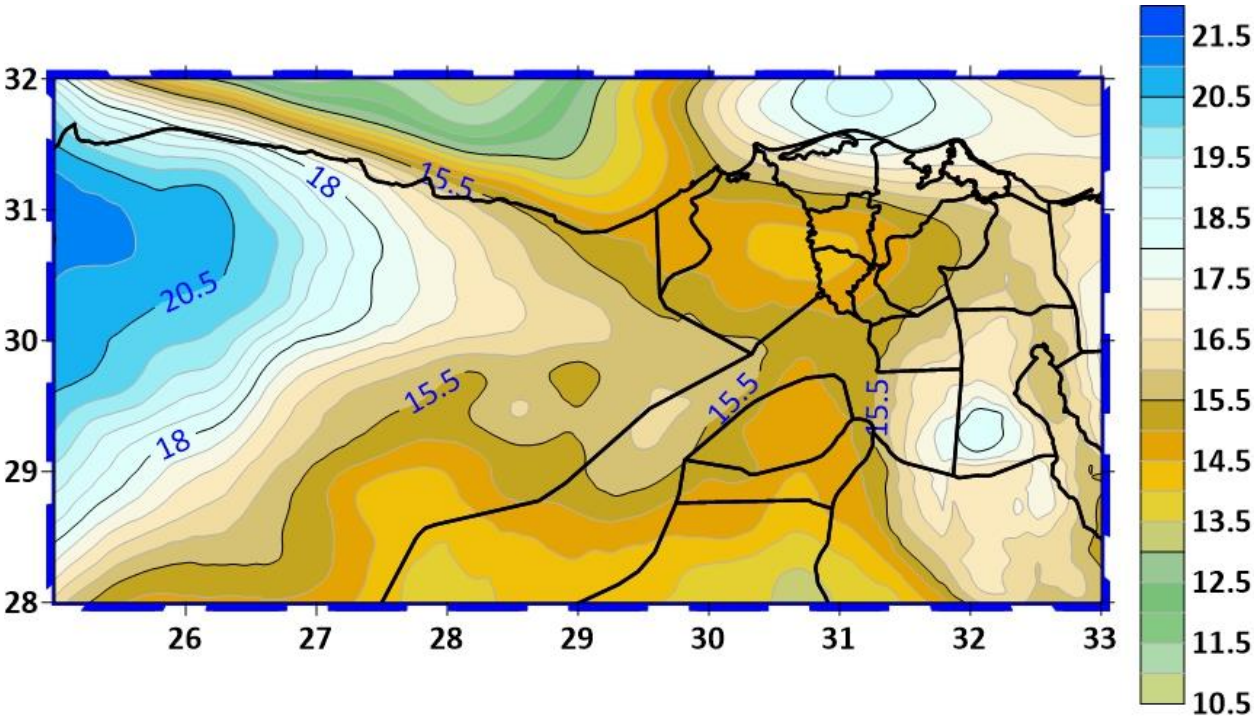

Figure 66 General Surface of the high-resolution geoid $N_{c\ [m]}$ of Area 01 (in m)

Table 26 Basic statistical data of the high-resolution geoid N_c of Area 01 (unit: m).

Parameter	Number of points	Min	Max	Mean	Std. Dev.
N_c	93961	10.686	21.202	16.235	2.012

6.2.15 Residual Assessment

The combined solution should be the last step in evaluating geoid undulations that can be used in practical work to transform ellipsoidal heights into orthometric ones.

However, in differences

$$R = N_c - N_{GPS/H} \tag{6.34}$$

which are formed at points where discrete undulations are known, in most cases, significant deviations can be noticed and called residuals (Table 28 and Fig. 67).

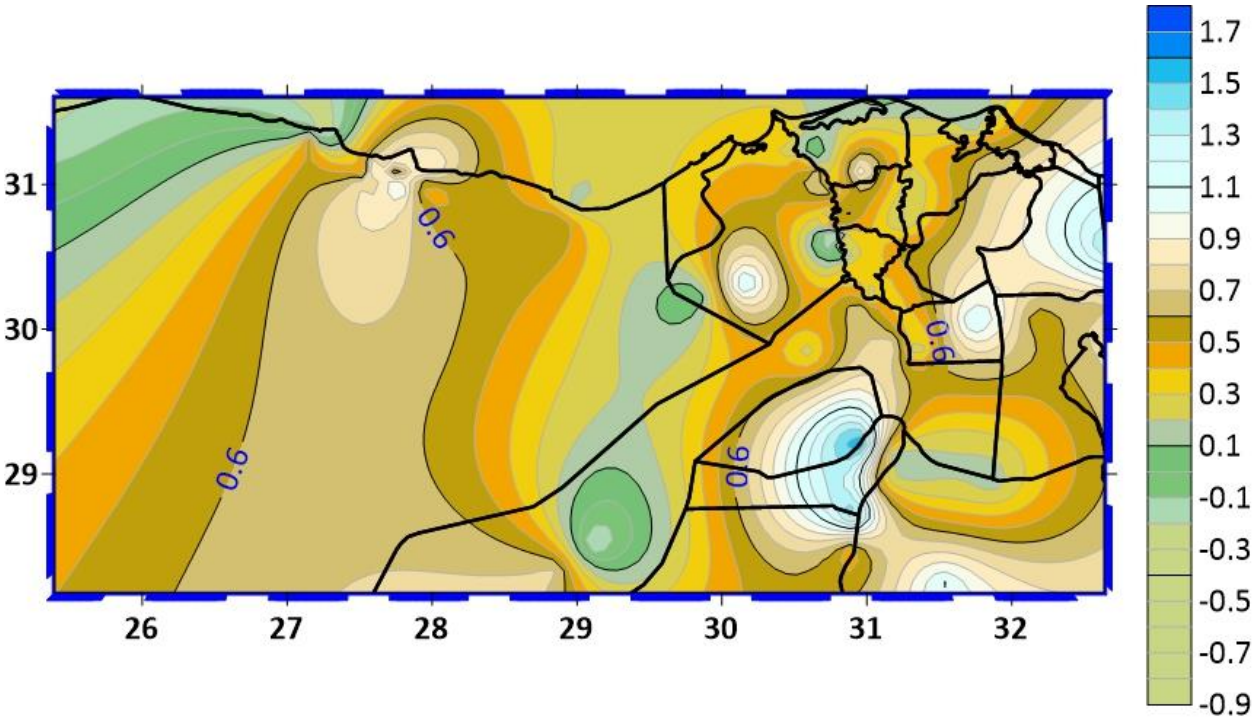

Figure 67 General surface of the residuals R *for internal check (unit: m).*

Table 27 Basic statistical data of the residuals R for internal check (unit: m).

Parameter	Number of points	Min	Max	Mean	Std. Dev.
R	180	-0.91947	1.649404	0.484733	0.338604

These residues at arbitrary points of the area under consideration are most often estimated by collocation, where stochastic deviation properties are modeled using the Gaussian analytical function of covariance:

$$C(\rho) = C_0 e^{-A^2\rho^2}, \qquad (6.35)$$

or by applying the Hirvonen covariance analytical function

$$C(\rho) = \frac{C_0}{(1 + B^2\rho^2)^m}, \qquad (6.36)$$

where A, B, and m are unknown parameters of the above functions.

Unknown parameters of covariance functions can be estimated based on empirical covariances of residuals R and residual values can be estimated in each TG.

To control the process of residual assessment in TG, it is necessary to divide the set of points where discrete values of undulations are known into two parts:

• the first part consists of 80 GPS/dh discrete points to be used for the assessment of residues in TG

• and the second part that will be used to control the residual assessment process - external verification consists of 100 GPS/dh discrete points (Table 29 and Fig. 68).

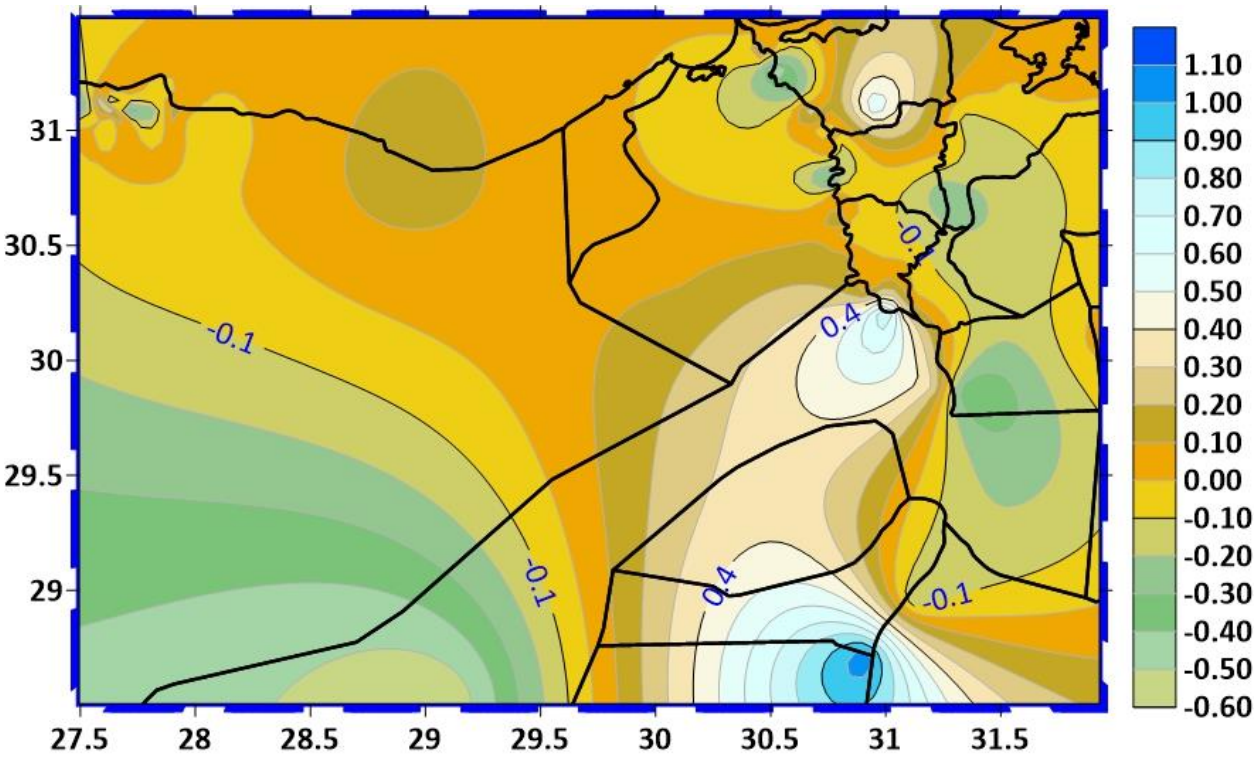

Figure 68 General surface the residuals R *for external check (in* m*)*

Table 28 Basic statistical data of the Residuals R for external check (unit: m).

Parameter	Number of points	Min	Max	Mean	Std. Dev.
R	100	-0.600	1.081	-0.005	0.262

After the external check, it is necessary to evaluate the residues in TG using all available residues.

The mentioned residual assessment procedure was applied for further calculations, where only the values assessed in the fundamental benchmarks and points of the reference network of Egypt were used for residual assessments.

6.2.16 Surface of Transformation

Finally, after adding the estimated residual values to the undulations determined in the combined solution, there are undulations that define the surface of the transformation of ellipsoidal heights into the national Egyptian height system for the chosen Area01:

$$N_{ST} = N_c - \widehat{R} \ . \qquad (6.37)$$

Table 30 and Fig 96 show the values of the Residuals $\hat{R}$ of the transformation of ellipsoidal heights into the national Egyptian height system for the chosen Area01.

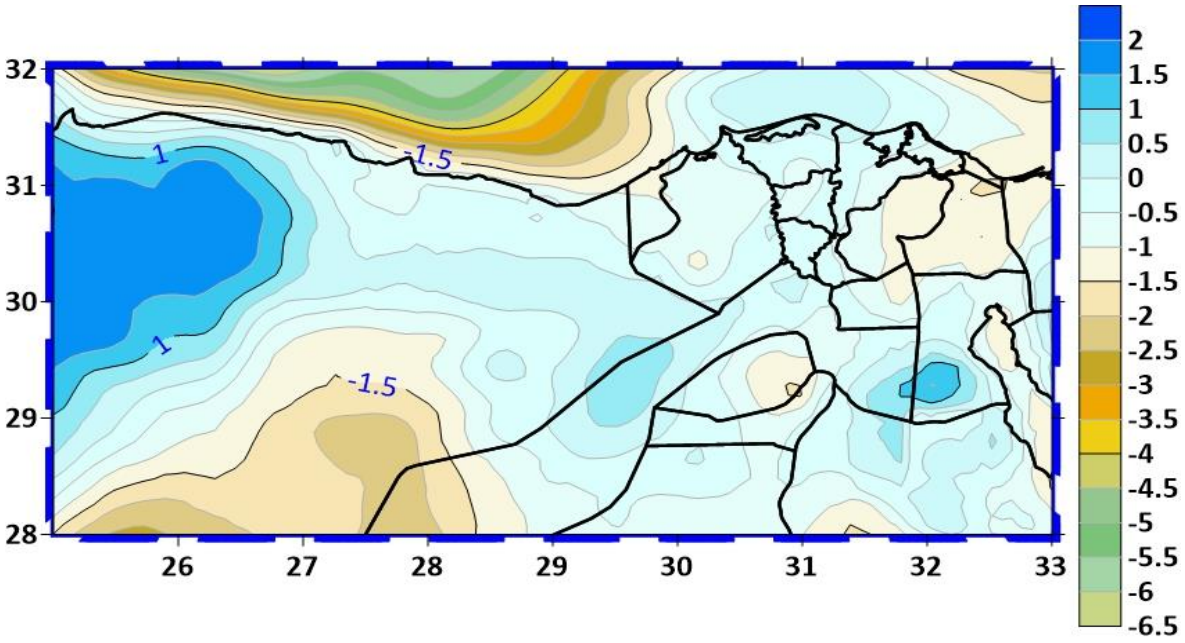

Figure 69 General Surface of the residuals $\hat{R}$ of Surface of Transformation (in m)

Table 29 Basic statistical data of the Residuals $\hat{R}$ of the transformation of ellipsoidal heights into the orthometric height system (unit: m).

Parameter	Number of points	Min	Max	Mean	Std. Dev.
$\hat{R}$	93961	-6.435	1.939	-0.605	1.320

Table 31 and Fig 71 show the obtained combined solution geoid after removing the residuals of the surface of transformation of ellipsoidal heights into the national Egyptian height system for the chosen Area01.

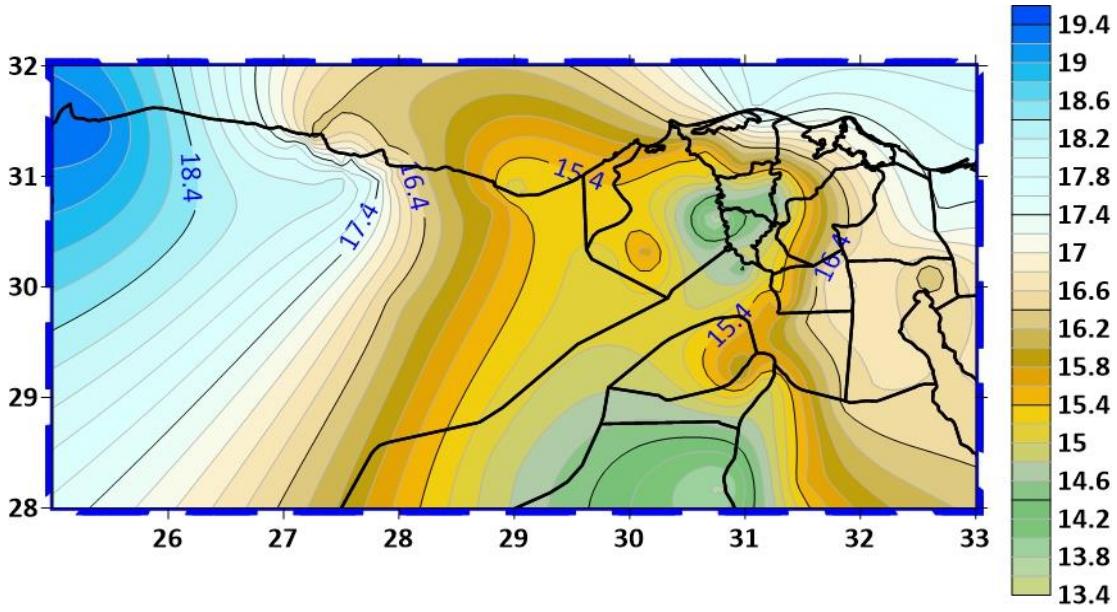

Figure 70 combined solution Geoid for Area 01 (in m)

Table 30 Basic statistical data of the geoid of the chosen AREA 01 (unit: mGal).

Parameter	Number of points	Min	Max	Mean	Std. Dev.
N_{ST}	93961	13.100	19.329	16.488	1.248

6.3 Concluding Remarks

Based on everything shown, and especially external controls (Fig. 71), the following can be concluded:

- at 43% of points where discrete values of anomalous heights/undulations of geoids are known, the remaining residues in the transformation of ellipsoidal heights into the system of orthometric heights do not exceed 50 cm, as shown in (Fig. 71 A),
- in 52% of points, the residues are less than 80 cm shown in (Fig. 71 B), and
- in 68% of points, the residues are less than 1.20 m shown in (Fig. 71 C), and
- in 77% of points, the residuals do not exceed the value of 1.5 m shown in (Fig. 71 D).

A

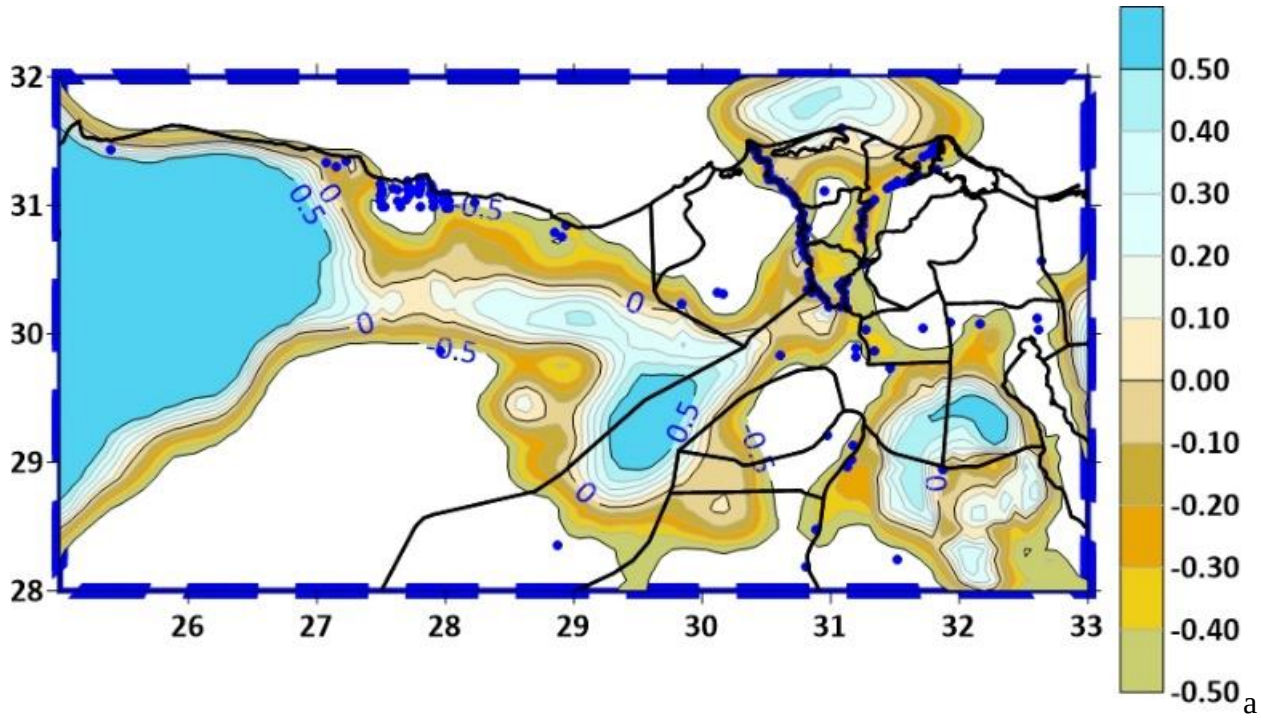

B

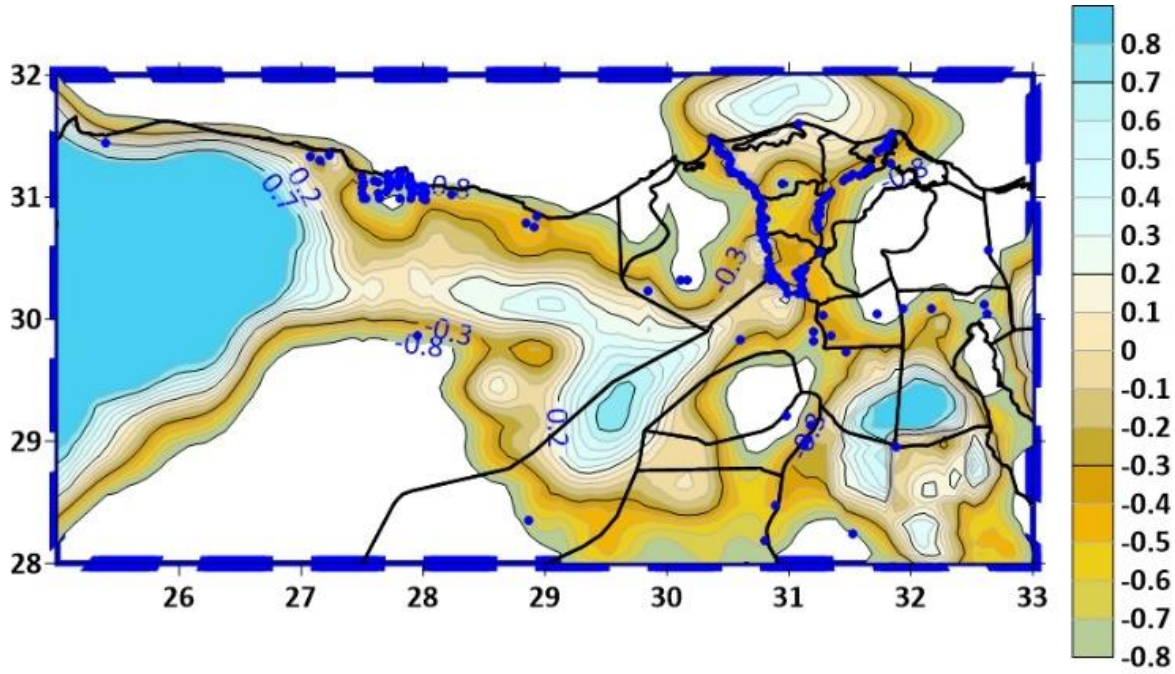
32
31
30
29
28
26
27
28
29
30
31
32
33
0.8
0.7
0.6
0.5
0.4
0.3
0.2
0.1
0
-0.1
-0.2
-0.3
-0.4
-0.5
-0.6
-0.7
-0.8

C

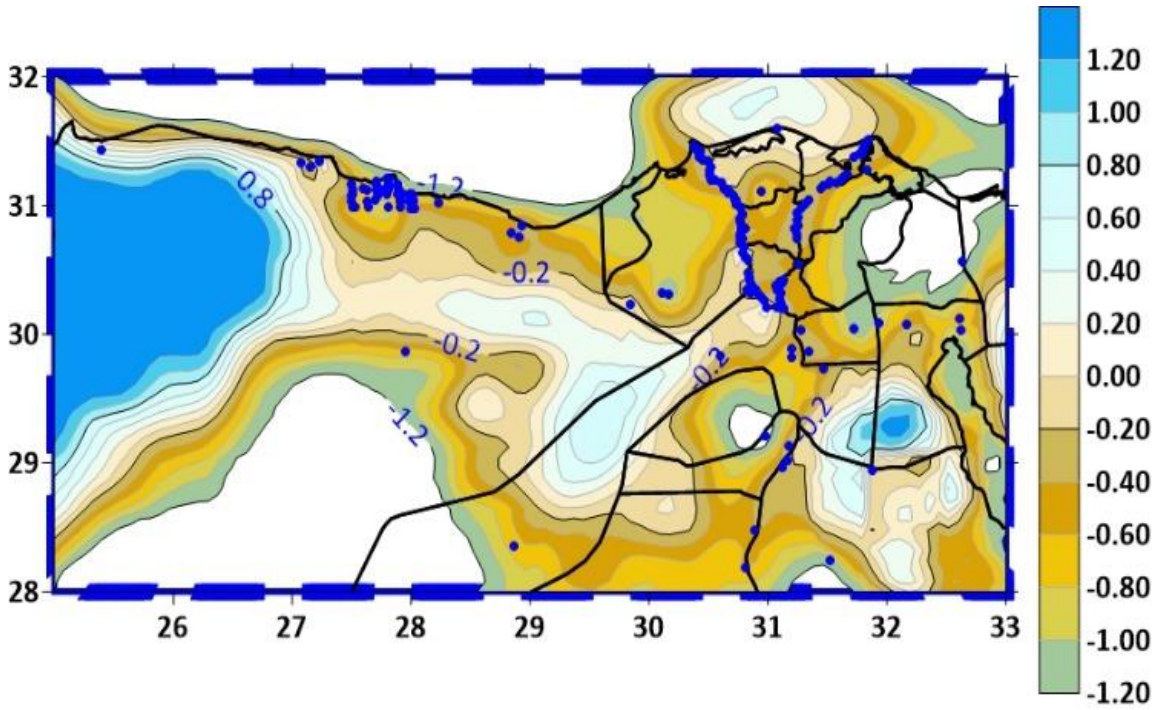
32
31
30
29
28
26
27
28
29
30
31
32
33
1.20
1.00
0.80
0.60
0.40
0.20
0.00
-0.20
-0.40
-0.60
-0.80
-1.00
-1.20

D

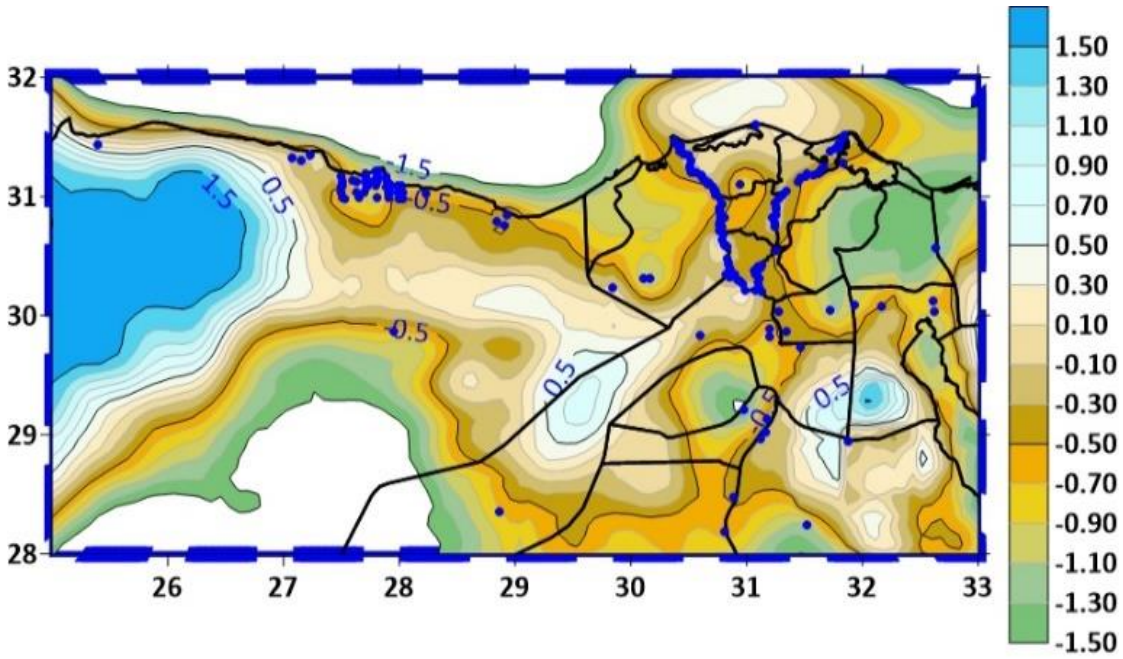

Figure 71 Residuals assessment for Area 01 geoid (Unit: m)

6.4 Geoid determination in the rest of EGYPT territory (Area 02)

As mentioned, there is sparse gravimetric data, especially in the rest of Egypt's territory (Area02). These gabs were filled using the XGM2019e geopotential model, and the geoid was computed in several steps similar to Area01 geoid computations:

- GGM-XGM2019e was used to comput the long wavelength of the height anomalies quasi-geoid,
- The short-wavelength component was computed using reduced gravity anomalies in a two-dimensional convolution representation of the Stokes' integration,
- DEM (SRTM 3arecsec) was used to compute the terrain effect (Molodensky term) (Hastings and Dunbar, 1998).

The height anomalies were converted to geoidal heights using (Rapp, 1997) spherical harmonic representation of the separation between the two surfaces.

6.4.1 The long-wavelength component of the height anomalies (quasi-geoid) of AREA02

To determine the long-wavelength component, the evaluations of EGM 2008 and XGM2019e (Table 32) were performed first and compared to all gravimetric data for Egypt territory. The statistical results are summarised in Tables 33 and 34 and spatially represented in Figs. 46 and 72.

Table 31 Global Geopotential Models used for Area02 (A is for altimetry, S is for satellite (e.g., GRACE, GOCE, LAGEOS), G for ground data (e.g., terrestrial, shipborne, and airborne measurements), and T is for topography)

Global Geopotential Model	Degree/order	Data	References
EGM 2008	2190	A, G, S(Grace)	(Pavlis, N.K. et al, 2012)
XGM2019e	2190	A, G, S(GOCO06s), T	(Zingerle et al., 2020)

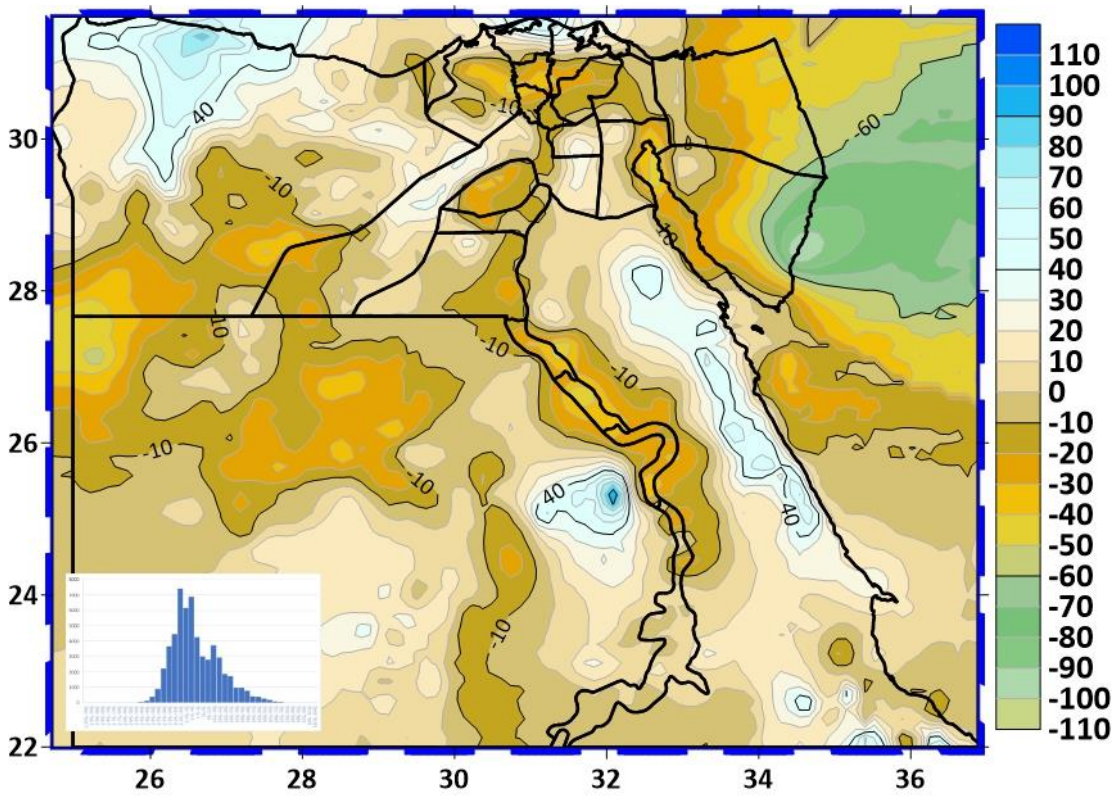

Figure 72 Free air gravity anomaly residuals obtained from EGM2008 and discrete Free air gravity anomaly points over whole territory of Egypt. The histogram of residuals shown on the below left corner of the map

Table 32 Statistical computation of the free air anomaly data sets computed from GGMs (unit: mGal)

δ Δg [mGal]	Free air gravity anomaly	Min	Max	Mean	Std. Dev.
	2190 EGM2008	-103.601	104.387	-2.236	20.883
	2190 XGM2019e	-52.471	41.144	0.422	7.779

Table 33 Statistical computation of the residuals between height anomaly from GGMs and corresponding discrete GPS/H data points (unit: m)

	GPS/H and Height anomaly	Min	Max	Mean	Std. Dev.
δ N[m]	2190 EGM2008	-1.150	2.168	0.537	0.510
	2190 XGM2019e	-2.036	0.837	-0.371	0.487

6.4.2 Determination of Short-Wave Characteristics of Anomalous Potential Functionals for the Purpose of Determining the Geoid of Area 02

Expression 6.10 from section 6.2.3.2 was used to determine the short-wave length characteristics of anomalous potential functionals to determine geoid in Area 02. The statistical results are summarized in Table 35 and represented as a contour map (Fig. 73).

Table 34 Basic statistical data of short-wave characteristics of free air anomalies (unit: mGal)

Parameter	Numbers	Min	Max	Mean	Std. Dev.
Δg_{TOPO}	15733	-48.370	13.180	-0.160	1.490

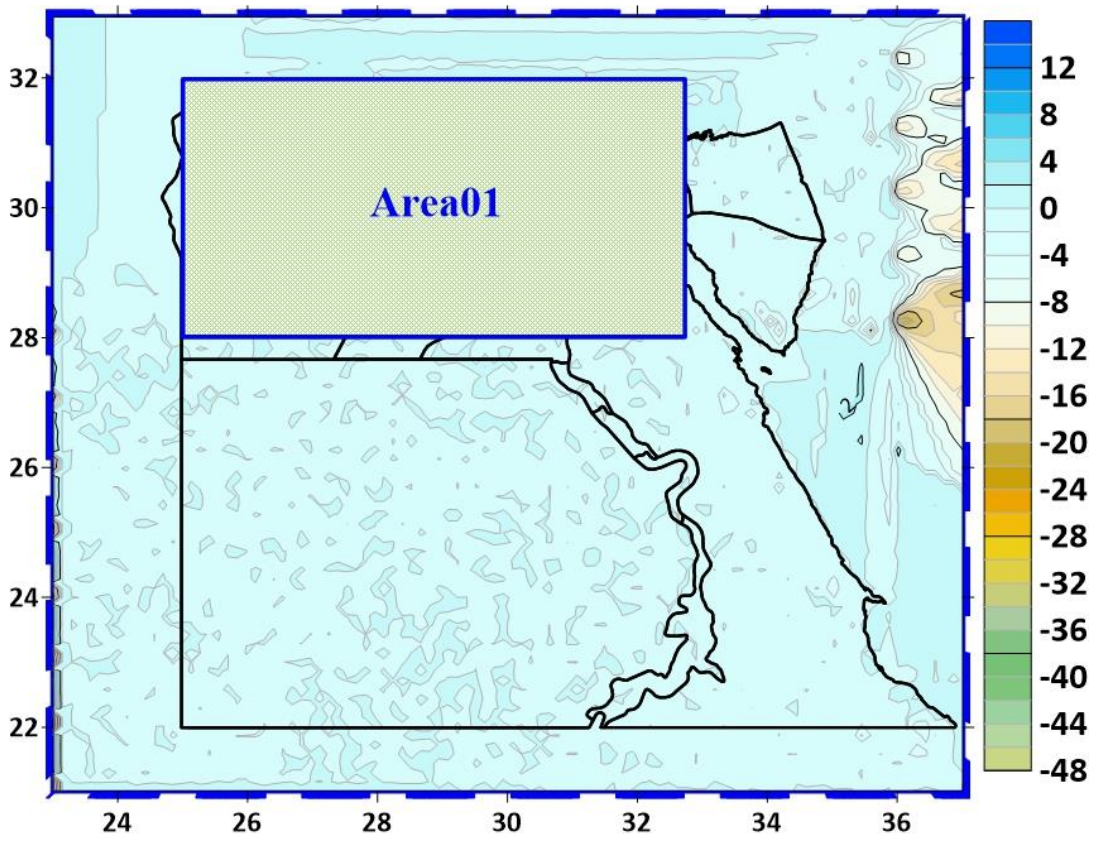

Figure 73 The surface of shortwave characteristics of free air anomalies (contour interval 5 mGal*) for Area 02.*

6.4.3 Residual Anomalies

Expression 6.11 was used for the calculation of residual anomalies. The results were summarized hereafter in Table 36 and represented as a contour map shown in Fig. 74.

Table 35 Basic statistics of residual anomalies (unit: mGal).

Parameter	Numbers	Min	Max	Mean	Std. Dev.
Δg_R [mGal]	15733	-99.330	147.346	0.034	8.389

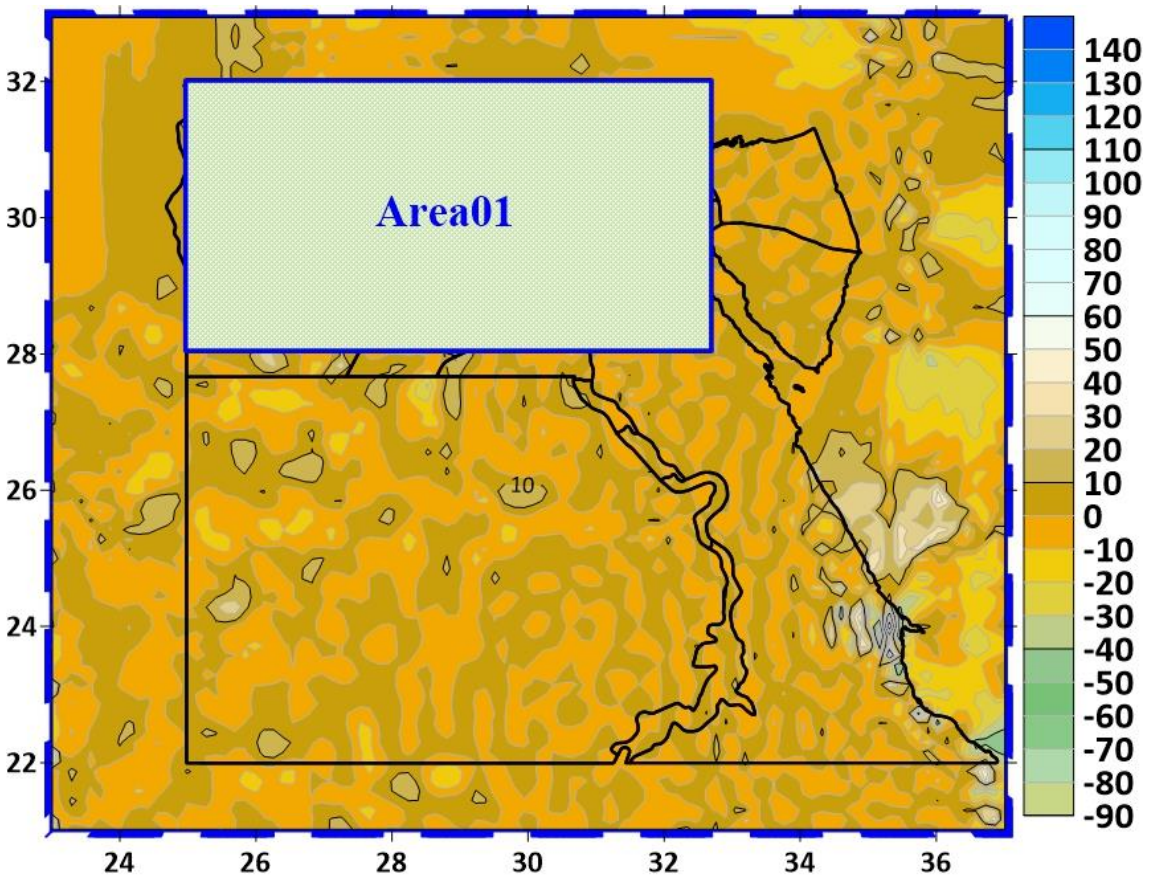

Figure 74 General surface shape of residual anomalies for Area 02 (in mGal)

6.4.4 Empirical covariances and analytical function of covariances for Area 02

Expressions from section 6.2.5 have been used to determine the empirical covariance function and parameters of the analytical function, as shown hereafter in Fig. 75 and Table 37, respectively.

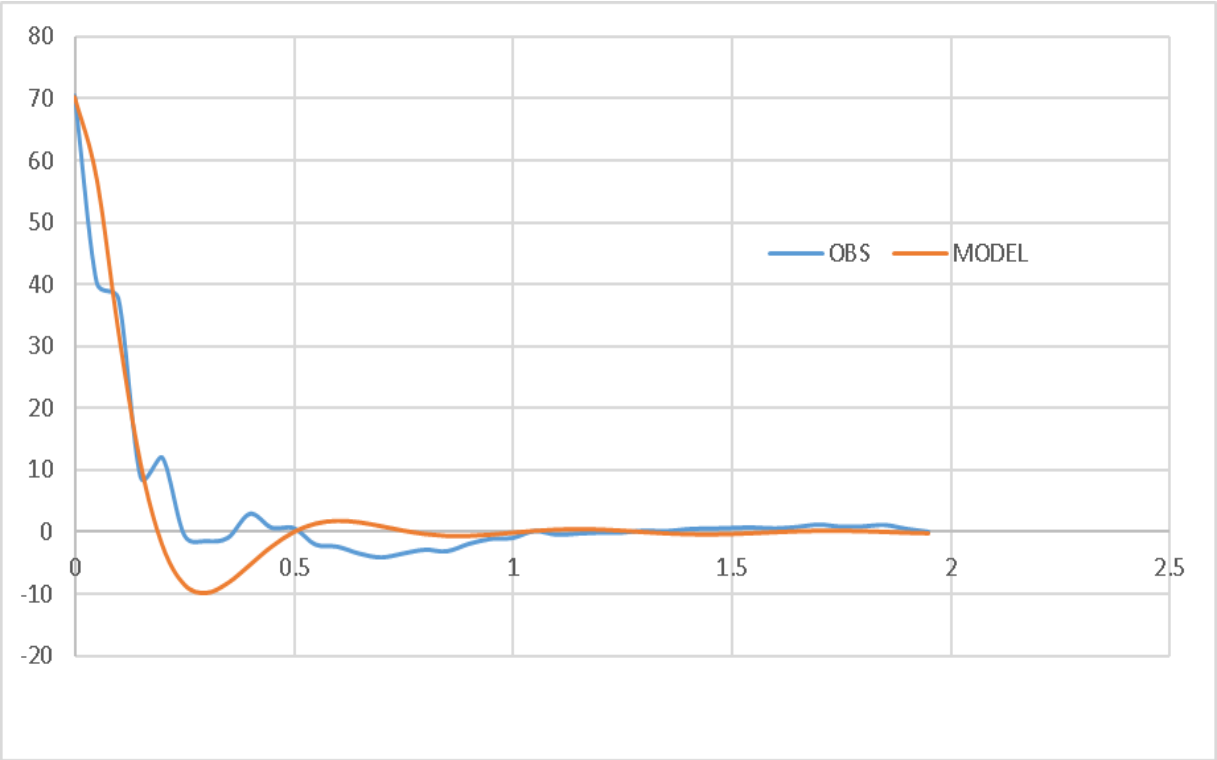

Figure 75 Empirical covariances and analytical function of covariances for Area 02

Table 36 Parameters of the analytical function of covariances of residual anomalies

α [−]	$R_B - R_E$ [km]	$C_{H=0.03}$ [mGal^2]	C_0 [mGal^2]	ζ [arc minute]
-0.000009	-2.118	79.09	70.4	5.00

6.4.5 Anomalous l height residuals for GPS/H points

LSC method was used to predict anomaly height residuals for GPS/H points ζ_{Coll} using GEOCOL software from the Gravsoft package.

Table 38 and Fig. 76 show the statistical computation and spatial representation as contour map for the obtained residual from collocation.

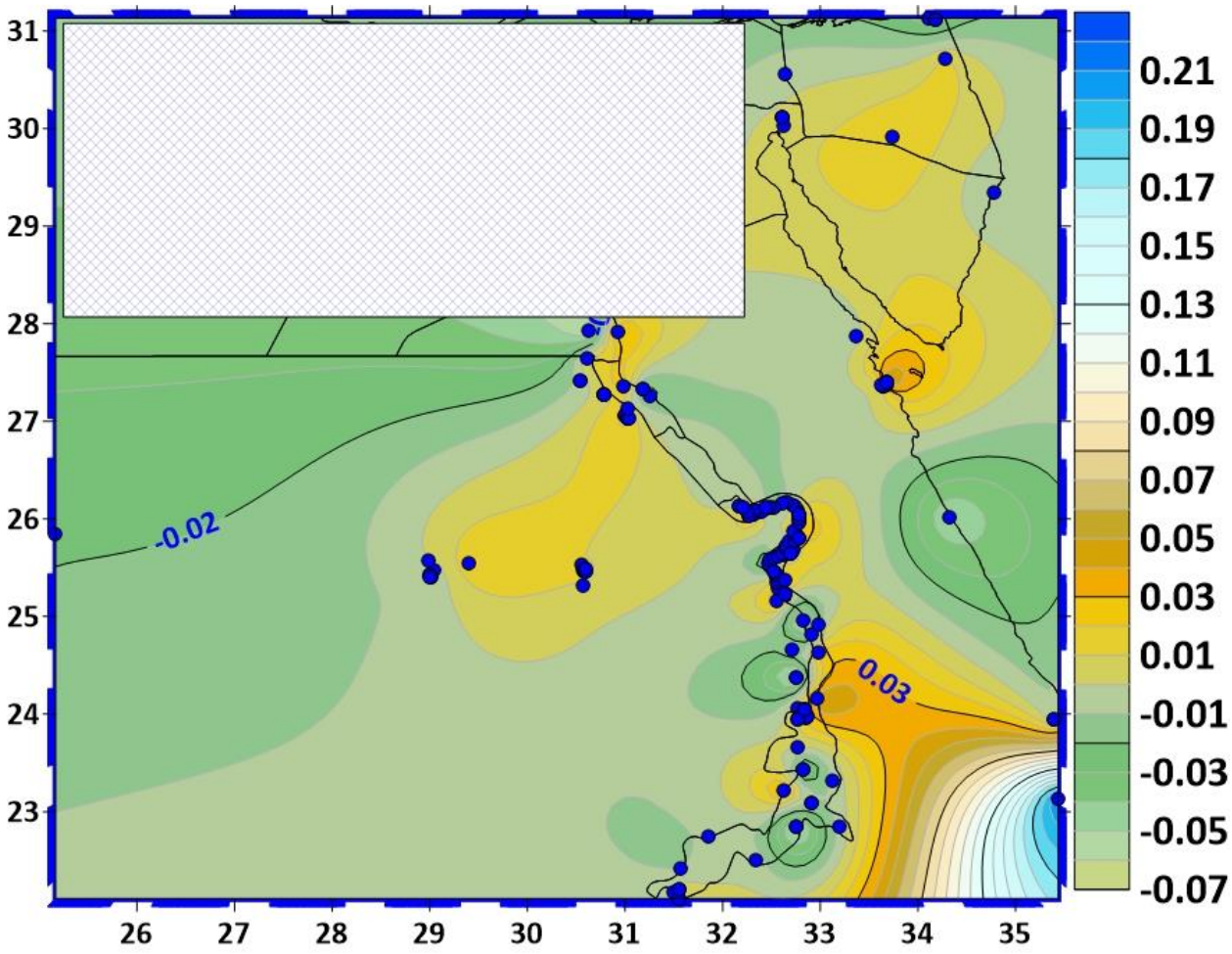

Figure 76 Anomalous residual heights for GPS/H points located at Area 02

Table 37 Basic statistics of anomalous residual heights for GPS/H points (unit: m).

Parameter	Numbers	Min	Max	Mean	Std. Dev.
ζ_{Coll}	162	-0.069	0.212	-0.004	0.028

6.4.6 Residual anomalous heights on (TG - geoid points)

Residual anomaly height prediction over a grid 5*5 arc-min generated from SRTM3 arc- sec, considered similar to the previous section 6.4.5 but performed on grid 5*5 arc-min instead of GPS/H points. Table 39 and Fig. 77 described the results as statically computation and spatially representation using the contoured map.

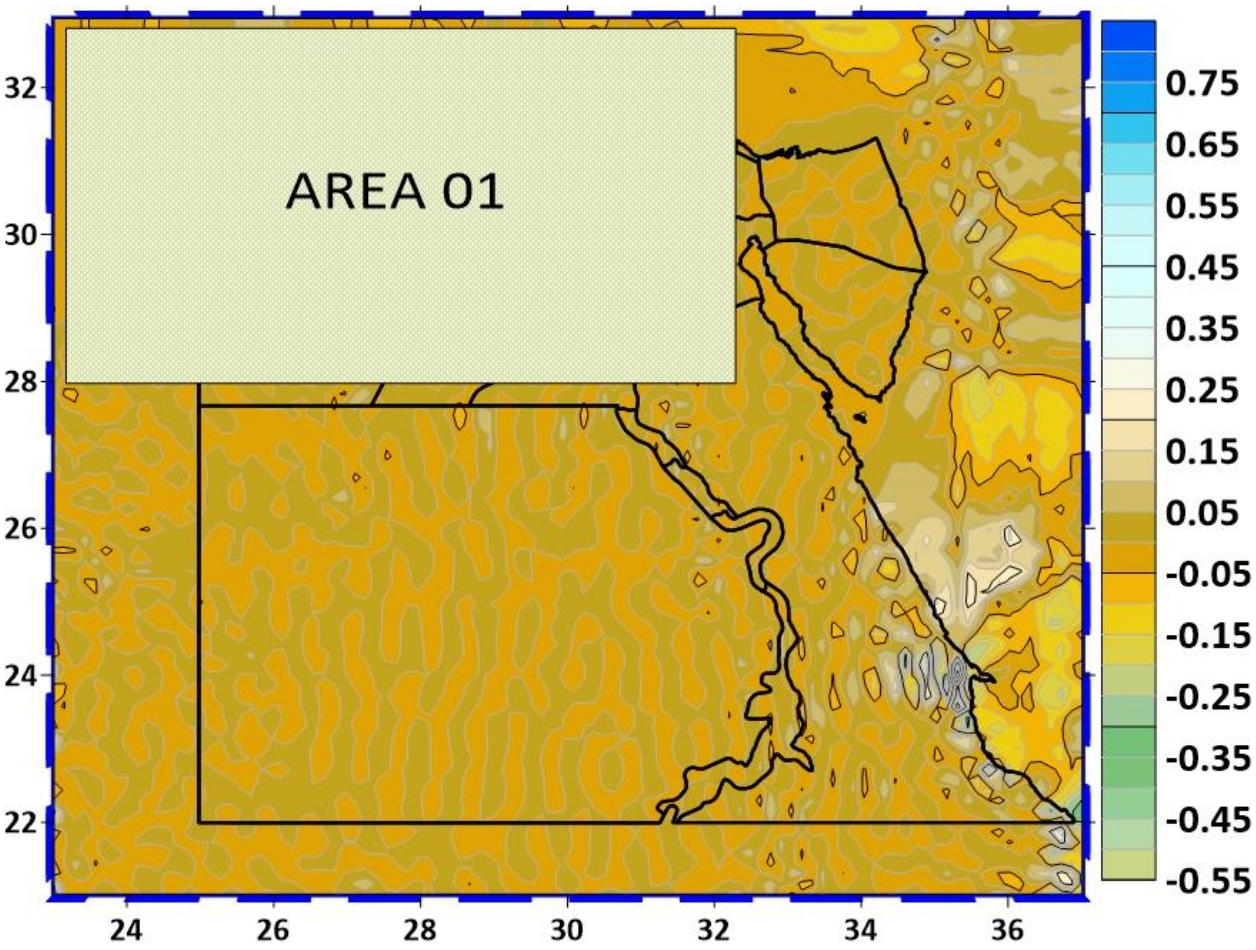

*Figure 77 Residual anomaly height prediction over a grid 5*5 arcmin generated from SRTM 3 arcsec*

Table 38 Basic statistics of residual Anomaly height prediction over a grid from SRTM 5*5 arcmin (unit: m).

Parameter	Numbers	Min	Max	Mean	Std. Dev.
ζ_{Coll}	15733	-0.536	0.981	-0.000	0.046

6.4.7 Short Wave Characteristics of Anomaly Heights

Short wave characteristics of the functional height anomaly were determined using STRM 3 arc-sec in both directions according to section 6.2.3, Table 40 and Fig. 78 show residual terrain model over a grid from SRTM 5*5 arc-min over Area 02.

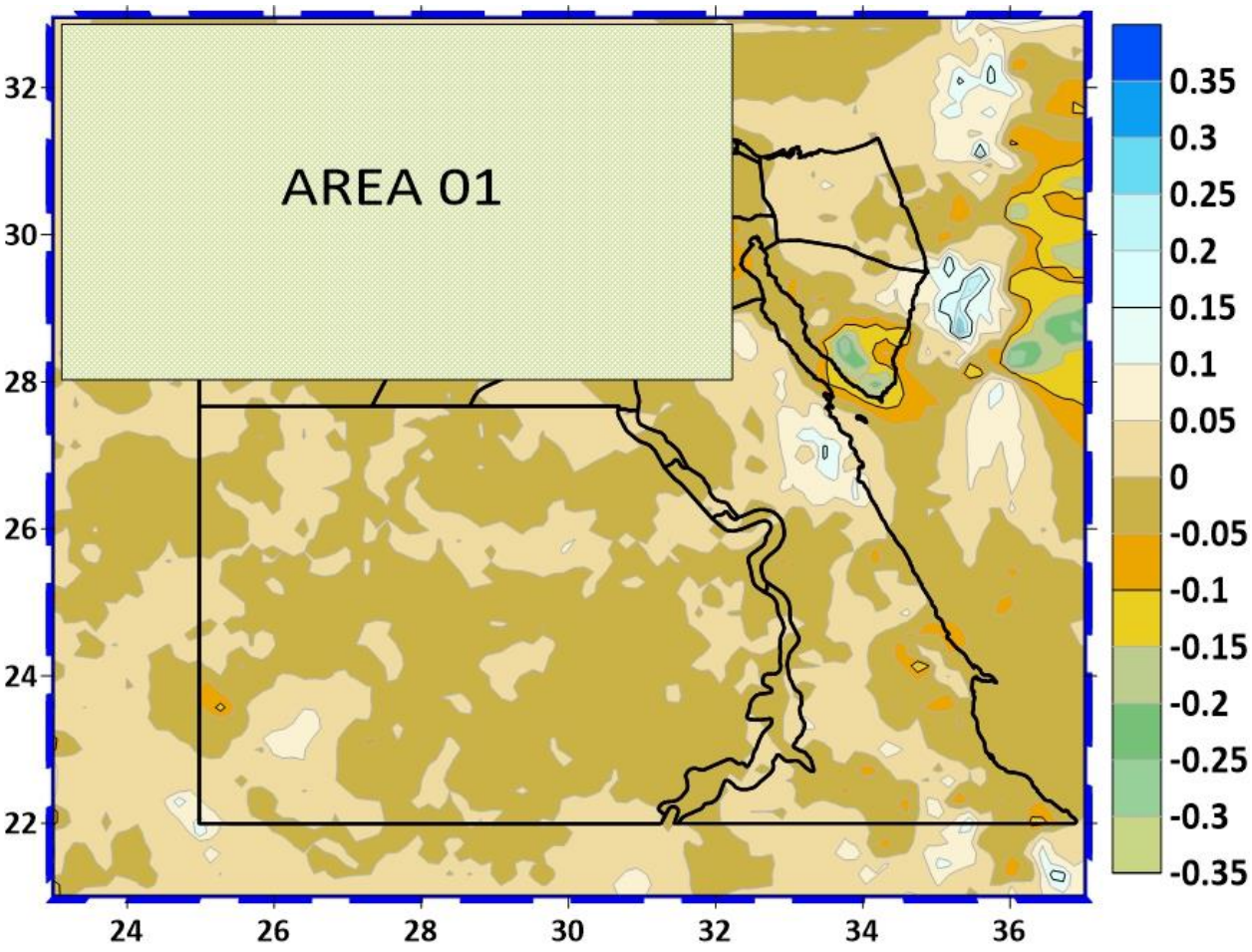

*Figure 78 Residual terrain model over a grid 5*5 arcmin from SRTM 3arcsec*

Table 39 Basic statistics of residual terrain model over a grid from SRTM 5*5 arc-min (unit: m).

Parameter	Numbers	Min	Max	Mean	Std. Dev.
ζ_{TOPO}	15733	-0.331	0.381	-0.003	0.035

6.4.8 Height Anomaly over a grid 5*5 arc-min from EGM GOCE 05c

Expression 6.6 was used to compute height anomaly over a grid 5*5 arc-min for Area 02 the statistical computation and spatial representation are shown in Table 41 and Fig. 79.

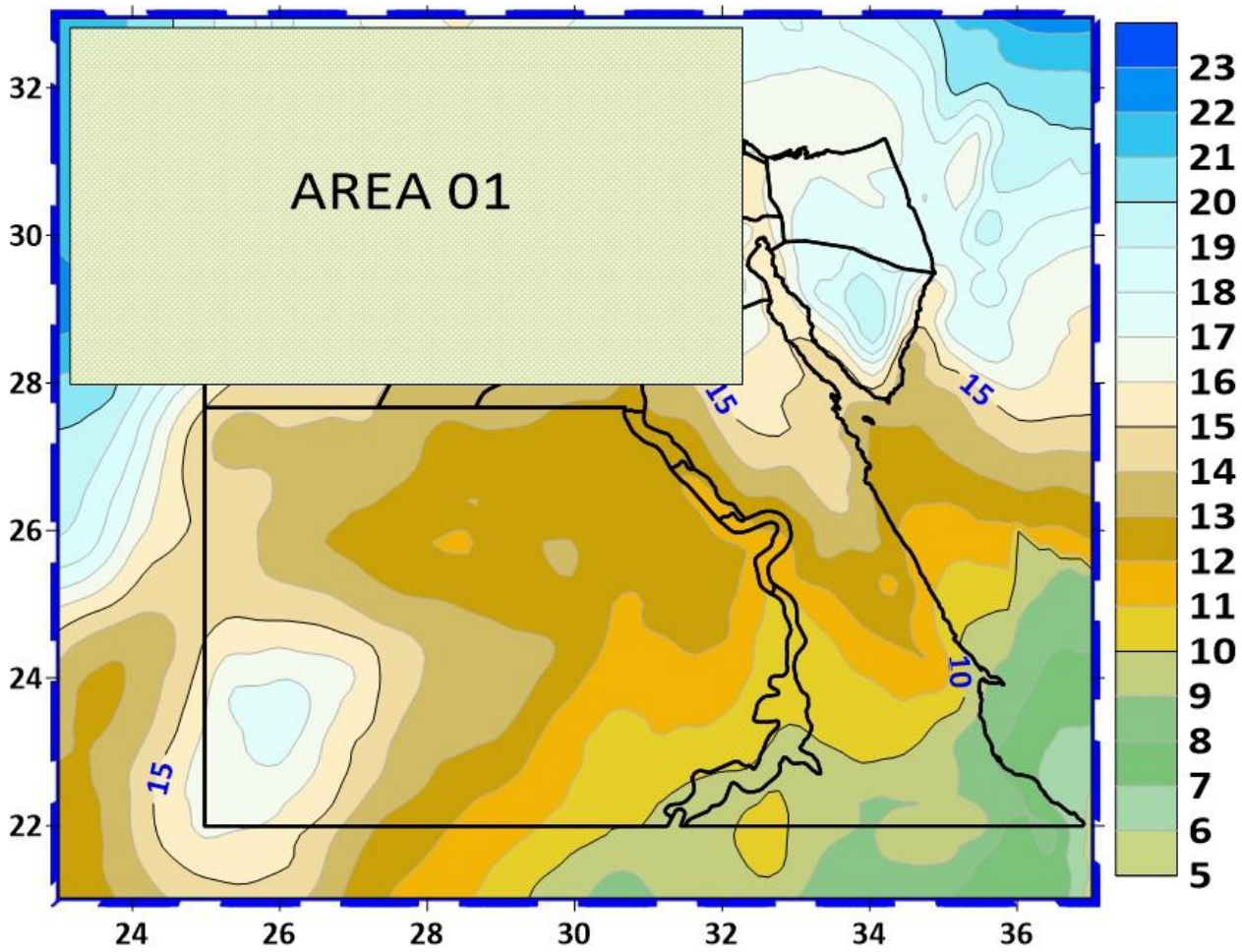

*Figure 79 Height anomaly over a grid 5*5 arcmin from EGM GOCE 05c*

Table 40 Basic statistics of height anomaly over a grid 5*5 arc-min (unit: m).

Parameter	Numbers	Min	Max	Mean	Std. Dev.
$\zeta_{GOCO05c}$ [m]	15733	5.576	22.477	13.677	2.895

6.4.9 Total Anomaly Heights

Total anomalous heights are determined using expressions from section 6.2.8, Table 42 and Fig. 80 describe total height anomaly over a grid 5*5 arc-min over Area 02.

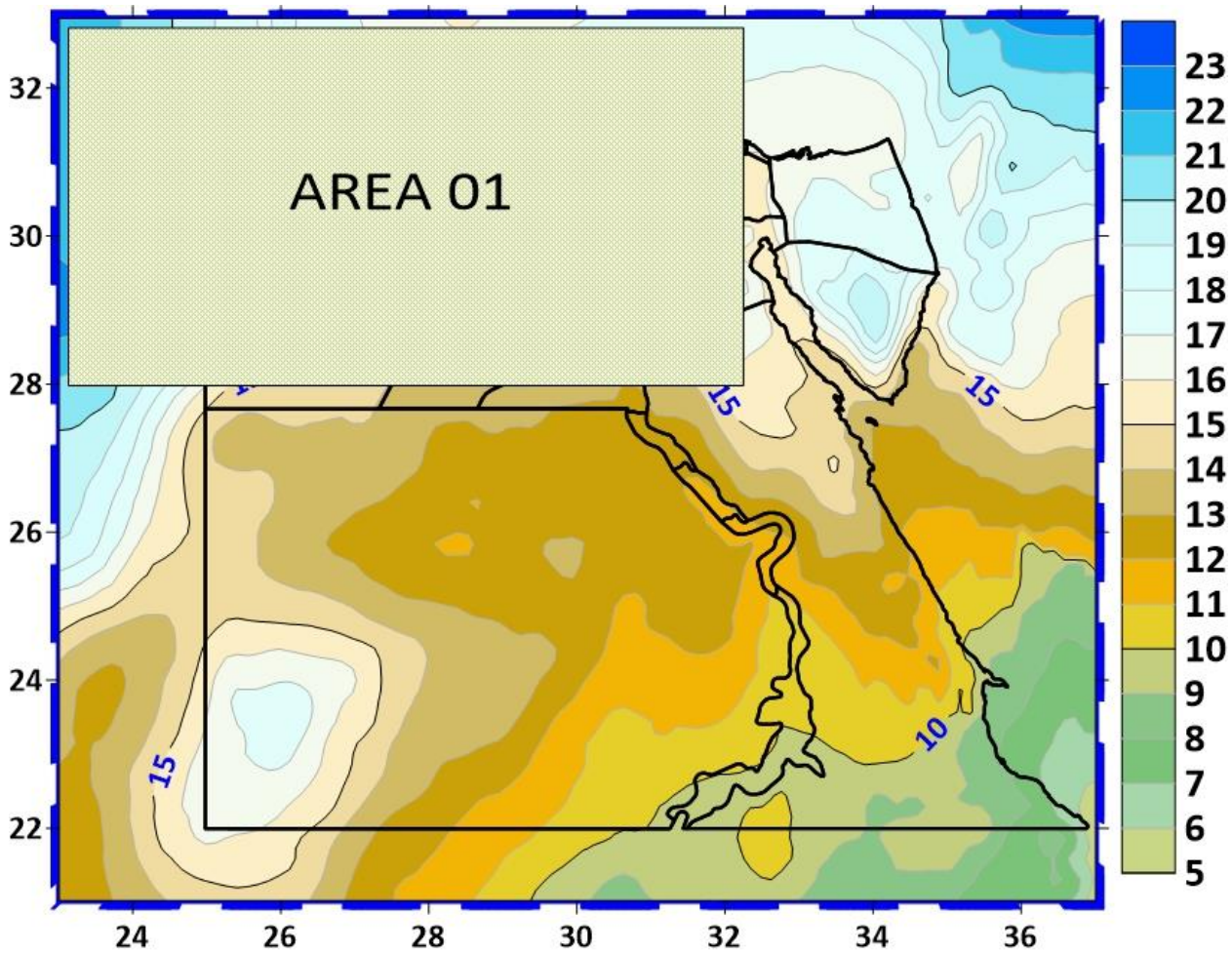

*Figure 80 Total height anomaly over a grid 5*5 arcmin*

Table 41 Basic statistics of total height anomaly over a grid 5*5 arc-min (unit: m).

Parameter	Numbers	Min	Max	Mean	Std. Dev.
$\zeta_{GOCO05c}$ [m]	15733	5.507	22.673	13.680	2.900

6.4.10 Quasi-geoid Corrections

The difference between geoid and quasi-geoid using the expression 6.26 mentioned in section 6.2.9, Table 43 and Fig. 81show geoid/quasi-geoid correction over a grid 5*5 arcmin for Area 02.

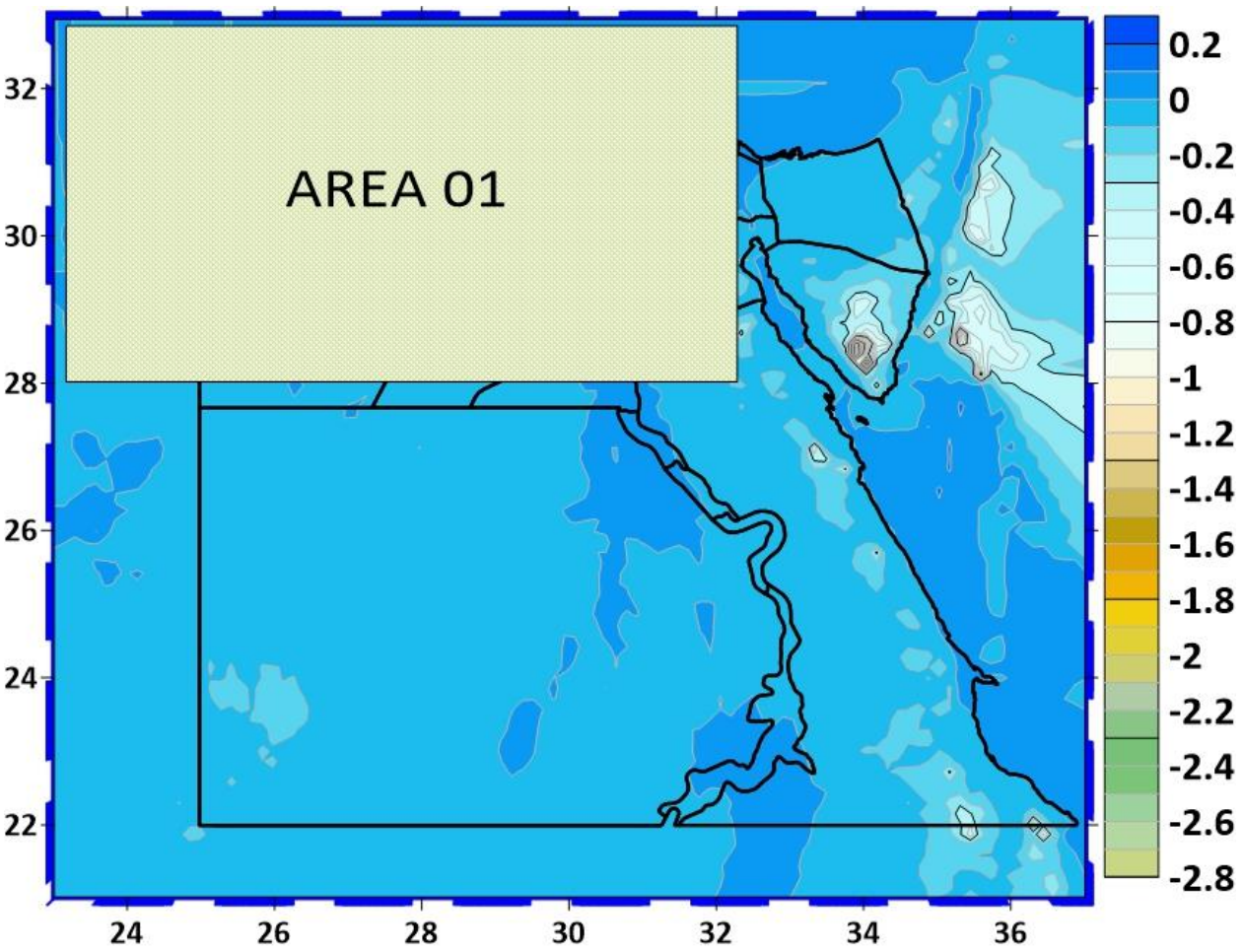

*Figure 81 Geoid/Quasi-geoid correction over a grid 5*5 arcmin (Unit in* cm*)*

Table 42 Basic statistics Geoid/Quasi-geoid correction over a grid 5*5 arc-min (unit: cm).

Parameter	Numbers	Min	Max	Mean	Std. Dev.
$\zeta_{\text{Geoid/Quasigeoid}}$	15733	-4.774	0.105	0.041	0.104

6.4.11 Ellipsoid correction

it is necessary to calculate ellipsoidal corrections using the expression 6.28 from the previous section 6.2.11 to eliminate the introduced spherical approximation at all points where the differences between geoids and quasi-geoids are determined, Table 44 and Fig. 82 illustrated values of the ellipsoidal correction over a grid 5*5 arc-min for Area 02.

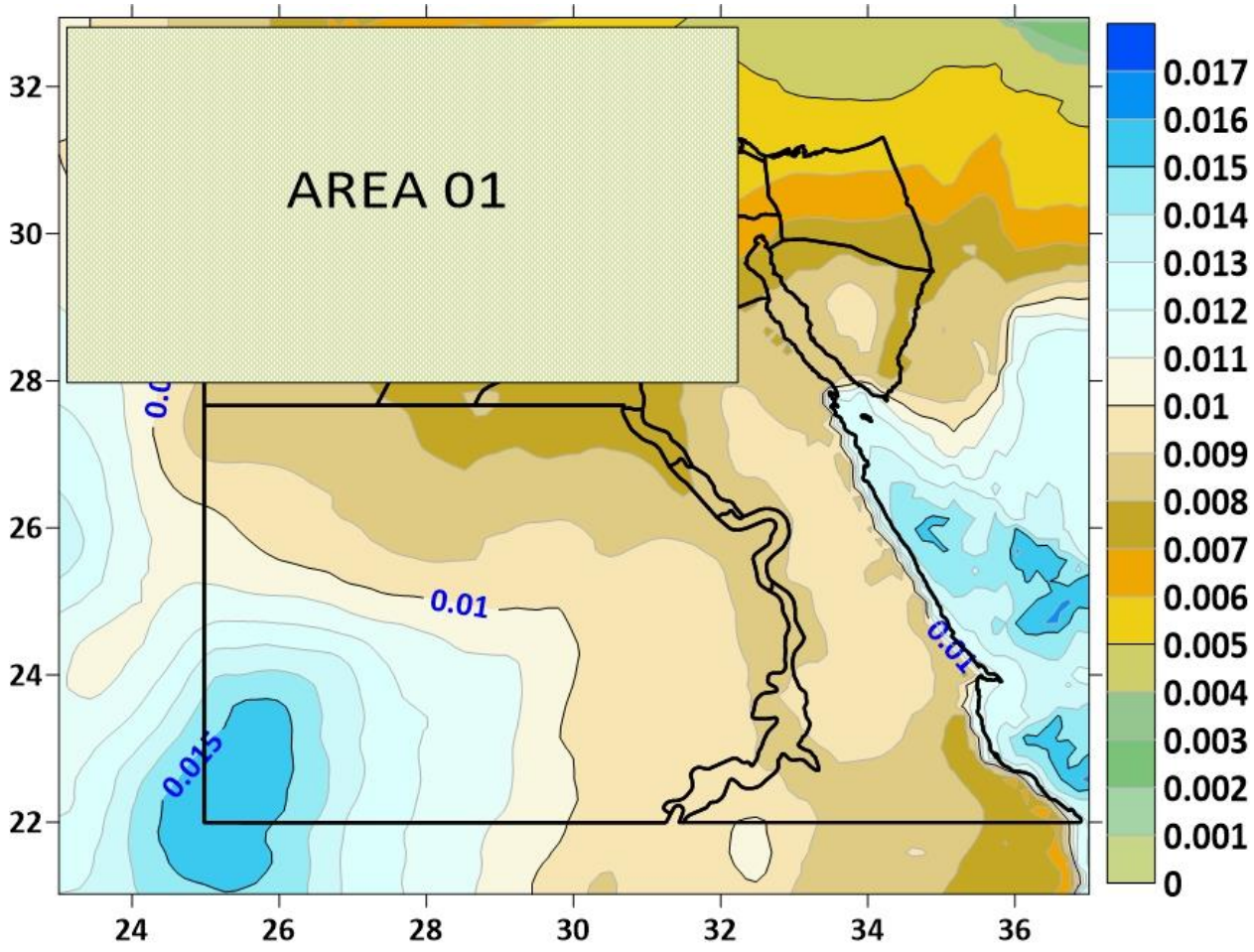

*Figure 82 Statistics ellipsoidal correction over a grid 5*5 arcmin (Unit in* m*)*

Table 43 Basic statistics ellipsoidal correction over a grid 5*5 arc-min (unit: m).

Parameter	Numbers	Min	Max	Mean	Std. Dev.
ζ_{EC} [m]	15733	0.000	0.016	0.009	0.002

6.4.12 Geoid for Area 02

Expression 6.29 was used from section 6.2.12 to add the values of certain ellipsoidal corrections to the values of undulations at the spherical approximation:

Such undulations define the geoid, often called the scientific geoid, and can be considered as the high-resolution geoid of the c AREA 01, Table 45 and Fig. 83 show the geoid over a grid 5*5 arcm for Area 02.

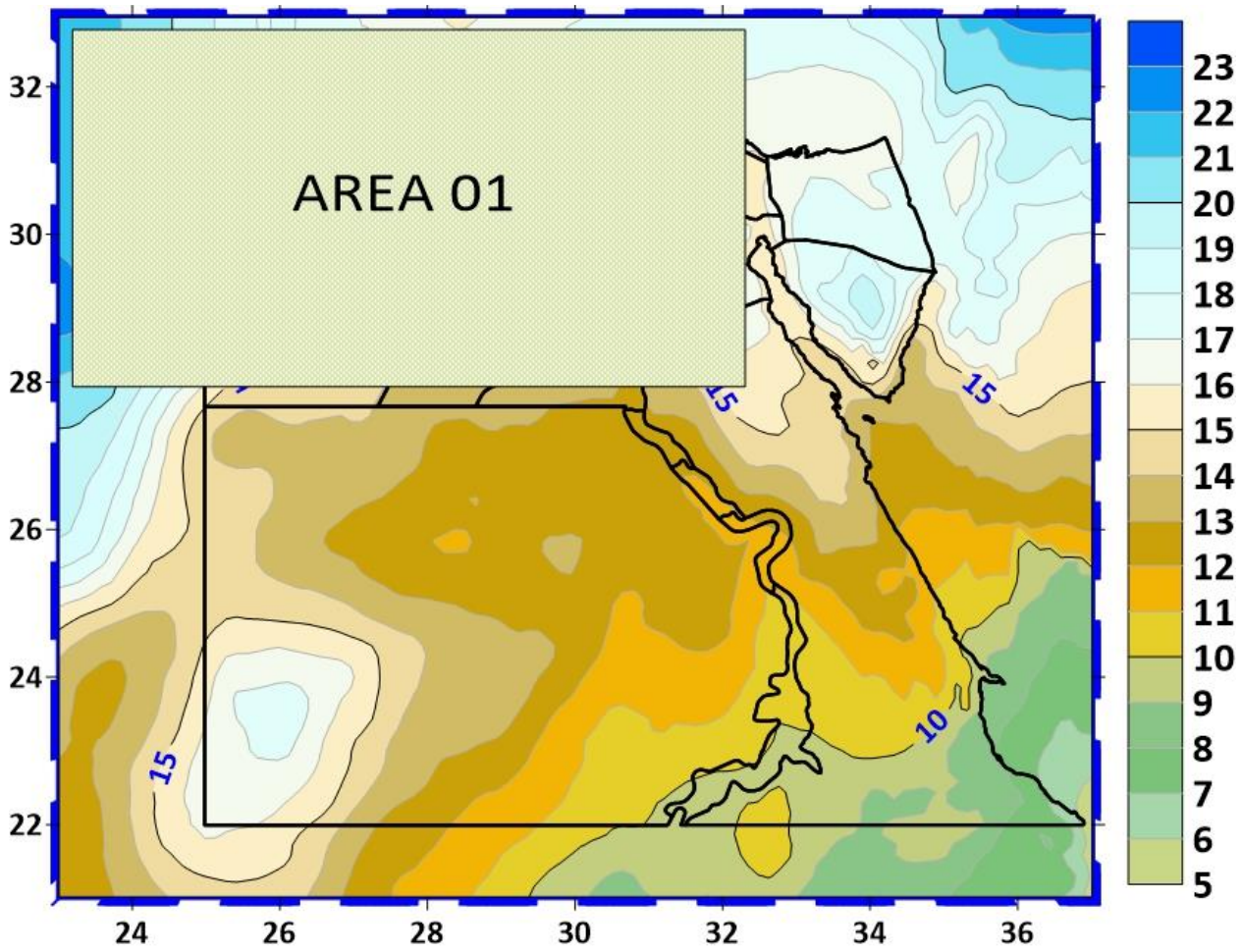

*Figure 83 Area 02 geoid over a grid 5*5 arcmin (Unit in* m*)*

Table 44 Basic statistics of Area 02 Geoid over a grid 5*5 arc-min (unit: m).

Parameter	Numbers	Min	Max	Mean	Std. Dev.
N_E	15733	5.516	22.645	13.650	2.884

6.4.13 Evaluation of Translation Parameters

Recall the expressions and the values of translation parameters from section 6.2.13 to fit the geoid into the national Egyptian height system for Area 02, Table 47 and Fig. 84 show the values of statistical data of differences $\hat{t}$.

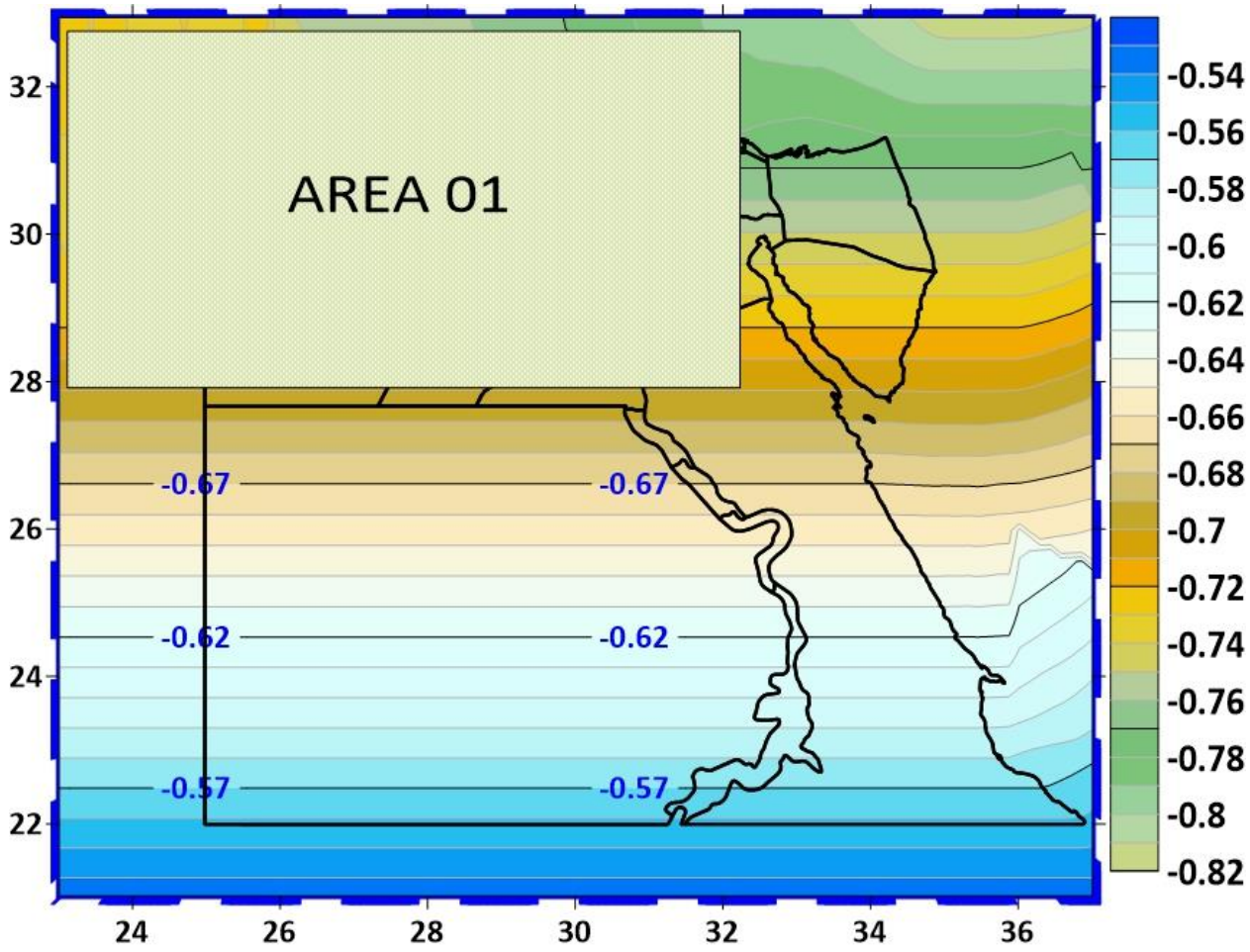

Figure 84 General surface of differences $\hat{t}$ (in m)

Table 45 Basic statistical data of differences $\hat{t}$ (unit: m).

Parameter	Numbers	Min	Max	Mean	Std. Dev.
$\hat{t}$	15733	-0.816	-0.534	-0.640	0.068

6.4.14 Combined Solution

Table 48 and Fig. 85 shown the combined solution which have been obtained as expressions 6.32 and 6.33 mentioned above in section 6.2.14

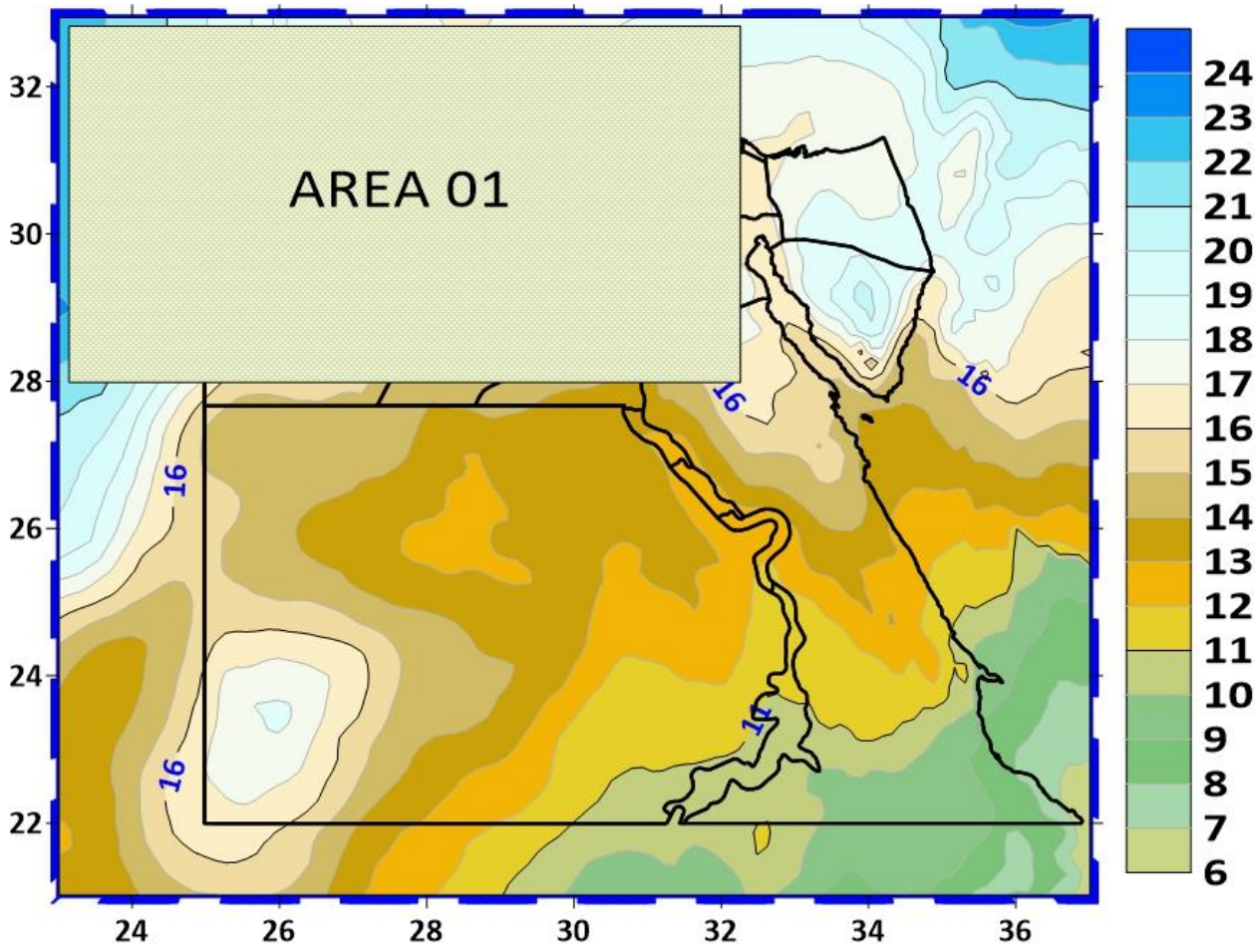

Figure 85 General surface of the high-resolution geoid N_K of Area 02 (in m)

Table 46 Basic statistical data of the high-resolution geoid N_K of Area 02 (unit: m).

Parameter	Numbers	Min	Max	Mean	Std. Dev.
N_C	15733	6.054	23.461	14.289	2.930

6.4.15 Residual Assessment

The combined solution should be the last step in evaluating geoid undulations that can be used in practical work to transform ellipsoidal heights into orthometric ones.

Expression from section 6.2.15 and Eq. 6.34 have been used to determine the residuals R for the internal check as shown hereafter in Fig. 86 and Table 49, respectively.

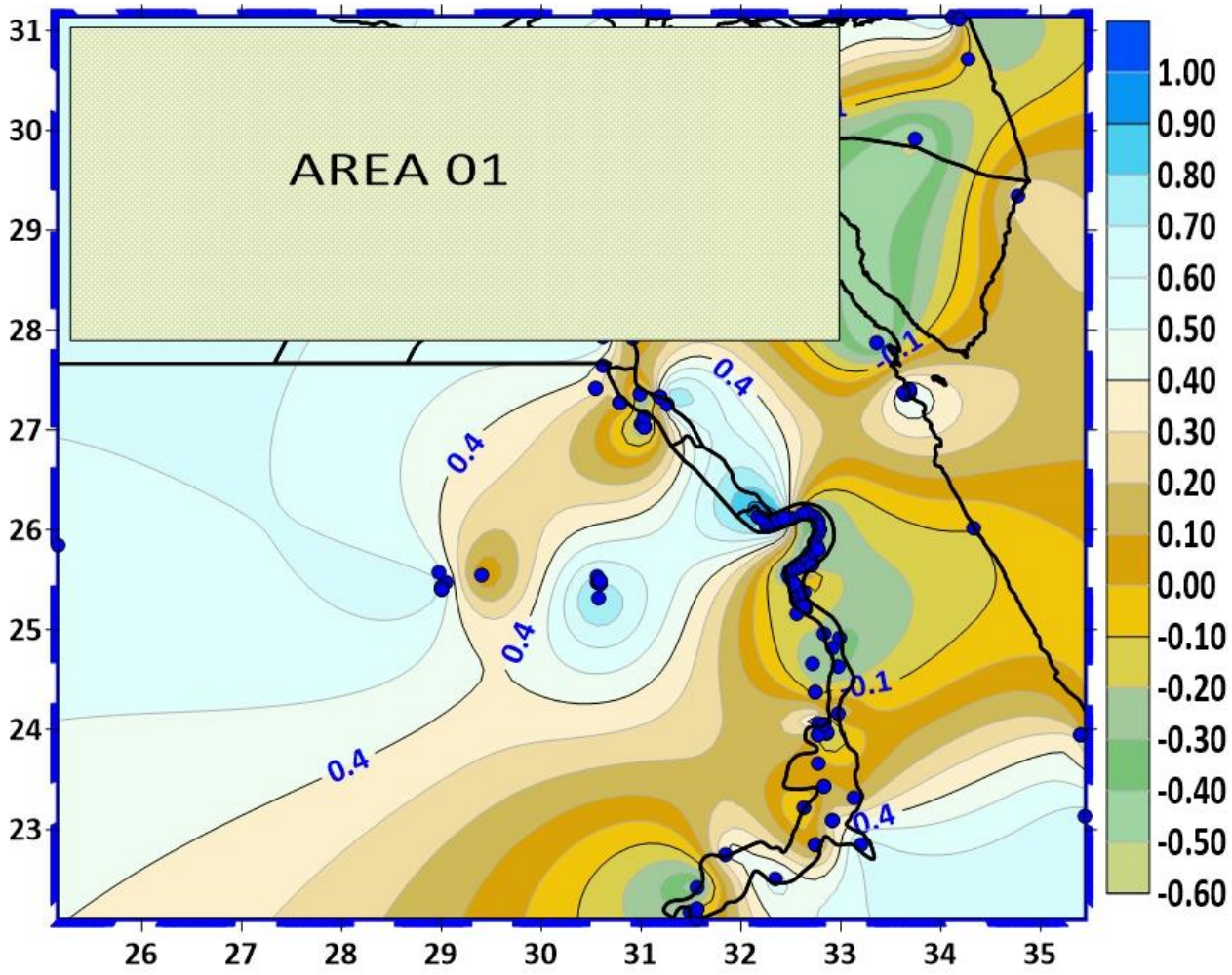

Figure 86 Residuals R for internal check (in m*).*

Table 47 Basic statistical data of the Residuals R for internal check (unit: m).

Parameter	Numbers	Min	Max	Mean	Std. Dev.
$R_{\text{Internal check}}$ [m]	162	-0.971	1.175	0.113	0.479

7. Conclusions and Recommendations

The subject of this research is the determination of geoid and quasi-geoid in areas where only the irregular spatial distribution of observations is available. Among other things, that includes the following:

- the number of observation results is too small concerning the area under consideration (sparse data),
- observation results are grouped in only one part of the relevant area and very rarely in other parts,

and especially

- the results of observations cannot be taken over by classical geodetic methods due to the inaccessibility or continuous change of the Earth's physical surface of the relevant area.

The appropriate approach implies

- the use of a global geopotential model (XGM2019e), digital models of topographic masses (SRTM 3aresec), and available observation results to model the parameters of the Earth's potential, this approach tries to distribute data in the relevant area, to be suitable and sufficient for geoid solution attempt.

- Then, the reference surfaces (geoid and quasi-geoid) are determined from observations and newly modeled parameters of the Earth's gravity potential.

Based on the studied Area 01 results, as outlined in Table 28 and shown in Fig. 67, the accuracy obtained by the LSC technique in terms of the standard deviation is 0.338 m of the differences, and it is considered rather satisfactory.

Geoid solution for Area 01 has been fitted using 80 GPS/H points, while 100 points were used for external checking, the results show that.

The obtained accuracy in terms of the standard deviation of the differences at control points GPS/H, given as the external check outlined in Table 29, and showed by Fig. 68, was 0.262 m.

To generalize this solution to Egypt's whole area, some alternative solutions were applied for the rest of Egypt territory called Area 02, to obtain a geoid solution, especially in the eastern and northern deserts. The data has inadequate and insufficient distribution all over Area 02, and it is recommended to have new gravimetric measurements in Area 02. While these data are not available at present, alternative methods were used to provide data for Area 02 as follows:

- GGMs GOCE05c and XGM2019e were used for modelling Long-wavelength component for Area 02 as qusi-geoid for this region.

- Used DEM (SRTM 3arcsec) for modelling Short-wavelength component for Area 02

The gravimetric and combined geoid solutions for Area 02 were computed using GGMs GOCE05c and XGM2019e in addition to DEM (SRTM 3arc-sec), in the RCR technique through 3D least-squares collocation (3D LSC), geoid solutions for Area 02 have been fitted using 162 GPS/ data points.

Finally, Table 49 and Fig. 86 show the internal check for the geoid model for Area 02, which has ±0,479 cm as internal accuracy in terms of the standard deviation of the residuals when compared to 162 GPS/H points.

Evidently, from the two obtained Area 01 and Area 02 geoid accuracies, Area01 geoid has better accuracy, nearly about 30%, than Area 02 geoid as an internal check.

Based on all of the above-mentioned conclusions we recommended the following recommendations for the future producing a one-centimeter geoid model to replace the existing vertical reference for Egypt.

It is advisable to use the satellite-only models of the GOCO series in combination with the available local geodetic data for better modelling the Egyptian gravity field. It is also necessary to cooperate actively between the Egyptian surveying authority representatives and the responsible organizations dealing with GGM computations.

It is recommend to redefination the datums of the currently available gravity and GPS/H data, where different organizations have collected this data set. Data will likely be affected with several types of errors, e.g., datum errors (horizontal, vertical, and gravity datum).

We strongly recommend the creation of a new gravity network with 5*5 arc-min spacing for the entire area of Egypt, as the current observations suffer from poor spatial distribution, as well as a scarcity of data (cf. Fig.4.12), especially in areas that contain Egypt's reserves of raw materials, such as the eastern and western deserts, Until this happens, it is recommended to fill the current gaps by the following methods:

- airborne gravity surveys may contribute to filling the voids, especially in mountainous areas, sand dunes, lagoons ،and all areas where ground observations are difficult to perform;

- The Egyptian government should work on a unified project to collect observed gravity data from all state institutions, public and private, especially the petroleum companies working in Egypt, as well as making communication channels with the foreign countries and companies that may have any information or data about the Egypt gravity field to integrate them with the rest data collected from inside.

- the combination of the observations of three gravity field mapping missions (CHAMP, GRACE, and GOCE) and available gravity data should be used for better gravity field modelling in Egypt.

GPS/H stations should be increased as well as distributed all over egypt area to determine a precise corrective surface to fit the geoid models to the Egyptian vertical datum.

Since the new GGMs often do not contain terrestrials gravity data from Egypt, therefore we recommend tailoring/ integrating those GGMs with all the ground data obtained in a repetitive process to be applied when a new GGM publishes or new terrestrial data is observed.

Based on the obtained result of the present research, it is recommended to re-develop the reference geopotential model GOCE05c with the available and new observation of Egyptian gravity data.

References

Abdalla, A., Fairhead, D. (2011). *A new gravimetric geoid model for Sudan using the KTH method. Journal of African Earth Sciences*. 60, 213-221. https://doi.org/10.1016/j.jafrearsci.2011.02.012.

Abdalla, A., and Tenzer, R. (2011). *The evaluation of the New Zealand's geoid model using the KTH method.* Journal of Geodesy and Cartography, 37(1), 5–14. https://doi.org/10.3846/13921541.2011.558326

Abd-Elmotaal, H. (2006). *High-degree geopotential model tailored to Egypt*. (eds) Kılıçoğlu and Forsberg R, Gravity Field of the Earth, Map Journal 18 187–192.

Abd-Elmotaal, H. A., Kühtreiber, N., Seitz, K., and Heck, B. (2020). *A Precise Geoid Model for Africa: AFRgeo2019* (pp. 1–11). Springer. https://doi.org/10.1007/1345_2020_122

Adam, M. O. (1967). *A Geodetic Datum for the Sudan* [Master Thesis,]. Cornell University.

Ågren, J., Kiamehr, R., and Sjöberg, L. E. (2008). *Computation of a new gravimetric model over Sweden using the KTH method Integrating Generations FIG Working Week 2008*.

Al-Krargy, E. M., Doma, M. I., Dawod, G. M. *Towards an accurate definition of the local geoid model in Egypt using GPS/leveling Data. a case study at Rosetta zone Int.* International Journal of Innovative Science and Modern Engineering (IJISME) 2 , 10-15.

Ameti, P., and Jäger, R. (2016). *On the definition of height reference surfaces over an arbitrary selected area by means of DFHRS approach*. Geodesy and Cartography, 42(4), 115–121. https://doi.org/10.3846/20296991.2016.1268431

Amin, M., El-Fatairy, S., and Hassouna, R. (2002). *The "EGM96EGIT" Geopotential Model Tailored to Egypt by the Stokes' Integral Technique.* Scientific Bulletin of Matarya Faculty of Engineering,Helwan University, Cairo, Egypt, 84.

Amin, M., El-Fatairy, S., and Hassouna, R. (2003). *Two Techniques Of Tailoring A Global Harmonic Model: Operational Versus Model Approach Applied To The Egyptian Territory*. Port-Said Engineering Research Journal PSERJ,Faculty of Engineering, Suez Canal University, Port-Said, Egypt.

Amin, M. M. (1983). *Investigation of the Accuracy of some Methods of Astrogravimetric Levelling using an Artificial Test Area"* [Ph.D. dissertation]. Geophysical Institute, Czechoslovac Acad. Sci.

Amos, M. J. (2007). *Quasigeoid modelling in New Zealand to unify multiple local vertical datums* [PhD Thesis,]. Department of Spatial Sciences, Curtin University of Technology.

Amos, M. J. (2016). *Improving New Zealand's Geoid Based Datum with Airborne Gravimetry.* In FIG Working Week.

Arabelos, D. (1989). *Gravity Field Approximation in The Area of Greece with Emphasis on Local Characteristics*. Bulletin Geodesique, 63, 69–84.

Arabelos, D. N., and Tscherning, C. C. (2010). *A comparison of recent Earth gravitational models with emphasis on their contribution in refining the gravity and geoid at continental or regional scale*. Journal of Geodesy, 84(11), 643–660.

Ardestani, V., and Martinec, Z. (2000). *Geoid Determination Through Ellipsoidal Stokes Boundary-value Problem*. Studia Geoph. et Geod, 44, 353–363.

Avalos Naranjo, M. S. G., and Abundes, R. M. (2010). *The Mexican gravimetric geoid: GGM2010. V. 1.0. GFZ Data Services*. https://doi.org/10.5880/isg.2010.001

Avramiuc, N., Erhan, C., Spiroiu, I., Crişan, R.-D.-N., and Flueraş, M. (2019). *Determination of a new gravimetric quasigeoid for Romania*. Journal of Geodesy, 7.

Barthelmes, F. (2014). *Global models.* Encyclopedia of Geodesy, Springer International Publishing, 1–9.

Barzaghi, R., Betti, B., Borghi, A., Sona, G., and Tornatore, V. (2002). *The Italian quasi-geoid ITALGEO99.* Bollettino di Geodesia e Scienze Affini, 61(1), 33–51.

Barzaghi, R., Borghi, A., Carrion, D., and Sona, G. (2007). Refining the estimate of the Italian quasi-geoid. Bollettino di Geodesia e Scienze Affini, 66(3), 145–159.

Barzaghi, R., Borghi, A., Ducarme, B., and Everaerts, M. (2003). *Quasi-geoid BG03 computation in Belgium*. Newton's Bulletin, 1, 78–94.

Basic, T., and Bjelotomic, O. (2014). *HRG2009: New High Resolution Geoid Model for Croatia*. In U. Marti (Ed.), Gravity, Geoid and Height Systems, IAG Symposia Series 141, 187-191. Springer Verlag. https://doi.org/10.1007/978-3-319-10837-7_24

Belay, E. Y., Godah, W., Szelachowska, M., and Tenzer, R. (2021). *ETH-GM21: A new gravimetric geoid model of Ethiopia developed using the least-squares collocation method.* Journal of African Earth Sciences, 22, 104313. https://doi.org/10.1016/j.jafrearsci.2021.104313

Benahmed Daho S. A.,. (2000). *The new gravimetric geoid in Algeria.* IGeS Bulletin, 10, 1128-3955-85.

Benahmed Daho, S. A., and Kahlouche, S. (1998). *The gravimetric geoid in Algeria.* First Results. Geodesy on the Move. IAG.

Benaim, E. H. (1995). *Strate´gies de calcul d'un geoid gravimetrique sur le de´troit de Gibraltar*. In Pub. Institut Agronomique et Veterinaira.

Benaim, E. H., Swassi, A. M., and Sevilla, M. J. (1998). *The first northern Moroccan gravimetric geoid.* Phys. Chem. Earth, 23(1), 65–70.

Benciolini, B., Mussio, L., Sanso', F., Gasperini, P., and Zerbini, S. (1984). *Geoid Computations in the Italian Area.* Bollettino di Geodesia e Scienze Affini, 43(3), 213–243.

Beutler, G., Moore, A. W., and Mueller, I. I. (2009). *The international global navigation satellite systems service (IGS): Development and achievements.* Journal of Geodesy. https://doi.org/10.1007/s00190-008-0268-z

Bilker-Koivula, M. (2010). *Development of the Finnish Height Conversion Surface FIN2005N00.* Nordic Journal of Surveying and Real Estate Research, 2010, 76–88.

Bjelotomić, O., Bašić, T., and Markovinović, D. (2015). *Refinement of the geoid model on the islands with sparse terrestrial gravity data.* 26th IUGG General Assembly, Prag.

Bjerhammar, A. (1973). *On the Discrete Boundary Value Problem.* Proceedings of the Symposium on Earth's Gravitational Field and Secular Variations in Position, 475–488.

Blitzkow, D., Matos, A. C. O. C., Machado, W. C., Nunes, M. A., Lengruber, N. V., Xavier, E. M. L., and Fortes, L. P. S. (2016). MAPGEO2015: *The New Geoidal Undulation Model of Brazil.* Revista Brasileira de Cartografia, 68(10), 1873–1884.

Bonneville, A., Barriot, J.-P., and Bayer, R. (1988). *Evidence from Geoid Data of a Hotspot Origin for the Southern Mascarene Plateau and Mascarene Islands (Indian Ocean).* Journal of Geophysical Research, 93, 4199. https://doi.org/10.1029/JB093iB05p04199

Borge, A. (2013). *Geoid determination over Norway using global Earth gravity Models*. Published MSc Thesis of the Department of Civil and Transport Engineering, Norwegian University of Science and Technology.. https://ntnuopen.ntnu.no/ntnu-xmlui/handle/11250/232486

Bosy, J. (2014). *Global, Regional and National Geodetic Reference Frames for Geodesy and Geodynamics*. Pure and Applied Geophysics. https://doi.org/10.1007/s00024-013-0676-8

Bucha, B., Hirt, C., Meng, Y., Kuhn, M., and Rexer, M. (2019). *Residual terrain modelling (RTM) in terms of the cap-modified spectral technique: RTM from a new perspective.* Journal of Geodesy, 93. https://doi.org/10.1007/s00190-019-01303-4

Burša, M. (1971). *Single-Layer Density as Function of Stokes' Constants*. Studia Geoph. et Geod, 15, 113–123.

Catalao, J. (2008). *Um modelo de geoide para Portugal continental*. Universidade de Lisboa.

Catalao, J., and Sevilla, M. J. (2009). *Mapping the geoid for Iberia and the Macaronesian Islands using multi-sensor gravity data and the GRACE geopotential model.* Journal of Geodynamics, 48(1), 6–15. https://doi.org/10.1016/j.jog.2009.03.001

Catalao, J., Sevilla, M. J., and Koll, H. (2007). *The ICAGM07 Geoid Model for the North-East Atlantic (Iberia – Canary - Azores.* In IUGG2007 General Assembly.

Chandler, G., and Merry, C. L. (2010). *The South African Geoid 2010: SAGEOID10*. Position IT, June, 29–33.

Chen, J. Y., Li, J. C., Chao, D. B., and Ning, J. S. (2003). *Geoid determination on China sea and its merge with the geoid in China mainlandChin.* J. Geophys, 46(1), 31–35.

Chen, J. Y., and Schwarz, K. P. (1985). *Report on the International Summer School on Local Gravity Field Approximation.* Bulletin Géodésique, 59(1), 107–108. https://doi.org/10.1007/BF02519346

Claessens, S. J., Hirt, C., Amos, M. J., Featherstone, W. E., and Kirby, J. F. (2011). *The NZGEOID09 model of New Zealand.* Survey Review, 43, 2–15. https://doi.org/10.1179/003962610X12747001420780

Cole, J. (1944). *Geodesy in Egypt*. Ministry of Finance.

Colombo, O. L. (1980). *A World Vertical Network"* [Report No. 296,]. Department of Geodetic Science, The Ohio State University.

Conventions, I. E. R. S. (2010). In G. Petit and B. Luzum (Eds.), *IERS Technical Note* (Vol. 36, p. 179 ,). Verlag des BundesamtsfürKartographie und Geodäsie.

Corchete, V. (2008). *The high-resolution gravimetric geoid of North Iberia: NIBGEO*. Terra Nova, 20, 489–493. https://doi.org/10.1111/j.1365-3121.2008.00844.x

Corchete, V. (2010). *The high-resolution gravimetric geoid of Italy: ITG2009.* Journal of African Earth Sciences, 58, 580–584. https://doi.org/10.1016/j.jafrearsci.2010.05.010

Corchete, V. (2013a). *The first high-precision gravimetric geoid of Hungary: HGG2013*. https://doi.org/10.13140/RG.2.2.10552.16646.

Corchete, V. (2013b). *The first high-resolution gravimetric geoid for Ukraine: UGG2013*. https://doi.org/10.13140/RG.2.2.12649.31848.

Corchete, V., Chourak, M., and Khattach, D. (2005). *The high-resolution gravimetric geoid of Iberia: IGG2005*. Geophysical Journal International, 162, 676–684. https://doi.org/10.1111/j.1365-246X.2005.02690.x

Corchete, V., Chourak, M., Khattach, D., and Benaïm, E. H. (2007). *The high-resolution gravimetric geoid of Morocco: MORGEO*. Journal of African Earth Sciences, 48(4), 267–272. https://doi.org/10.1016/j.jafrearsci.2007.04.002

Corchete, V., Chourak, M., Khattach, D., and Benaim, E. H. (2008). *A new high-resolution gravimetric geoid for South Spain and the Gibraltar Strait area: SOSGIS*. Terra Nova, 20, 489–493.

Corchete, V., Flores, D., and Oviedo, F. (2006). *The first high-resolution gravimetric geoid for the Bolivian tableland: BOLGEO*. Physics of the Earth and Planetary Interiors, 157, 250–256. https://doi.org/10.1016/j.pepi.2006.04.004

Corchete, V., and Pacino, M. C. (2007). *The first high-resolution gravimetric geoid for Argentina: GAR*. Physics of the Earth and Planetary Interiors, 161, 177–183. https://doi.org/10.1016/j.pepi.2007.01.012

Cornero, C., Pereira, A., Sanchez, M. V., Matos, A. C. O. C. D., Blitzkow, D., and Pacino, M. C. (2018). *Modelado del geoide gravimetrico estatico para la provincia de Santa Fe, Argentina*. Geoacta, 42(2), 82–95.

Crombaghs, M., and Bruijne, A. (2004). *NLGEO2004 - Een nieuw geoide- model voor Nederland*. In Adviesdienst Geo-informatie en ICT, Report AGI-GAP-2004-25 (p. 41).

Dahl, O. C., and Forsberg, R. (1998). *Geoid models around Sognefjord using depth data*. Journal of Geodesy, 72, 547–556.

Dawod, G. (1998). *The National Gravity Standardization Network for Egypt 'ENGSN-97*. [Ph.D. dissertation].Department of Surveying Engineering, Shoubra Faculty of Engineering, Zagazig University.

Dawod, G. M. (2008). *Towards the redefinition of the Egyptian geoid: Performance analysis of recent global geoid and digital terrain models*. Journal of Spatial Science, 53(1), 31-42. https://doi.org/10.1080/14498596.2008.9635133

Dawod, G. M. (2009). *Geoid modeling in Egypt*. https://www.academia.edu/1741835/Geoid_modelling_in_Egypt

Dawod, G. M., and Hosny, M. (2017). *Towards to a Centimeter—Geoid Model for Engineering Surveying in Egypt: Status and Projected Activates.* Journal of Scientific and Engineer Research, 4(10), 312–319.

Dawod, G. M., and Ismail, S. S. (2005). *Enhancing the Integrity of the National Geodetic Data Bases in Egypt*. Proceedings of the FIG working week and GSDI-8 International Conference, Cairo, Egypt, April 16-21.

Denker, H. (2013). *Regional Gravity Field Modeling: Theory and Practical Results.* Science of Geodesy-II, apter 5, 185-291,. https://doi.org/10.1007/978-3-642-28000-9_5

Denker, H., Timmen, L., Voigt, C., Weyers, S., Peik, E., Margolis, S., Delva, P., Wolf, P., and Petit, G. (2018). *Geodetic methods to determine the relativistic redshift at the level of 10-18 in the context of international timescales – A review and practical results.* Journal of Geodesy, 92: 487-516. https://doi.org/10 1007 00190-017-1075–1.

Denker, H., and Torge, W. (1998). *The European Gravimetric Quasigeoid EGG97*. An IAG Supported Continental Enterprise.

Droscak, B. (2014). *Suradnicovy system Jednotnej trigonometrickej siete katastralnej a jeho vztahk Europskemu terestrickemu referencnemu systemu 1989.* Technicka sprava.

Duquenne. (1998). *QGF98, a new solution for the quasi-geoid in France*. Report of the Finnish Geodetic Institute, 98(4), 251–255.

Duquenne, F. (2010). *Evolution des references verticales.* Journee Geodesie.

Duquenne, H. (1997a). *Comparison between the EGM96 model and the French quasi-geoid model.* IGeS Bulletin, 6, 131–134.

Duquenne, H. (1997b). *Le modele de quasi-geoide francais QGF96 et la surface de reference d'altitude RAF96.* In Ecole Superieure des Geometres et Topographes (ESGT), F91055-Evry, and Institut Geographique National (IGN), F94160-SaintMande.

Duquenne, H. (1998). *Grille de rorrection pour effectuer du nivellement par GPS.* Revue Geometre, 6.

Duquenne, H., Everaerts, M., and Lambot, P. (2005). *Merging a gravimetric model of the geoid with GPS/levelling data: An example in Belgium.* In C. Jekeli, L. Bastos, and J. Fernandes (Eds.), Gravity, Geoid and Space Missions, IAG Symposia Series (Vol. 129, pp. 131-136,). Springer Verlag. https://doi.org/10.1007/3-540-26932-0_23

El Hassan, E. B. (2020). *Moroccan geoid determination from spatial gravity using recent GGM.* 2020 IEEE International Conference of Moroccan Geomatics (Morgeo), 1–4. https://doi.org/10.1109/Morgeo49228.2020.9121900

El shouny, A., Yakoub, N., and Hosny, M. (2017). *Evaluating the Performance of Using PPK-GPS Technique in Producing Topographic Contour Map.* Marine Geodesy, 40. https://doi.org/10.1080/01490419.2017.1321594

El-Ashquer, M., Elsaka, B., and El-Fiky, G. (2017). *EGY-HGM2016: An improved hybrid local.*

El-Fatairy, S. M. (1983). Investigation of Systems of Heights on an Earth's Model. [Ph.D. dissertation]. Geophysical Institute, Czechoslovac Acad. Sci.

Ellmann, A. (2004). *The geoid for the Baltic countries determined by the least squares modification of Stokes´formula*. http://urn.kb.se/resolve?urn=urn:nbn:se:kth:diva-3744

Ellmann, A., Märdla, S., and Oja, T. (2019). *The 5 mm geoid model for Estonia computed by the least squares modified Stokes formula.* Survey Review. https://doi.org/10.1080/00396265.2019.1583848

El-Sagheer, A. (1995). *Development of a Digital Terrain Model (DTM) for Egypt and its Application for a Gravimetric Geoid Determination* [Ph.D. dissertation]. Department of Surveying Engineering, Shoubra Faculty of Engineering, Zagazig University.

El-Shazly, A. (1995). *Towards the Redefinition of the vertical Datum of Egypt: an Analysis of Sea Surface Topography and Levelling byGPS.* [Ph.D. dissertation]. Cairo University, Cairo Egypt.

El-Tokhy, M. E. (1993). *Towards the redefinition of the Egyptian geodetic control networks: Geoid and best fitting reference ellipsoid by combination of heterogeneous data* [Ph.D. dissertation]. Ain-Shams University, Cairo, Egypt.

Erker, E., Hofmann-Wellenhof, B., Moritz, H., and Suenkel, H. (1996). *Austrian Geoid 2000.* Osterreichische Zeitschrift fuer Vermessung und Geoinformation, 84(3), 289–293.

Fairhead, J. D. (1988). *Mesozoic plate tectonic reconstructions of the central South Atlantic Ocean: The role of the West and Central African rift system.* Tectonophysics, 155(1), 181–191. https://doi.org/10.1016/0040-1951(88)90265-X

Fan, H. (1998). *On an Earth ellipsoid best-fitted to the Earth surface.* Journal of Geodesy, 72, 511–515.

Farr, T. G., and Kobrick, M. (2000). *Shuttle radar topography mission produces a wealth of data.* Eos, Transactions American Geophysical Union, 81(48), 583–585. https://doi.org/10.1029/EO081i048p00583

Fashir, H. (1991). *The gravimetric geoid of Sudan.* Journal of Geodynamics - J GEODYNAMICS, 14, 19–36. https://doi.org/10.1016/0264-3707(91)90005-Y

Fashir, H. H., and Kadir, A. M. A. (1998). *Gravity Prediction from Anomaly Degree Variances.* Buletin Geoinformasi, 2(2), 230–240.

Fashir, H., Majid, A., and Kadir, A. (1997). *The Sudanese gravimetric geoid 1998*. International Geoid Service, Bulletin, 10, 59–77.

Featherstone, W. E., Alexander, K., and Sideris, M. G. (1996). *Gravimetric Geoid Refinement Using High Resolution Gravity and Terrain Data*. Geomatics Research Australasia.

Featherstone, W. E., Evans, J. D., and Olliver, J. G. (1998). *A Meissl-modified Vaníček and Kleusberg kernel to reduce the truncation error in gravimetric geoid computations.* Journal of Geodesy, 72, 154–160.

Featherstone, W. E., Kirby, J. F., Hirt, C., Filmer, M. S., Claessens, S. J., Brown, N. J., Hu, G., and Johnston, G. M. (2010). *The AUSGeoid09 model of the Australian Height Datum.* Journal of Geodesy, 85(3), 133–150. https://doi.org/10.1007/s00190-010-0422-2

Featherstone, W. E., Kirby, J. F., Kearsley, A. H. W., Gilliland, J. R., Johnston, G. M., Steed, J., Forsberg, R., and Sideris, M. G. (2001). *The AUSGeoid98 geoid model of Australia: Data treatment, computations and comparisons with GPS-levelling data.* Journal of Geodesy, 75, 313–330. https://doi.org/10.1007/s001900100177

Featherstone, W. E., and Kuhn, M. (2006). *Height systems and vertical datums", a review in the Australian context.* Journal of Spatial Science, 51(1), 21–42.

Featherstone, W. E., McCubbine, J. C., Brown, N. J., Claessens, S. J., Filmer, M. S., and Kirby, J. F. (2018). *The first Australian gravimetric quasigeoid model with location-specific uncertainty estimates.* Journal of Geodesy, 92(2), 149–168. https://doi.org/10.1007/s00190-017-1053-7

Featherstone, W. E., and Olliver, J. G. (1993). *The gravimetric geoid of the British Isles computed using a modified Stokes integral*. In R. Forsberg and H. Denker (Eds.), The European Geoid Determination (pp. 19–25). Kort-og Martikelstyrelsen.

Featherstone, W. E., and Olliver, J. G. (1994). *A New Gravimetric Determination of the Geoid of the British Isles.* Survey Review, 32, 254.

Featherstone, W. E., and Sideris, M. G. (1998). *Modified Kernels in Spectral Geoid Determination: First Results from Western Australia.* In R. Forsberg, M. Feissl, and R. Dietrich (Eds.), Geodesy on move: Gravity, Geoid, Geodynamics and Antarctica (pp. 188–193). Springer.

Fecher, T., Pail, R., Gruber, T., and GOCO Project Team. (2016). *The combined gravity field model GOCO05c.* EPSC2016-7696.

Fischer, I., and Slutsky, M. (1967). *A preliminary geoid chart of Australia.* Australian Surveyor, 21(8), 327–332. https://doi.org/10.1080/00050326.1967.10440069

Forsberg, R. (1984). *A study of terrain reductions, density anomalies and geophysical inversion methods in gravity field modelling.* Ohio State Univ Columbus Dept of Geodetic Science and Surveying, OSU/DGSS-355.

Forsberg, R. (2016a). *GGEOID16 - Opdateret geoide for Grønland—Tilpasset havniveau i Nuuk*. Report of National Space Institute at the Technical University of Denmark.

Forsberg, R. (2016b). *Ny dansk geoide tilpasset revideret GPS og DVR90 – DKGEOID12*. Report of National Space Institute at the Technical University of Denmark.

Forsberg, R., Kaminskis, J., and Solheim, D. (1997). *Geoid for the Nordic and Baltic Region from Gravimetry and Satellite Altimetry*. In J. Segawa, H. Fujimoto, and S. Okubo (Eds.), Gravity, Geoid and Marine geodesy, IAG Symposia Series (Vol. 117, pp. 540-547,). Springer Verlag. https://doi.org/10.1007/978-3-662-03482-8_72

Forsberg, R., Strykowski, G., and Loon, J. (2002). *Ny GPS-tilpasset geoid for Greenland, GEOID2000*. IGC Thessaloniki.

Forsberg, R., Strykowski, G., and Solheim, D. (2004). *NKG-2004 geoid of the Nordic and Baltic area.* Proceedings on CD-ROM of the IAG International Symposium "Gravity, Geoid and Satellite Gravity Missions."

Forsberg, R., and Tscherning, C. C. (1981). *The use of height data in gravity field approximation by collocation.* Journal of Geophysical Research: Solid Earth, 86(B9), 7843–7854. https://doi.org/10.1029/JB086iB09p07843

Forsberg, R., and Tscherning, C. C. (1997). *Topographic Effects in Gravity Field Modelling for BVP". In F. Sanso and R. Rummel (Eds.), Geodetic Boundary Value Problems in View of the Centimeter Geoid.* Lecture Notes in Earth Sciences 65, 241–272.

Fukuda, Y., Kuroda, J., Takabatake, Y., Itoh, J., and Murakami, M. (1997). *Improvement of JGEOID93 by the geoidal heights derived from GPS/leveling survey.* In J. Segawa, H. Fujimoto, and S. Okubo (Eds.), Gravity, Geoid and Marine geodesy, IAG Symposia Series 117, 589-596. Springer Verlag. https://doi.org/10.1007/978-3-662-03482-8_78

Gad, M., Odalovic, O., and Naod, S. (2020). *Possibility to determine highly precise geoid for Egypt territory. Geodetski Vestnik, 64*, 578. https://doi.org/10.15292/geodetski-vestnik.2020.04.578-593

Geodesy and Cartography. (2021). *Publikacja nowego modelu quasi-geoidy* . In Polish.

Georgopoulos, G. D., Telioni, E. C. (2015). *Determination of local geoid model in Attica Basin Greece.* Survey Review, 47(341), 109–114. https://doi.org/10.1179/1752270614Y.0000000096

Gilardoni, M., Reguzzoni, M., and Sampietro, D. (2013). *A least-squares collocation procedure to merge local geoids with the aid of satellite-only gravity models: The Italian/Swiss geoids case study.* Bollettino Di Geofisica Teorica Ed Applicata, 54(4), 303–319.

Godah, W., and Krynski, J. (2014). *The Sudanese gravimetric geoid: SUD-GM2014* (1.0) [Data set]. GFZ Data Services. https://doi.org/10.5880/ISG.2014.001

Greaves, M., Downie, P., and Fitzpatrick, K. (2016). OSGM15 and OSTN15: *Updated transformations for UK and Ireland.* Geomatics World, 18–21.

Grigoriadis, V. N., and Vergos, G. S. (2020). *The AUTh geoid based on 1D FFT with Wong-Gore modification of the Stokes kernel for the Colorado Experiment: ColFFTWG2020. V. 1.0*. GFZ Data Services. https://doi.org/10.5880/isg.2020.004

Groten, E. (1981). Local and Global Gravity Field Representation". Reviews of Geophysics and Space Physics, 19 (2), 407–414.

Groten, E., and Roehrich, S. (1989). *Accuracy estimates of geoid computation and related quantities for GPS work across the Strait of Gibraltar*. In E. B. SCEG (Ed.), Workshop on Geodesy in the Strait of Gibraltar 36–45.

Gruber, T., Bode, A., Reigber, C., and Schwintzer, P. (1997). *D-PAF Global Earth Gravity Models Based on ERS"*. http://www.gfz-potsdam.de/pb1/pg3).

Gysen. V., HG., and Merry, C. L. (1987). *The gravity field in southern Africa.* University of Cape Town Department of Surveying Technical Report TR-3.

Hastings, D. A., and Dunbar, P. K. (1998). *Development and assessment of the global land one-km base elevation digital elevation model (globe).* D. Fritsch, M. Englich & M. Sester, eds, 'IAPRS', Vol. 32/4, ISPRS Commission IV Symposium on GIS - Between Visions and Applications,Stuttgart, Germany.

Hein, G. W., Leick, A., and Lambert, S. (1989). *Integrated Processing of GPS and Gravity Data*. Journal of Surveying Engineering, 115(1).

Heiskanen, W. A., and Moritz, H. (1967). *Physical Geodesy*. Freeman.

Higgins, M. B., Forsberg, R., and Kearsley, A. H. W. (1997). *The Effects of Varying Cap Sizes on Geoid Computations: Experiences with FFT and Ring Integration*. In IAG Scientific Assembly, Rio de Janeiro.

Higgins, M. B., Pearse, M. B., and Kearsley, A. H. W. (1996). *Using Digital Elevation Models in the Computation of Geoid Heights.* Geomatics Research Australasia, 65 December, 59–74.

Hirt, C., Yang, M., Kuhn, M., Bucha, B., Kurzmann, A., and Pail, R. (2019). *SRTM2gravity: An ultrahigh resolution global model of gravimetric terrain corrections.* Geophysical Research Letters, 46(9), 4618–4627. https://doi.org/10.1029/2019GL082521

Hirvonen, R. A. (1960). *New Theory of the Gravimetric Geodesy.* Geologica –Geographica, 56.

Hobson, E. W. (1931). *The Theory of Spherical and Ellipsoidal Harmonics"*. Cambridge University Press, UK.

Hotine, M. (1969). *Mathematical Geodesy"*. U.S. Dep. Of Commerce.

Huang, J., and Veronneau, M. (2013). *Canadian gravimetric geoid model 2010.* Journal of Geodesy, 87(8), 771–790. https://doi.org/10.1007/s00190-013-0645-0

Huang, J., and Véronneau, M. (2016). *The Canadian Geodetic Vertical Datum of 2013 (CGVD2013).* Geomatica, 70(1), 9–19. https://doi.org/10.5623/cig2016-101

Hwang, C. (1998). *Inverse Vening Meinesz formula and deflection geoid formula: Applications to the predictions of gravity and geoid over the South China Sea*. Journal of Geodesy, 72, 304–312.

Hwang, C. (2001). *Gravity recovery using COSMIC GPS data: Application of orbital perturbation theory*. Journal of Geodesy, 75, 117–136.

I.G.N. (1998). *Geoide Geometrique Francais - GGF97.* Notes Techniques. Institut Geographique National, Service de Geodesie et Nivellement.

I.G.N. (2010). *Descriptifs quasi-geoides et grilles de conversion altimetrique sur la France metropolitaine.* In Laboratoire de Recherche en Geodesie, Service de Geodesie et Nivellement.

I.G.N. (2018). *Comment obtenir des altitudes NGF – IGN69 ou IGN78 à partir de levés GPS.* In Laboratoire de Recherche en Geodesie, Service de Geodesie et de.

Ihde, J., Sánche, L., Barzaghi, R., Drewes, H., Förste, C., Gruber, T., Liebsch, G., Marti, U., Pail, R., Sideris, M. (2017). *Definition and Proposed Realization of the International Height Reference System (IHRS).* Surveys in Geophysics, 38(3), 549-570. https://doi.org/10.1007/s10712-017-9409-3

Iliffe, J. C., Ziebart, M., Cross, P. A., Forsberg, R., Strykowski, G., and Tscherning, C. C. (2003). OSGM02: *A new model for converting GPS-derived heights to local height datums in Great Britain and Ireland. Survey Review, 37*(290), 276–293. https://doi.org/10.1179/sre.2003.37.290.276

Işık, M. S., Erol, B., Erol, S., and Sakil, F. F. (2021). *High-resolution geoid modeling using Least Squares modification of Stokes and Hotine formulas in Colorado.* Journal of Geodesy, 95, 49. https://doi.org/10.1007/s00190-021-01501-z

Ismail, Z. (2016). *Détermination de l'exactitude d'un géoïde gravimétrique* . [Ph.D. dissertation]. at PSL Research University.

Jekeli, C. (2000). *Inertial navigation systems with geodetic application"*. walter de gruyter.

Jiang, T., Dang, Y., and Zhang, C. (2020). *Gravimetric geoid modeling from the combination of satellite gravity model, terrestrial and airborne gravity data: A case study in the mountainous area, Colorado.* Earth Planets Space, 72, 189. https://doi.org/10.1186/s40623-020-01287-y

Kadaj, R., and Świętoń, T. (2016). *Theoretical and applied research in the field of higher geodesy conducted in Rzeszow*. Reports on Geodesy and Geoinformatics, 100(2016), 79–100. https://doi.org/10.1515/rgg-2016-0008

Kadir, M. A., Fashir, H. H., and Omar, K. (1999). *A regional gravimetric co-geoid over South East Asia.* Geomatics Research Australasia, 71, 37–56.

Kamguia, J., Tabod, C. T., Nouayou, R., Tadjou, J. M., Manguelle-Dicoum, E., and Kande, H. L. (2007). *The Local Geoid Model of Cameroon: CGM05.* Nordic Journal of Surveying and Real Estate Research, 4(2), 7–23.

Kaminskis, J., and Forsberg, R. (1996). *A new detailed geoid for Latvia.* In J. Segawa, H. Fujimoto, and S. Okubo (Eds.), Gravity, Geoid and Marine geodesy, IAG Symposia Series, 117, 621-628. Springer Verlag. https://doi.org/10.1007/978-3-662-03482-8_82

Kearsley, A. H. W., and Ahmad, Z. (1996). *Report on the Geoid Computation for Papua New Guinea.* Australian Component of the Land Management Project for Papua New Guinea.

Kearsley, A. H. W., Forsberg, R., Olesen, A., Bastos, L., Hehl, K., Meyer, U., and Gidskehaug, A. (1998). *Airborne gravimetry used in precise geoid computations by ring integration.* Journal of Geodesy, 72, 600–605.

Kirby, J. F., and Featherstone, W. E. (1997). *A Study of Zero- and First-Degree Terms in Geopotential Models Over Australia.* Geomatics Research Australasia, 66, June, 93–108.

Kirby, J. F., Featherstone, W. E., and Kearsley, A. H. W. (1997). *Geoid Computations Using Ring Integration: Gridded Vs. Point Data.* Geomatics Research Australasia, 67 December, 33–46.

Kostelecky, J., Kostelecky, J., Jr., Pesek, I., Simek, J., Svabensky, O., Weigel, J., and Zeman, A. (2004). *Quasigeoids for the Territory of the Czech Republic.* Studia Geophysica et Geodaetica, 48(3), 503–518. https://doi.org/10.1023/B:SGEG.0000037469.70838.39

Kraiger, G. (1988). *Influence of the curvature parameter on least-squares prediction.* manuscripta geodetica, 13, 164–171.

Krarup, T. (1969). *A contribution to the mathematical foundation of physical geodesy*. Publ. 44, 80 pp., Dan. Geod. Inst.,' Copenhagen

Kucher, O., Stophai, U., and Renkevich, O. (2005). *Construction of the quasi geoid model on the territory of Republic of Moldova.* Internal Report of Ukrainian Research Institute of Geodesy and Cartography.

Kuczynska-Siehien, J., Lyszkowicz, A., and Birylo, M. (2016). *Geoid determination for the area of Poland by the least squares modification of Stokes' formula.* Acta Geodynamica et Geomaterialia, 13(1), 19–26. https://doi.org/10.13168/AGG.2015.0041

Kuroishi, Y. (1995). *Precise Gravimetric Determination of Geoid in the Vicinity of Japan.* Bulletin of the Geographical Survey Institute, 41, 1–93.

Kuroishi, Y. (2001). *An improved gravimetric geoid for Japan, JGEOID98, and relationships to marine gravity data.* Journal of Geodesy, 74(11), 745–755. https://doi.org/10.1007/s001900000129

Kuroishi, Y. (2009). *Improved geoid model determination for Japan from GRACE and a regional gravity field model.* Earth, Planets and Space, 61(7), 807–813. https://doi.org/10.1186/BF03353191

Kuroishi, Y., Ando, H., and Fukuda, Y. (2002). *A new hybrid geoid model for Japan, GSIGEO2000.* Journal of Geodesy, 76, 428–436. https://doi.org/10.1007/s00190-002-0266-5

Kuroishi, Y., and Keller, W. (2005). *Wavelet approach to improvement of gravity field-geoid modeling for Japan*. Journal of Geophysical Research, 110, 03402. https://doi.org/10.1029/2004JB003371

Lachapelle, G., and Tscherning, C. C. (1978). *Use of Collocation for Predicting Geoid Undulations and Related Quantities over Large Areas.* International Symposium on the Geoid in Europe and Mediterranean Area, 25–29.

Lacy, M. C., Rodriguez-Caderot, G., Marin, E., Ruíz, A., Borque, M. J., Gil, A. J., and Biagi, L. (2001). *A gravimetric geoid computation and comparison with GPS results in Northern Andalusia (Spain).* Studia Geophysica et Geodaetica, 45(1), 55–66. https://doi.org/10.1023/A:1021702514130

L'Ecu, F. (2017). *Calcul du quasi-géoïde QGF16 et de la grille de conversion altimétrique RAF16 état d'avancement et perspectives.* Revue XYZ, 150, 49–51.

Lehmann, R. (1999). *Boundary-value problems in the complex world of geodetic measurements*. Journal of Geodesy, 73, 491–500.

Lehmann, R. (2000). *Altimetry-gravimetry problems with free vertical datum.* Journal of Geodesy, 74, 327–334.

Lehmann, R., and Klees, R. (1999). Numerical solution of geodetic boundary value problems using a global reference field. Journal of Geodesy, 73, 543–554.

Lemoine, F. G., Smith, D. E., Kunz, L., Smith, R., Pavlis, E. C., Pavlis, N. K., Klosko, S. M., Chinn, D. S., Torrence, M. H., Williamson, R. G., Cox, C. M., Rachlin, K. E., Wang, Y. M., Kenyon, S. C., Salman, R., Trimmer, R., Rapp, R. H., and Nerem, R. S. (1996). *The Development of the NASA GSFC and NIMA Joint Geopotential Model*. Proceedings Paper for the International Symposium on Gravity, Geoid and Marine Geodesy (GRAGEOMAR) 1996.

Li, X., Ahlgren, K., Hardy, R., Krcmaric, J., and Wang, Y. M. (2019). *The Development and Evaluation of the Experimental Gravimetric Geoid Model 2019* [Technical Report,]. NOAA/National Geodetic Survey.

Liang, W., Li, J., Xu, X., Zhang, S., and Zhao, Y. (2020). *A High-Resolution Earth's Gravity Field Model SGG-UGM-2 from GOCE, GRACE, Satellite Altimetry, and EGM2008.* Engineering, 6(8), 860–878. https://doi.org/10.1016/j.eng.2020.05.008

Lobianco, M. C. B., Blitzkow, D., and Matos, A. C. O. C. (2004). *The Brazilian gravimetric geoid: MAPGEO2004. V. 1.0. GFZ Data Services*. https://doi.org/10.5880/isg.2004.002

Lyszkowicz, A. (2010*). QuasiGeoid for the Area of Poland computed by least squares collocation.* Technical Sciences, 13, 147–164.

Lyszkowicz, A., Birylo, M., and Becek, K. (2014). *A new geoid for Brunei Darussalam by the collocation method.* Geodesy and Cartography, 63(2), 183–198. https://doi.org/10.2478/geocart-2014-0013

Łyszkowicz, A., and Wahiba, A. A. (1998). *The Gravimetric Geoid for Libya. In R. Forsberg, M. Feissel, and R. Dietrich (Eds.),* Geodesy on the Move (pp. 275–280). Springer. https://doi.org/10.1007/978-3-642-72245-5_40

Mammar, G., Ahmed Daho, S. A. B., and Messaoud, H. (2019). *Description and validation of the new data to determine a geoid model in Algeria.* Energy Procedia, 157, 254–260. https://doi.org/10.1016/j.egypro.2018.11.188

Manisa, M., Das, R., Segobye, M., and Maphale, L. (2016). *Developing local geoid model to assess accuracy of orthometric heights from GPS-based ellipsoidal heights in Botswana.* Spatial Information Research. https://doi.org/10.1007/s41324-016-0057-3

Marchenko, A. N., Abrikosov, O. A., and Romanishin, P. O. (1995). *Improvement of the gravimetric geoid in the Ukraine area using absolute gravity data.* Reports of the Finnish Geodetic Institute, 95(7), 19–22.

Marchenko, A. N., and Kucher, O. (2008). *On the quasigeoid solutions for the Ukraine and Moldova area.* Proceedings of the EUREF Symposium 2008.

Marchenko, A. N., Kucher, O., and Renkevych, O. (2007). *Determination of the UQG2006 quasigeoid in the Ukraine area.* Bulletin of Geodesy and Cartography, 2, 3–13.

Marchenko, A. N., Kucher, O. V., and Marchenko, D. A. (2015). *Regional quasigeoid solutions for the Ukraine area*. Geodynamics, 2(16), 7–14. https://doi.org/10.23939/jgd2015.02.007

Marchenko, A. N., and Monin, I. F. (2004). *Regional quasigeoid solution for the Moldova area from GPS/levelling data*. Mitteilungen des Bundesamtes fur Kartographie und Geodasie, Band 35, Frankfurtn am Main (pp. 297–301).

Marchenko, A. N., Tretyak, K., Kulchicky, A., and Tretyak, N. P. (2012). *The study of the Earth's Gravity Field, Sea Surface Topography and the Crustal movements in the Antarctic area*. Lviv Polytechnic National University.

Marsh, J. G., Lerch, F. J., Klosko, S. M., Engelis, T. L., Patel, G. B., Robbins, J. W., and Williamson, R. G. (1989). *Geoid Determination Over Basin-Wide Scales Using a Combination of Satellite Tracking, Surface Gravity and Altimeter Observations*. International Symposium on Sea Surface Topography and the Geoid, 10–11.

Marti, U. (2007). *Comparison of high precision geoid models in Switzerland. In P. Tregonig and C. Rizos (Eds.), Dynamic Planet: Monitoring and Understanding a Dynamic Planet with Geodetic and Oceanographic Tools.* IAG Symposia Series, Springer Verlag, 130, 377-382.

Marti, U., and Schlatter, A. (2002). *The new Height System in Switzerland.* IAG Proceedings of the Symposium on Vertical Reference Systems.

Martinec, Z. (1998). *Construction of Green's function for the Stokes boundary-value problem with ellipsoidal corrections in the boundary condition.* Journal of Geodesy, 72, 460–472.

Martinec, Z., and Grafarend, E. W. (1997). *Solution to the Stokes Boundary-value Problem on an Ellipsoid of Revolution.* Studia Geoph. et Geod, 41, 103–129.

Matos, A. C. O. C., Blitzkow, D., Guimarães, G. N., Lobianco, M. C. B., and Costa, S. M. A. (2012). *Validação do MAPGEO2010 e comparação com modelos do geopotencial recentes.* Boletim de Ciencias Geodesicas, 18(1), 101–122. https://doi.org/10.1590/S1982-21702012000100006

Matsuo, K., and Forsberg, R. (2019). *Gravimetric geoid computation over Colorado based on Remove-Compute-Restore Stokes-Helmert scheme. In 27th International Union of Geodesy and Geophysics (IUGG) General Assembly.* *https://doi.org/10.5880/isg.2019.011*

McCubbine, J. C., Amos, M. J., F.C., F. C. T., Smith, E., Winefied, R., Stagpoole, V., and Featherstone, W. E. (2018). *The New Zealand gravimetric quasigeoid model 2017 that incorporates nationwide airborne gravimetry.* Journal of Geodesy, 92(8). https://doi.org/10.1007/s00190-017-1103-1

Mccubbine, J., Featherstone, W., and Brown, N. (2021). *Australian quasigeoid modelling: Review, current status and future plans.* Terrestrial Atmospheric and Oceanic Sciences, 32. https://doi.org/10.3319/TAO.2021.08.10.01

Medvedev, P., and Nepoklonov, V. (2003). RGQG-2003: *The new geoid and gravity field model for territory of Russia and sea areas around Russia.* In IUGG 2003 (p. 169). Abstracts Week B.

Meissl, P. (1971). *A study of covariance functions related to the Earth's disturbing potential*. Ohio State University Research Foundation.

Merry, C. L. (2003). *The African geoid project and its relevance to the unification of African vertical reference frames.* Proceedings of the 2nd FIG Regional Conference.

Merry, C. L., Blitzkow, D., Abd-Elmotaal, H., Fashir, H. H., John, S., Podmore, F., and Fairhead, J. D. (2005). *A Preliminary Geoid Model for Africa.* In F. Sansò (Ed.), A Window on the Future of Geodesy 374–379. Springer. https://doi.org/10.1007/3-540-27432-4_64

Milbert, D. G. (1993). GEOID93: *A high-resolution geoid for the United States, GandGS Update.* Coast and Geodetic Survey, 5(3).

Militar, S. G. (2007). *Calculo de un nuevo modelo geoidal para Uruguay (UruGeoide-2007).* Report of Servicio Geografico Militar.

Miyahara, B., Kodama, T., and Kuroishi, Y. (2014). *Development of new hybrid geoid model for Japan, (GSIGEO2011).* Bulletin of the Geographical Information Authority of Japan, 62, 11–20.

Molodensky, M. S. (1958). *New methods of studying the figure of the earth.* Bulletin Géodésique, 50(1), 17–21.

Moritz, H. (1972). *Determination of the gravity field by collocation.* International Symposium on Earth Gravity Models and Related Problems. St, 16–18.

Moritz, H. (1974). *The method of least-squares collocation in geometrical geodesy.* ANNO XXXIII – BOLLETTINO DI GEODESIA E SCIENZE AFFINI: 2, 193–207.

Moritz, H. (1978). *Least-squares collocation*. https://doi.org/10.1029/RG016I003P00421

Moritz, H. (1980). *Advanced Physical Geodesy*. Herbert Wichmann.

Moritz, H. (1989). *Advanced physical geodesy*. Wichmann.

Moritz, H. (1990a). *The Figure of the Earth*. Herbert Wichmann Verlag, GmbH.

Nakagawa, H., Wada, K., Kikkawa, T., Shimo, H., Andou, H., Kuroishi, Y., Hatanaka, Y., Shigematsu, H., Tanaka, K., and Fukuda, Y. (2003). *Development of a New Japanese Geoid Model, (GSIGEO2000).* Bulletin of the Geographical Survey Institute, 49, 1–10.

Naranjo, D. A. (2004). *Nuevo modelo geoidal mexicano GGM04.* Revista Cartográfica, 78(79), 53–58.

Naranjo, D. A., Abundes, R. M., and Gaytan, M. S. (2006). *Datos involucrados en el desarrollo del GGM05.* In Report of the Instituto Nacional de Estradistica y Geografia (INEGI).

Naranjo, D. A., Abundes, R. M., and Gaytan, M. S. (2007). *Datos involucrados en el desarrollo del GGM06*. In Report of the Instituto Nacional de Estradistica y Geografia (INEGI).

Nassar, M. M. (1976). *The Earth gravity field.* In Lecture notes, In the courseof Physical Geodesy laboratory assignments, given at the Department ofSurveying Engineering. University of New Brunswick, N.B., Canada..

Nassar, M. M., Hanafy, M. S., and El-Tokhey, M. (1993). *The 1993 Ain Shams University (ASU93) Geoid Solutions for Egypt*. Al-Azhar Engineering 3rd International Conference, Faculty of Engineering.

Nsombo, P. (1998). *Preliminary geoid over Zambia.* Journal of Geodesy, 72, 144–153.

Nyamangunda, P. (1997). *Towards a 10cm local gravimetric geoid for Zimbabwe using FFT* [Doctoral, UCL (University College London),]. https://discovery.ucl.ac.uk/id/eprint/10101424/

Odalović, O. (2000). *Determination of high-resolution local geoid using the model of integral geodesy* [Master's thesis,]. Faculty of Civil Engineering, University of Belgrade.

Odalović, O. (2006). *Geoid determination in Serbia.* Adria Microplate GPS Geodesy, Tectonics and Hazards, 61, 237–246.

Odera, A., Musyoka, S. M., and Gachari, M. K. (2014). *Practical application of the geometric geoid for heighting over Nairobi County and its Environs.* Journal of Agriculture, Science and Technology, 16(2), 175–185.

Odumosu, J. O., Kelly, K. M., Omogunloye, O. G., Adejare, Q. A., Adeleke, O. O., and Olaniyi, A. M. (2016). *Empirical geoid modelling using classical gravimetric method.* Proceedings of the FIG Working Week.

Olliver, J. G. (1980). *The gravimetric geoid of Great Britain and Ireland.* Geophysical Journal International, 63(1), 253–270. https://doi.org/10.1111/j.1365-246X.1980.tb02619.x

Olliver, J. G. (2007). *The Gravimetric geoid of Tanzania.* Survey Review, 39(305), 212–225. https://doi.org/10.1179/003962607X165186

Olujimi, O., Ono, M. N., and Sylvester Okiemute, E. (2019). *Practical Local Geoid Modelling of Benin City, Nigeria from Gravimetric Observations Using the Modified Stokes Integral.* International Journal of Advanced Engineering, Management and Science, 5, 608–617. https://doi.org/10.22161/ijaems.512.1

Otsubo, T., Matsuo, K., Aoyama, Y., Yamamoto, K., Hobiger, T., Kubo-oka, T., and Sekido, M. (2016). *Effective expansion of satellite laser ranging network to improve global geodetic parameters.* Earth, Planets and Space. https://doi.org/10.1186/s40623-016-0447-8.

Pail, R., Kühtreiber, N., Wiesenhofer, B., Hofmann-Wellenhof, B., Ullrich, C., Höggerl, N., Ruess, D., and Imrek, E. (2009). *The official Austrian geoid solution 2008: Data, Method and Results.* In Poster presentation at EGU General Assembly 2009.

Pavlis, N. K., Holmes, S. A., Kenyon, S. C., and Factor, J. K. (2012). *The development and evaluation of the Earth Gravitational Model 2008 (EGM2008).* Journal of Geophysical Research: Solid Earth, 117(B4). https://doi.org/10.1029/2011JB008916

Peneva, E. (2001). *Gravimetric method for determination of the geoid of the territory of Bulgaria* [Ph.D. Dissertiation,]. University of Architecture, Civil Engineering and Geodesy.

Petrović, S. (1996). *Determination of the potential of homogeneous polyhedral bodies using line integrals.* Journal of Geodesy, 71, 44–52. https://doi.org/10.1007/s001900050074

Piña, W. H. S., Gemael, C., and Sá, N. C. (2001). *URUGEOIDE 2000 project: A gravimetric geoid for Uruguay.* IGeS Bulletin, 11, 11–20.

Piñón, D. A., Zhang, K., Wu, S., and Cimbaro, S. R. (2016). *A New Argentinean Gravimetric Geoid Model: GEOIDEAR. In J. T. Freymueller and L. Sánchez (Eds.), International Symposium on Earth and Environmental Sciences for Future Generations, IAG Symposia Series 147, 53-62. Springer Verlag. https://doi.org/10.1007/1345_2017_267*

Pribicevic, B. (2000). *Uporaba geološko-geofizicnih in geodetskih baz podatkov za racunanje ploskve geoida Republike Slovenije* [Ph.D. dissertiation,]. Faculty of Civil Engineering and Geodesy, University of Ljubljana, Slovenia.

Forsberg, R. Tscherning, CC . (1997). *Topographic effects in gravity field modelling for BVP*. In: Sansò F, Rummel R (eds). Geodetic boundary-value problems in view of the one centimeter geoid. Lecture notes in earth sciences, Springer, Berlin Heidelberg New York, 65, 241–272.

Rabah, M., and Kaloop, M. (2013). *The use of minimum curvature surface technique in geoid computation processing of Egypt.* Arab J Geosci, 6, 1263–1272. https://doi.org/10.1007/s12517-011-0418-0

Ramouz, S., Afrasteh, Y., Reguzzoni, M., and Safari, A. (2020). Assessment of local covariance estimation through Least Squares Collocation over Iran. Advances in Geosciences, 50, 65–75. https://doi.org/10.5194/adgeo-50-65-2020

Ramouz, S., Afrasteh, Y., Reguzzoni, M., Safari, A., and Saadat, A. (2019). *IRG2018: A regional geoid model in Iran using Least Squares Collocation.* Studia Geophysica et Geodaetica, 63(2), 191–214. https://doi.org/10.1007/s11200-018-0116-4

Ramouz, S., and Safari, A. (2020). *Assessment of the improved covariance in local geoid modeling using Least Squares Collocation - Case study: Tehran Province.* Journal of the Earth and Space Physics, 46(3), 517–535. https://doi.org/10.22059/jesphys.2020.303845.1007221

Rapp, R. H. (1972a). *Geopotential Coefficient Behavior to High Degree and Geoid Information by Wavelength.* Report No, 180, Department of Geodetic Science, The Ohio State University

Rapp, R. H. (1972b). *Improved Models for Anomaly Computations from Potential Coefficients*. Report No, 181, Department of Geodetic Science, The Ohio State University

Rapp, R. H. (1973). *Accuracy of Geoid Undulation Computations.* Journal of Geophysical Research, 78(32), 7589–7595.

Rapp, R. H. (1977). *The relationship between mean anomaly block sizes and spherical harmonic representations.* Journal of Geophysical Research, 82(33), 5360–5364.

Rapp, R. H. (1979). *Global Anomaly and Undulation Recovery Using GEOS-3 Altimeter Data"* [Report No. 285,]. Department of Geodetic Science, The Ohio State University.

Rapp, R. H. (1982). *Aspects of Geoid Definition and Determination.* Proceedings of the General Meeting of the IAG.

Rapp, R. H. (1997). *Use of potential coefficient models for geoid undulation determinations using a spherical harmonic representation of the height anomaly/geoid undulation difference.* Journal of Geodesy, 71(5), 282–289. https://doi.org/10.1007/s001900050096

Roman, D. R., Wang, Y. M., Henning, W., and Hamilton, J. (2004). *Assessment of the New National Geoid Height Model, GEOID03.* Surveying and Land Information Science, 64(3), 153–162.

Roman, D. R., Wang, Y. M., Saleh, J., and Li, X. (2009). *A Gravimetric Geoid Model for the United States: The Development and Evaluation of USGG2009* [Technical Report,]. NOAA/National Geodetic Survey.

Rülke, A., Liebsch, G., Schäfer, U., Schirmer, U., and Ihde, J. (2012). *Geoid determination in Central Europe based on terrestrial data and GOCE observations.* EGU General Assembly.

Saad, A. (1993). *Towards the redefinition of the Egyptian vertical control network* [Ph.D. Dissertation]. Shoubra Faculty of Engineering, Zagazig University, Cairo, Egypt.

Saad, A., and Dawod, G. (2002) *A precise integrated GPS/gravity geoidmodel for Egypt.* Civil Engineering Research Magazine (CERM),Al-Azhar University, 24(1), 391-405.

Saadat, A., Safari, A., and Needell, D. (2018). *IRG2016: RBF-based regional geoid model of Iran.* Studia Geophysica et Geodaetica, 62(3), 380–407. https://doi.org/10.1007/s11200-016-0679-x

Saadat, S. A. (2016). *Regional gravity field modeling combining terrestrial and satellite gradiometry data based on radial basis functions* [Ph.D. Dissertation,]. University of Tehran.

Saka, S. (2019). *Determination of an improved Geoid Model over Zambia* [Ph.D. Dissertation]. University of Zambia]. http://dspace.unza.zm/handle/123456789/6528

Sánchez, L. (2003). *Determinación de la superficie vertical de referencia para Colombia.* In Thesis at Technische Universität Dresden, Germany (in Spanish and in German).

Sansò, F., and Sideris, M. G. (2013). *Geoid Determination: Theory and methods*. Springer-Verlag. https://doi.org/10.1007/978-3-540-74700-0.

Schwabe, J., Liebsch, G., and Schirmer, U. (2016). *Refined computation strategies for the new German Combined Quasigeoid GCG2016.* Symposium on Geoid, Gravity and Height Systems (GGHS2016), 19-23 September 2016, Thessaloniki, Greece.

Schwarz, K. P., and Lachapelle, G. (1980). *Local characteristics of the gravity anomaly covariance function.* Bulletin Geodesique, 54, 21–36. https://doi.org/10.1007/BF02521093

Schwarz, K. P., Sideris, M. G., and Forsberg, R. (1990). *The use of FFT techniques in physical geodesy.* Geophysical Journal International, 100(3), 485–514. https://doi.org/10.1111/j.1365-246X.1990.tb00701.x

Sevilla, M. J. (1995). *A new gravimetric geoid in the Iberian Peninsula.* BGI Bull, 4(77), 163–180.

Sevilla, M. J. (1997). *A high-resolution gravimetric geoid in the Strait of Gibraltar*. J. Geodesy, 7(1), 402–410.

Sevilla, M. J. (2006). *IBERGEO 2006: Nuevo Geoide centimetrico de la Peninsula Iberica.* In Topografia y cartografia: Revista del Ilustre Colegio Oficial de Ingenieros Tecnicos en Topografia, 23(135), 3–11.

Shaker, A. (1982). *Three-Dimensional Adjustment and Simulation of the Egyptian Geodetic Network.* [Ph.D. Dissertation,]. Technische Universität Graz.

Shen, W., and Han, J. (2013). *Improved Geoid Determination Based on the Shallow-Layer Method: A Case Study Using EGM08 and CRUST2.0 in the Xinjiang and Tibetan Regions.* Terrestrial, Atmospheric and Oceanic Sciences, 24(4), 591–604. https://doi.org/10.3319/TAO.2012.11.12.01(TibXS)

Shoganbekova, D., Fan, H., and Pentayev, T. (2015). *Gravimetric geoid model over Kazakhstan.* Proceedings of the 15th International Multidisciplinary Scientific GeoConference Surveying Geology and Mining Ecology Management (SGEM, 2(2), 283–290. https://doi.org/10.5593/SGEM2015/B22/S9.035

Sigurdsson, T., and Valsson, G. (2014). *National Report from Iceland.* In 17th NKG General Assembly.

Sjöberg, L. E. (2003). *A general model for modifying Stokes' formula and its least-squares solution.* Journal of Geodesy, 77(7), 459–464. https://doi.org/10.1007/s00190-003-0346-1

Skiba, Y. (2017). *Mathematical Problems of the Dynamics of Incompressible Fluid on a Rotating Sphere.* Springer International Publishing AG. Cham, Switzerland, 239. https://doi.org/10.1007/978-3-319-65412-6

Slobbe, C., Klees, R., Farahani, H. H., Huisman, L., Alberts, B., Voet, P., and Doncker, F. D. (2018). *The Belgian hybrid quasi-geoid.* HBG18. V. 1.0. GFZ Data Services. https://doi.org/10.5880/isg.2018.003

Slobbe, C., Klees, R., Farahani, H. H., Huisman, L., Alberts, B., Voet, P., and Doncker, F. D. (2019). *The impact of noise in a GRACE/GOCE global gravity model on a local quasi-geoid.* Journal of Geophysical Research: Solid Earth, 124(3), 3219–3237. https://doi.org/10.1029/2018JB016470

Smith, D. A. (1998). *There is no such thing as 'The' EGM96 geoid: Subtle points on the use of a global geopotential model.* IGeS Bulletin, 8, 17–28.

Smith, D. A., and Milbert, D. G. (1999). *The GEOID96 high-resolution geoid height model for the United States.* Journal of Geodesy, 73(5), 219–236. https://doi.org/10.1007/s001900050239

Smith, D. A., and Small, H. J. (1999). *The CARIB97 high-resolution geoid height model for the Caribbean Sea.* Journal of Geodesy, 73(1), 1–9. https://doi.org/10.1007/s001900050212

Sneeuw, N. (1996). *Global Spherical Harmonic Computation by Two-Dimensional Fourier Methods.* Journal of Geodesy, 70, 224–232.

Ssengendo, R., Sjoberg, L., and Gidudu, A. (2015). *The Uganda Gravimetric Geoid Model 2014 computed by the KTH Method.* Journal of Geodetic Science, 5, 36–46. https://doi.org/10.1515/jogs-2015-0007

Stanaway, R. (2012). *PNG08 - A new geoid model for Papua New Guinea.* In 46th Association of Surveyors of Papua New Guinea Congress, Port Moresby.

Steed, J., and Holtznagel, S. (1994). *AHD heights from GPS using AUSGEOID93.* The Australian Surveyor, 39(1), 21–27. https://doi.org/10.1080/00050326.1994.10558404

Stewart, M. P., and Hipkin, R. G. (1989). *A High Resolution, High Precision Geoid for the British Isles.* Proceedings of the International Symposium on Sea Surface Topography and the Geoid.

Swassi, A. M. (2000). *Geoid determination for Libya* [PhD dissertation,]. Institut Agronomique et veterinare Hassan II, Rabat, Morocco.

Tierra, A. R., and de Freitas, S. R. C. (2005). *Artificial Neural Network: A Powerful Tool for Predicting Gravity Anomaly from Sparse Data.* In C. Jekeli, L. Bastos, and J. Fernandes (Eds.), Gravity, Geoid and Space Missions, Springer, 208–213. https://doi.org/10.1007/3-540-26932-0_36

Torge, W. (1989). *Gravimetry"*. W. de Gruyter.

Torge, W. (2001). *Geodesy"* (3rd. ed.,W). de Gruyter, Berlin-NewYork.

Tscherning, C. C. (1974). *A FORTRAN IV program for the determination of the anomalous potential using stepwise least squares collocation.* Report, 212. Ohio State University and Department of Geodefic Scienc

Tscherning, C. C. (1981). *Comparison of Some Methods for the Detailed Representation of the Earth's Gravity Field.* Reviews of Geophysics and Space Physics, 19(1, February), 213–221.

Tscherning, C. C. (1982). *Determination of a (quasi) geoid for the Nordic Countries from heterogeneous data using collocation.* Meeting of the Nordic Geodetic Commission.

Tscherning, C. C. (1993). *An experiment to determine gravity from geoid heights in Turkey.* In book:

GEOMED rep. no. 3 Publisher: POLOMI

Tscherning, C. C. (1994a). *Geoid Determination by Least-Squares Collocation Using GRAVFSOFT.* Paper originated as lecture notes prepared for the International School for the Determination and Use of the Geoid.

Tscherning, C. C. (1994b). *Potential field collocation and density modelling".* Preprint IAG section IV review book, prepared for IAG/IUGG, 1995.

Tscherning, C. C. (1999). *Construction of an-isotropic covariance functions using Riesz-representers.* Journal of Geodesy, 73, 333–336.

Tscherning, C. C., Arabelos, D., and Strykowski, G. (2000). *The 1-cm geoid after GOCE.* In Gravity, Geoid and Geodynamics (GGG2000).

Tscherning, C. C., and Forsberg, R. (1986a). *Geoid determination in the Nordic Countries from gravity and height data.* International Symposium on the Definition of the Geoid.

Tscherning, C. C., and Forsberg, R. (1986b). *Geoid determination in the Nordic Countries from gravity and height data.* International Symposium on the Definition of the Geoid, 26–30.

Tscherning, C. C., and Rapp, R. H. (1974a). *Closed covariance expressions for gravity anomalies, geoid undulations and deflections of the vertical implied by anomaly degree variance models.* Volume 208 of Department of Geodetic Science: Report, Ohio Ohio State University Columbus.

Tscherning, C. C., and Rapp, R. H. (1974b). *Closed covariance expressions for gravity anomalies, geoid undulations, and deflections of the vertical implied by anomaly degree variance models.* In Scientific Interim Report Ohio State Univ. https://ui.adsabs.harvard.edu/abs/1974osu..reptQ....T

Tscherning, C. C., Rapp, R. H., and Goad, C. (1983). *A Comparison of Methods for Computing Gravimetric Quantities from High Degree Spherical Harmonic Expansions.* Manuscripta Geodetica, 8, 249–272.

Tscherning, C. C., Sanso, F., and Arabelos, D. (1987). *Merging Regional Geoids: Preliminary Considerations and Experiences.* In ANNO XLVI – BOLLETTINO DI GEODESIA E SCIENZE AFFINI, 3, 191–206.

Tscherning, C., Radwan, A., Tealeb, A., Mahmoud, S., Mohamed, A., Hassan, R., and Saker, K. (2001). *Local geoid determination combining gravity disturbances and GPS/levelling: A case study in the Lake Naser area, Aswan. Egypt.* Journal of Geodesy,75(7–8), 343–348. https://doi.org/10.1007/s001900100185

Tsuei, G.-C., Arabelos, D., Forsberg, R., Sideris, M. G., and Tziavos, I. N. (1994). *Geoid Computations in Taiwan*. IGC/ICG JEOIT Symposium, 11–17.

Tziavos, I. N., and Andritsanos, V. D. (1997). *Improvements in the computation of deflections of the vertical by FFT*. Physics and Chemistry of the Earth, 23(1), 71-75. https://doi.org/10.1016/S0079-1946(97)00244-9.

Tziavos, I. N., and Sideris, M. G. (2013). *Topographic Reductions in Gravity and Geoid Modeling*. in Lecture Notes in Earth System Sciences, Springer, Berlin Heidelberg, 110, 337– 400,

Tziavos, I. N., Vergos, G. S., and Grigoriadis, V. N. (2010). *Investigation of topographic reductions and aliasing effects to gravity and the geoid over Greece based on various digital terrain models*. Surveys in Geophysics, 31(3), 23–67. https://doi.org/10.1007/s10712-009-9085-z

Tziavos, I., Vergos, G. S., Grigoriadis, V., and Stylianidis, S. (2017). *Geoid and Moho-depth modeling in Cyprus*. Conference: IAG-IASPEI2017, Kobe, Japan https://doi.org/10.13140/RG.2.2.16574.18248

Ulotu, P. E. (2009). *Geoid Model of Tanzania from Sparse and Varying Gravity Data Density by the KTH Method*. [Ph.D. Dissertation], Royal Institute of Technology (KTH).

Vanicek, p, E, K., and G. (1986). *The concepts* (2nd revised ed"). north Holland.

Vanicek, P. (1975). *Vertical crustal movements in Nova Scotia asdetermined from scattered relevellings*. Tectonophysics, 29, 183–189.

Vaníček, P., and Featherstone, W. E. (1998). *Performance of three types of Stokes's kernel in the combined solution for the geoid*. Journal of Geodesy, 72, 684–697.

Vaníček, P., Sun, W., Ong, P., Martinec, Z., Najafi, M., Vajda, P., and Horst, B. (1996). *Downward continuation of Helmert's gravity*. Journal of Geodesy, 71, 21–34.

Vergos, G. S., Tziavos, I. N., and Sideris, M. G. (2006). *On the validation of CHAMP-and GRACE-type EGMs and the construction of a combined model*. Geodezja I Kartografia, Geodesy and Cartography, 55(3), 115–131.

Vermeer, M. (1992). *A frequency domain approach to optimal geophysical data gridding*. Man Geod, 17, 141–154.

Vermeer, M. (1995). *Two new geoids determined at the FGI*. Report of the Finnish Geodetic Institute, 95(5), 24.

Veronneau, M. (1996). *The GSD95 geoid model for Canada. In J. Segawa, H. Fujimoto, and S. Okubo (Eds.)*. Gravity, Geoid and Marine Geodesy, IAG Symposia Series , Springer Verlag, 117, 573-580. https://doi.org/10.1007/978-3-662-03482-8_76

Veronneau, M. (2001). *The Canadian Gravimetric Geoid Model of 2000 (CGG2000).* Report of Geodetic Survey Division, Natural Resources Canada.

Veronneau, M., and Huang, J. (2007). *The Canadian Gravimetric Geoid Model of 2005 (CGG2005).* Report of Geodetic Survey Division, Natural Resources Canada.

Veronneau, M., and Mainville, A. (1992). *Computation of a Canadian geoid model using the FFT technique to evaluate Stokes' and Vening-Meinesz' formulas in a planar approximation.* AGU-CGU-MSA Joint Spring Meeting.

Visser, P. N. A. M., and IJssel, J. (2000). *GPS-based precise orbit determination of the very low Earth-orbiting gravity mission GOCE.* Journal of Geodesy, 74, 590–602.

Wang, Y. M. (1993). *Comments on proper use of the terrain correction for the computation of height anomalies.* Manuscripta Geodetica, 18, 53–57.

Wang, Y. M. (1999). *On the ellipsoidal corrections to gravity anomalies computed using the inverse Stokes integral.* Journal of Geodesy, 73, 29–34.

Wang, Y. M., Li, X., Ahlgren, K., Krcmaric, J., Hardy, R., Veronneau, M., Huang, J., and Avalos, D. (2021). *The experimental geoid 2020 andndash; the first joint geoid model for the North American and Pacific Geopotential Datumandnbsp;* (No. EGU21-6011). EGU21. Copernicus Meetings. https://doi.org/10.5194/egusphere-egu21-6011

Wang, Y. M., Saleh, J., Li, X., and Roman, D. R. (2012). *The US Gravimetric Geoid of 2009 (USGG2009): Model development and evaluation.* Journal of Geodesy, 86(3), 165–180. https://doi.org/10.1007/s00190-011-0506-7

Wellenhof, B., and Moritz, H. (2005). *Physical geodesy"*. Springer-Verlag.

Williams, J. G., Turyshev, S. G., Boggs, D. H., and Ratcliff, J. T. (2006). *Lunar laser ranging science.* Gravitational physics and lunar interior and geodesy, 37(1), 67-71. https://doi.org/10.1016/j.asr.2005.05.013.

Willis, P., Lemoine, F. G., Moreaux, G., Soudarin, L., Ferrage, P., Ries, J. C., Otten, M., Saunier, J., Noll, C. E., Biancale, R., and Luzum, B. (2016). In *The International DORIS Service (IDS), Recent Developments in Preparation of ITRF2013, IAG Symposia 143*.

Yakubu, C. I., Ferreira, V. G., and Asante, S. (2017). *Towards the Selection of an Optimal Global Geopotential Model for the Computation of the Long-Wavelength Contribution: A Case Study of Ghana.* Geosciences, 7(4), 113. https://doi.org/10.3390/geosciences7040113

Yearbook, I. U. G. G. (2021). *International Union of Geodesy and Geophysics*. (p. 155). https://www.iugg.org/

Zhang, C. (1998). *Estimation of dynamic ocean topography in the Gulf Stream area using the Hotine formula and altimetry data.* Journal of Geodesy, 72, 499–510.

Zingerle, P., Pail, R., Gruber, T., and Oikonomidou, X. (2020). *The combined global gravity field model XGM2019e.* Journal of Geodesy, 94(7), 66. https://doi.org/10.1007/s00190-020-

Biography

Moamen Awad Habib Gad

Born on 20.05.1978 in the city of Sohag, Egypt, where he finished primary and secondary school with great success.

He enrolled at the Faculty of Engineering in Shoubra, Benha University, in 1998, where he graduated in 2003. At the same faculty, he also obtained the title of master in geodesy and surveying in 2013. In parallel with his master's studies, he completed a project management course at the University of Cairo.

The mother tongue of Moamen Awad Habib Gad is Arabic, and he speaks, reads and writes English. After graduating, he constantly improved by participating in the implementation of a large number of projects, mainly in Egypt, so, so far Moamen Awad Habib Gad has over 17 years of work experience. The projects in which he participated are mostly in the field of geodesy, construction and landscape architecture.

He enrolled in doctoral studies at the Faculty of Civil Engineering, University of Belgrade in 2016 (in Geodesy, Specialized scientific field Determination of the gravitational field) and completed all anticipated obligations on February 21, 2019. by successfully defending the Accession Work.

Moamen Awad Habib Gad is married and has three children.

Биографија

Моамен Авад Хабиб Гад

Рођен 20.05.1978. год. у граду Сохаг, Египат, где је завршио основну и средњу школу са одличним успехом.

Уписао се на факултет инжињерства Схоубра, Универзитета Бенха, 1998. године, где је и дипломирао 2003. године. На истом факултету стекао је и титулу мастера из геодезије и премера 2013. године.

Паралелно са мастер студијама завршио је на универзитеу у Каиру и курс за управљање пројектима.

Матерњи језик Моамен Авад Хабиб Гад је арапски, а говори, чита и пише енглески.
Након дипломирања све време се усавршавао учествовањем у реализацији великог броја пројеката, углавном на територији Египта, тако да до сада Моамен Авад Хабиб Гад има и преко 17 година радног искуства. Пројекти у којима је учествовао су већим делом из области геодезије, грађевинарства и пејзажне архитектуре.

На докторске студије Грађевинског факултета Универзитета у Београду уписао се 2016. године (смер Геодезија, ужа научну област Одређивање гравитационог поља) и све предвиђене обавезе завршио је 21.02.2019. успешно одбрањеним Приступним радом.
Моамен Авад Хабиб Гад је ожењен и има троје деце.

образац изјаве о ауторству

Изјаве о ауторству

Име и презиме аутора Moamen Awad Habib Gad

Број индекса 914_16

Изјављујем

да је докторска дисертација под насловом

Одређивање референтних нивоских површи висина у подручјима са неправилним просторним распоредом резултата опажања параметара потенцијала Земљине теже

1. резултат сопственог истраживачког рада;
2. да дисертација у целини ни у деловима није била предложена за стицање друге дипломе према студијским програмима других високошколских установа;
3. да су резултати коректно наведени и
4. да нисам кршио/ла ауторска права и користио/ла интелектуалну својину других лица.

У Београду, јун 2022 Потпис аутора

образац изјаве о истоветности штампане и електронске верзије докторског рада

Изјаве о истоветности штампане и електронске верзије докторског рада

Име и презиме аутора Moamen Awad Habib Gad

Број индекса 914_16

Студијски програм Геодезије и геоинформатике

Наслов рада Одређивање референтних нивоских површи висина у подручјима са неправилним просторним распоредом резултата опажања параметара потенцијала Земљине теже

Ментор проф. др. Oleg Odalović

Изјављујем да је штампана верзија мог докторског рада истоветна електронској верзији коју сам предао/ла ради похрањивања у **Дигиталном репозиторијуму Универзитета у Београду.**

Дозвољавам да се објаве моји лични подаци везани за добијање академског назива доктора наука, као што су име и презиме, година и место рођења и датум одбране рада.

Ови лични подаци могу се објавити на мрежним страницама дигиталне библиотеке, у електронском каталогу и у публикацијама Универзитета у Београду.

У Београду, јун 2022 Потпис аутора

Образац изјаве о коришћењу

Изјаве о коришћењу

Овлашћујем Универзитетску библиотеку „Светозар Марковић“ да у Дигитални репозиторијум Универзитета у Београду унесе моју докторску дисертацију под насловом:

Одређивање референтних нивоских површи висина у подручјима са неправилним просторним распоредом резултата опажања параметара потенцијала Земљине теже

која је моје ауторско дело.

Дисертацију са свим прилозима предао/ла сам у електронском формату погодном за трајно архивирање.

Моју докторску дисертацију похрањену у Дигиталном репозиторијуму Универзитета у Београду и доступну у отвореном приступу могу да користе сви који поштују одредбе садржане у одабраном типу лиценце Креативне заједнице (Creative Commons) за коју сам се одлучио/ла.

1. Ауторство (CC BY)
2. Ауторство – некомерцијално (CC BY-NC)
3. Ауторство – некомерцијално – без прерада (CC BY-NC-ND)
4. Ауторство – некомерцијално – делити под истим условима (CC BY-NC-SA)
5. Ауторство – без прерада (CC BY-ND)
6. Ауторство – делити под истим условима (CC BY-SA)

(Молимо да заокружите само једну од шест понуђених лиценци.
Кратак опис лиценци је саставни део ове изјаве).

У Београду, јун 2022 Потпис аутора

1. Ауторство. Дозвољавате умножавање, дистрибуцију и јавно саопштавање дела, и прераде, ако се наведе име аутора на начин одређен од стране аутора или даваоца лиценце, чак и у комерцијалне сврхе. Ово је најслободнија од свих лиценци.

2. Ауторство – некомерцијално. Дозвољавате умножавање, дистрибуцију и јавно саопштавање дела, и прераде, ако се наведе име аутора на начин одређен од стране аутора или даваоца лиценце. Ова лиценца не дозвољава комерцијалну употребу дела.

3. Ауторство – некомерцијално – без прерада. Дозвољавате умножавање,
дистрибуцију и јавно саопштавање дела, без промена, преобликовања или употребе дела у свом делу, ако се наведе име аутора на начин одређен од стране аутора или даваоца лиценце. Ова лиценца не дозвољава комерцијалну употребу дела. У односу на све остале лиценце, овом лиценцом се ограничава највећи обим права коришћења дела.

4. Ауторство – некомерцијално – делити под истим условима. Дозвољавате умножавање, дистрибуцију и јавно саопштавање дела, и прераде, ако се наведе име аутора на начин одређен од стране аутора или даваоца лиценце и ако се прерада дистрибуира под истом или сличном лиценцом. Ова лиценца не дозвољава комерцијалну употребу дела и прерада.

5. Ауторство – без прерада. Дозвољавате умножавање, дистрибуцију и јавно саопштавање дела, без промена, преобликовања или употребе дела у свом делу, ако се наведе име аутора на начин одређен од стране аутора или даваоца лиценце. Ова лиценца дозвољава комерцијалну употребу дела.

6. Ауторство – делити под истим условима. Дозвољавате умножавање, дистрибуцију и јавно саопштавање дела, и прераде, ако се наведе име аутора на начин одређен од стране аутора или даваоца лиценце и ако се прерада дистрибуира под истом или сличном лиценцом. Ова лиценца дозвољава комерцијалну употребу дела и прерада. Слична је софтверским лиценцама, односно лиценцама отвореног кода.